Microstructure and Mechanical Properties of Aluminium Based Nanocomposites Strengthened with Alumina and Silicon Carbide

A thesis submitted in fulfilment
of the requirements for the degree
of
Doctor of Philosophy
at
The University of Waikato
by

Amro A. Gazawi

The University of Waikato

2014

THE UNIVERSITY OF
WAIKATO
Te Whare Wānanga o Waikato

!!

أنك تنام في أي مكان في المنزل،

ولكنك تستيقظ وأنت في سريرك ..

" ربي إرحمهما كما ربّياني صغيرا"

To my Loving Parents

"وَقَالَ رَبِّ أَوْزِعْنِي أَنْ أَشْكُرَ نِعْمَتَكَ الَّتِي أَنْعَمْتَ عَلَيَّ وَعَلَى وَالِدَيَّ وَأَنْ أَعْمَلَ صَالِحًا تَرْضَاهُ"

Abstract

Al-Al_2O_3 and Al-4wt%Cu-SiC metal matrix nanocomposites were studied because these materials have a potential for offering good ductility, high strength, and high electrical and/or thermal conductivity, which make them ideal for engineering applications such as aerospace and automobile components. In order to achieve these goals the reinforcement phase needs to be in a particulate form, and the size of the particles needs to be small.

Samples of aluminium based nanocomposites were produced with different volume fractions, ranging from 2.5-10 vol.% of alumina (Al_2O_3) and silicon carbide (SiC) nanoparticles. High energy mechanical milling (HEMM) with various milling times ranging from 6-12 hours was used to produce these samples. Optical microscopy, XRD, SEM, TEM and microindentation were used to characterize the milled powder and bulk samples. Bulk solid Al-(2.5-10) vol. % Al_2O_3 and Al-4wt%Cu-(2.5-10) vol. %SiC nanocomposites samples were produced using different powder consolidation techniques such as powder compact forging and powder compact extrusion.

The microstructure of the composite powder/balls/granules produced was studied in details to understand the morphology, macrostructure and microstructural evolution during the HEMM and with changing volume percent of the reinforcements in the matrix. The nano SiC and Al_2O_3 were imbedded into the aluminium matrix due to the high forces and strains affecting particle surfaces during milling and the very small size of the reinforcement relative to the size of the Al particles. The average microhardness was increased with increasing volume fraction of reinforcement within the matrix. HEMM was used to fabricate Ultra-Fine Grained (UFG) and nanostructured Al- (2.5-10) vol. %Al_2O_3 composites

with a dispersion of nano alumina within the matrix and Al-4wt%Cu- (2.5-10) vol%SiC with two different sizes of SiC in the micro and nano ranges.

A UFG structure in the Al and Al-(2.5-10)vol.% Al_2O_3 nanocomposites can be synthesized by a combination of high energy mechanical milling and severe plastic deformation used to consolidate the powder compacts into nearly fully dense forged discs and extruded bars. No significant microscopic yielding was found in the Al-2.5 and 10 vol. %Al_2O_3 composites produced by powder compact forging. However, Al-5vol. % Al_2O_3 showed plastic yielding of 8%, and the best fracture strength of 343 MPa. No significant microscopic yielding was noticed for the Al- 10 vol. %Al_2O_3 composite produced by powder compact extrusion. Al-2.5vol. % Al_2O_3 showed plastic yielding of ~1% with the highest tensile strength of 364 MPa while Al-5vol. % Al_2O_3 showed plastic yielding of 8% with a yield strength of 318 MPa.

The average microhardness of the extruded bars for Al-4wt%Cu-(2.5-10)vol.% SiC increased from 104 HV to 205 HV with increasing the volume fraction of SiC nanoparticles from 2.5 to 10%. The ultimate tensile strength increased from 168 MPa to 400 MPa with increasing volume fraction of SiC nanoparticles from 2.5 to 5% while the ductility dropped from 6.8% to 1.2 %. The fracture strength of the Al-4wt%Cu-micro-SiC was increased from 225 MPa for Al-4wt%Cu-2.5vol. %SiC to 412 MPa for Al-4wt%Cu-10vol. % SiC. The Al-4wt%Cu-2.5vol. %SiC forged disc did not show any macroscopic plastic yielding, while the Al-4wt%Cu-(7.5 and 10)vol. %SiC forged disk showed macroscopic plastic yielding with a small plastic strain to fracture (~1%).

Acknowledgements

I would like to express my gratitude to my former chief supervisor Prof. Deliang Zhang for his guidance, support, motivation and future vision during the entire period of my research that enabled me to keep up my motivation and focus through this important step in my life. I would like also to thank my co-supervisor Prof. Kim Pickering for providing advice when needed.

I would like to express my sincere gratitude to my chief supervisor Prof. Brian Gabbitas, for his inspiration, constant encouragement, and assistance during the course of this research work.

I would like to thank Prof. Paul Munroe and Dr. Charlie Kong, from the University of New South Wales, Sydney, for their collaboration during my PhD study. I would like to thank the Foundation for Research, Science and Technology (FRST), New Zealand, for the financial support.

Special thanks for my parents; Dr. Abdul-Karim Ghazzwi and Eman Al-Tall for their encouraging words, all what they have given me through my lifetime, financial support during this journey and to my siblings Lubna and Haitham and their families.

Many thanks for the continuous support and being around for Maria Gherca and her family, Martin Danisik, Alison Pope, Refa`at Al-Shunnaq, Mohammad Malkawi and his family, Ahmad Al Selati , Abdul-Rahman Al Omari , Ghaith Alomari, Moeen Alkhatib and his family, Adel Alghamedi, Essam George, Jose Nunez, Sam George, Irene Albuquerque, Neto Cazuma, Roanna Richards and all the other friends whom supported me.

I am thankful for the Department of Engineering technicians who provided the technical support for this research, especially Helen Turner, Yunaji Zhang, Brett

Nichole, Indar Singh, Steve Hardy, Stuart Finlay, and Annette Rodgers. I would like to thank Mary Dalbeth and Cheryl Ward for their official support.

I also want to thank the new and old members of the metallic group (Vijay, Aamir, Asma, Stella, Maselyatti, Mingtu, Paul, Ken, Qain, Huiyang, Dengshan, Izhar, Jai lou, Venni, Nav, and Fei) for their constant support and encouragement through the progress of my experimental work and writing up this thesis.

I am also thankful for Dr.Fantao Kong from the School of Materials Science and Engineering, Harbin Institute of Technology-China for his kind help.

Finally I would like to thank all the people who directly and indirectly helped me during the project work.

Table of Contents

List of Figures

List of Tables

List of Publications

1. A. Gazawi, D.L. Zhang, K. Pickering, The Effect of Volume Fraction of Al_2O_3 on the Morphology and Hardness of Nanostructured Al_2O_3 Composite Produced by High Energy Mechanical Milling, In Proc. of SMNZI Materials Conference 2009, 10-11 December 2009, Hamilton, New Zealand.

2. Amro A. Gazawi, D. L. Zhang, K. L. Pickering, and A. Mukhtar, Microstructure and Mechanical Behaviour of Ultrafine Grained Al-4wt%Cu-(2.5-10) vol.% SiC Metal Matrix Composites Produced by Powder Compact Forging. International Conference on Structural Integrity and Failure (SIF 2010), 4-7 July 2010, Auckland, New Zealand.

3. Amro A. Gazawi, Deliang Zhang, Charlie Kong, Paul Munroe, Microstructure and Tensile Properties of an Ultrafine Structured Al-5vol. %Al_2O_3 Nanocomposite Produced by Using a Powder Metallurgy Processes, Unpublished research.

Chapter One: Introduction

Materials are classified into five main types: metallic, ceramic, polymeric materials, advanced and composite materials [1, 2]. A Composite is a mixture of two or more distinct constituents or phases. However, this definition is not sufficient and three other criteria have to be satisfied before a material can be said to be a composite. Firstly, both constituents have to be present in reasonable proportions, >5%. Secondly the constituent phases should have different properties and finally a man-made composite is usually produced by intimately mixing and combining the constituents by various means [3]. Composites are commonly classified at two distinct levels. The first level of classification is usually made with respect to the matrix constituent. The major composite classes include organic-matrix composites (OMCs), metal-matrix composites (MMCs), and ceramic-matrix composites (CMCs). The second level of classification refers to the reinforcement form—particulate reinforcements, short fibres, continuous fibre laminated composites, and woven composites (braided and knitted fibre architectures are included in this category), as depicted in Fig. 1 [4]. Reinforcements, characterized as either continuous or discontinuous, may constitute from 10 to 60 vol% of the composite. Continuous fibre or filament reinforcements include graphite (Gr), silicon carbide (SiC), boron, aluminium oxide (Al_2O_3), and refractory metals. Discontinuous reinforcements consist mainly of SiC in whisker (w) form, particulate (p) types of SiC, Al_2O_3, or titanium diboride (TiB2), and short or chopped fibres of Al_2O_3 or graphite [5].

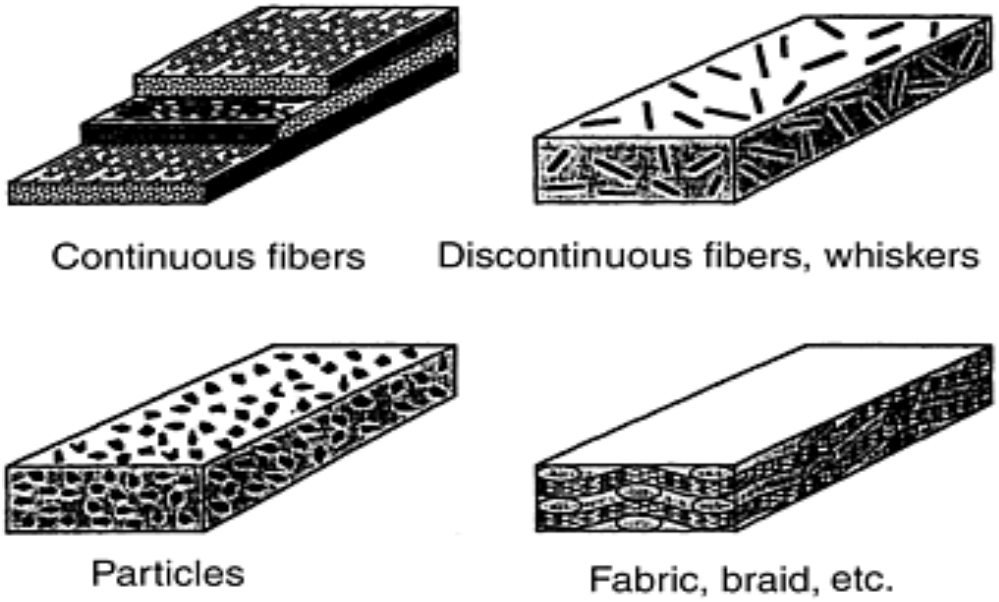

Figure 1.1: Common forms of reinforcement phase [4].

The most common matrix materials of MMCs are: aluminium, titanium, magnesium, copper, nickel, and various alloys of these metals [6]. Most of the commercial work on MMCs has focused on aluminium as the matrix metal. The combination of light weight, corrosion resistance, high mechanical properties, and relatively low melting point makes aluminium alloys attractive as engineering materials. These properties also make aluminium well suited for use as a matrix metal and suitable to be produced by powder metallurgy, and by casting methods. The melting point of aluminium is high enough to satisfy many application requirements, yet low enough to render composite processing reasonably convenient. Also, aluminium can accommodate a variety of reinforcing agents, including continuous boron, Al_2O_3, SiC, and graphite fibres, and various particles, short fibres, and whiskers [5, 7].

We chose to study Al-Al_2O_3 and Al-4wt%Cu-SiC metal matrix composite as these materials offer good ductility, high strength, and high electrical and thermal conductivity, making them ideal for engineering applications such as aerospace

and automotive. In order to achieve these goals the reinforcement phase needs to be in a particulate form, and the size of the particles needs to be small.

In this PhD research, samples of aluminium based matrix nanocomposites were produced with different volume fractions, ranging from 2.5-10 %, of alumina (Al_2O_3) and silicon carbide (SiC) nanoparticles. High energy mechanical milling (HEMM) with various milling times ranging from 6-12 hours was used to produce these samples. Optical microscopy, XRD, SEM, TEM and micro-indentation were used to characterize the mechanically milled powder and final bulk samples. Bulk solid Al-(2.5-10) vol. % Al_2O_3 and Al-4wt%Cu-(2.5-10) vol. %SiC nanocomposite samples were produced using powder compact forging and powder compact extrusion.

The hypothesis to be investigated in this thesis is whether high energy mechanical milling, followed by powder consolidation can produce a fine distribution of alumina and/or silicon carbide particles in the aluminium microstructure, which enhances the mechanical properties of aluminium without adversely affecting its electrical conductivity.

The objectives of this study are:

- To understand the effect of the various milling conditions on the microstructure and microhardness of Al with (2.5-10) vol. % of Al_2O_3 and Al-4wt%Cu with (2.5-10) vol. % of SiC processed to give an ultra fine-grained structure as a result of mechanical milling.
- To understand the effects of powder consolidation techniques and conditions on the microstructure and mechanical properties of the bulk aluminium composites with ultrafine microstructure.
- To understand the relationship between microstructure and mechanical properties of the ultrafine aluminium composite materials.

The thesis is divided into seven chapters. The first chapter is an introduction, chapter two presents a review of the literature on aluminium matrix nanocomposites (AMNC`s), with some general background information, processing techniques and the relationship between microstructure and mechanical properties of these composites. Chapter three describes the experimental procedure used in this work. Chapter four to chapter six presents and discusses the results of the research. Chapter seven summarizes the conclusions and gives recommendations for future work.

References

[1] D. R. Askeland, F. Haddelton, P. Green, and RobertsonHoward, *The Science and Engineering of Materials*, Third Edition ed.: Chapman & Hall, 1996.

[2] W. F. Smith and J. Hashemi *Foundations of Materials Science and Engineering* Fifth Edition ed.: Mc Graw Hill, 2010.

[3] F. L. Matthews and R. D. Rawlings, *Composite Materials: Engineering and Science*, First edition ed.: Chapman and Hall, 1994.

[4] C. Zweben, *Composite Materials and Mechanical Design, Mechanical Engineer's Handbook*, Second Edition ed. New York: John Wiley & Sons, Inc, 1998.

[5] A.S.M Handbook, *Properties and selection: Non ferrous alloys and special -purpose Materials* vol. 2, 1990.

[6] A. B. Strong, *Fundamentals of Composites Manufacturing*, Second Edition ed.: Society of Manufacturing Engineers, 2002.

[7] D. O. Defense and Handbook, Metal Matrix Composites, vol. 4, 2002.

Chapter Two: Literature Review

2.1 Introduction

A composite material in the broad sense refers to all solid material composed of more than one component wherein those components are in separate phase. This definition includes a wide range of materials such as, fibre reinforced plastics, regular and steel reinforced concrete, particle filled plastics, and rubber reinforced plastics, wood laminates, and ceramic mixtures. MMCs have higher strength-to-density ratios, better fatigue resistance (Fatigue damage in composites is very complex, due to several damage mechanisms occurring at many locations. Such as matrix cracking, fibre fracture, longitudinal cracking, crack coupling. As a result, composites components generally do not fail due to single, large macrocracks, but rather fail due to a series of interdependent damage events), better elevated temperature properties (such as high strength and low creep rate), and lower coefficients of thermal expansion, high thermal conductivity, good damping characteristics, excellent wear properties and flexibility in design attributes [1, 2]. Table 2.1 below shows the advantages and disadvantages of composite materials.

Table 2.1: Advantages and disadvantages of composites [3].

Advantages	Disadvantages
• Lightweight • High Specific Stiffness • Tailored properties (anisotropic) • High specific strength • Easily mouldable to complex (net) shapes • Part consolidation leading to lower overall system cost • Easily bondable • Good fatigue resistance • Good Damping • Crash worthiness • Internal energy storage and release • Low thermal expansion • Low electrical conductivity • Stealth (low radar visibility) • Thermal Transport (carbon fibre only)	• Cost of material • Lack of well-proven design rules • Metal and composite designs are seldom directly interchangeable • Long development time • Manufacturing difficulties (manual, slow, environmentally problematic, poor reliability) • Fasteners • Low ductility (joints inefficient, stress risers, more critical than in metals) • Solvent/moisture attack • Temperature limits • Damage susceptibility • Hidden damage • EMI shielding sometimes required

Metal-matrix composites (MMCs) are a class of materials with potential for a wide variety of structural and thermal applications. Metal-matrix composites are capable of providing higher-temperature operating limits than their base metal counterparts, and they can be tailored to give improved strength, stiffness, thermal

conductivity, abrasion resistance, creep resistance, or dimensional stability. Unlike resin-matrix composites, they are non-flammable, do not outgas in a vacuum, and suffer minimal attack by organic fluids such as fuels and solvents. A desire to extend the structural efficiency (high specific strength and high specific stiffness) of metallic materials motivated the development of metal matrix composites in the 1950s and early 1960s [1, 4]. Early work on sintered aluminium powder was a precursor to discontinuously reinforced MMCs. The development of high-strength monofilaments—first boron and then silicon carbide (SiC)—led to significant research effort on fibre- reinforced MMCs throughout the 1960s and early 1970s. A wide range of aluminium alloys in various forms have been used in MMCs. These are attractive because the density of most aluminium alloys is near that of pure aluminium, approximately (2698 kg/m^3) and pure aluminium melts at (660.32 °C). This relatively low melting temperature facilitates processing of Al-based MMC's by solid state routes, such as powder metallurgy, and casting [5, 6].

Lightweight, high specific strength and Young`s modulus, good wear resistance and high temperature strength are some of the properties that aluminium matrix composites possess [7-10]. Aluminium based metal matrix composites (AlMMCs) are ideal materials because the melting point of aluminium is high enough to satisfy many application requirements, yet low enough to render composite processing reasonably convenient so that they can be widely used in aerospace, defence and automotive industries [11, 12].

Niihara proposed the concept of structural ceramic nanocomposites in 1991[13]and in the last 2-3 decades, interest in the processing, microstructure and properties of metallic materials with grain sizes in the range of tens to several hundreds of a nanometres has increased considerably [14-16].

2.2 Fabrication of Metal Matrix Nanocomposites

Discontinuous reinforced composites have been rapidly developed during the 1980s, with a focus on Al-based composites reinforced with particles and short fibres of SiC and Al_2O_3 [17]. The use of aluminium alloys (like Al-Si alloys) for the matrix is preferred because of its advantages, including low cost and ease of handling. The major fabrication methods used for aluminium metal matrix composites are stir casting, squeeze casting, compocasting and infiltration, spray deposition and powder metallurgy. Wide applications were found for the alumina-reinforcing aluminium metal matrix composites in the automotive and aerospace industries along with carbon and silicon carbide-reinforced composites [18].

Powder metallurgy is used to synthesize both aluminium metal matrix composites (AlMMC`s) and ceramic matrix composites through the relativity low-cost methods of single compaction, double compaction and mechanical deformation following hot pressing as well as through high cost hydrostatic and isostatic compaction methods [17, 19]. High energy, high rate processing (solid-phase synthesis) was used successfully to consolidate rapidly quenched powders containing a fine distribution of ceramic particulates, where the consolidation of a metals-ceramic mixture involves the application of high energy in a short period of time [20].

There has been considerable effort to produce in-situ nanocomposites by mechanical alloying. In-situ particle composites that have been prepared include aluminium based MMCs such as Al-Al_2O_3, Al-TiC, and Al-TiBs [17].

Metal matrix nanocomposites can be synthesized either through the separate addition of particles to the matrix (ex-situ) or the formation of the reinforcement at the time of synthesising the matrix metal (in-situ). Ex-situ nanocomposites are prepared by incorporating ceramic nanoparticles into the ductile matrix via either

powder metallurgy (PM) or liquid metallurgy routes, whilst in-situ nanocomposites are prepared by producing the nanoparticles inside a matrix through exothermic reactions between the constituent elements during the fabrication process. The particles synthesized in-situ is normally extremely fine (nano sized), homogeneously distributed in the matrix, and are thermally stable, and therefore more effectively reinforce the matrix resulting in higher mechanical properties [21-24].

Powder metallurgy is a common technique for producing MMNCs especially AlMMNCs, where ceramic nanoparticles are incorporated into Al and its alloys [14, 25]. Powder blending and/or premixing using ex-situ or in-situ methods followed by consolidation is one of the ways used for the fabrication of MMNCs. The powders are blended for certain times (20 minutes [26] and 4 hours have been used with5 wt.% of nanosized alumina [27] for example), with different weight fractions of nanometre sized ceramic particles before being milled and put into moulds [7, 26, 27]. Powders of the Al matrix and reinforcement powders are then mechanically alloyed to develop a new matrix. As an example, figure 2.1 (a)–(e) shows the SEM microstructure taken from an Al–5%Al_2O_3 composite after 75, 150, 230, 450 and 900 min milling. As expected, the particle distribution was not uniform and the distance between alumina particles was large after relatively short milling times [28].

Spray deposition is an advanced technique used to synthesize MMNCs. Spray deposition facilitates through cost savings, the production of alloys with compositions that are difficult, if not impossible to produce conventionally. It also offers the possibility for modifying the properties of the sprayed deposit. MMNC`s produced using this technique include Al alloys, Cu alloys, stainless steels, high Cr alloy steels, and superalloys [29-31].

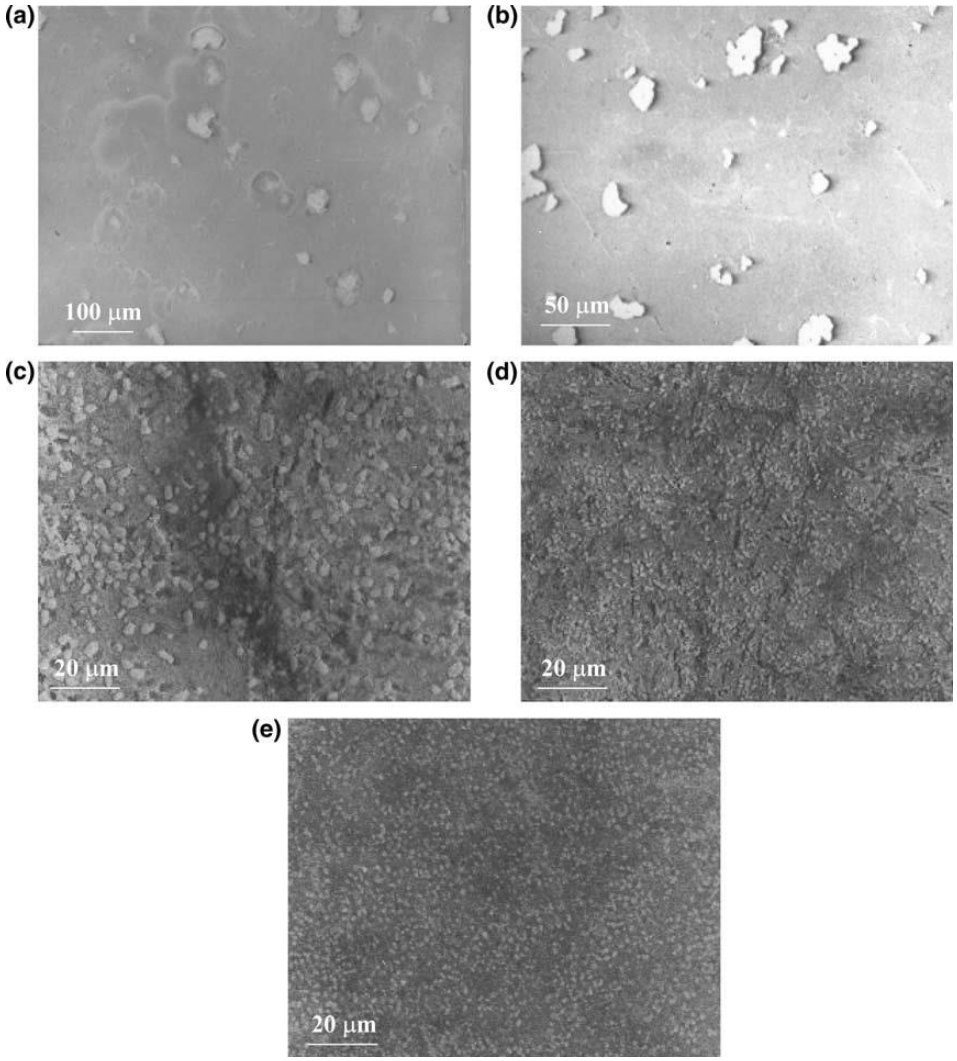

Figure 2.1: SEM micrographs of Al–5%Al_2O_3 composite milled after: (a) 75 min; (b) 150 min; (c) 230 min; (d) 450 min; (e) 900 min [28].

Another technique used to fabricate MMNCs is squeeze casting in which the melt solidifies under pressure [32, 33]. Figure 2.2 shows an SEM micrograph of a hybrid consisting of 20 vol.% SiC whiskers and 5 vol.% SiC nanoparticles. Aluminium, magnesium, and copper alloy components are readily manufactured using this process [34], while the reinforcement materials include ceramics, carbon and graphite.

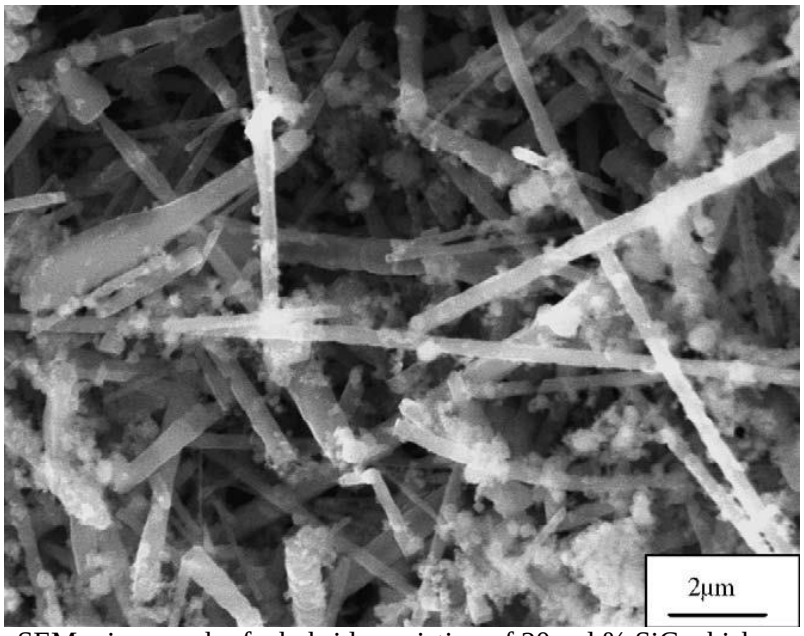

Figure 2.2: SEM micrograph of a hybrid consisting of 20 vol.% SiC whiskers and 5 vol.% SiC nanoparticles fabricated by squeeze casting route[35].

2.3 High Energy Mechanical Milling

Mechanical milling is a very effective method used for producing alloys and composite powders. Milling is carried out under an inert atmosphere to prevent the oxidation of the powders. Process control agents (PCAs) are normally used to prevent sticking of the milled powders to the surface of the balls and inner walls of the vial and to achieve a proper balance between cold welding and fracture when milling ductile materials. There are a variety of high energy mechanical mills including planetary ball mill (Figure 2.3), vibratory ball mill, tumbler ball mill, and discus mill.

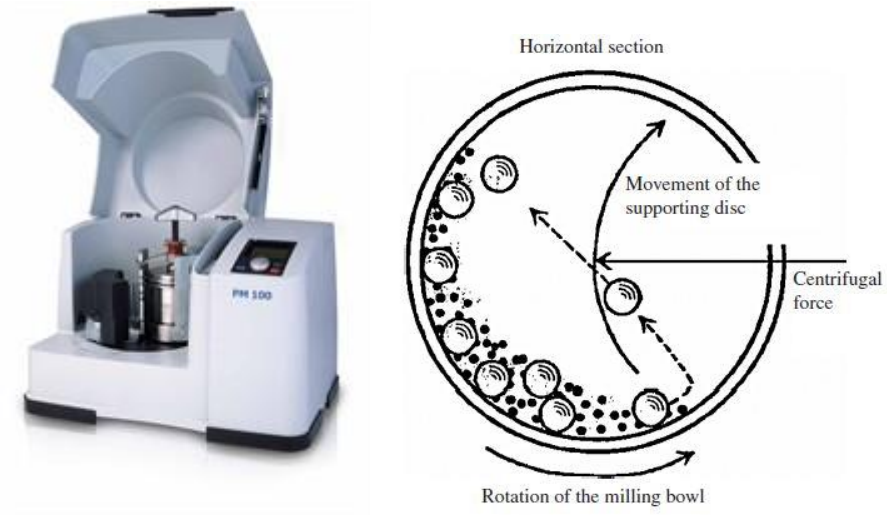

Figure 2.3: Picture and **s**chematic drawing of a high-energy planetary ball mill.

According to El-Eskandarani [36] the objectives of milling are particle size reduction, mixing and blending, particle shaping and mechanical alloying. These objectives are accomplished by means of continuous plastic deformation, fracturing and welding of powder particles. The MA process is affected by several factors such as the type of mill, the milling tool material, atmosphere, temperature, time, media types, and media to powder weight ratio.

One of the most common systems for mechanical alloying to produce composites is the ductile/brittle system. This system involves powder particles of a ductile metal such as Al, Cu, or Ni and a brittle phase which might be an oxide or carbide. During milling, the ductile particles become flattened, while the brittle particles undergo fragmentation. When the ductile flattened particles start to weld together due to ball collision, the fragmented brittle particles are embedded between the ductile layers. In this way, the brittle phase is uniformly distributed within the matrix [28, 37-40]. Cu-Al_2O_3, Al-Al_2O_3, NiAl/Al_2O_3 are common ductile/brittle systems. The microstructural evolution of the system during mechanical milling is schematically described in Figure 2.4.

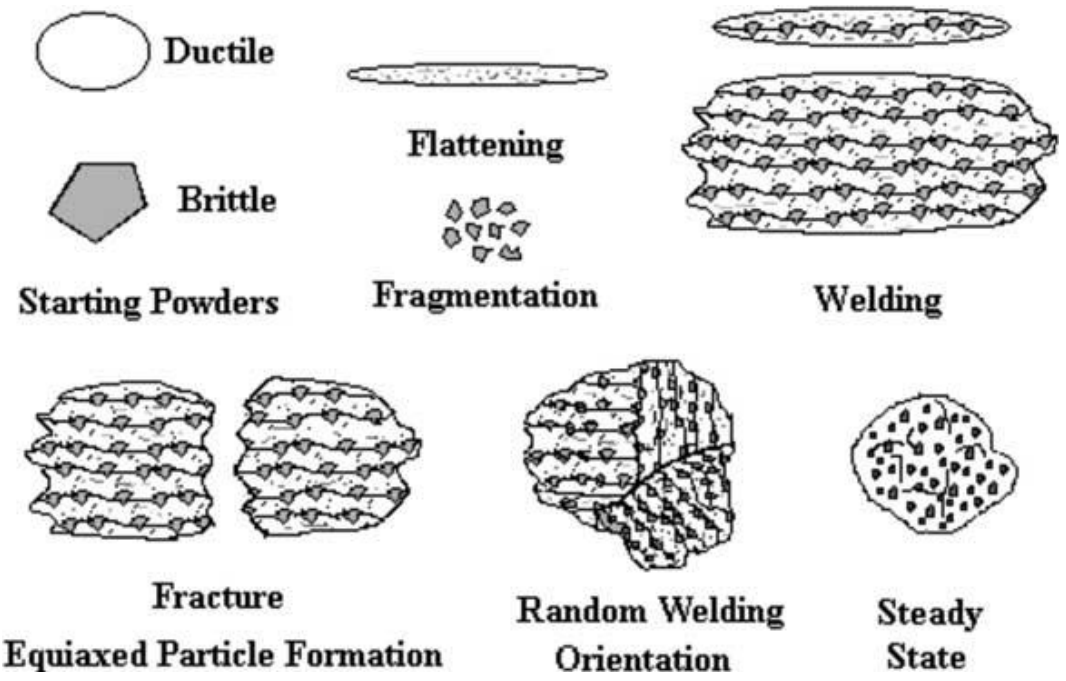

Figure 2.4: The various stages of a ductile-brittle system during mechanical alloying [41].

2.4 Microstructure of MMNCS Powder Particles Produced by MA

A feature of nanocomposites is the control of grain size of both the matrix and reinforcement to within nanometre (10^{-9} m) size. Fine grain sizes, homogenous reinforcement distribution and strong bonding of reinforcements with the matrix will certainly improve mechanical properties [42, 43]. It is essential to obtain a fine and homogenous microstructure for better mechanical properties.

The morphology of the nanocomposite powder particles changes during milling due to plastic deformation driven by impact forces from the milling media. Figure 2.5 shows the morphologies of atomized Al powder particles and the powder particles of milled Al-5vol. %Al_2O_3 and Al-5083/SiCp nanocomposites. During mechanical milling of metal powders, the morphology and structure of the particles undergo continuous changes. Plastic deformation, welding, and fracture of the particles are dominant mechanisms which influence the characteristics of milled powders. When soft aluminium powder is milled, the energy of milling deforms the particles and changes their morphology from equiaxed to a flatten profile. This can be accompanied by welding of the flattened particles to form

larger agglomerates. As shown in Figure 2.6[44], Al-5wt%Al_2O_3 nanocomposite powder particles milled for 15 h showed flattening and coarsening, while after 20 h of milling, the powder particles became finer and changed their shape from flat and elongated to almost equiaxed. It is noteworthy to mention that an Al–Mg alloy 5083 matrix is more brittle than pure Al due to the solid solution hardening effect of the Mg. This accelerates particle fracturing and shortens the different mechanical milling stages [44].

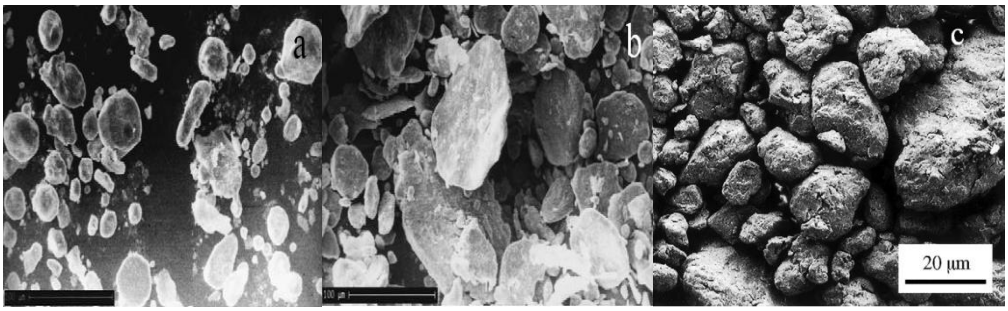

Figure 2.5: (a) Particle morphologies of the as-received atomised Al powders [45] , (b) particle morphologies of Al–5 vol% Al_2O_3 powder after 8 hours of milling time [45], (c) particle morphologies of cryomilled Al-5083/SiCp composite powder [46].

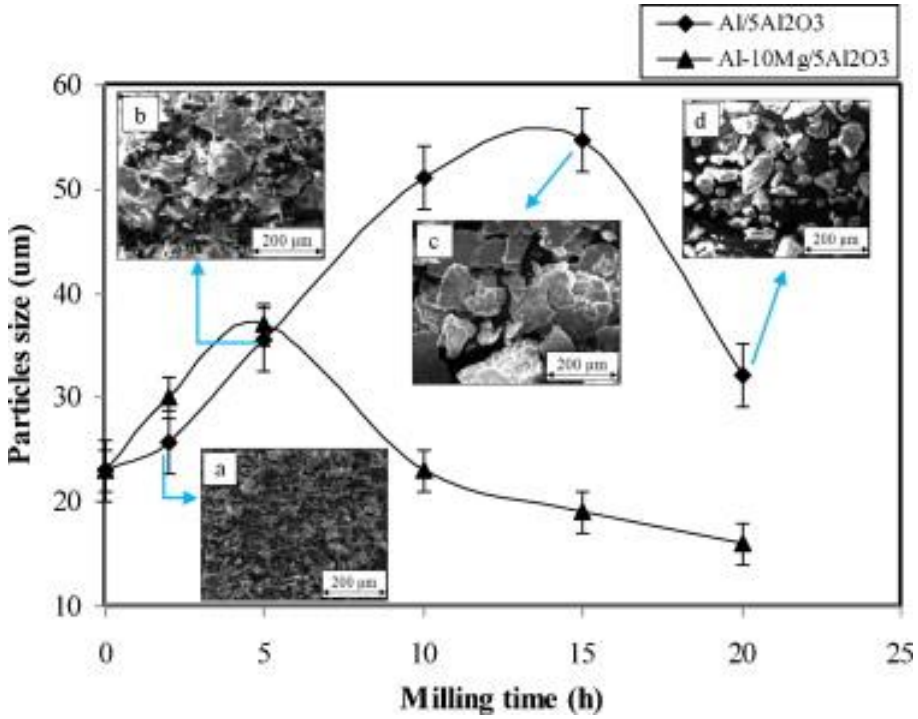

Figure 2.6: Variation of particles size as a function of milling time for Al/5wt.%Al_2O_3 and Al–10Mg/5Al_2O_3 powder mixture [44].

Mechanical alloying is a feasible method of adding alloying elements to improve both the mechanical and physical properties [28, 41] and distribution of

reinforcement within the matrix. But with increasing milling time beyond a certain point there is no significant effect on microstructure because mechanical alloying reaches a steady-state condition. This behaviour can be attributed to the cold welding of initial ductile particles followed by work hardening and thus the fracturing of powder particles. When the rate of the processes of cold welding and fracturing are equal, a steady state is achieved.

During milling, aluminium powder particles undergo cold working and the tendency for them to incorporate alumina nanoparticles decreases with increasing milling time [28, 45, 47]. Figure 2.7 shows a uniform distribution of Al_2O_3 particles in an Al matrix and an Al (Cu) solid solution matrix. The high energy milling process reduces the reinforcement size and tends to eliminate reinforcement defects and sharp edges, producing a rounder reinforcement morphology, which will result in better composite properties [41, 48, 49]. Increasing the volume fraction and/or decreasing the particle size of the reinforcement particles results in more frequent interactions between dislocations and the hard particles which accelerates the mechanical milling[45, 50]. An increasing amount of reinforcement in the matrix results in larger numbers of particles embedded within the metal matrix. Since a higher volume fraction of reinforcement causes a smaller interparticle spacing, matrix relaxation is more difficult, which increases the dislocation density because of strain accumulation. All these effects accelerate the milling action since the induced reinforcement will act as milling media during mechanical alloying.

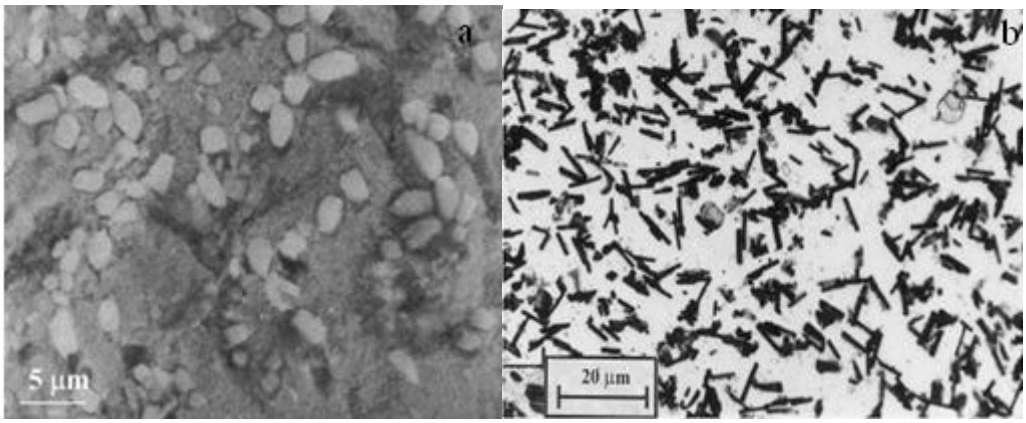

Figure 2.7: (a) SEM microstructure of Al–5%Al_2O_3 composite after 900 min milling[28] ,(b) Optical micrograph of the Al–4wt%Cu matrix composite reinforced with α-alumina platelets[51].

2.5 Consolidation of MMNC Powders

Thermomechanical powder consolidation (TPC) has been used widely to consolidate nanostructured powders and nanopowders to produce bulk nanostructured and ultrafine-structured metallic materials including metals, alloys, and metal matrix composites. Powder compact forging, powder compact extrusion, equal channel angular pressing/extrusion, hot pressing/sinter forging are among the common techniques for TPC [52-59]. Severe plastic deformation (SPD) of a bulk solid or consolidation of mechanically milled nanostructured powders are two widely used techniques for synthesizing bulk nanostructured or ultra-fine grained (UFG) Al alloys. These methods achieve fully dense bulk materials and are capable of making near net shaped parts for technological applications [53, 54, 60]. Thermomechanical powder consolidation requires the application of both heat and pressure and the consolidation of milled powders into fully dense and fully bonded compacts while preserving manometer scale grain sizes is not easy to achieve [56, 61-65]. Adherence to clean powder handling and optimised powder compaction conditions play a major role in achieving effective interparticle bonding and high density. Severe plastic deformation (SPD) is one of the effective methods for making materials with nanometre or submicrometer sized grains. Al, Cu nanocomposites and SiO_2, SiC and Al_2O_3 nanopowders are examples of

materials produced using this technique [60, 64]. The challenges are due to the fact that nanocrystalline materials are thermally unstable and grain growth occurs during high temperature consolidation [62, 64, 66, 67].

Ball milled powders are also more difficult to consolidate, since they possess higher hardness and yield strength than powders in the unmilled state due to dispersions of hard particles, grain boundary strengthening and work hardening of the powder particles. High temperatures are required for good consolidation of powders into bulk materials in order to remove all the porosity and to obtain good interparticle bonding, which makes retention of a nanocrystalline structure in the consolidated material a serious challenge. Knowing the applied pressure and the temperature required to achieve good consolidation helps to control the recrystallization and grain growth during the TPC process.

Another drawback is that layers of oxide/hydroxide, about 5nm in thickness cover the mechanically alloyed Al powder surfaces. These layers have to be broken and disturbed because they act as a barrier to sintering and prevent the formation of necks between metal particles. There will be some rupturing of the oxide film during pressing creating metal-metal contacts between particles. Al powders produced by mechanical alloying (MA) have reduced plasticity, and hence they are typically consolidated by hot deformation such as forging or extrusion [55, 68]. Hot deformation processes are used to consolidate mechanically alloyed powders to achieve full density. Grain growth has to be minimized so the matrix and reinforcement remain nanocrystalline with a mean crystallite size of less than 100 nm [61, 62, 67, 69]. Cold isostatic pressing (CIP) and cold pressing consolidation take longer, but there is no significant grain growth during consolidation [54, 56, 70, 71], it is well known that high pressure reduces diffussion rate but increases nucleation sites. The nucleation rate increases but grain growth decreases with

increasing pressure. On the other hand, using hot isostatic pressing (HIP), which requires shorter times for powder consolidation, there is more opportunity for grain growth with the grain size reaching 500nm [59, 66, 72, 73]. By controlling the HIP conditions especially the HIP temperature, grain sizes in the range of 200-500 nm have been obtained during consolidation of a silicon nitride based nanocomposite [74], an Al_2O_3/SiC nanocomposite [75], TiAl and Ti_3Al [76] powders produced by MA.

The consolidated composite powders have a more homogeneous distribution of reinforcements compared with those mixed by conventional methods. Secondary manufacturing processes such as extrusion, rolling and forging have important roles in the P/M fabrication of MMCs. These processes are combined with cold or hot compaction in the consolidation of the composite powders. The combinations have many advantages such as (1) a breakup of agglomerating reinforcements, (2) a more homogeneous distribution of reinforcements in the matrix, (3) an improvement of the mechanical properties and microstructures, (4) high productivity and lower costs [77].

2.5.1 Powder Compact Forging

Powder compact forging is an important thermomechanical processing technique for improving the quality of composites because low strain rates and high temperatures are adopted during the process [78, 79]. Previous studies have reported that the tendency for composite damage during plastic deformation, in terms of particle fracture, interfacial decohesion or growth of pre-existing voids, decreases using strain rates lower than 0.1 s^{-1} and temperatures near to 500 °C, because the stresses within the particles are reduced[80, 81]. An advantage of forging from powder compared with conventional casting and forging is lower cost and dimensional and weight control [82, 83]. Powder forged parts can

outperform parts machined from a forged blank, probably as a consequence of being fully dense, and with a very fine, uniform grained microstructure [84].

A schematic of the powder compact forging process is shown in Figure 2.8 [85] where h_f is the height of a work piece after deformation, D_{TC} is the top contact diameter, D_{BC} is the bottom contact diameter and D_B is the bulged diameter. Aluminium based particulate reinforced MMCs have limitations because of their low forgability resulting from defect regions. A geometrical defect *(i.e.*, variation in cross-sectional area) that can concentrate stresses and strain and accelerate local deformation was assumed to represent all possible defects. Thus, in effect, the local stress concentrations around nondeformable particles, a non-uniform distribution of particles and grain sizes, porosity and cracked particles, were assumed to be simulated adequately by such a defect factor (geometrical defect)[55, 79, 86].

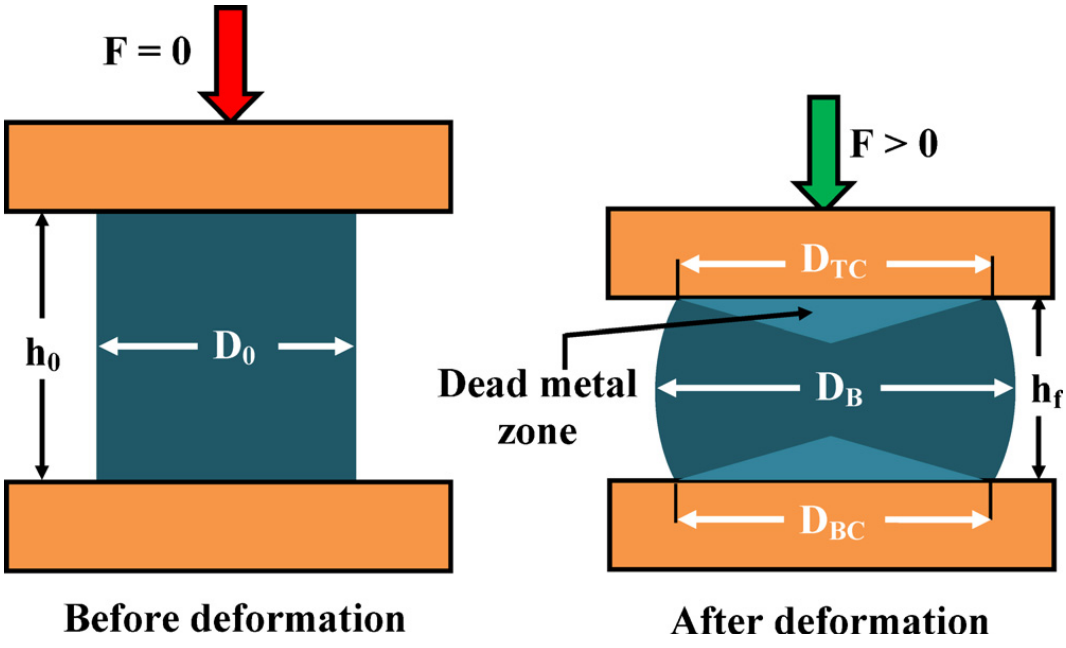

Figure 2.8: The upset forging test – before and after deformation [85].

2.5.2 Powder Compact Extrusion

Powder compact extrusion has two main advantages over other manufacturing processes. These are the ability to create very complex cross-sections and to work materials that are brittle, because the material only encounters compressive and

shear stresses. It also forms finished parts with an excellent surface finish. Extrusion can substantially decrease the number of pores and improve the density and more importantly, increase the interfacial bonding strength between second phase particles and matrix. All of the above mentioned factors can lead to increased yield and tensile strengths of a composite after extrusion [77, 87]. Key extrusion parameters are [88]: (i) the extrusion temperature. Extruding a composite material at a relatively high temperature imposes a non-uniform distribution of reinforcing, but severe particle breakage occurs during extrusion of a composite at lower temperatures [89]. As expected, the extrusion process breaks the reinforcing hard particles and thereby a uniform distribution of the particles in the matrix becomes evident [90] (ii) the extrusion rate, and (iii) the extrusion ratio. A further rise of this ratio leads to deterioration of local interfacial cohesion between the ceramic phase and the matrix leading to a deterioration in tensile properties, especially when there is a high volume fraction of crystals and intermetallic dispersiods [91]. In contrary, it is reported that by increasing the extrusion ratio, the ultimate tensile strength (UTS) and elongation values of the composite are also increased [90]. Nanometre and submicrometer sizes were achieved in consolidating $Nd_2Fe_{14}B/\alpha$-Fe nanocomposite powder at 1200K with an extrusion ratio of 5.54:1 [92], Al-5vol.%Al_2O_3 nanocomposite powder at 737K with an extrusion ratio of 16:1 [93, 94], AZ91- 1vol.% SiC composite powder at 623K with an extrusion ratio of 12:1 [95], and W–40wt% Cu composite powder at a temperature in the range of 1273-1373K with an extrusion ratio of 64 [96]. It is very important to control the extrusion ratio in the powder compact extrusion process to obtain a high density material with good mechanical properties.

Figure 2.9 shows the powder compact extrusion process. If sufficient diffusion and bonding occur at the extrusion temperature then good grain boundary

strengthening will be achieved. Powder compact extrusion has been used to consolidate metal nanopowders and nanostructured powders to obtain bulk materials with a fine grain structure [59, 93, 97].

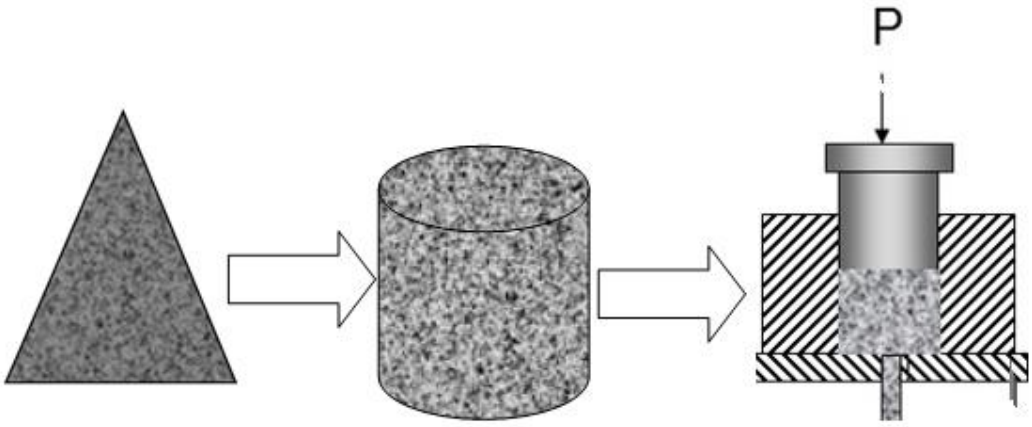

Figure 2.9: The extrusion process from loose powders to final product.

2.6 Mechanical Properties

Metal matrix composites (MMCs) are advanced materials with highly desirable property combinations, well suited to numerous aerospace and automotive applications such as aircraft structural parts, cylinders, and pistons. Some of these property combinations are high strength to density, high stiffness to density ratio. The grain size, reinforcement size, matrix/particle interface bonding, dislocations, all affect the mechanical properties of metallic materials [26, 98-101].

The mechanical properties of MMCs depend on their microstructure, reinforcement content, and homogeneity. Several studies have shown that the strength of MMC`s follows the Hall-Pitch relationship [102-105]. Traditional modelling of grain size effects on strength/hardness, using the Hall–Pitch (H–P) equation ($\sigma = \sigma_0 + kd^{-1/2}$ or $H = H_0 + Kd^{-1/2}$) does indeed predict increasing strength/hardness accompanying grain refinement [97, 106, 107]. With decreasing grain size and a more uniform distribution of the reinforcement particles within the matrix, the strength of the MMCs increases. The grain refinement was caused by the severe plastic deformation affecting the elemental powders and the refining

effect of adding the hard reinforcing particles to the Al powders. This is in agreement with Hesabi et.al [45] who reported that the crystallite size of the Al powder decreased with the addition of ceramic particles especially in the case of nanoscaled alumina.

The tensile and yield strength of Al-(1-20)vol.%Al_2O_3 composites from different studies were reported to be in the range of 80-400 MPa and 100-350 MPa, respectively [93, 97, 98, 108, 109].The tensile and yield strength of Al-Cu- (6.5-22)vol.% SiC composites were reported in different studies to be in the range of 120-600 MPa and 60-220 MPa, respectively [46, 100, 102, 110].

The reasons for the broad range of mechanical properties are related to the difference in the composites preparation methods. For example Kang et al [97] employed wet mixing, cold isotropic pressing (CIP) and sintering. The aluminium powder was mixed with different volume fractions (1–7 vol.%) of Al_2O_3 powder in a pure ethanol slurry. Mixed powders were dried at 150 °C and then compacted by CIP. All compacted billets were sintered in vacuum at 620 °C for 2 h. Finally, the sintered compacts were extruded at 420 °C with a reduction ratio of approximately 36:1, to form bars of 15 mm in diameter. All specimens were subjected to an anneal heat treatment at 350 °C for 2 h. On the other hand, Hesabi et al [93] synthesised the aluminium mixture, containing nanometric alumina with an average particle size of 35 nm, by mechanical milling followed by a severe plastic deformation process using hot powder extrusion. Wang et al [102] produced Al–Cu powder using inert gas atomization (Figure 2.10). The volume fraction of SiC particles in the composites is 20%. The SiC reinforcements are in particulate form with an average diameter of about 4.7 μm and 77 μm, respectively. Al–Cu and SiC powders were ball-mixed for 2 h, 7 h, 16 h and 40 h using a V-shaped powder rotator mixer with the rotation speed of about 35 r min^{-1}.

The mixed powders were die-pressed at room temperature under a pressure of 200 MPa in a cylindrical steel die with the diameter of 44 mm. The specimens were then heated in a vacuum furnace (pressure of 7×10^{-3} Pa) to 420 °C with a heating rate of 10 °C per minute. At 420 °C, the specimens were sintered for 1 h. Then the specimens were heated to 570 °C with a heating rate of 10 °C per minute. At 570 °C, the specimens were further sintered for 5 h. After sintering, the specimens were hot extruded to rods (with a diameter of ~14.7 mm) at 430 °C with an extrusion ratio of 9:1.

Hardness is a simple and non-destructive mechanical test for assessing yield strength and how the material will behave in wear testing [37, 111-114]. With increasing volume fraction of reinforcement within the matrix, the hardness continues to increase until a certain volume fraction is reached and beyond this the hardness will start to decrease due to clustering of reinforcement particles. Gupta et al [114] revealed the existence of a linear relationship between microhardness and tensile strength when silicon carbide particulate (SiCp) reinforced aluminium alloy-based composites were synthesized using the technique of disintegrated melt deposition (DMD). Narayanasamy et. al [84] reported that with increasing amounts of SiC in the composites, the SiC particles impeded the motion of dislocations and hence the stress required for further plastic deformation increased. It was found that the hardness and tensile strength of an aluminium matrix composite reinforced with nanometric alumina particles (50 nm) increased with increasing volume fraction of reinforcement, as shown in Table 2.2 below [97]. It was also reported that by reducing the Al_2O_3 particle size from 400 to 4 nm the nanocomposite powder particle hardness increased by 11%, this trend is probably due to the difference in Al grain sizes for the different Al_2O_3 sizes [40]. Contrary to this, other workers found that small volume

fractions of SiC are more effective at increasing the strength of nanocomposite SiC than larger ones. At higher SiC content (>2 vol.%) the strength and ductility of a nanocomposite were found to decrease to the detriment of the nanocomposite. Particle clustering was considered to be the main cause of this decrease [115], because as the concentration of SiC in the matrix increases, damage accumulates leading to increased porosity, thus weakening the nanocomposite. This can be explained by, enhanced void formation between neighbouring particles which can effectively increase the porosity of a fairly dense material. The presence of microspores between adhering particles and the SiC concentration increases damage accumulations

Grain refinement of the matrix and a more uniform distribution of reinforcement within the matrix will improve the ductility of the composite [78, 116]. It was reported by Koch that most nanostructured materials with grain sizes in the range of 20- 30 nm are "brittle" in tension (<5% elongation).Three major limitations to ductility for nano-composite materials can be identified. These are: (1) artifacts from processing (Pores); (2) force instability in tension; (3) crack nucleation or propagation instability. A major difficulty in the study of the mechanical properties of nanostructured materials has been the problem of processing nanostructured samples with well characterized microstructures and free from the artifacts that can mask the inherent mechanical properties [117, 118].

Jorge et.al [119] showed that the ductility of bulk material consolidated from powders is extremely dependant on the densification of the powder compacts and on the bonding level between powder particles. It is believed that good properties can only be obtained for the consolidated nanostructured aluminium powder when the extrusion temperature is around 400°C. That’s because, the ductility of the consolidated material increases significantly within the range of 375 °C to

400 °C.A slight decrease in ductility with rising temperature was observed at higher temperatures (400 °C to 425 °C).

According to Koch et. al [118], there are two major sources of limited ductility of nanostructured materials: (a) artifacts present in the consolidated particulate samples, and (b) the degree of interparticle bonding and any embrittling phase at grain boundaries. These reduce the strength and ductility of materials [97].

Table 2.2: Grain sizes and hardness of composites [97]**.**

	Pure Al	**1vol.% Al_2O_3/ Al**	**2vol. % Al_2O_3 / Al**	**3vol. % Al_2O_3 / Al**	**4vol. % Al_2O_3/ Al**	**5vol. % Al_2O_3/ Al**	**6vol. % Al_2O_3/ Al**	**7vol.% Al_2O_3/ Al**	**10 vol. % SiC/Al**
Grain size (µm)	4.6	3	2.3	1.9	1.2	1.1	1.2	1.3	-
Hardness (HRF)	31.8	45.6	50.1	57.7	66.6	64.7	63.2	68.4	48.6
Tensile strength (MPa)	150	180	210	225	245	240	250	247	185

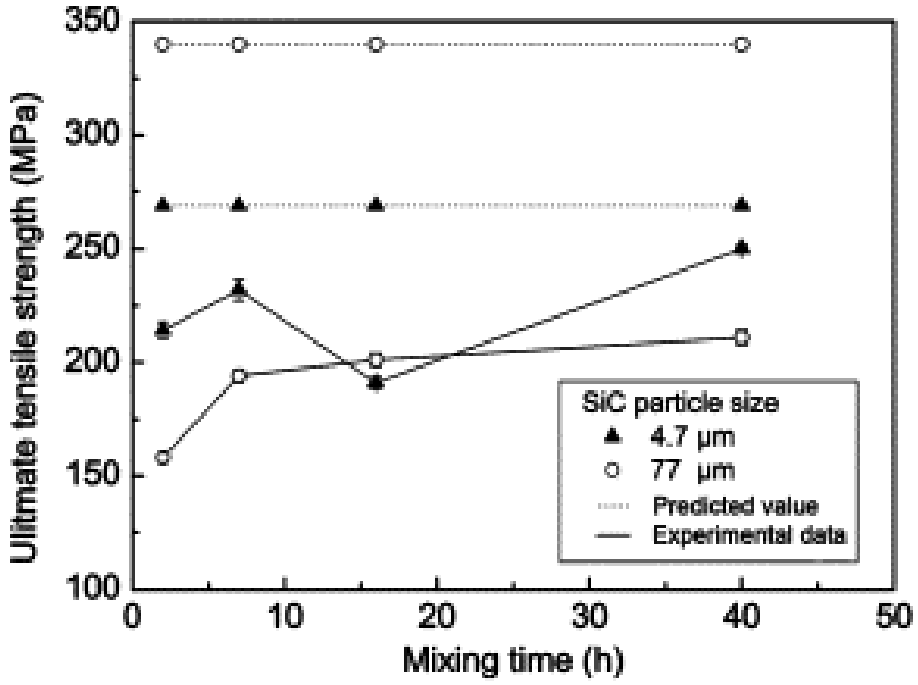

.

Figure 2.10: Ultimate tensile strength of the composites containing 20 vol.% SiC particles with different mixing time and different reinforcement particle sizes [102].

Fracture in nano-composites derives from propagation of nano and/or micro voids or cracks. It was reported in several places that for Al metal matrix composites

ductile fracture occurs in the inter-particle regions by grain boundary separation. Brittle fracture or cleavage across the reinforcement particles in the inner-particle regions [22, 46, 55, 120]. Park et al [120] reported that for Al-20vol.%Al_2O_3 metal matrix composites the proportion of particles (broken or debonded) present on the fracture surfaces increased with increasing particle volume fraction. Tjong et al. [121] reported that the fracture surface for Al based composites reinforced with in situ TiB_2 and Al_2O_3 submicron particles were characterized by typical tear ridges and shallow dimple morphologies with submicron ceramic particles remaining intact with the matrix. Also, fracture of reinforcing particles does not occur due to their small sizes. This is opposite to what was reported for a different composite by Badini et al. [81] in which voids nucleate in the matrix at SiC particles and at Al-Cu-Mg precipitates. The examined composite samples showed that SiC particles had fractured to different extents due to an increase in stress within the particles, as shown in Fig 2.11 below. For other SiC reinforced specimens a partially ductile fracture was observed and dimples could be observed with SiC embedded in them. No clean separation at the SiC/matrix interface can be observed, indicating good interfacial bonding [122].

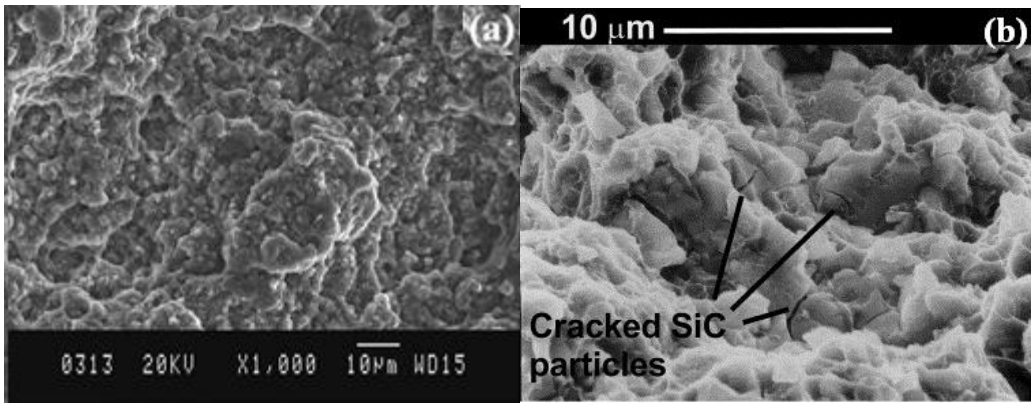

Figure 2.11: (a) SEM micrograph showing fractograph of TiO2–Al–B composite. Microcracks are initiated at brittle Al_3Ti blocks [121], and (b) Fracture surface of 2124/SiC_p specimen tensile tested at room temperature, showing particle fractures [81].

Fracture toughness is a property which describes the ability of a material containing a crack to resist fracture, and is one of the most important properties of any material for most structural applications. Facture toughness is a quantitative way of expressing a material's resistance to brittle fracture when a crack is present. It was found that the fracture toughness decreased progressively with particle volume fraction, but at a decreasing rate [120]. Which is attributed to growth of the microvoids nucleated at the fractured at the fractured particles becoming more limited as the interparticle spacing decreases.

2.7 Electrical and Thermal Properties

Electrical conductivity is a measure of a materials ability to conduct an electrical current. Copper is the standard by which electrical materials are rated and conductivity ratings are frequently expressed as a percentage of IACS which is the abbreviation for International Annealed Copper Standard. Pure copper is taken to be 100% IACS. The electrical conductivity of aluminium in general is 61 IACS. The electrical resistivity of MMCs increases with increasing volume fraction and decreasing size of non-conducting reinforcement particles [123-125]. Al–5 wt% Al_2O_3 composite materials produced by a combination of mechanical alloying and powder consolidation show that since the electrical resistivity of alumina is much higher than that of aluminium (2.7×10^{-6} Ω cm for aluminium vs 1×10^{14} Ω cm for alumina), the electrical conductivity of the composite is much lower than that for pure aluminium [108]. Figure 2.13 shows the resistivity of the Al_2O_3/aluminium alloy composite versus the aluminium content in the composite. The resistivity decreases dramatically from $6.41 * 10^{12}$ to $9.77 * 10^{-4}$, $7.28 * 10^{-4}$, and $6.24 * 10^{-4}$ Ω m with Al_2O_3/A356, Al_2O_3/6061 and Al_2O_3/1050 composites, respectively, by increasing the aluminium alloy content in the composites from 0 to 40 vol.% [126].

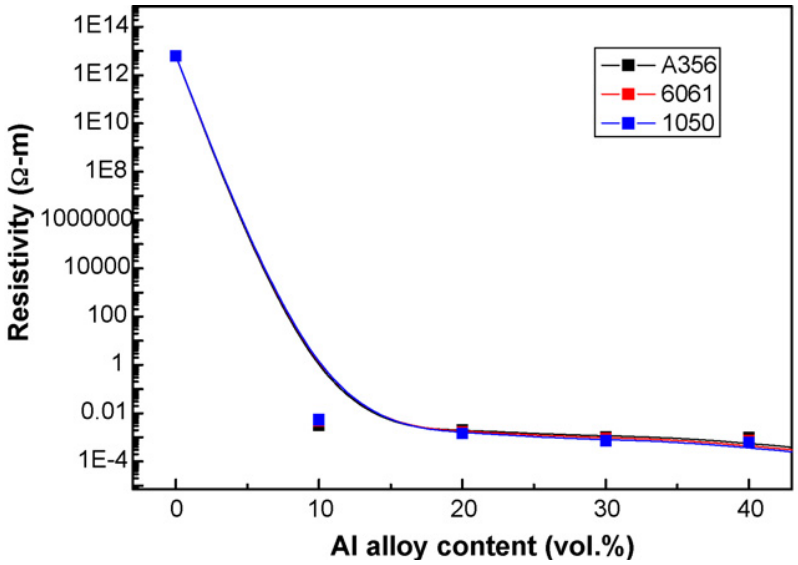

Figure 2.12: Resistivity versus aluminium alloy content in the Al_2O_3/ Al alloy composites [126] .

Metal matrix composites are especially attractive materials for applications where a maximum thermal conductivity (λ) with a minimum coefficient of thermal expansion (α) and a low density are needed. The influence of thermal stresses on composite behaviour is much larger in MMCs than PMCs for two main reasons: (a) the operating temperatures and fabrication for MMCs are much higher and (b) a much higher yield strength is needed in the metallic matrix for thermal stresses to relax by plastic yielding. Mechanical alloying is used to produce metal matrix ceramic nanocomposites (MMCNs) with fine grains, supersaturated solid solutions and fine thermally stable dispersiods. A homogeneous distribution of thermally stable second phase particles provides good elevated temperature properties in the composite and the thermal stability of a microstructure is important during the consolidation stage of nanostructured powder processing. Grain growth in nanocrystalline Al with an initial grain size of ~ 26 nm and produced by mechanical milling has been studied. Stabilization of nanograins with sizes around 50~60 nm at temperatures as high as 0.78 T_m was observed, where T_m is993.1 K. The high degree of grain size stability was considered to be due to the pinning forces arising from impurities as well as ultrafine dispersiods

formed during the milling process [127]. In another study on nanocrystalline Al, the critical temperature above which the grain size becomes unstable was defined to be equal to 0.8 T_m [128].

In MMCs the interface between the reinforcements and the matrix largely controls the properties of the composites and with increased interfacial area, which is the case with smaller reinforcement diameters, increased interactions result between the reinforcements and the matrix. This is because the thermal mismatch between the reinforcement phase and the matrix is only in thermal equilibrium at the temperature at which they are brought into contact during processing. When cooled from the processing temperature, the thermal stresses in the composite can be large enough to cause plastic deformation of the matrix, especially in the interface regions as a result of the differences in the coefficient of thermal expansion between the reinforcement and the matrix. This will lead to generation of various defects such as dislocations [3, 129].

Aluminium matrix composites reinforced with a mixture of diamond and SiC particles of equal size were produced by gas pressure assisted liquid metal infiltration. Replacing SiC gradually by diamond particles resulted in a steady increase of thermal conductivity from 220 to 580 W m^{-1} K^{-1} [130]. The thermal conductivity of an Al matrix composite with a high volume fraction of SiCp ((56–65 vol.%) and prepared by pressure infiltration was 248Wm^{-1} K^{-1}[131]. Tatar et.al [132] has found a linear relationship between the thermal conductivity of the composites and the volume fraction of alumina in the composites as follows:

K= -0.0261*V+2.67767,

Where K is thermal conductivity ($Wm^{-1}K^{-1}$) and the V is the volume fraction of alumina.

2.8 Summary

The main conclusions from the literature review are as follow:

- A mechanical alloying route has been reported to be a promising technique for producing ultra-fine grain and nanostructured metal matrix composites.
- The microstructure of metal matrix nanocomposites depends on the composition, processing temperature, and processing technique.
- High quality material with a homogeneous reinforcement distribution is very important for improving the mechanical properties.

For simple and economic production of aluminium-based nanocomposites, more research to investigate the advantages of powder compact forging and extrusion is required. In particular their efficiency at maintaining a nanostructure through controlled processing is important. Additionally the effect of process variables in achieving full density with a minimum of porosity and the effect on mechanical properties has received little attention and warrants further investigation.

2.9 References

[1] A. International, *ASM Handbook: Composites* vol. 21, 2001.

[2] Y.Zhu and H.A.Kishawy, "Influence of alumina particles on the mechanics of machining metal matrix composites," *International Journal of Machine Tools and Manufacture,* vol. 45, pp. 389-398, 2005.

[3] R. U. Vaidya and K. K. Chawla, "Thermal expansion of metal-matrix composites," *Composites Science and Technology,* vol. 50, pp. 13-22, // 1994.

[4] A. Varvani-Farahani, "Composite Materials: Characterization, Fabrication and Application-Research Challenges and Directions," *Applied Composite Materials,* vol. 17, pp. 63-67, 2010.

[5] I. Oguocha, "Characterization of Aluminium Alloy 2618 and Its Composites Containing Alumina Particles," Doctor of Philosophy (Ph.D.) Mechanical Engineering University of Saskatchewan, 1999.

[6] D. O. Defense, *Composite Materials Handbook* vol. MILHDBK 17-4, 1999.

[7] J.M.Wu and Z.Z.Li, "Nanostructured composite obtained by mechanicall driven reducton reaction of Cu and Al powder mixture," *Journal of Alloys and Compounds,* vol. 299, pp. 9-16, 2000.

[8] A.Santos-Beltran, V.Gallegos-Orozco, I.Estrada-Guel, L.Bejar-Gomez, F.Espinosa-Magana, M.Miki-Yoshida, and R.Martinez-Sanchez, "TEM characterization of Al-C-Cu-Al_2O_3 compsoites produced by mechanical milling," *Journal of Alloys and Compounds,* vol. 434-435, pp. 514-517, 2007.

[9] K. D. Woo and H. B. Lee, "Fabrication of Al alloy matrix composite reinforced with subsieve-sized Al_2O_3 particles by the in situ displacement reaction using high-enegy balkl-milled powder," *Materials Science and Engineering A,* vol. 449-451, pp. 829-832, 2007.

[10] L.Carroll, M.Sternitzke, and B.Derby, "Silicon carbide particle size effects in alumina-based nanocomposites," *Acta Materialia,* vol. 44, pp. 4543-4552, 1996.

[11] J. M. Wu and Z. Z. Li, "Nanostructured composite obtained by mechanically driven reduction reaction of CuO and Al powder mixture," *Journal of Alloys and Compounds,* vol. 299, pp. 9-16, 3/14/ 2000.

[12] T. W. Clyne and P. J. Withers, *An Introduction to Metal Matrix Composites*. Press Syindicate of the University of Cambridge: Cambridge University Press, 1995.

[13] N. Koichi, "New design concept of structural ceramics. Ceramic nanocomposites," *Journal of the Ceramic Society of Japan,* vol. 99, pp. 974-982, 1991.

[14] S.C.Tjong and H. Chen, "Nanocrystalline Materials and Coatings," *Materials Science and Engineering R,* vol. 45, pp. 1-88, 2004.

[15] K. S. Kumar, H. V. Swygenhoven, and S. Suresh, "Mechanical behavior of nanocrystalline metals and alloys," *Acta Materialia,* vol. 51, pp. 5743-5774, 2003.

[16] N.Lane, "The grand challanges of nanotechnology," *Journal of Nanoparticles Research,* vol. 3, pp. 95-103, 2001.

[17] X. Luo, "Processing of Al-Al2O3 Metal Matrix Composites Using aPowder Metallurgy Approach " Master of Science(Technology), Materials and Process Engineering, University of Waikato, Hamilton, 2001.

[18] T. P. D. RAJAN, R. M. PILLAI, and B. C. PAI, "Review Reinforcement coatings and interfaces in aluminium metal matrix composites," *JOURNAL OF MATERIALS SCIENCE,* vol. 33, pp. 3491-3503, 1998.

[19] J. U. Ejiofor and R. G. Reddy, "Effects of porous carbon on sintered Al-Si-Mg matrix composites," *Journal of Materials Engineering and Performance* vol. 6, pp. 785-791 1997.

[20] I. A. Ibrahim, F. A. Mohamed, and E. J. Lavernia, "Particulate reinforced metal matrix composites — a review," *Journal of Materials Science* vol. 26, pp. 1137-1156, 1991.

[21] S. Kleiner, F. Bertocco, F. A.Khalid, and O. Beffort, "Reactivley Synthesized Nanostructured PM Aluminium Composite-Microstructure stability and elevated Temperature Hardness Response," *Advanced Engineering Materials,* vol. 7, pp. 380-383, 2005.

[22] S. C. Tjong, "Novel Nanoparticle-reinforced Metal Matrix Composites with Enhanced Mechanical properties," *Advanced Engineering Materials,* vol. 9, pp. 639–652, 2007.

[23] A. Mukhtar, "MicroStructure, Thermal Stability and Consolidation of Nanostructured and Ultrafine Structured Cu based Metal Matrix Composite and Alloy powders Produced by High Energy Mechanical Milling," Doctor of Philosophy, Materials and Process Engineering, University of Waikato, Hamilton, 2010.

[24] V. Rajkovic, D. Bozic, and M. T. Jovanovic, "Properties of copper matrix reinforced with nano- and micro-sized Al2O3 particles," *Journal of Alloys and Compounds,* vol. 459, pp. 177-184, 2008.

[25] Z. Y. Ma, S. C. Tjong, Y. L. Li, and Y. Liang, "High temperature creep behavior of nanometric Si3N4 particulate reinforced aluminium

composite," *Materials Science and Engineering: A,* vol. 225, pp. 125-134, 1997.

[26] H.Arami and A.Simchi, "Reactive milling synthesis of nanocrystalline Al-Cu/Al_2O_3 nancomposite," *Materials Science and Engineering A,* vol. 464, pp. 225-232, 2007.

[27] R.Ismail and I.I.Yaacob, "The formation of aluminides in intermetallic nickel aluminide-based nanocomposites," *Journal of Alloys and Compounds,* vol. 392, pp. 214-219, 2005.

[28] S.M.Zebarjad and S.A.Sajjadi, "Microstructure evaluation of Al-Al_2O_3 composites produced by mechanical alloying method," *Materials and Design,* vol. 27, pp. 684-688, 2006.

[29] T. E. P. M. Association. (2002). *Spray Deposition - A Metal Forming Process.* Retrieved

[30] S. Zhang, Y. Chen, and Q. Li, "Research on microstructure and properties of aluminum-matrix composite fabricated by spray deposition," *Journal of Materials Processing Technology,* vol. 137, pp. 168-172, 2003.

[31] H. Zhang, Y. He, and L. Li, "Tensile deformation and fracture behavior of spray-deposition 7075/15SiCp aluminum matrix composite sheet at elevated temperatures," *Materials Characterization,* vol. 59, pp. 1078-1082, 2008.

[32] A. Papworth and P. Fox, "Oxide film casting defects in squeeze cast metal matrix composites," *Materials Letters,* vol. 29, pp. 209-213, 1996.

[33] K. Sukumaran, K. K. Ravikumar, S. G. K. Pillai, T. P. D. Rajan, M. Ravi, R. M. Pillai, and B. C. Pai, "Studies on squeeze casting of Al 2124 alloy and 2124-10% SiCp metal matrix composite," *Materials Science and Engineering: A,* vol. 490, pp. 235-241, 2008.

[34] A. M. Handbook, *Casting* vol. 15: ASM Handbook Committee, 1992.

[35] X. N. Zhang, L. Geng, and G. S. Wang, "Fabrication of Al-based hybrid composites reinforced with SiC whiskers and SiC nanoparticles by squeeze casting," *Journal of Materials Processing Technology,* vol. 176, pp. 146-151, 2006.

[36] M. S. El-Eskandarany, *Mechanical Alloying For Fabrication of Advanced Engineering Materials*. United states of America: Noyse publication/ William Andrew Oublishing, 2001.

[37] V. Rajkovic, D. Bozic, and M. T.Jovanovic, "Effects of copper and Al_2O_3 particles on characteristics of Cu-Al_2O_3 composites," *Materials and Design,* vol. 31, pp. 1962-1970, 2010.

[38] S. Tahamtan, A. Halvaee, M. Emamy, and M. S. Zabihi, "Fabrication of Al/A206–Al2O3 nano/micro composite by combining ball milling and stir casting technology," *Materials & Design,* vol. 49, pp. 347-359, 2013.

[39] I. Mobasherpour, A. A. Tofigh, and M. Ebrahimi, "Effect of nano-size Al2O3 reinforcement on the mechanical behavior of synthesis 7075 aluminum alloy composites by mechanical alloying," *Materials Chemistry and Physics,* vol. 138, pp. 535-541, 2013.

[40] D. Poirier, R. A. L. Drew, M. L. Trudeau, and R. Gauvin, "Fabrication and properties of mechanically milled alumina/aluminum nanocomposites," *Materials Science and Engineering: A,* vol. 527, pp. 7605-7614, 2010.

[41] J. B. Fogagnolo, F. Velasco, M. H. Robert, and J. M. Torralba, "Effect of mechanical alloying on the morphology, microstructure and properties of aluminium matrix composite powders," *Materials Science and Engineering A,* vol. 342, pp. 131-143, 2003.

[42] C.C.Koch, "Processing-Structure-Property Relationships in Ultrafine Grain and Nanocrystalline Materials," in *The 13th International Conference on Rapidly Quenched and Metastable Materials*, Dresden, Germany 2008.

[43] F. Shehata, A. Fathy, M. Abdelhameed, and S. F. Moustafa, "Preparation and properties of Al2O3 nanoparticle reinforced copper matrix composites by in situ processing," *Materials and Design,* vol. 30, pp. 2756-2762, 2009.

[44] J. Safari, G. H. Akbari, A. Shahbazkhan, and M. Delshad Chermahini, "Microstructural and mechanical properties of Al-Mg/Al2O3 nanocomposite prepared by mechanical alloying," *Journal of Alloys and Compounds,* vol. 509, pp. 9419-9424, 2011.

[45] Z. r. Hesabi, A.Simchi, and S. M. S. Reihani, "Structural evolution during mechanical milling of nanometric and micrometric Al_2O_3 reinforced Al matrix composites," *Materials Science and Engineering A,* vol. 428, pp. 159-168, 2006.

[46] F. Tang, M. Hagiwara, and J. M. Schoenung, "Microstructure and tensile properties of bulk nanostructured Al-5083/SiCp composites prepared by cryomilling," *Materials Science and Engineering: A,* vol. 407, pp. 306-314, 2005.

[47] B.Prabhu, C.Suryanarayana, L.An, and R.Vaidyanathan, "Synthesis and characterization of high volume fraction Al-Al_2O_3 nanocomposite powders by high-energy milling " *Materials Science and Engineering A,* vol. 425, pp. 192-200, 2006.

[48] J.Y.Huang, Y.K.Wu, and H.Q.Ye, "Ball milling of ductile metals," *Materials Science and Engineering A,* vol. 199, pp. 165-172, 1995.

[49] Z. Razavi Hesabi, H. R. Hafizpour, and A. Simchi, "An investigation on the compressibility of aluminum/nano-alumina composite powder prepared by blending and mechanical milling," *Materials Science and Engineering: A,* vol. 454-455, pp. 89-98, 2007.

[50] I. Ozdemir, S. Ahrens, S. Mucklich, and B. Wielage, "Nanocrystalline Al-Al_2O_3 and SiC_p composites produced by high-energy ball milling," *Journal of Materials Processing Technology,* vol. 205, pp. 111-118, 2008.

[51] V. Massardier, L. Pelletier, and P. Merle, "Influence of the introduction of ceramic particles in Al-Cu alloys on GP zone formation," *Materials Science and Engineering: A,* vol. 249, pp. 121-133, 1998.

[52] A.Mukhtar, D.L.Zhang, C.Kong, and P.Munroe, "Consolidation of ultrafine-grained Cu powder and nanostructured Cu-(2.5-10) vol%Al_2O_3 composite powders by powder compact forging," *Journal of Materials Science,* vol. 45, pp. 4594-4605, 2010.

[53] B. Q.Han and E. J.Lavernia, "Deformation Mechanisms of Nanostructured Al Alloys," *Advanced engineering materials,* vol. 7, pp. 457-465, 2005.

[54] D. Canadinc, H. J. Maier, M. Haouaoui, and I. Karaman, "On the cyclic stability of nanocrystalline copper obtained by powder consolidation at room temperature," *Scripta Materialia,* vol. 58, pp. 307-310, 2008.

[55] F. Tang, H. Meeks, J. E. Spowart, T. Gnaeupel-Herold, H. Prask, and I. E. Anderson, "Consolidation effects on tensile properties of an elemental Al matrix composite," *Materials Science and Engineering: A,* vol. 386, pp. 194-204, 2004.

[56] K. I. Moon, H. S. Hong, K. T. Hong, K. S. Lee, and S. J. Kim, "Consolidation behavior of L12 phase (Al + 12.5 at.% Cu)3Zr powder with nanocrystalline structure during CIP and subsequent sintering," *Materials Science and Engineering: A,* vol. 380, pp. 46-51, 2004.

[57] R. Narayanasamy, T. Ramesh, and K. S. Pandey, "Some aspects on cold forging of aluminium-alumina powder metallurgy composite under triaxial stress state condition," *Materials & Design,* vol. 29, pp. 1212-1227, 2008.

[58] Y. V. R. K. Prasad, K. P. Rao, and M. Gupta, "Hot workability and deformation mechanisms in Mg/nanoAl2O3 composite," *Composites Science and Technology,* vol. 69, pp. 1070-1076, 2009.

[59] O. N. Senkov, S. V. Senkova, J. M. Scott, and D. B. Miracle, "Compaction of amorphous aluminum alloy powder by direct extrusion and equal channel angular extrusion," *Materials Science and Engineering: A,* vol. 393, pp. 12-21, 2005.

[60] A. L. Ortiz and L. Shaw, "X-ray diffraction analysis of a severely plastically deformed aluminum alloy," *Acta Materialia,* vol. 52, pp. 2185-2197, 2004.

[61] M. Krasnowski, A. Antolak, and T. Kulik, "Nanocrystalline Ni3Al alloy produced by mechanical alloying of nickel aluminides and hot-pressing consolidation," *Journal of Alloys and Compounds,* vol. 434-435, pp. 344-347, 2007.

[62] M. Krasnowski and T. Kulik, "Nanocrystalline FeAl matrix composites reinforced with TiC obtained by hot-pressing consolidation of mechanically alloyed powders," *Intermetallics,* vol. 15, pp. 1377-1383, 2007.

[63] B. H. Kear, J. Colaizzi, W. E. Mayo, and S. C. Liao, "On the processing of nanocrystalline and nanocomposite ceramics," *Scripta Materialia,* vol. 44, pp. 2065-2068, 2001.

[64] I. V. Alexandrov, Y. T. Zhu, T. C. Lowe, R. K. Islamgaliev, and R. Z. Valiev, "Consolidation of nanometer sized powders using severe plastic torsional straining," *Nanostructured Materials,* vol. 10, pp. 45-54, 1998.

[65] D.L.Zhang, "Processing of advanced materials using high-energy mechanical milling," *Progress in Materials Science,* vol. 49, pp. 537-560, 2004.

[66] K. I. Moon, H. S. Park, and K. S. Lee, "Consolidation of nanocrystalline Al-5 at.% Ti alloy powders by ultra high-pressure hot pressing," *Materials Science and Engineering: A,* vol. 323, pp. 293-300, 2002.

[67] M. Jafari, M. H. Abbasi, M. H. Enayati, and F. Karimzadeh, "Mechanical properties of nanostructured Al2024-MWCNT composite prepared by optimized mechanical milling and hot pressing methods," *Advanced Powder Technology,* 2011.

[68] J.Cintas, J.M.Montes, F.G.Cuevas, and E.J.Herrera, "Influence of milling media on the microstructure and mechanical milled and sintered aluminium " *Journal of Materials Science,* vol. 40, pp. 3911-3915, 2005.

[69] J. H. Choi, K. I. Moon, J. K. Kim, Y. M. Oh, J. H. Suh, and S. J. Kim, "Consolidation behavior of nanocrystalline Al-5at.%Ti alloys synthesized by cryogenic milling," *Journal of Alloys and Compounds,* vol. 315, pp. 178-186, 2001.

[70] M. Azabou, M. Khitouni, and A. Kolsi, "Characterization of nanocrystalline Al-based alloy produced by mechanical milling followed by cold-pressing consolidation," *Materials Characterization,* vol. 60, pp. 499-505, 2009.

[71] S. Sharafi and S. Gomari, "Effects of milling and subsequent consolidation treatment on the microstructural properties and hardness of the

nanocrystalline chromium carbide powders," *International Journal of Refractory Metals and Hard Materials,* vol. 30, pp. 57-63, 2012.

[72] A. Kaiser, R. Vassen, D. Stöver, and H. P. Buchkremer, "Heat treatment of ultrafine SiC powders to reduce oxidation sensitivity and grain growth," *Nanostructured Materials,* vol. 4, pp. 795-802, 1994.

[73] Y.-K. Jeong and K. Niihara, "Microstructure and properties of alumina-silicon carbide nanocomposites fabricated by pressureless sintering and post hot-isostatic pressing," *Transactions of Nonferrous Metals Society of China,* vol. 21, Supplement 1, pp. s1-s6, 2011.

[74] O. Tapasztóa, P. Kuna, F. Wébera, G. Gergelya, K. Balázsia, J. Pfeifera, P. Aratóa, A. Kidarib, S. Hampshireb, and C. Balázsia, "Silicon nitride based nanocomposites produced by two different sintering methods," *Ceramics International,* vol. 37, pp. 3457-3461, 2011.

[75] C. E. Borsa, H. S. Ferreira, and R. H. G. A. Kiminami, "Liquid phase sintering of Al2O3/SiC nanocomposites," *Journal of the European Ceramic Society,* vol. 19, pp. 615-621, 1999.

[76] C. Suryanarayana, G. E. Korth, G. H. Chen, A. Frefer, and F. H. Froes, "Thermal stability of nanostructured titanium aluminides," *Nanostructured Materials,* vol. 2, pp. 527-535, 1993.

[77] K.Hanadaa, Y.Murakoshib, H.Negishia, and T.Sanob, "Microstructures and Mechanical Properties of Al-Li/SiCp Composite Produced by Extrusion Processing," *Journal ofMaterials Processing Technology,* vol. 63, pp. 405-410, 1997.

[78] L. Ceschini, G. Minak, and A. Morri, "Forging of the AA2618/20 vol.% Al2O3p composite: Effects on microstructure and tensile properties," *Composites Science and Technology,* vol. 69, pp. 1783-1789, 2009.

[79] K. S. See and T. A. Dean, "The effects of the disposition of SiC particles on the forgeability and mechanical properties of co-sprayed aluminium-based MMCs," *Journal of Materials Processing Technology,* vol. 69, pp. 58-67, 1997.

[80] P. Cavaliere, "Isothermal forging of AA2618 reinforced with 20% of alumina particles," *Composites Part A: Applied Science and Manufacturing,* vol. 35, pp. 619-629, 2004.

[81] C. Badini, G. M. La Vecchia, P. Fino, and T. Valente, "Forging of 2124/SiCp composite: preliminary studies of the effects on microstructure and strength," *Journal of Materials Processing Technology,* vol. 116, pp. 289-297, 2001.

[82] J.-O. Park, K.-J. Kim, D.-Y. Kang, Y.-s. Lee, and Y.-H. Kim, "An experimental study on the optimization of powder forging process parameters for an

aluminum-alloy piston," *Journal of Materials Processing Technology,* vol. 113, pp. 486-492, 2001.

[83] J.-B. Yang, C.-C. Wang, and W.-S. Lin, "Study of the powder forging process on an Aluminium alloy," *Advances in Powder Metallurgy:proceedings of the powder metallurgy conference and exhibition,* vol. 6, pp. 237-249, 1991.

[84] R.Narayanasamy, T.Ramesh, and m.Prabhakar, "Effects of particle size of SiC in aluminium matrix on workability and strain hardening behaviour of P/M composite," *Materials Science and Engineering A,* vol. 504, pp. 13-23, 2009.

[85] S. Sivasankaran, K. Sivaprasad, and R. Narayanasamy, "Microstructure, cold workability and strain hardening behavior of trimodaled AA 6061â€“TiO2 nanocomposite prepared by mechanical alloying," *Materials Science and Engineering: A,* vol. 528, pp. 6776-6787, 2011.

[86] D.G.C.SYU and A.K.Ghosh, "Forging limits for an aluminium matrix composite:Part II.Analysis," *Metallurgical and Materials Transactions A,* vol. 25A, p. 2039, 1994.

[87] Z. Wang, M. Song, C. Sun, D. Xiao, and Y. He, "Effect of extrusion and particle volume fraction on the mechanical properties of SiC reinforced Al–Cu alloy composites," *Materials Science and Engineering: A,* vol. 527, pp. 6537-6542, 2010.

[88] B. F. Luan, N. Hansen, A. Godfrey, G. H. Wud, and Q. Liu, "High strength Al–Al2O3p composites: Optimization of extrusion parameters," *Materials and Design,* vol. 32, pp. 3810–3817, 2011.

[89] R. R. Fard and F. Akhlaghi, "Effect of extrusion temperature on the microstructure and porosity of A356-SiCp composites," *Journal of Materials Processing Technology* vol. 187–188, pp. 433-436, 2007.

[90] K. Tavighi, M. Emamy, and A. R. Emami, "Effects of extrusion temperature on the microstructure and tensile properties of Al–16wt% Al4Sr metal matrix composite," *Materials & Design,* vol. 46, pp. 598-604, 2013.

[91] J. Zhou, A. T. Drużdżel, and J. Duszczyk, "The effect of extrusion parameters on the fretting wear resistance of Al-based composites produced via powder metallurgy," *Journal of Materials Science,* vol. 34, pp. 5089-5097, 1999.

[92] Y. Wang and E. Wang, "Research on preparing compact bulk nanocomposite Nd2Fe14B/Î±-Fe magnetic materials by hot extrusion," *Journal of Magnetism and Magnetic Materials,* vol. 312, pp. 220-223, 2007.

[93] Z. R. Hesabi, A.Simchi, S. M. S. Reihani, and F.Simanick, "Fabrication and characterization of ultrafinee-grained Al-5vol%Al_2O_3 nanocomposite," *international Journal of Nanomanufacturing,* vol. 5, p. 341, 2010.

[94] A. H. Monazzah, A.Simchi, and S. M. S. Reihani, "Creep behavior of hot extruded Al-Al_2O_3 nanocomposite powder," *Materials Science and Engineering A,* vol. 527, pp. 2567-2571, 2010.

[95] K. B. Nie, X. J. Wang, L. Xu, K. Wu, X. S. Hu, and M. Y. Zheng, "Effect of hot extrusion on microstructures and mechanical properties of SiC nanoparticles reinforced magnesium matrix composite," *Journal of Alloys and Compounds,* vol. 512, pp. 355-360, 2012.

[96] D. Li, Z. Liu, Y. Yu, and E. Wang, "The influence of mechanical milling on the properties of W–40 wt.%Cu composite produced by hot extrusion," *Journal of Alloys and Compounds,* vol. 462, pp. 94-98, 2008.

[97] Y.-C. Kang and S. L.-I. Chan, "Tensile properties of nanometric Al2O3 particulate-reinforced aluminum matrix composites," *Materials Chemistry and Physics,* vol. 85, pp. 438-443, 2004.

[98] E. Gariboldi and A. Lo Conte, "Damage mechanisms at room and high temperature in notched specimens of Al6061/Al2O3 particulate composites," *Composites Science and Technology,* vol. 68, pp. 260-267, 2008.

[99] I. C. Stone and P. Tsakiropoulos, "The effect of reinforcement on the notched and unnotched room temperature tensile properties of Al-4wt.%Cu/SiCp MMCs," *Materials Science and Engineering: A,* vol. 241, pp. 19-29, 1998.

[100] A. M. S. Hamouda and M. S. J. Hashmi, "Mechanical properties of aluminium metal matrix composites under impact loading," *Journal of Materials Processing Technology,* vol. 56, pp. 743-756, 1996.

[101] S. C, "Synthesis of nanocomposites by mechanical alloying," *Journal of Alloys and Compounds,* vol. 509, Supplement 1, pp. S229-S234, 2011.

[102] Z. Wang, M. Song, C. Sun, and Y. He, "Effects of particle size and distribution on the mechanical properties of SiC reinforced Al-Cu alloy composites," *Materials Science and Engineering: A,* vol. 528, pp. 1131-1137, 2011.

[103] S. Cheng, E. Ma, Y. M. Wang, L. J. Kecskes, K. M. Youssef, C. C. Koch, U. P. Trociewitz, and K. Han, "Tensile properties of in situ consolidated nanocrystalline Cu," *Acta Materialia,* vol. 53, pp. 1521-1533, 2005.

[104] J. Ye, B.Q.Han, and J.M.Schoenung, "Mechanical behaviour of an Al-matrix composite reinforced with nanocrystalline Al-coated B_4C particulates," *Philosophical Magazine Letters,* vol. 86, pp. 721-732, 2006.

[105] Y. Ji and J. A. Yeomans, "Processing and mechanical properties of Al2O3-5 vol.% Cr nanocomposites," *Journal of the European Ceramic Society,* vol. 22, pp. 1927-1936, 2002.

[106] M. Dollár and A. Dollár, "On the strength and ductility of nanocrystalline materials," *Journal of Materials Processing Technology,* vol. 157-158, pp. 491-495, 2004.

[107] R. W. Siegel and G. E. Fougere, "Mechanical properties of nanophase metals," *Nanostructured Materials,* vol. 6, pp. 205-216, 1995.

[108] S. M. Zebarjad and S. A. Sajjadi, "Dependency of physical and mechanical properties of mechanical alloyed Al-Al2O3 composite on milling time," *Materials & Design,* vol. 28, pp. 2113-2120, 2007.

[109] M.Kok, "Production and mechanical properties of Al2O3 particle-reinforced 2024 aluminium alloy composites," *Journal of Materials Processing Technology,* vol. 161, pp. 381-387, 2005.

[110] Ä. s. Ozdemir, Ã. Cocen, and K. Onel, "The effect of forging on the properties of particulate-SiC-reinforced aluminium-alloy composites," *Composites Science and Technology,* vol. 60, pp. 411-419, 2000.

[111] D. Roy, S. S. Singh, B. Basu, W. Lojkowski, R. Mitra, and I. Manna, "Studies on wear behavior of nano-intermetallic reinforced Al-base amorphous/nanocrystalline matrix in situ composite," *Wear,* vol. 266, pp. 1113-1118, 2009.

[112] C. E. da Costa, W. C. Zapata, F. Velasco, J. M. Ruiz-Prieto, and J. M. Torralba, "Wear behaviour of aluminum reinforced with nickel aluminide MMCs," *Journal of Materials Processing Technology,* vol. 92-93, pp. 66-70, 1999.

[113] A. M. Al-Qutub, I. M. Allam, and T. W. Qureshi, "Effect of sub-micron Al2O3 concentration on dry wear properties of 6061 aluminum based composite," *Journal of Materials Processing Technology,* vol. 172, pp. 327-331, 2006.

[114] M. Gupta and T. S. Srivatsan, "Interrelationship between matrix microhardness and ultimate tensile strength of discontinuous particulate-reinforced aluminum alloy composites," *Materials Letters,* vol. 51, pp. 255-261, 2001.

[115] A. F. Zimmerman, G. Palumbo, K. T. Aust, and U. Erb, "Mechanical properties of nickel silicon carbide nanocomposites," *Materials Science and Engineering: A,* vol. 328, pp. 137-146, 2002.

[116] K. Wu, K. Deng, K. Nie, Y. Wu, X. Wang, X. Hu, and M. Zheng, "Microstructure and mechanical properties of SiCp/AZ91 composite

deformed through a combination of forging and extrusion process," *Materials & Design,* vol. 31, pp. 3929-3932, 2010.

[117] C.C.Koch, "Ductility in nanostructured and ultra fine-grained materials: Recent evidence for optimism," *Journal of metastable and Nanocrystalline Materials,* vol. 18, pp. 9-20, 2003.

[118] C.C.Koch, D.G.Morris, K.Lu, and A.Inoue, "Ductility of nanostructured materials," *MRS Bulletin* vol. 24 pp. 54-58, 1999.

[119] J. A.M.Jorge, M.M.Peres, J.B.Fogagnolo, C.S.Kiminami, and C.Bolfarin, "Hot Extrusion of Nanostructured Al-Powder Alloys: Grain Growth Control and the Effect of Process Parameters on Their Microstructure and Mechanical Properties," *Metallurgical and materials transactions A,* vol. 40A, pp. 3314-3321, 2009.

[120] B. G. Park, A. G. Crosky, and A. K. Hellier, "Fracture toughness of microsphere Al2O3-Al particulate metal matrix composites," *Composites Part B: Engineering,* vol. 39, pp. 1270-1279, 2008.

[121] S. C. Tjong, G. S. Wang, and Y. W. Mai, "High cycle fatigue response of in-situ Al-based composites containing TiB2 and Al2O3 submicron particles," *Composites Science and Technology,* vol. 65, pp. 1537-1546, 2005.

[122] B. Ogel and R. Gurbuz, "Microstructural characterization and tensile properties of hot pressed Alâ€“SiC composites prepared from pure Al and Cu powders," *Materials Science and Engineering: A,* vol. 301, pp. 213-220, 2001.

[123] S.-Y. Chang, C.-F. Chen, S.-J. Lin, and T. Z. Kattamis, "Electrical resistivity of metal matrix composites," *Acta Materialia,* vol. 51, pp. 6191–6302, 2003.

[124] F. Akhtara, S. J. Askaria, K. A. Shaha, X. Dua, and S. Guoa, "Microstructure, mechanical properties, electrical conductivity and wear behavior of high volume TiC reinforced Cu-matrix composites," *Materials Characterization,* vol. 60, pp. 327-336, 2009.

[125] J. Li, L. Gao, and J. Guo, "Mechanical properties and electrical conductivity of TiN-“Al2O3 nanocomposites," *Journal of the European Ceramic Society,* vol. 23, pp. 69-74, 2003.

[126] S.-N. Chou, H.-H. Lu, D.-F. Lii, and J.-L. Huang, "Processing and physical properties of Al2O3/aluminum alloy composites," *Ceramics International,* vol. 35, pp. 7-12, 2009.

[127] F. Zhou, J. Lee, and E. J. Lavernia, "Grain growth kinetics of a mechanically milled nanocrystalline Al," *Scripta Materialia,* vol. 44, pp. 2013-2017, 2001.

[128] H. Abdoli, M. Ghanbari, and S. Baghshahi, "Thermal stability of nanostructured aluminum powder synthesized by high-energy milling," *Materials Science and Engineering: A,* vol. 528, pp. 6702-6707, 2011.

[129] S. K. Shee, S. K. Pradham, and M. De, "Effect of thermal stress on the microstructures of aluminium metal matrix composites," *Materials Chemistry and Physics,* vol. 52, pp. 228-234, 1998.

[130] J. M. Molina, M. Rheme, J. Carron, and L. Weber, "Thermal conductivity of aluminum matrix composites reinforced with mixtures of diamond and SiC particles," *Scripta Materialia,* vol. 58, pp. 393-396, 2008.

[131] K. Chu, C. Jia, X. Liang, H. Chen, and H. Guo, "The thermal conductivity of pressure infiltrated SiCp/Al composites with various size distributions: Experimental study and modeling," *Materials and Design,* vol. 30, pp. 3497–3503, 2009.

[132] C. Tatar and N. Ã–zdemir, "Investigation of thermal conductivity and microstructure of the α-Al_2O_3 particulate reinforced aluminum composites (Al/Al2O3-MMC) by powder metallurgy method," *Physica B: Condensed Matter,* vol. 405, pp. 896-899, 2010.

Chapter Three: Materials and Experimental Procedure

3.1 Starting materials

The starting materials were, Al and, Cu powders, and Al_2O_3, and SiC nano powders, and their details are shown in Table 3.1.

Table 3.1: Details of starting materials

Powders	Manufacturer	Purity	Particle size
Al	Eckagranuels,Australia	99.7%	40 µm
Cu	Merck, Germany	99.7%	<63 µm
Al_2O_3	Allied, USA	99.9%	~50nm
SiC	Aldrich, China	99.5%	<100nm

3.2 Material preparation

3.2.1 High Energy Mechanical Milling

The composite powders were produced by high energy mechanical milling (HEMM) of mixture of Al powders and Al_2O_3 nanopowders, and mixtures of Al and Cu powders and SiC nanopowders, respectively. The HEMM was carried out by using a PM 100 Retsch planetary ball mill as shown in Figure 3.1. The ball mill has a steel vial, with a cylindrical cavity of 60 mm in depth and a 100 mm in diameter (as shown in Figure 3.1). 72 stainless steel balls with a diameter of 12 mm were used for the milling. The milling rotational speed was 400 rpm. The vial which contained steel balls and 100 grams of powder mixture was sealed in a glove box filled with high purity argon. Two groups of composite powders, each with four nominal compositions; were produced: the first group of composite powders are based on Al- Al_2O_3 and their compositions are : Al-2.5vol.% Al_2O_3 ,Al-5vol.% Al_2O_3 , Al-7.5vol.% Al_2O_3, and Al-10vol.% Al_2O_3. The second groups of the composite powders are based on Al-4wt%Cu-SiC and their compositions are : Al-4wt%Cu-2.5vol.%SiC, Al-4wt%Cu-5vol.%SiC, Al-

4wt%Cu-7.5vol.%SiC, and Al-4wt%Cu-10vol.%SiC. 1 wt% of stearic acid which worked as a process control agent (PCA) was added to each batch of the powder charge for the milling experiments. The ball to powder weight ratio used was 5:1. The powder charge was first mixed for 6 hours with a rotational speed of 100 rpm then 400 rpm high energy milling started. The total net milling time for each batch of the powder was 12 hours and the milling process was interrupted after 6 hours to take a small powder sample for characterization.

Figure 3.1: PM 100 Retsch Planetary ball mill with the steel vial.

3.2.2 Powder Consolidation

The ultrafine structured Al-Al_2O_3 and Al-4wt%Cu-SiC nanocomposite powders produced by milling were consolidated by using powder compact forging and powder compact extrusion, respectively. For powder compact forging, the powder was compacted by using uniaxial hot pressing at 300 ºC for 15 minutes under a pressure of 240 MPa using a cylindrical H13 steel die (internal diameter: 25mm) . For powder compact extrusion, the powder was compacted by using uniaxial cold pressing at room temperature for 5 minutes under a pressure of 1000 MPa using the same die. For powder compact forging experiments, the powder compacts were heated to 450 ºC using an induction heating coil under an argon atmosphere, and then forged using an open die kept at room temperature , and a 100-ton hydraulic press with a ram travelling speed of 7.7 mm/s. Circular disks were

produced from the powder compact forging experiments. For the powder compact extrusion experiments, the powder compacts were heated to 500 ºC using an induction heating coil under an argon atmosphere, and then extruded using an extrusion die and cylinder kept at 450 ºC and the same 100-ton hydraulic press. The extrusion ratio was 10:1. Cylindrical bars were produced from the powder compact extrusion experiments.

3.3 Microstructure Characterization

Samples from the as-milled powders and granules and small pieces cut from the consolidated disks and bars were cold mounted in epoxy resin to prepare the metallographic samples which were kept at room temperature for at least 12 hours to allow the resin to fully harden. The resin (105 Epoxy Resin, Adhesive technologies NZ LTD) to hardener weight ratio was 4.44:1. The cylindrical metallographic samples were ground using SiC papers with grit numbers of 320, 600, 1000, 2000, and 4000 under flowing water, and then, polished using Diamond paste and Al_2O_3particle suspension.

The optical microscopy examination of the samples was done using an Olympus BX60 microscope, which was equipped with Polaroid digital camera (NIKON).

X-ray diffraction analysis (XRD) was performed to determine the phase constituents in both powder and consolidated samples using a Philip X-pert system diffractometer with Cu and Kα radiation. The XRD patterns were obtained using a 0.03° step size averaging for 1 second per increment, with voltage of 40 kV and a current of 40 mA.

The microstructures of the powders and granules and consolidated samples were examined using a Hitachi S4700 scanning electron microscope (SEM) operated with a voltage of 20 kV. Energy dispersive x-ray spectrometry (EDS) analysis was also carried out using a Kevex microanalyser attached to the SEM.

An FEI Nova xT nanolab 200 dual beam (focused ion beam (FIB) and electron beam) microscope was used to cut specimens for examination using transmission electron microscopy (TEM). The TEM specimen had dimensions of 15 µm in length, ~ 5 µm in width, and ~100nm in thickness. The TEM specimen cut from the powder particle and consolidated samples were retrieved by using a Kleindiek ex-situ nanomanipulator, and deposited onto standard 150-mesh Au grids each of which were covered with a carbon film. A Philips CM200 transmission electron microscope equipped with a field emission gun and an EDAX energy dispersive X-ray spectrometer (EDS) and operated at a voltage of 200 kV was used for the microstructure examination and compositional analysis of the TEM specimens. The TEM specimens were prepared and examined at the Electron Microscopey Unit, University of New South Wales, Sydney, Australia.

3.4 Microhardness Measurement

The microhardness of the powder particles and consolidated samples was measured using a digital Vickers microindentation tester, LECO LM700, with a load of 25 gf and a 15 second dwell time. 15 measurements were made to obtain an average value of the microhardness measurement.

3.5 Density Measurement

The density of the powder compacts was measured by dividing the weight of the compact in air by the volume of the compact. The scale used was Mettler Toledo (Ag204) with accuracy of 0.1 mg.

The density of the bulk consolidated samples was measured using the Archimedes method as shown in Equation 3.1[1].

$$Density = \frac{weight\,of\,sample\,in\,air}{weight\,of\,sample\,in\,air - weight\,of\,sample\,in\,water} \quad \textbf{(3.1)}$$

3.6 Mechanical Testing

For tensile testing flat dog-bone shaped specimens with a rectangular cross section of 2.2 mm in width and 2 mm in thickness and a gauge length of 20 mm for the extruded samples and 9.5 mm for the forged samples (Figure 3.2).Samples were cut from the powder forged disks and extruded bars using electrical discharge machining (EDM) (DK 77 series). The tensile test specimens were tested at room temperature using an Instron 4204 testing machine at a crosshead speed of 0.1 mm/min which corresponds to an initial strain rate of $6x10^{-5}$/sec for the forged and extruded samples. All reported data were the average of at least two test results.

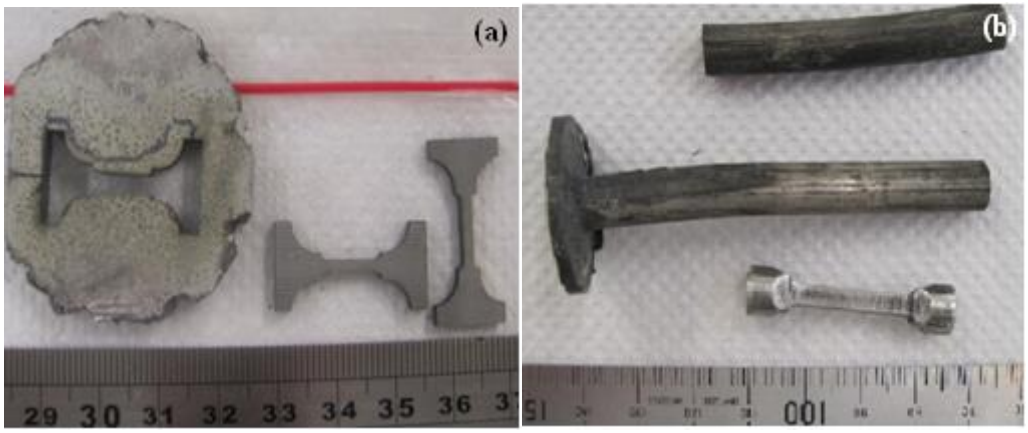

Figure 3.2: Tensile test specimens from the forged disks (a), and the extruded bars (b).

3.7 References

[1] *Wikipedia: Archimedes' Principle.* Retrieved from http://en.wikipedia.org/wiki/Archimedes'_principle

Chapter Four: Morphology, Microstructure and Thermal Stability of Aluminium Based nano-composites powder

4.1 Introduction

This chapter describes and discusses the results of a study on the effect of milling time and powder charge composition on the morphology and microstructure of ultrafine structured (UFS) and nanostructured Al-(2.5-10)vol.%Al_2O_3 nanocomposite balls /granules/powder particles and Al-4wt%Cu-(2.5-10) vol. % SiC nanocomposite powder particles. The purpose of this study is to achieve an understanding of the morphological and microstructural changes taking place in the powder particles during milling and the effects of different volume fractions of reinforcement nanoparticles on these microstructural changes. Of interest is the effect of increasing the volume fraction and/or decreasing the particle size of the reinforcement particles on the progress of mechanical milling. Some studies [1, 2] stated that after sintering and with increasing volume fraction of reinforcement within the matrix the hardness continues to increase until a certain volume fraction is reached and beyond this the hardness will start to decrease due to clustering of reinforcement particles. In this study increasing the volume fraction of reinforcement continued to increase the hardness of the powders even after reaching a steady state condition. This study also investigates the effect on powder yield of carrying out mechanical milling on aluminium composites without the use of a process control agent (PCA). This is an area of research that has hitherto received little attention.

4.2 Al and Al-(2.5-10)vol.%Al_2O_3 nanocomposites granules/balls/powder particles produced by HEMM

Nearly spherical hollow balls, having diameters in the range of 1-10 mm, were obtained after 6 and 12 hours of milling of Al powder (Figure 4.1(a)) using route one (with steel balls of 12 mm in diameter) (Figure 4.1 (b)). After continued

milling using route two (with a mix of steel balls of two diameters: 25 mm and 12 mm) for another 6 and 12 hours, respectively, plate like granules with diameters in the range of 2-20 mm were produced, as shown in Figure 4.1(c). Since a process control agent was not added to the starting powder charge, aluminium powder was stuck on the inner surface of the milling vial and on the surface of the steel balls (Figure 4.1(d)). When 1 wt % of stearic acid was added to the Al powder charge, fine Al granules were produced after 12 hours of milling, using route one (Figure 4.1 (e)).

As a result of milling a mixture of Al powder with2.5, 5, 7.5 and 10 vol.% of Al_2O_3 nanoparticles without using PCA, nearly spherical balls and discs were formed after 6 hours of milling using route one and 24 hours using route two, the results are summarized in Table 4.1. Figure 4.2 shows the granules and discs produced from milling Al powder with 2.5-10 vol.%Al_2O_3 nanoparticles without using PCA. Table 4.1 shows that under the milling condition in Route 1, with increasing the Al_2O_3 content the particle size appears to decrease. Similarly for Route 2.

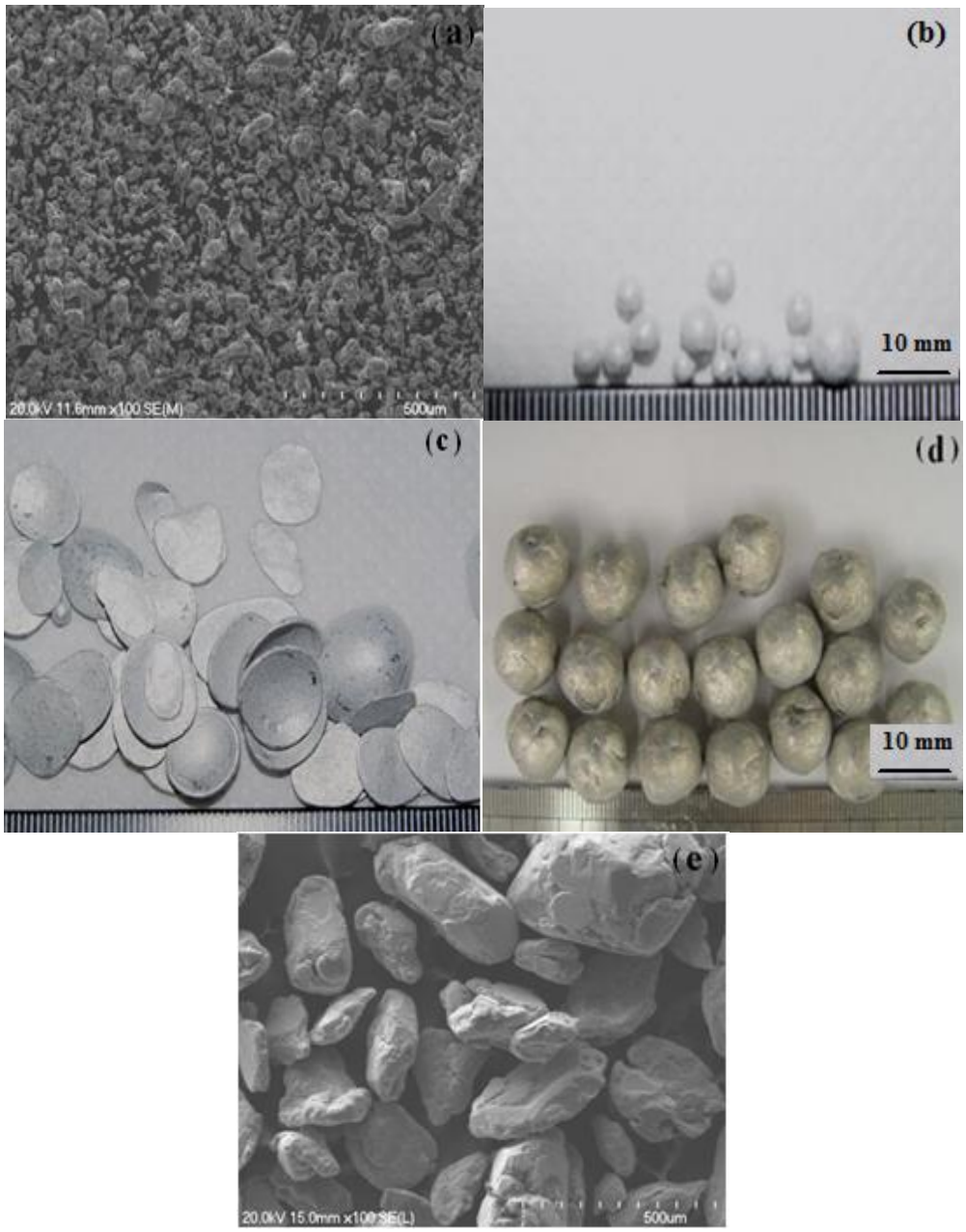

Figure 4.1: (a) As received Al powder; (b) Al balls produced after 6 hours of milling using route one; (c) Al discs produced after 24 hours of milling using route 1 and 2; (d) image showing Al adhered to the surface of the steel balls ;and (e) Al granules produced after 12 hours of milling with 1wt%PCA.

Table 4.1: Particle and granules sizes for Al-(2.5-10)vol.% Al_2O_3 produced without PCA addition.

Composition	Milling condition	Milling Time	Particle/ Granule sizes (mm)
Al-2.5vol.%Al_2O_3	Route 1	6 hr	2-5
Al-2.5vol.%Al_2O_3	Route 2	24 hr	5-12
Al-5vol.%Al_2O_3	Route 1	6 hr	1-5
Al-5vol.%Al_2O_3	Route 2	24 hr	5-12
Al-7.5vol.%Al_2O_3	Route 1	6 hr	1-4
Al-7.5vol.%Al_2O_3	Route 2	24 hr	3-8
Al-10vol.%Al_2O_3	Route 1	6 hr	0.5-2
Al-10vol.%Al_2O_3	Route 2	24 hr	0.5-3

Figure 4.3 shows images of the cross sections of the Al-(2.5-10) vol.%Al_2O_3 balls and granules produced after milling for different times ranging from 6-24 hours. Examination of the cross sections of the balls and granules showed that those with a low Al_2O_3volume fraction of up to 5vol.% had some cavities and those with a higher $Al_2O_3$of 7.5 or 10 % had no cavities.

Figure 4.2: (a) Al-2.5vol.% Al_2O_3 balls and discs produced after 6 hours of milling; (b) Al-2.5vol.% Al_2O_3 balls and discs produced after 24 hours of milling; (c) Al-5vol.% Al_2O_3 granules and discs produced after 6 hours of milling; (d)Al-5vol.% Al_2O_3 granules and discs produced after 24 hours of milling; (e) Al-7.5vol.% granules produced after 6 hours of milling; (f) Al-7.5vol.%Al_2O_3 granules produced after 24 hours of milling; (g) Al-10vol.% Al_2O_3 granules produced after 6 hours of milling, (h) Al-10vol.% Al_2O_3 coarse powder particles and granules produced after 24 hours of milling.

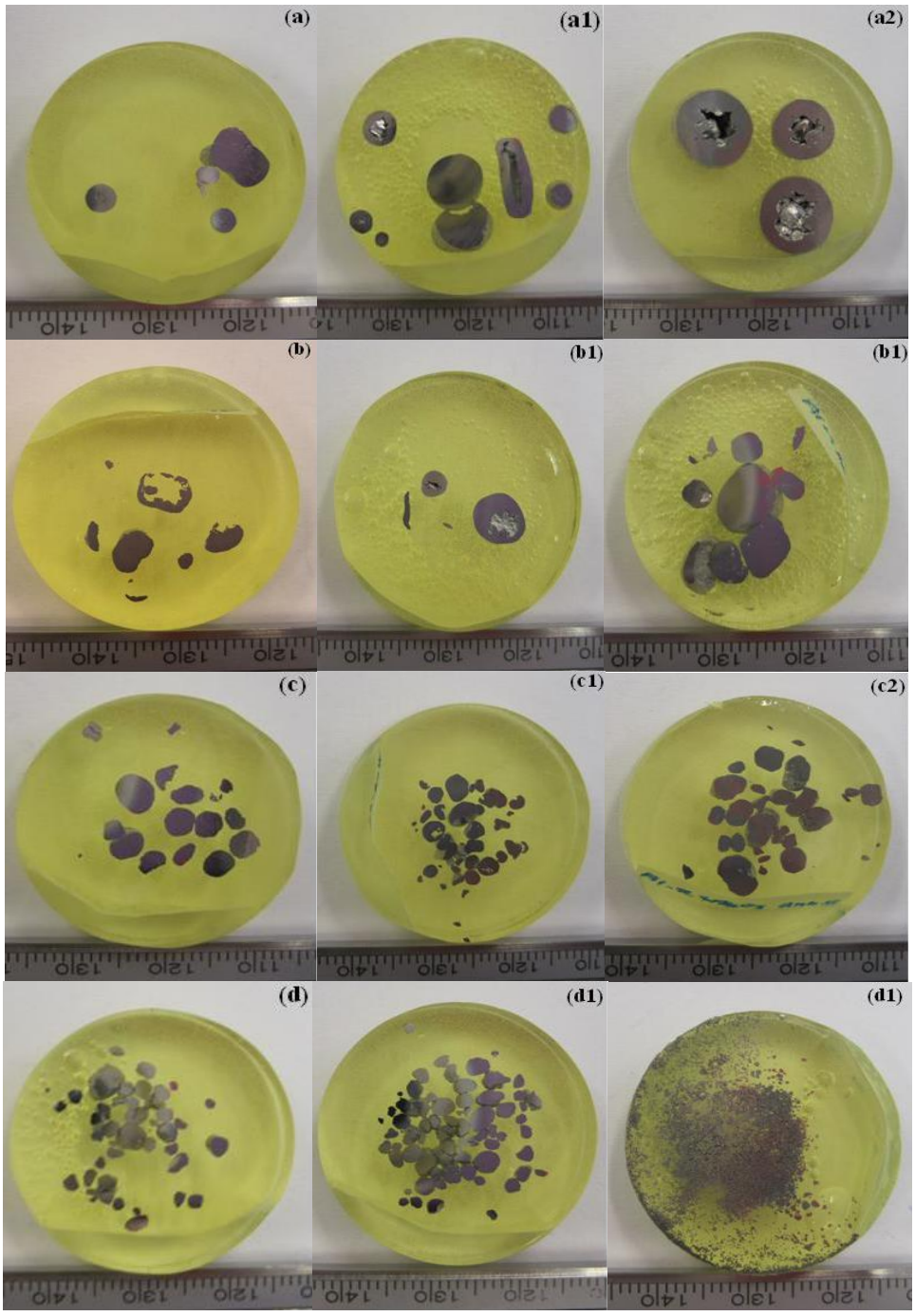

Figure 4.3: Images of cross sections of balls, granules and coarse powder particles of Al-(2.5-10)vol.%Al_2O_3 nanocomposite produced by HEMM without PCA: (a) 2.5vol.%Al_2O_3, 6 hours of milling, (a1) 2.5vol.%Al_2O_3, 12 hours of milling , (a2) 2.5vol.%Al_2O_3, 24 hours of milling; (b) 5vol.%Al_2O_3, 6 hours of milling, (b1) 5vol.%Al_2O_3,12 hours of milling (b2) 5vol.%Al_2O_3, 24hours of milling; (c) 7.5vol.%Al_2O_3,6 hours of milling,(c1) 7.5vol.%Al_2O_3,12 hours of milling (c2) 7.5vol.%Al_2O_3, 24 hours of milling; (d) 10vol.% Al_2O_3, 6 hours of milling, (d1) 10vol.% Al_2O_3, 12 hours of milling , (d2) 10vol.% Al_2O_3, 24 hours of milling.

The XRD patterns of the Al-(2.5-10)vol.%Al_2O_3 nanocomposite balls/granules produced after 12 hours of milling (Figure 4.4) and 24 hours of milling (Figure 4.5), only showed the Al peaks. The absence of the Al_2O_3 peaks in the

XRD patterns might be due to the small volume fraction and very small size of the Al_2O_3 nanoparticles embedded in the milled powder particles. The low volume fraction of Al_2O_3 results in lower intensities and the fine particle size leads to broadening of the peaks and consequently the height of the peak is smaller. with Prabhu et al [3] found that for uniform 50 nm to 150 nm alumina dispersions in aluminium, the expected diffraction peaks for γ-alumina are not clearly observed. This was found for alumina volume contents as high as 50%, where only the high intensity 440 peak for alumina was observed. XRD analysis of the as-milled nano-structured Al-(2.5-10)vol.%Al_2O_3nanocomposite showed that extensive milling using Route 2 (Figure 4.5) caused clear broadening of the Al peaks with a reduction in intensity which is an indication of grain size reduction with increased milling time. The average grain sizes and lattice strains of the Al phase of the milled powders were determined using the Williamson-Hall method (Appendix A) [4] which correlate $\beta Cos\theta/\lambda$ and $\xi Sin\theta/\lambda$ with a linear relationship expressed by the following equation:

$$\beta Cos\theta = \xi Sin\theta + 0.9\lambda/d, \qquad (4.1)$$

Where β is the width of the peak at the half of the maximum intensity, λ the wavelength of the x-ray used, *d* is the average grain size, θ the Bragg angle, and ξ the average lattice strain. Based on the Williamson-Hall method (Figure 4.6), the estimated average grain sizes of 12 and 24 hours milled Al-(2.5-10) vol.%Al_2O_3 nanocomposite balls/granules and their lattice strain are summarized in table 4.2.

Table 4.2: Average grain size and lattice strain for milled Al-(2.5-10)vol.%Al_2O_3 nanocomposite balls/granules after 12 and 24 hours of milling.

Composition	Milling Time (Hr)	Average grain size (nm)	Lattice Strain (%)
Al-2.5vol.%Al_2O_3	12	64	0.155
Al-2.5vol.%Al_2O_3	24	105	0.186
Al-5vol.%Al_2O_3	12	138	0.247
Al-5vol.%Al_2O_3	24	125	0.228
Al-7.5vol.%Al_2O_3	12	68	0.136
Al-7.5vol.%Al_2O_3	24	121	0.327
Al-10vol.%Al_2O_3	12	217	0.4
Al-10vol.%Al_2O_3	24	73	0.162

The average grain sizes and lattice strains of the Al-(2.5-10)vol.%Al_2O_3nanocomposite after 12 hours of milling were changing with increasing volume fraction of Al_2O_3 due to cold welding through not using a PCA. With increasing percentage of alumina particles, the amount of agglomeration in the composite powders was increased. After the ball milling process, the aluminium particles are cold welded to the wall of the milling cup and balls due to the applied normal force in this process. This phenomenon is due to the locally increasing temperature at the contact point between the balls and vial [5]. However after 24 hours of milling the grain size changes were negligible suggesting that the effect of increased milling time leads to a steady-state condition [6, 7] when there is no further decrease in grain size with increased milling time. The peaks shift because 2Ɵ has changed which implies a change in `d` spacing. The changes in the lattice parameters are considered to result from the combined effect of the residual stress due to the mechanical milling, and to

variations in composition [8]. Another explanation is due to Fe dissolution in the Al lattice regarding the higher atomic radius of Fe than Al.

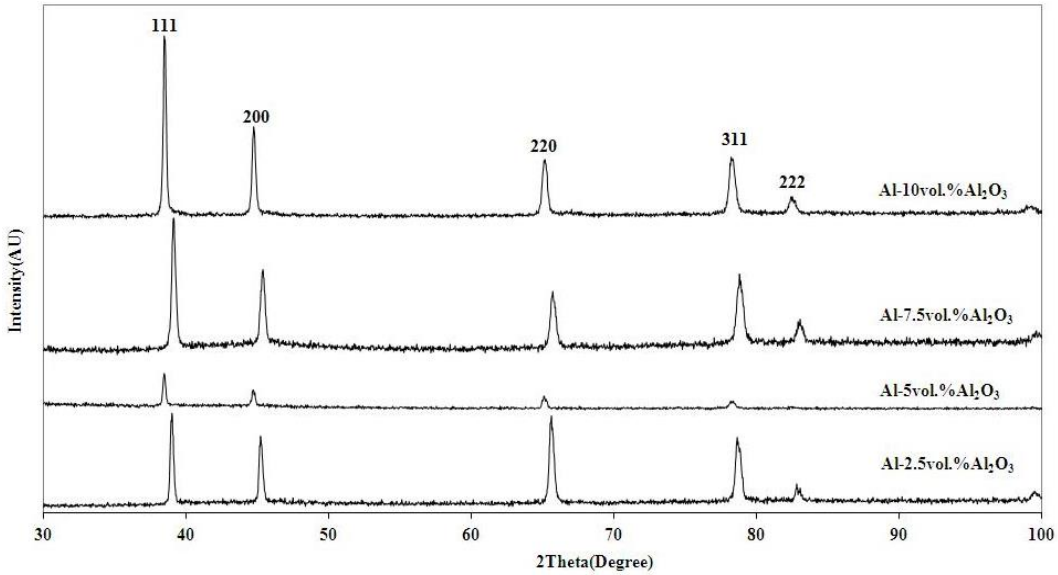

Figure 4.4: X-Ray diffraction patterns of the 12 hours milled Al-(2.5-10)vol.%Al_2O_3 nanocomposites balls/granules.

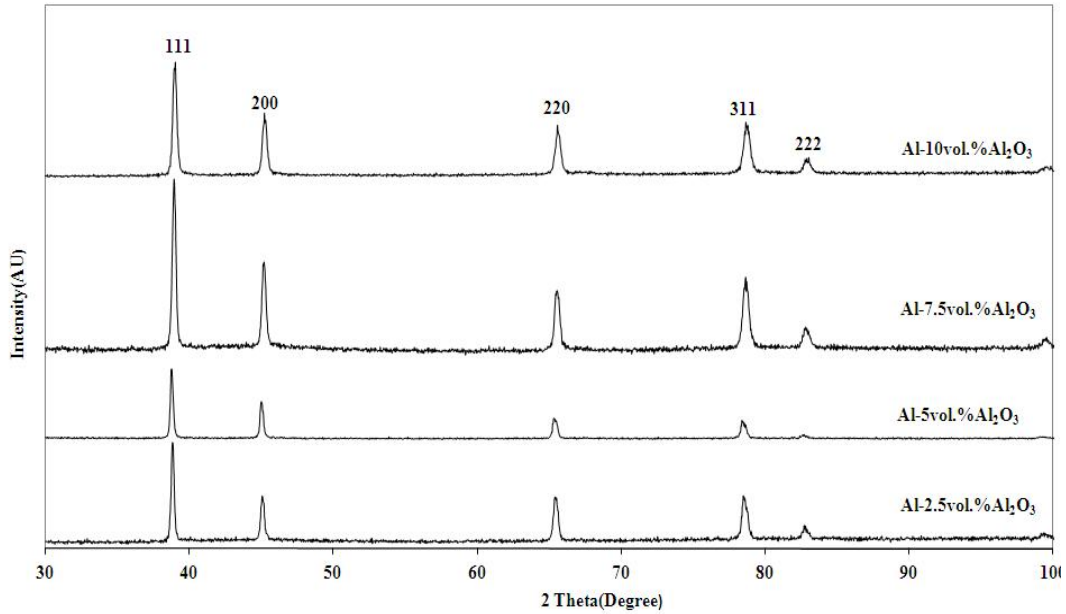

Figure 4.5: X-Ray diffraction patterns of the 24 hours milled Al-(2.5-10)vol.%Al_2O_3 nanocomposites balls/granules.

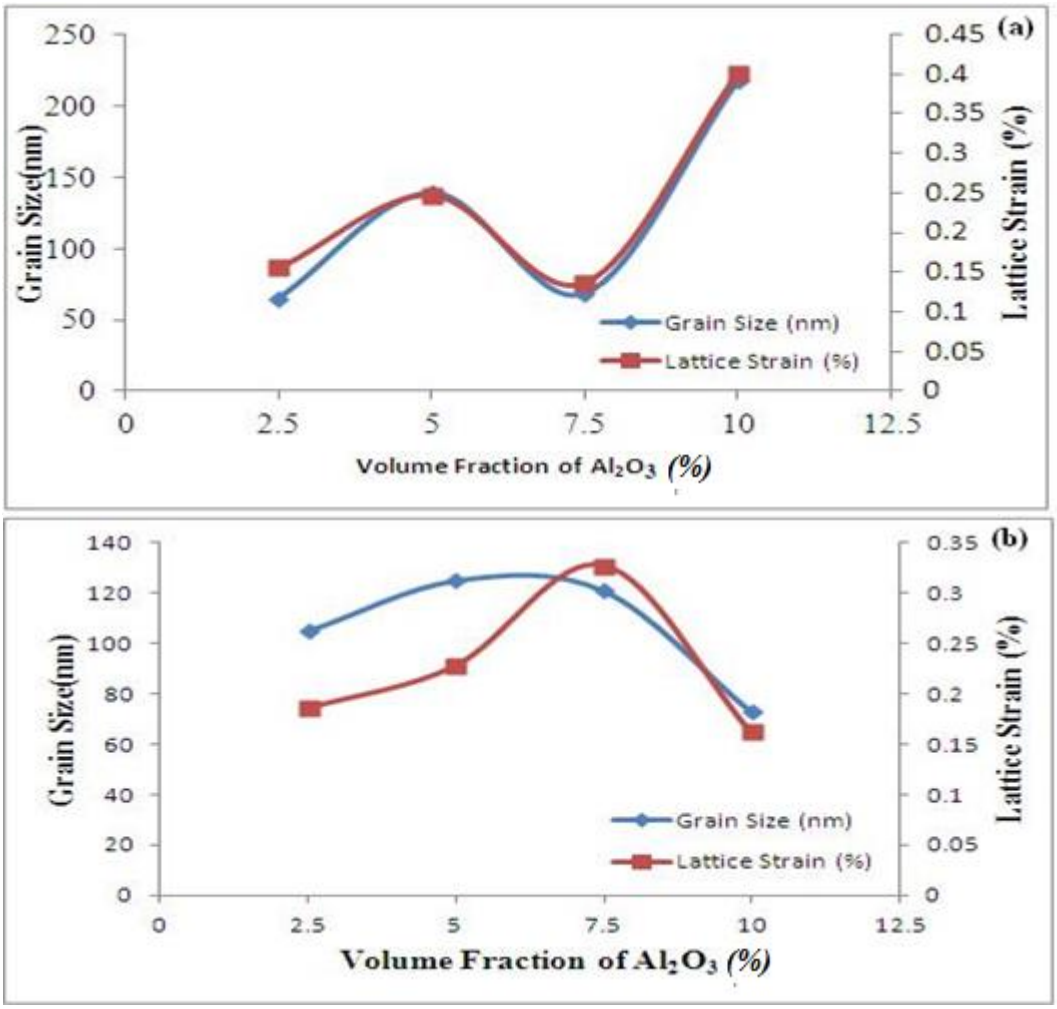

Figure 4.6: Average grain size and lattice strain of Al-(2.5-10)vol.%Al_2O_3 nanocomposites balls/granules as functions of the volume fraction of Al_2O_3 : (a) after 12 hours of milling ,(b) after 24 hours of milling.

A TEM examination was carried out on specimens of as milled Al-Al_2O_3 composite granules for all compositions investigated in the work (Figures 4.7-4.9). In all cases, a STEM analysis (Figures 4.11, 4.14, 4.16) showed through EDX elemental mapping, a uniform distribution of oxygen rich areas. These regions contain Al_2O_3 nanoparticles of varying size depending on the Al_2O_3 content and processing conditions. The results for changes in composition and processing conditions are summarized in Table 4.3. From the TEM figures it can be noticed a high density of dislocations within the Al matrix grains. The SAD patterns did not show well-defined single crystal spot patterns but a tendency towards ring patterns confirming a very small aluminium grain size, as shown in Figure 4.13.

If we look carefully at the images in Figures 4.10, 4.12, and 4.15 there is a sub-structure associated with the Al_2O_3 particle and the reinforcement nanoscaled particles distributed mostly at the grain boundaries, which is in agreement with the findings of Arami [9], who carried out work on nanocrystalline Al–4 wt% Cu alloy reinforced with nanometric Al_2O_3 particles which was synthesized by in situ reactive milling of Al and CuO powder mixture. The size of alumina particles was in the range of 10–50 nm and they were mostly distributed at the grain boundaries. The processed nanocomposite powder has fine and equiaxed particles with relatively high bulk density.

Table 4.3: Grain size summary of Al-(2.5-10)vol.%Al_2O_3 nanocomposites balls/granules as functions of the volume fraction of Al_2O_3 , after 12 and 24 hours of milling.

Composition	Grain Size (nm)	
	12 hrs milling time	24 hrs milling time
Al-2.5vol. %Al_2O_3	200-700	150-450
Al-5vol. %Al_2O_3	200-600	100-450
Al-7.5vol. %Al_2O_3	200-400	100-250
Al-10vol. %Al_2O_3	50-200	10-100

Randomly selected Al-(2.5-10) vol. %Al_2O_3 nanocomposites balls/granules were mounted ground and polished to produce flat surfaces for microhardness testing. 15-20 indents were taken for each measurement with the distances between indents being at least 100 µm to reduce the variability and the error of the measurements. As shown in Figure 4.17, for the Al-(2.5-10)vol.%Al_2O_3 nanocomposites granules produced after 12 hours of milling, with an increasing volume fraction ofAl_2O_3 nanoparticles from 2.5 to 10 vol. %, the average microhardness increased from 108 HV to 143 HV. The microhardness of 24 hours milled Al- (2.5-10) vol. %Al_2O_3 nanocomposite granules increased from102.9HV to 156 HV as the Al_2O_3 content increased from 2.5 to 10 vol.%.

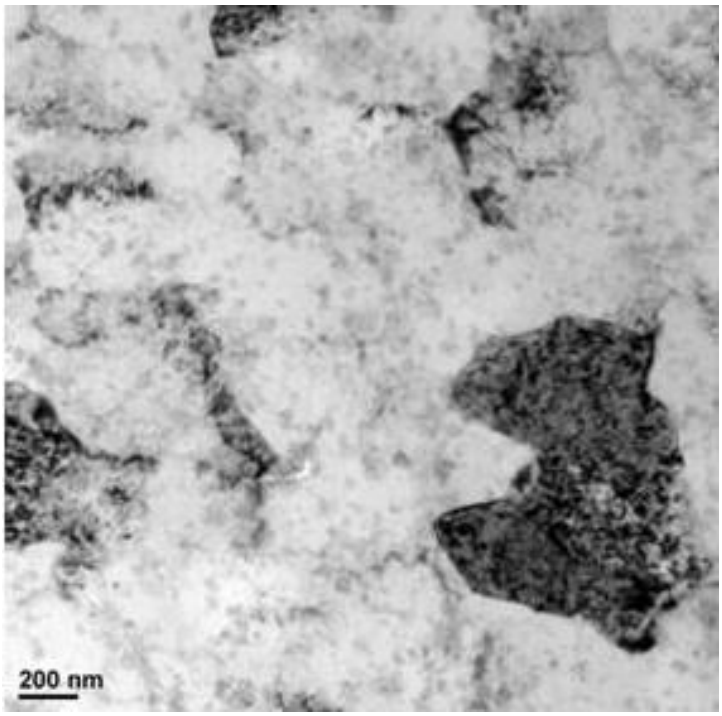

Figure 4.7: TEM bright field image of a specimen cut from a randomly selected 12 hours milled Al-2.5vol.%Al_2O_3 nanocomposite granules.

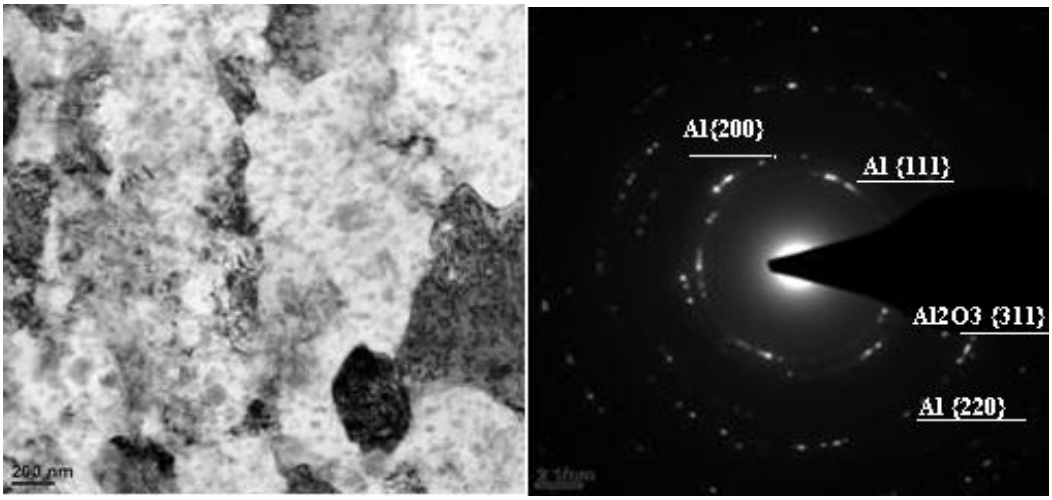

Figure 4.8: TEM bright field image and SADP of a specimen cut from a 24 hours milled Al-2.5vol.%Al_2O_3 granules.

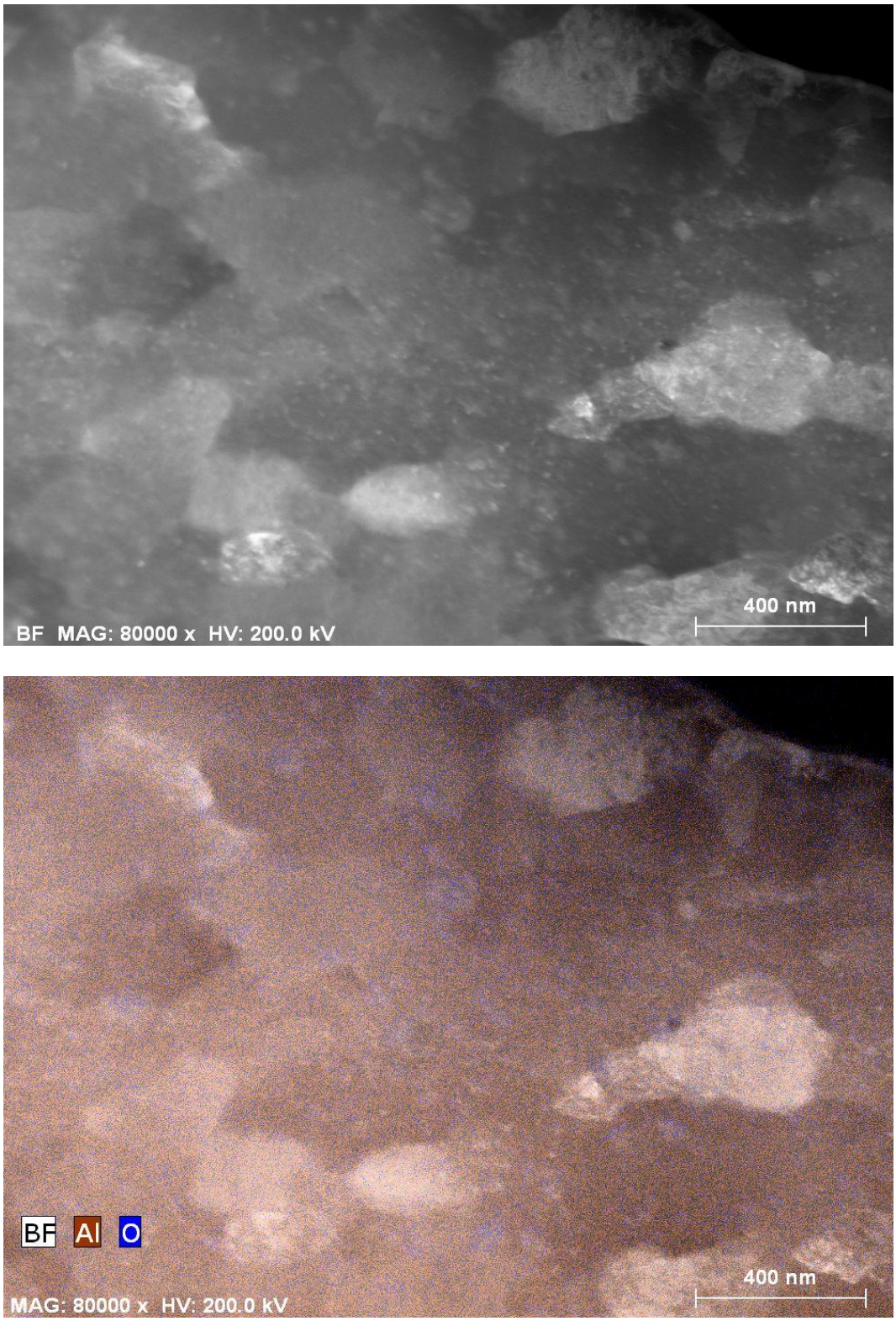

Figure 4.9: STEM image and the corresponding EDX elemental mapping of 24 hours milled Al-2.5vol. %Al_2O_3 nanocomposite granules.

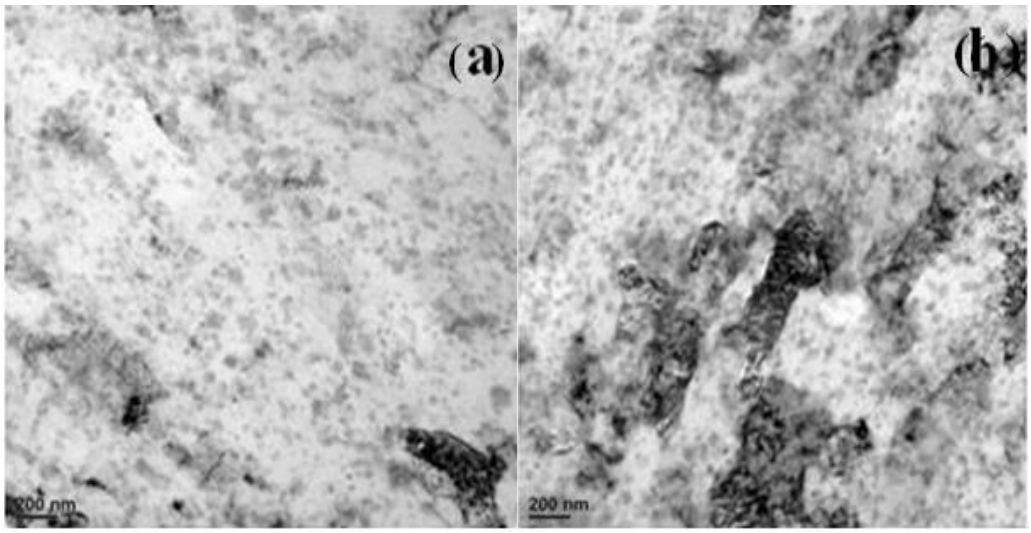

Figure 4.10: TEM bright field image of Al-5vol. %Al_2O_3 nanocomposite granules (a) after12 hours of milling, (b) after 24 hours of milling.

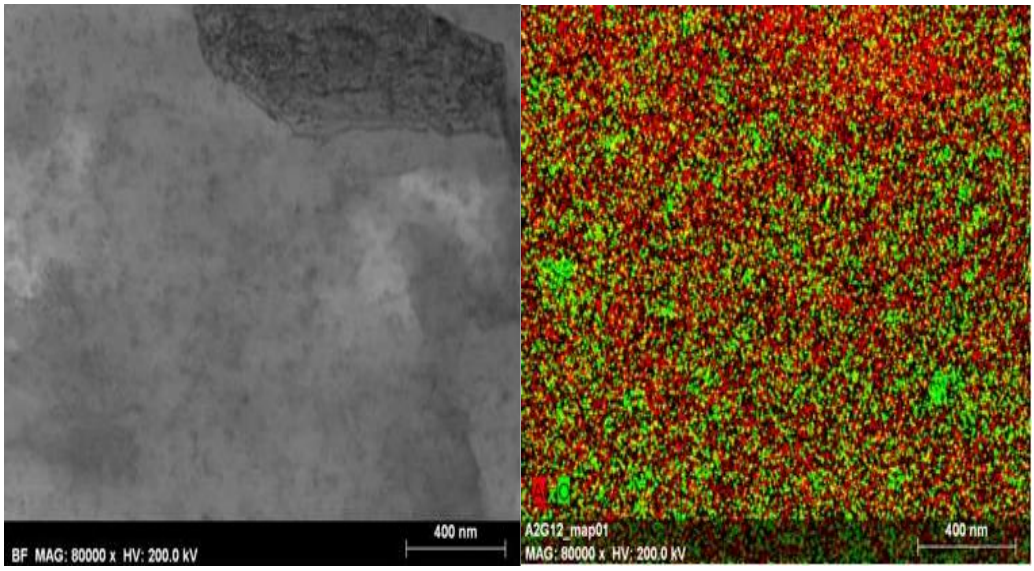

Figure 4.11: STEM image and EDX elemental mapping of a 12 hours milled Al-5vol. %Al_2O_3 nanocomposite granule showing the distribution and clustering of Al_2O_3 within the Al matrix. (Red colour: Al; green colour: O)

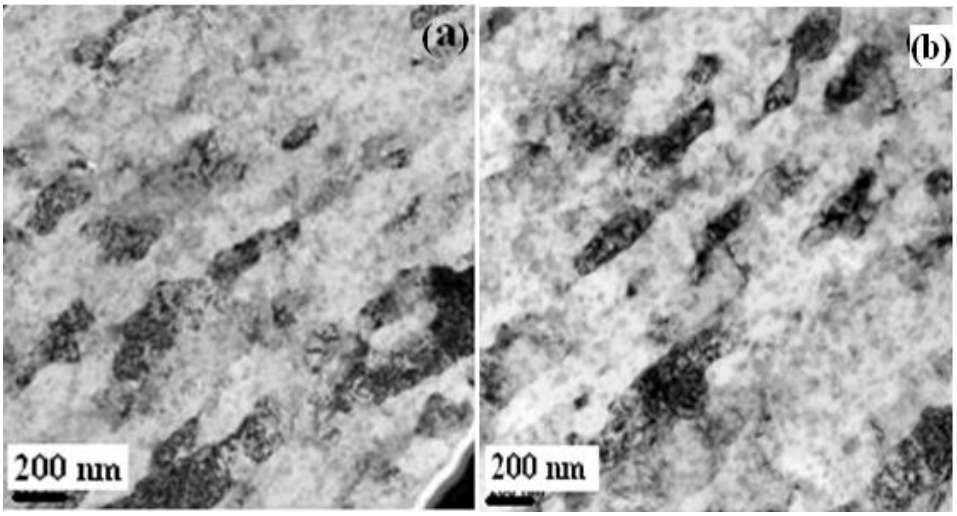

Figure 4.12: TEM bright field image of Al-7.5vol.%Al_2O_3nanocomposites granules produced by HEMM, (a)after 12 hours of milling , (b) after 24 hours of milling, respectively.

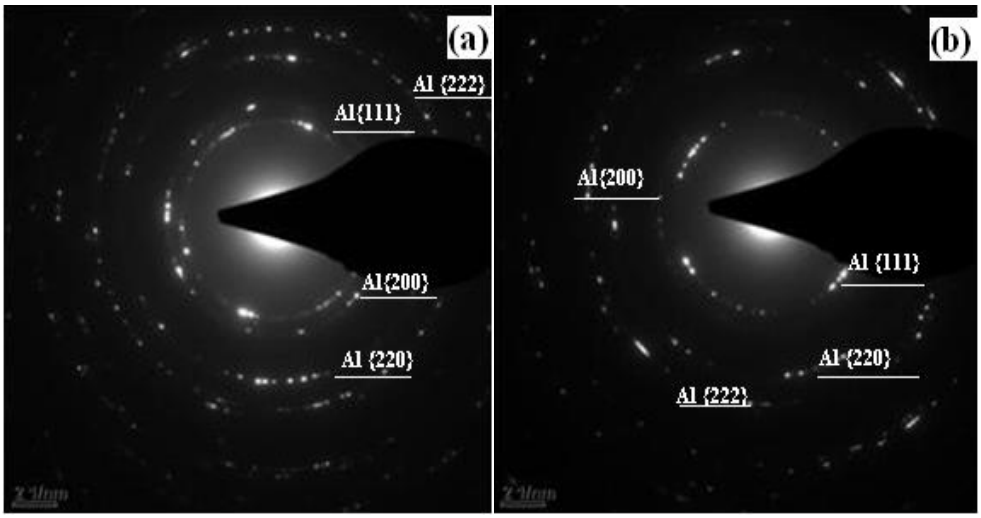

Figure 4.13: SADPs of Al-7.5vol.%Al_2O_3 nanocomposites granules produced by HEMM, (a) after 12 hours of milling, (b) after 24 hours of milling, respectively.

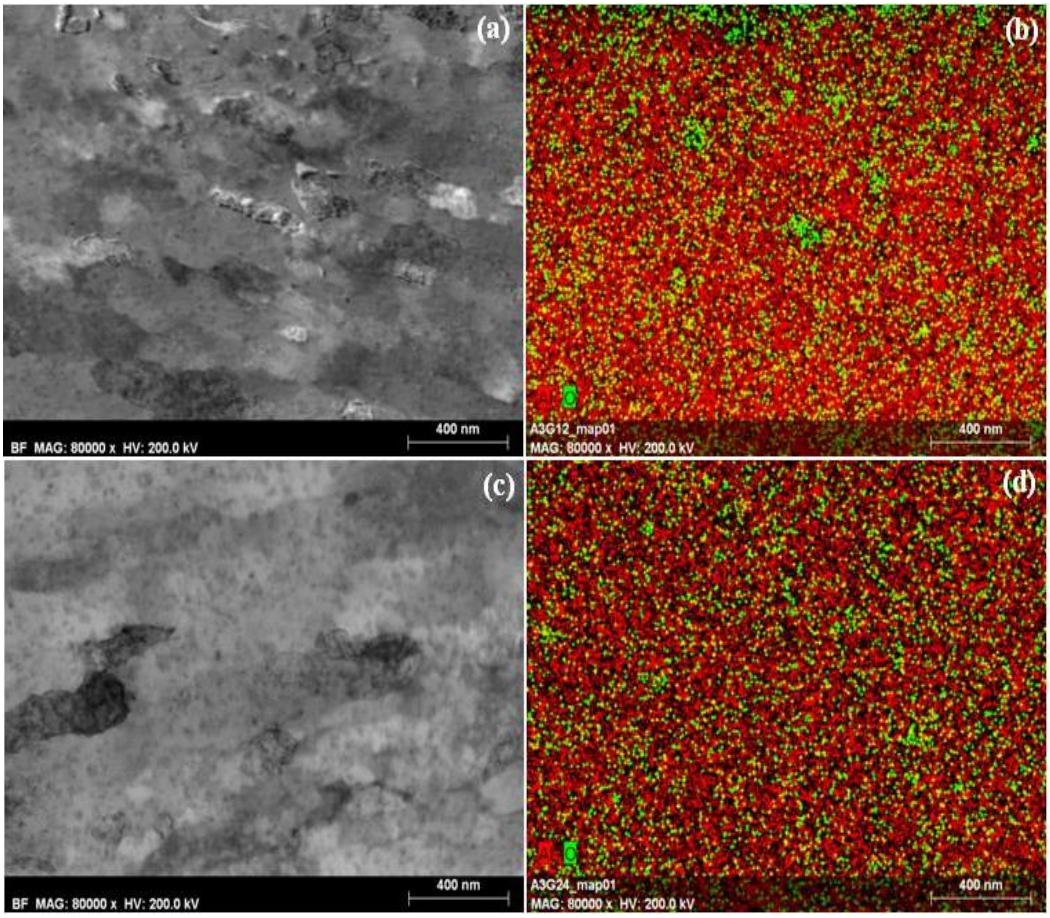

Figure 4.14: STEM images ((a) and (c)) and EDX elemental mappings ((b) and (d)) of 12 and 24 hours milled Al-7.5vol. %Al_2O_3nanocomposite granules produced by HEMM, (a)-(b) after 12 hours of milling, (c)-(d) after 24 hours milling. (Red colour: Al; green colour: O)

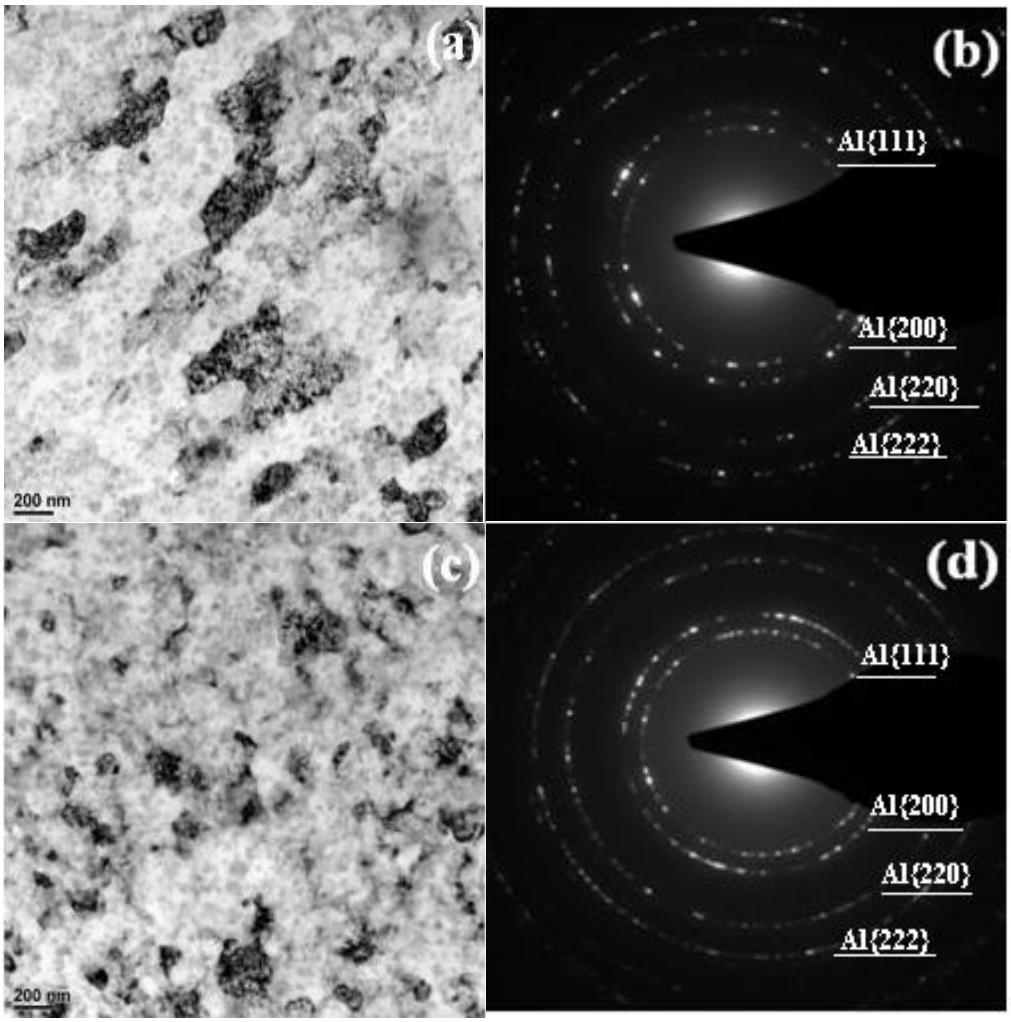

Figure 4.15: TEM bright filed image and SADPs of nanostructured Al-10 vol. %Al_2O_3 particles produced by HEMM, (a) and (b) after 12 hours of milling, (c) and (d) after 24 hours of milling, respectively.

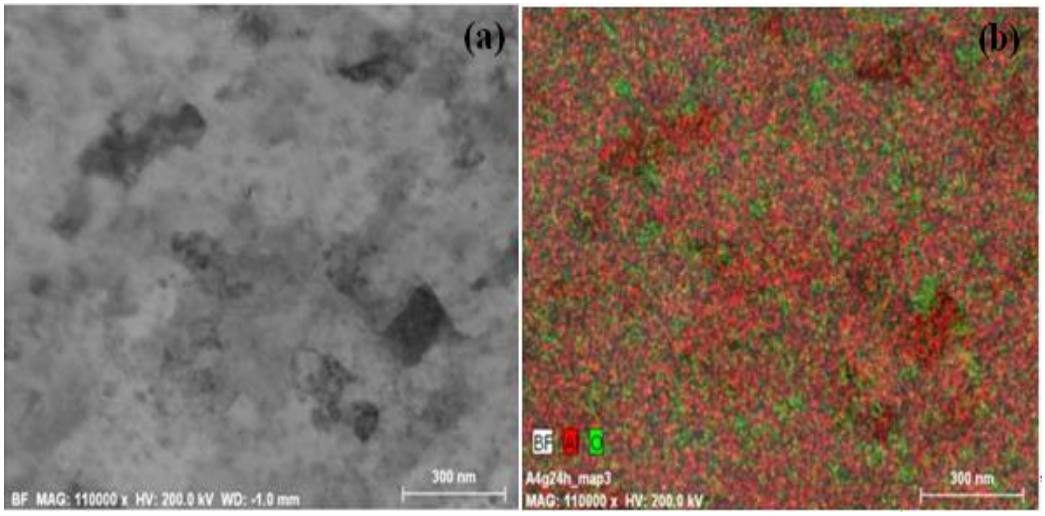

Figure 4.16: (a) STEM image and (b) EDX elemental mapping of 24 hours milled Al-10vol.%Al_2O_3 nanocomposite granules.

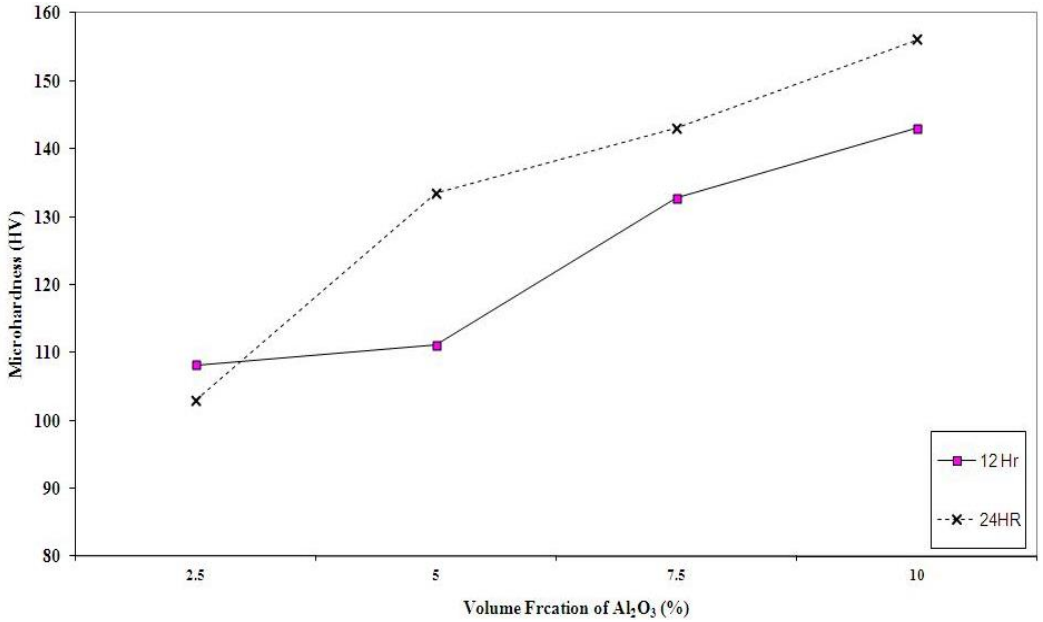

Figure 4.17: Microhardness of 12 and 24 hours milled Al- (2.5-10) vol. %Al_2O_3 nanocomposite granules as functions of the volume fraction of Al_2O_3.

4.3 Al-(2.5-10)vol.%Al_2O_3 nanocomposites powders

This section talks about producing Al-(2.5-10)vol.%Al_2O_3 nanocomposite powders with the use of 1wt% of PCA and two different milling times (6 and 12 hours). Because PCA is used during milling a sufficient amount of powder was produced without the need for route two (18 and 24 hours of milling). The powder particle sizes are summarized in table 4.4 below. The particle size distribution as a function of volume fraction of reinforcement (Figure 4.18) showed that the particle mean diameter D (V, 0.1) was 114, 95, 40, and 26 um for Al-2.5vol.%Al_2O_3, Al-5vol.%Al_2O_3, Al-7.5vol.%Al_2O_3, Al-10vol.%Al_2O_3 nanocomposite powders, respectively. The particle size was calculated using a Malvern Mastersizer 2000 where samples are dispersed in water and circulated through the mastersizer and analysed using laser diffraction to give the particle size results. Figure 4.19 shows SEM images of the Al-(2.5-10)vol.%Al_2O_3 nanocomposite powders produced by HEMM with 1wt%PCA.

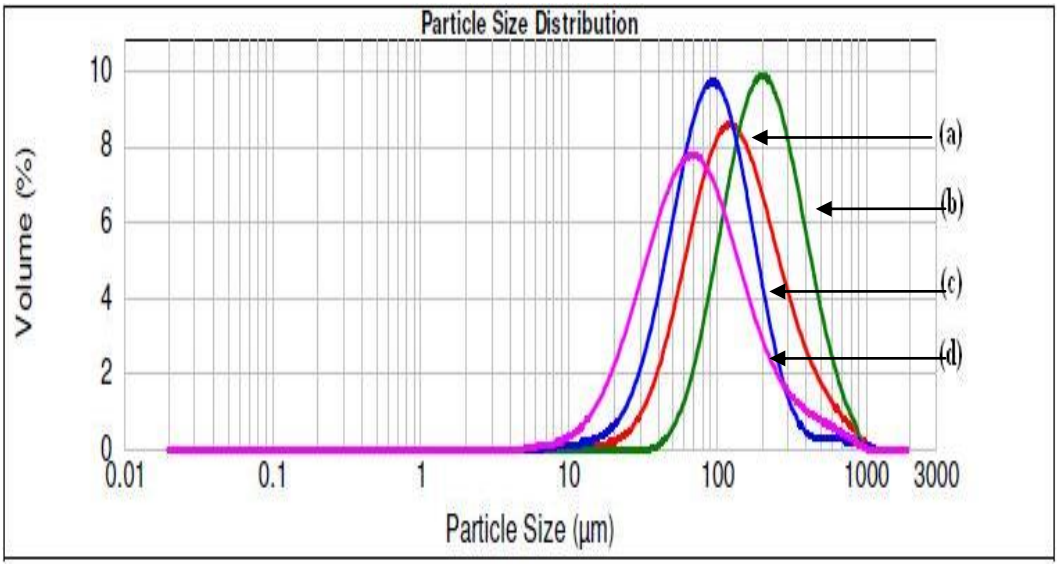

Figure 4.18: Particle size distribution of the Al-(2.5-10) vol.%Al_2O_3 nanocomposite powder produced after 12 hours of milling: : (a) 2.5vol.%Al_2O_3 ;(b) 5vol.%Al_2O_3 ; (c) 7.5vol.%Al_2O_3; (d) 10vol.%Al_2O_3 .

Table 4.4: The particle size of the Al-(2.5-10)vol.%Al_2O_3 nanocomposite powders produced by HEMM with 1wt%PCA.

Composition	**Milling condition**	**Milling Time**	**Powder particle sizes (µm)**
Al-2.5vol.%Al_2O_3	Route 1	6 hr	20-100
Al-2.5vol.%Al_2O_3	Route 1	12 hr	10-120
Al-5vol.%Al_2O_3	Route 1	6 hr	40-110
Al-5vol.%Al_2O_3	Route 1	12 hr	20-80
Al-7.5vol.%Al_2O_3	Route 1	6 hr	30-120
Al-7.5vol.%Al_2O_3	Route 1	12 hr	20-70
Al-10vol.%Al_2O_3	Route 1	6 hr	10-60
Al-10vol.%Al_2O_3	Route 1	12 hr	5-50

The cross sectional morphologies of the 12 hours milled powder particles with different volume fractions of Al_2O_3 are shown in Figure 4.20.These micrographs show that the powder particles were irregular and as the volume fraction of Al_2O_3 nanoparticles increased from 2.5 to 10%, the sizes of the nanocomposite powder particles correspondingly decreased, for the same milling time.

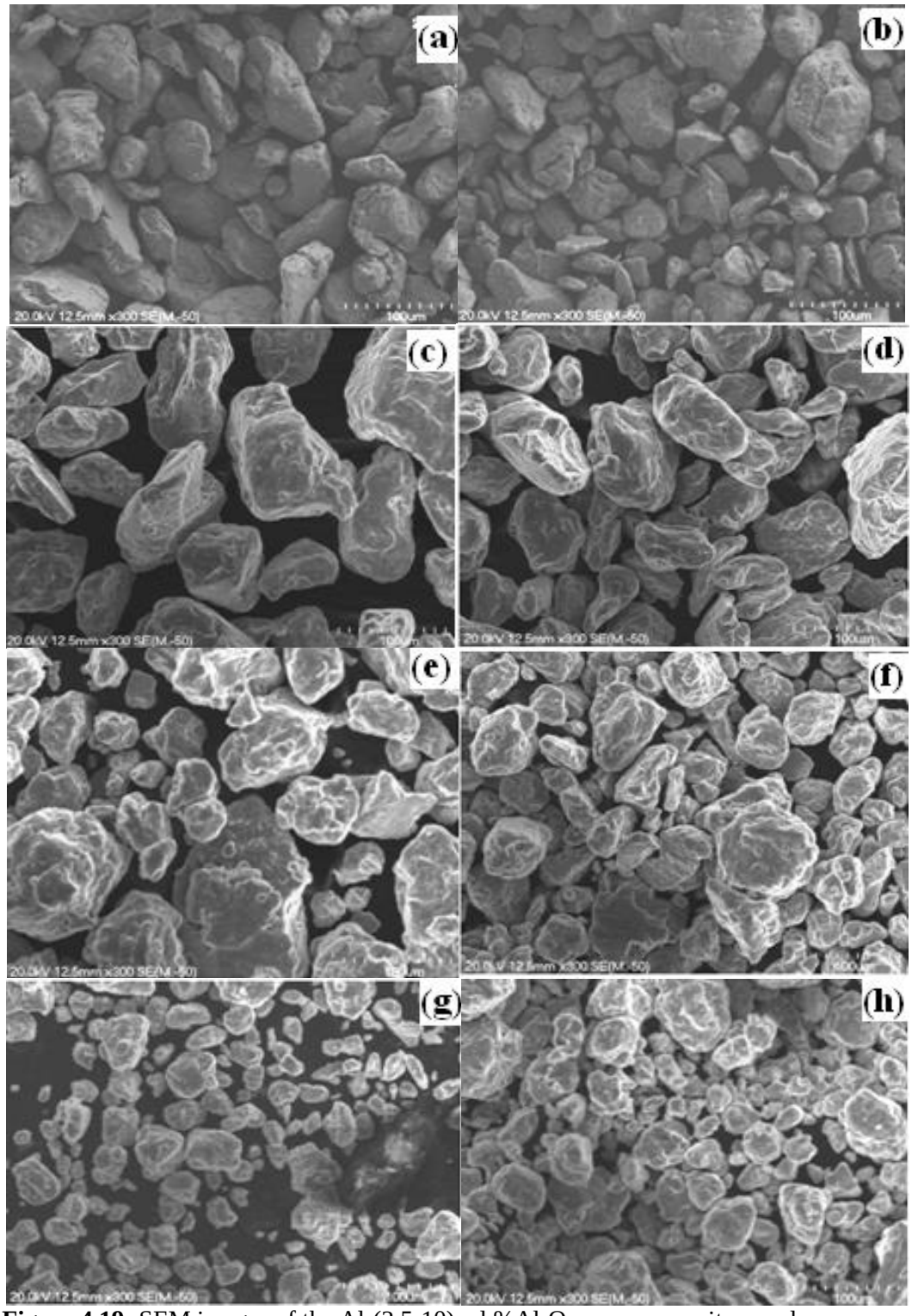

Figure 4.19: SEM images of the Al-(2.5-10)vol.%Al_2O_3 nanocomposite powders produced by HEMM with 1wt%PCA: (a) 2.5vol.%Al_2O_3, 6 hours of milling; (b) 2.5vol.%Al_2O_3, 12 hours of milling; (c) 5vol.%Al_2O_3 ,6 hours of milling; (d) 5vol.%Al_2O_3 , 12 hours of milling; (e) 7.5vol.%Al_2O_3 ,6 hours of milling, (f) 7.5vol.%Al_2O_3 , 12 hours of milling; (g) 10vol.% Al_2O_3 ,6 hours of milling, (h) 10vol.%Al_2O_3,12 hours of milling.

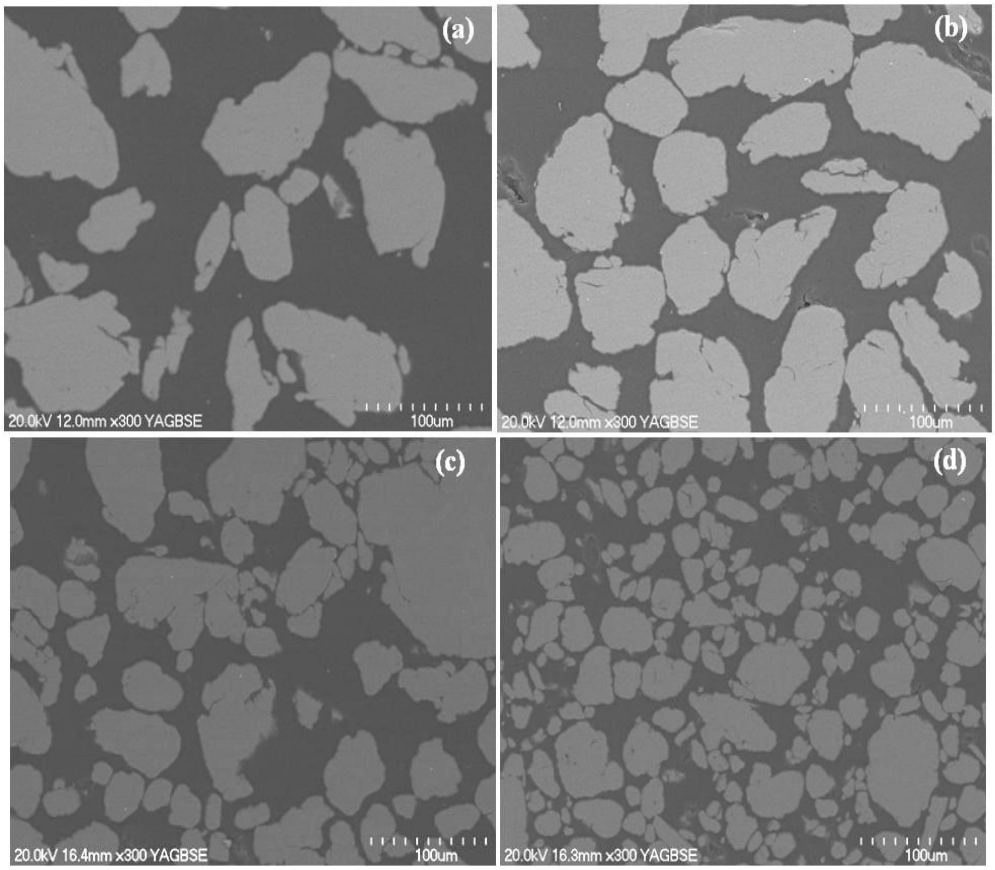

Figure 4.20: SEM backscattered electron images of the cross sections of the Al-(2.5-10)vol.% Al_2O_3 nanocomposite powder particles produced by 12 hours of milling: (a) 2.5vol.% Al_2O_3 ;(b)5vol.% Al_2O_3;(c)7.5vol.% Al_2O_3 ;and (d)10vol.% Al_2O_3.

Figure 4.21 shows the XRD patterns of Al and Al-(2.5-10) vol.% Al_2O_3 nanocomposite powders produced after 12 hours of milling. The XRD patterns showed only the Al peaks for the same reasons discussed in section 4.2 above. An Al_2O_3 peak was noticed with the composite of Al-10vol.% Al_2O_3 but still a weak and broadened peak. The fine particle size leads to broadening of the peaks and consequently the height of the peak is smaller. Which agree with Prabhu et al [3]. It is clear that with increasing volume fraction of Al_2O_3 nanoparticles the XRD peaks for aluminium became broader, suggesting that the sizes of Al grains had decreased. As before, the average grain sizes and lattice strains of the Al phase of the milled powders were determined using the Williamson-Hall method. Figure 4.22 shows the $\beta Cos\theta/\lambda$ vs $\xi Sin\theta/\lambda$ data points for the Al-2.5vol.%Al_2O_3 and Al-10vol.%Al_2O_3 nanocomposite powders after 12 hours of milling, respectively. Based on the broadening of the XRD peaks of the Al phase, the average grain size and lattice strain due to the alumina phase distributed in the Al matrix of the nanocomposite powder were

estimated, and the results are shown in Figure 4.23. The average grain size and lattice strain in the Al-2.5vol.%Al_2O_3 nanocomposite powders were 111 nm, 0.22%, respectively. With 5 % volume fraction of Al_2O_3 nanoparticles, the average grain size and lattice strain remained almost unchanged, but a further increase in the volume fraction of Al_2O_3 nanoparticles to 7.5 % increased the grain size and lattice strain to 1111 nm and 0.47% respectively. At a volume fraction of 10% Al_2O_3 the grain size and lattice strain decreased to 500 nm and 0.39%, respectively. One reason for the variations in the grain size and lattice strain is caused by the introduction of dislocations, vacancies, impurities and other lattice defects during milling [10, 11]. The lattice parameter increases for Al are possibly due to the substitution of larger Fe atoms produced from the collision of the balls with the internal surface of the milling vial into the Al lattice. Also an increase in the amount of alumina particles leads to an increase in the dislocation density, and causes grain refinement. Figure 4.14 shows a TEM bright field images of 12 hours milled Al-(2.5-10)vol.% Al_2O_3 nanocomposites powders. If we look carefully at those images there is a sub-structure associated with the Al_2O_3 particle and the reinforcement nanoscaled particles distributed mostly near the grain boundaries.

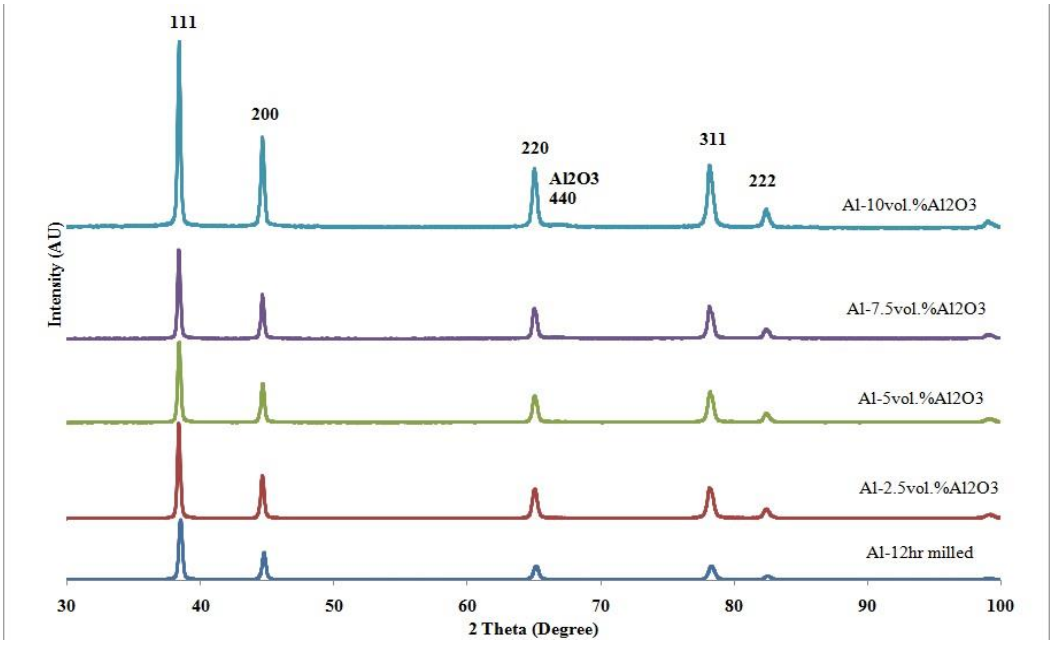

Figure 4.21: XRD patterns of 12 hours milled Al powder and Al-(2.5-10)vol.% Al_2O_3 nanocomposites powders.

Figure 4.22: βCosθ/λ vs Sinθ/λ plot of the 12 hours milled (a) Al-2.5vol.% Al_2O_3 nanocomposites powder and(b) Al-10vol.% Al_2O_3 nanocomposites powder.

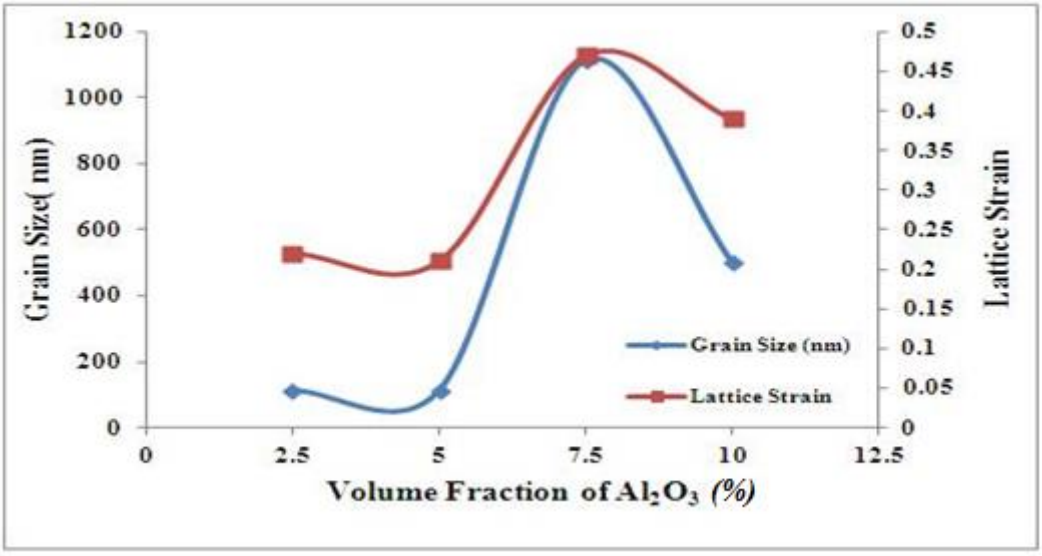

Figure 4.23: Average grain size and lattice strain of Al-(2.5-10)vol.%Al_2O_3 nanocomposite powders produced by 12 hours of milling as a functions of the volume fraction of Al_2O_3.

The changes in microstructure of the Al-(2.5-10)vol.%Al_2O_3powders was examined using TEM. This showed that after 12 hours milling time, a mixture of equiaxed and elongated aluminium grains were present in the microstructure. The range of grain-sizes varied with alumina volume fraction and these are summarized in the table below:

Table 4.5: The grain sizes of Al-(2.5-10) vol.%Al_2O_3 powders.

Composition	Milling condition	Milling Time	Grain sizes (nm)
Al-2.5vol.%Al_2O_3	Route 1	12 hr	100-500
Al-5vol.%Al_2O_3	Route 1	12 hr	100-400
Al-7.5vol.%Al_2O_3	Route 1	12 hr	50-400
Al-10vol.%Al_2O_3	Route 1	12 hr	50-300

It is clear that, for Al-7.5vol.% Al_2O_3, the average grain size estimated from the XRD data in figure 4.21 is larger than the sizes obtained by TEM. From the TEM examination, we can see that the grain size of the Al matrix decreased slightly with increasing volume fraction of Al_2O_3 nanoparticles. The SADPs of the

nanocomposites showed {111}, {200}, {220}, and {222} diffraction rings of the Al matrix and weak diffraction spots from {311} and {400} planes of the Al_2O_3 nanoparticles (Figure 4.25).

Figure 4.26 shows the average microhardness of as-milled Al powder particles and Al- (2.5-10)vol.%Al_2O_3 nanocomposite powders produced by 12 hours of milling. There is a small increase in the microhardness with a 2.5 vol. % Al_2O_3 addition, and further increases in the Al_2O_3 nanoparticle content to 10vol.% continues the trend of microhardness increase to 143 HV.

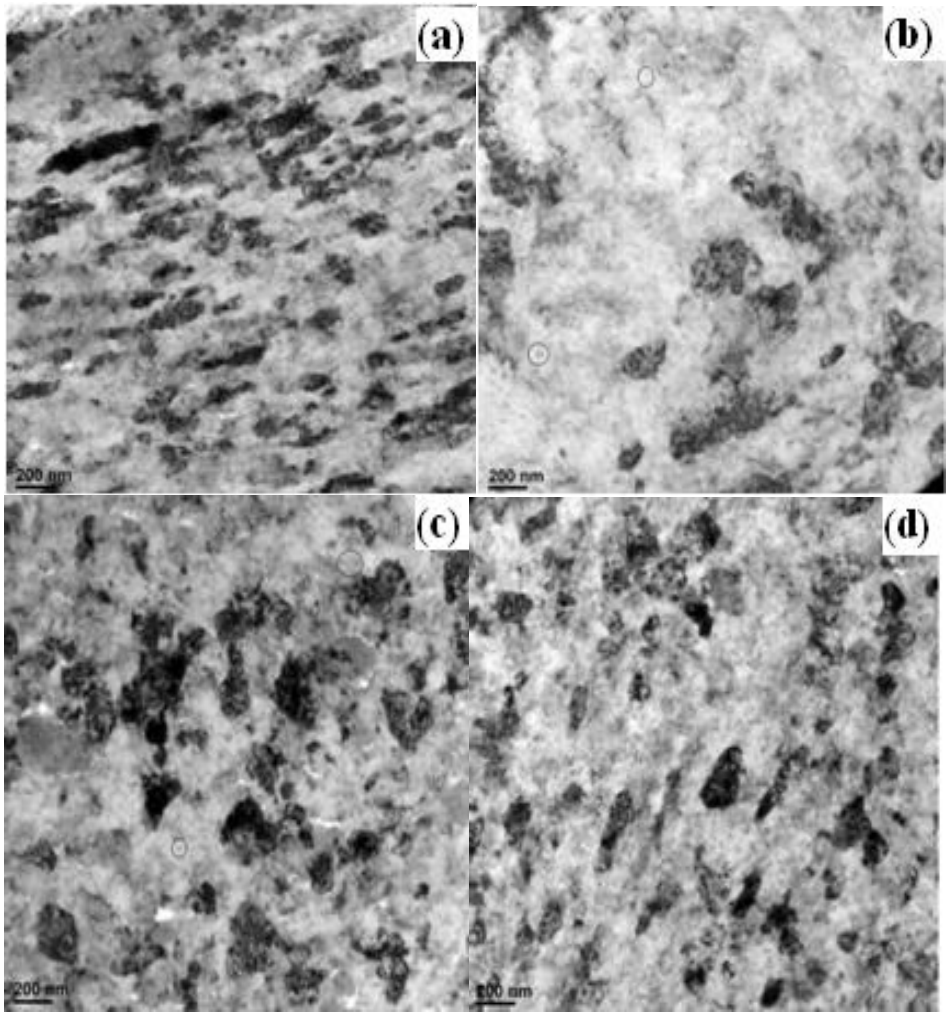

Figure 4.24: TEM bright field images of 12 hours milled Al-(2.5-10)vol.% Al_2O_3 nanocomposite powders particles (a) 2.5vol.% Al_2O_3, (b) 5vol.% Al_2O_3, (c) 7.5vol.% Al_2O_3, (d) 10vol.% Al_2O_3.

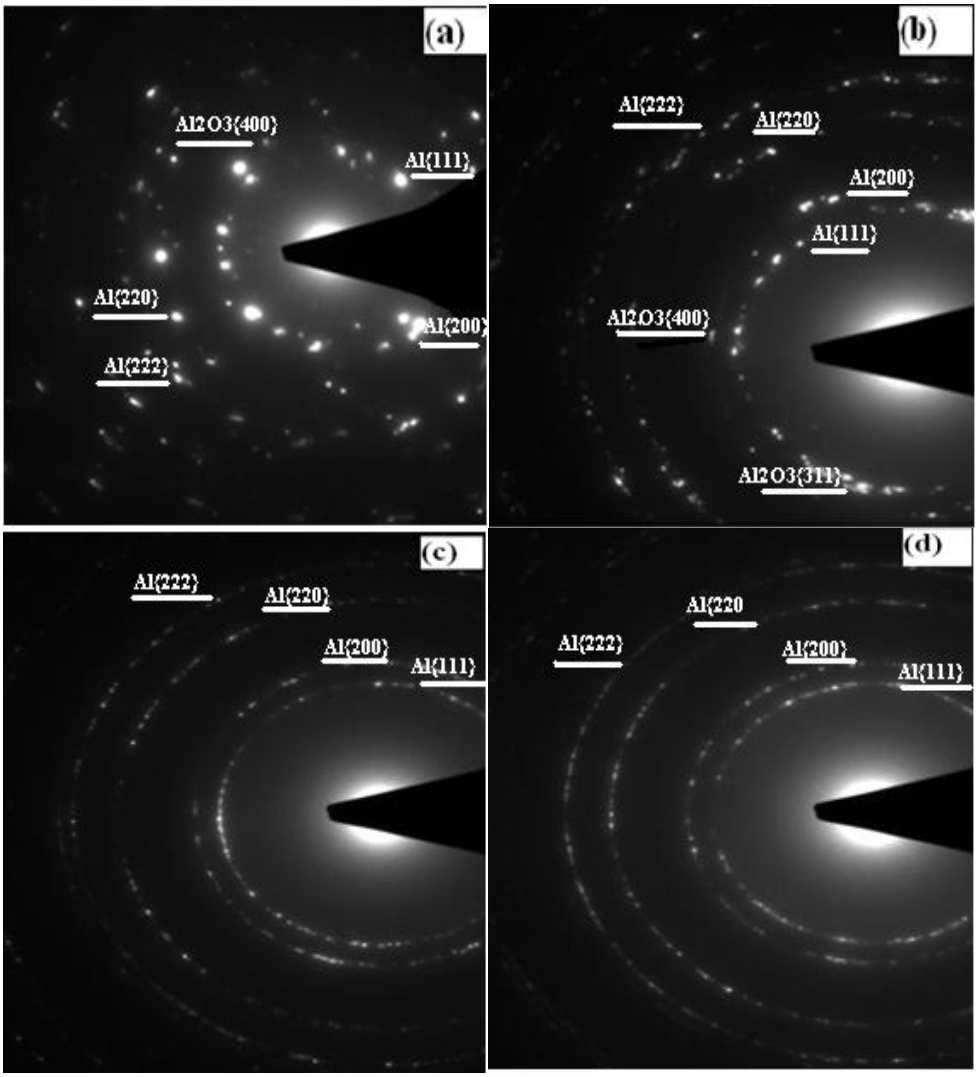

Figure 4.25: SADPs of (a) Al-2.5vol.% Al_2O_3 nanocomposite, (b) Al-5vol.% Al_2O_3 nanocomposite, (c) Al-7.5vol.% Al_2O_3 nanocomposite, and (d) Al-10vol.% Al_2O_3 nanocomposite, corresponding to the TEM images shown in Figure 4.24.

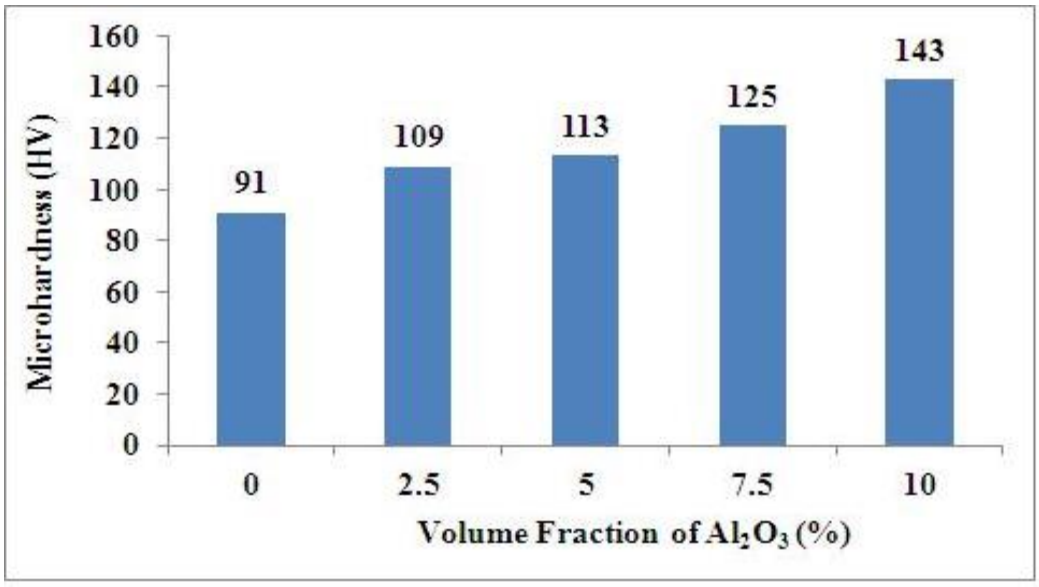

Figure 4.26: Average microhardness of Al and Al-(2.5-10)vol.%Al_2O_3 nanocomposites powder particles produced after 12 hours of milling.

4.4 Al-4wt%Cu-(2.5-10)vol.%SiC nanocomposites powders

Coarse powder particles with sizes in the range of 20-150 µm formed after 12 hours of milling a mixtures of Al powder with 4wt%Cu and 2.5vol.%SiC nanoparticles together with 1wt%PCA(Figure 4.27(a)). When the volume fraction of SiC nanoparticles was 5%, 7.5 % and 10%, the nanocomposite powder particle sizes were in the range of 10-90 µm, 5-120 µm and 5-70µm respectively.

The XRD patterns of the 12 hours milled Al-4wt%Cu- (2.5-10) vol%SiC nanocomposite powders (Figure 4.28) showed a mix of the Al, Cu, and SiC peaks. The Cu and SiC peaks are very weak, and this can be explained by the small volume fractions of Cu and SiC phases. It was clear that with increasing volume fraction of SiC nanoparticles the Al peaks became broader, suggesting a decrease in the Al grain size. The shift in the Al peaks is thought to be caused by a change in lattice parameter as a result of incorporation of alloying elements into the Al lattice to form a solid solution [12]. The average grain sizes and lattice strains of the 12 hours milled Al-4wt.%Cu-(2.5-10)vol.%SiC nanocomposite powders were determined using the Williamson-Hall method, and the results are shown in Figure 4.29.It can be seen that with increasing volume fraction of SiC

nanoparticles inside the nanocomposite powder from 2.5% to 10%, the average grain size of the Al matrix decreased from 333 nm to 83 nm, but the lattice strain changed little and was in the range of 0.25% - 0.37%. One reason of the variations of the lattice strain is caused by the introduction of dislocations, vacancies, impurities and other lattice defects during milling [10, 11].

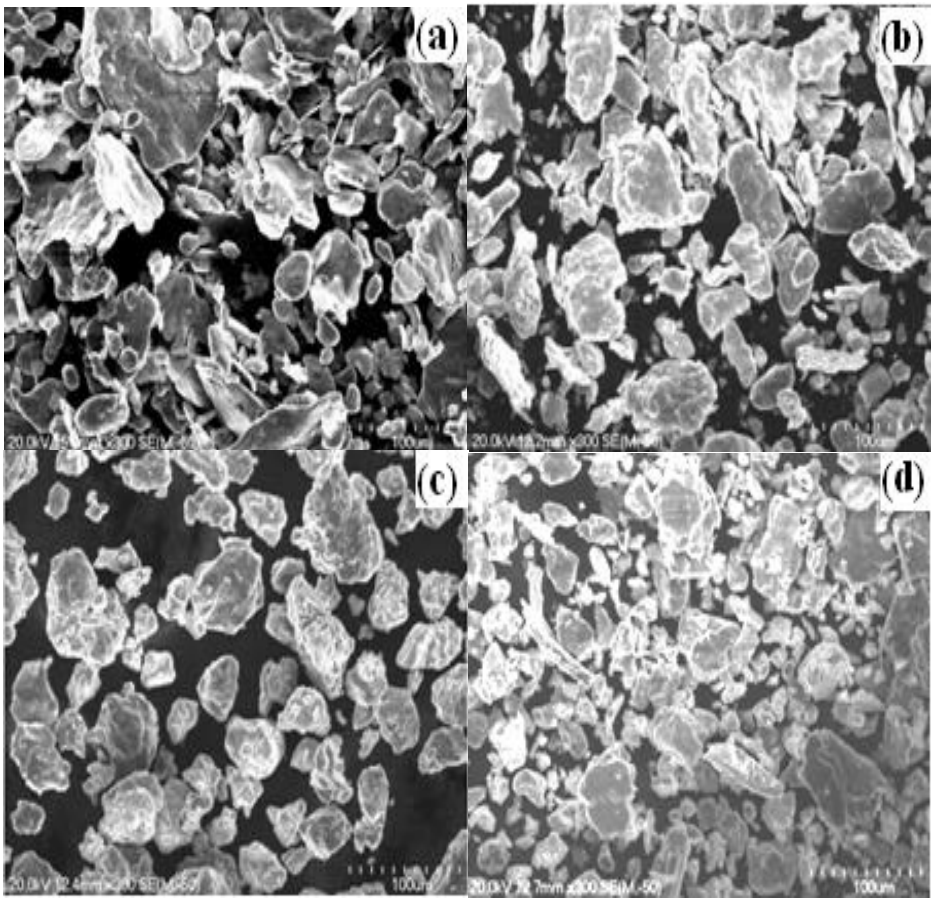

Figure 4.27: SEM micrographs of Al-4wt%Cu-SiC nanocomposites powder particles produced by 12 hours of milling with 1 wt% PCA: (a) 2.5vol.%SiC, (b) 5vol.%SiC, (c) 7.5vol.%SiC, (d) 10vol. %SiC.

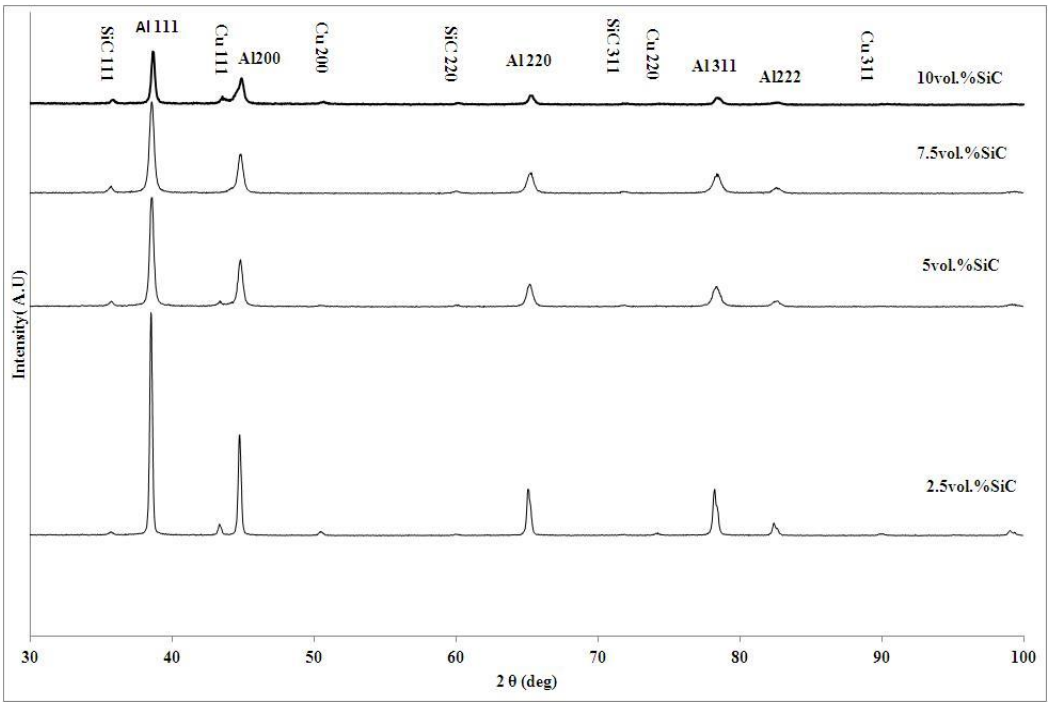

Figure 4.28: XRD patterns of Al-4wt%Cu- (2.5-10)vol% SiC nanocomposite powders produced by 12 hours of milling.

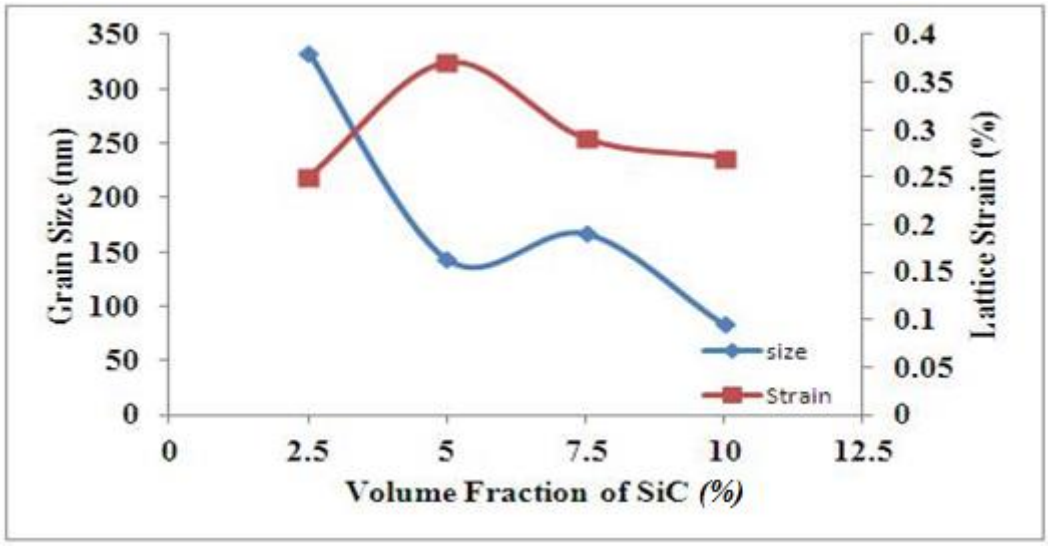

Figure 4.29: Average grain size and lattice strain of Al-4wt.%Cu-(2.5-10)vol.%SiC nanocomposite powders produced by 12 hours of milling as a functions of the volume fraction of SiC nanoparticles.

The microstructure of the Al-4wt%Cu-(2.5-10)vol.%SiC nanocomposite powders particles was examined using TEM. Based on the TEM examination (Figures 4.30 and 4.31), it was clear that the microstructure of the powder particles produced after 12 hours of milling consisted of slightly elongated or equiaxed Al grains containing high dislocation density and had sizes in the range 100-500 nm for Al-4wt%Cu-2.5vol.% SiC, 50-200 nm for Al-4wt%Cu-5vol.% SiC, 50-350 nm for

Al-4wt%Cu-7.5vol.% SiC, and 50-250 nm for Al-4wt%Cu-10vol.% SiC. From the TEM examination, we can see that the grain sizes of the Al matrix decreased slightly as the volume fraction of SiC nanoparticles increased. The SADPs of the nanocomposites powder particles showed {111}, {200}, {220}, and {222} diffraction rings of the Al matrix and weak diffraction spots of {111} and {220} planes of the SiC nanoparticles.

The average microhardness for Al-4wt%Cu- (2.5-10)vol.%SiC composite was also measured and for 12 hours milled Al-4wt%Cu with 2.5%,5%,7.5% and 10% SiC powder particles the microhardness was 122, 154, 180 and 192 HV, respectively. This shows that the microhardness of the nanocomposite powder particles increased significantly with increasing volume % of SiC nanoparticles incorporated within the Al-4wt%Cu matrix.

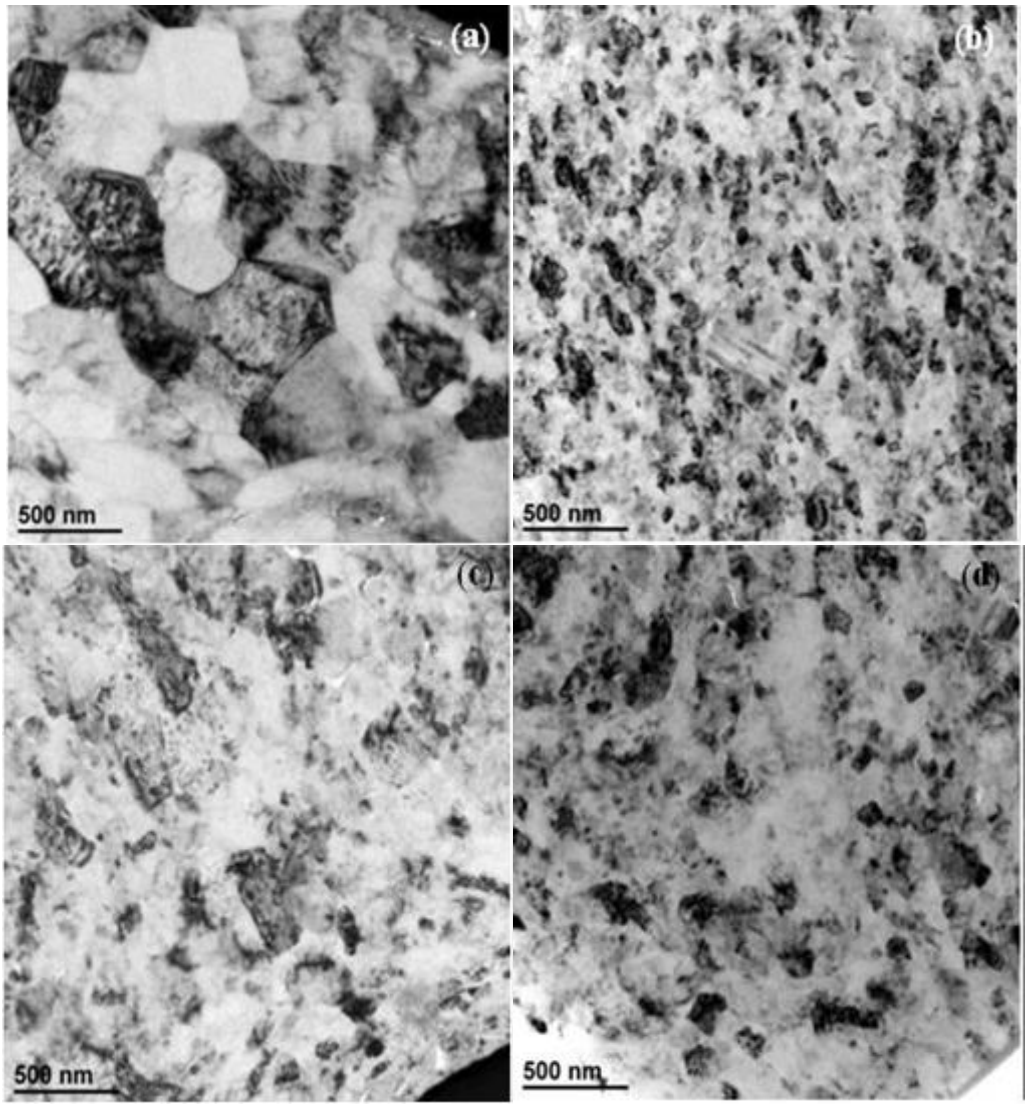

Figure 4.30: TEM bright field images of the microstructures of Al-4wt%Cu-(2.5-10)vol.% SiC nanocomposite powder particles: (a) 2.5vol.% SiC , (b) 5vol.% SiC, (c) 7.5vol.% SiC, (d) 10vol.% SiC.

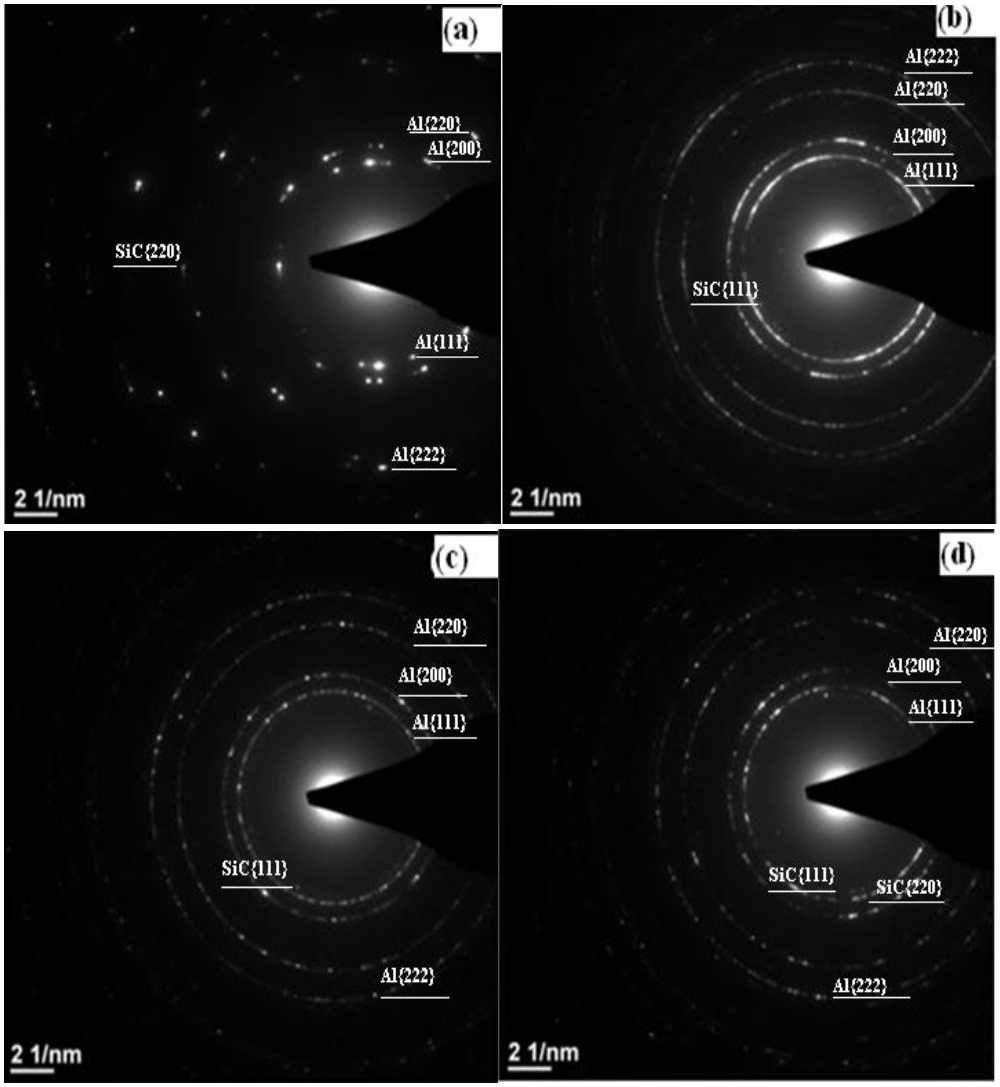

Figure 4.31: SADFs corresponding to the TEM images shown in Figure 3.31: (a) 2.5vol.% SiC , (b) 5vol.% SiC, (c) 7.5vol.% SiC, (d) 10vol.% SiC.

4.5 Al-4wt%Cu-(2.5-10)vol.%SiC micro-composite powders

SEM back scattered electron images of 12 hours milled Al-4wt%Cu- (2.5-10)vol%SiC microcomposites powder particles after different milling times and reinforcement volume fractions are shown in Figure 4.32. The Al_2Cu particles (bright particles in the SEM images in Fig. 4.32) were formed by the reaction between Al and Cu, and had shapes ranging from equiaxed to elongated with diameter or thickness being in the range of 1-20 μm. Figure 4.33 shows the backscattered images for the cross sections of the 12 hours milled Al-4wt.%Cu-(2.5-10)vol.%SiC microcomposites powder particles. Figure 4.34 shows a cross

section of Al-4wt.%Cu-(2.5-10)vol.%SiC but at higher magnification and the SiC micro particles embedded in the Al matrix can be seen.

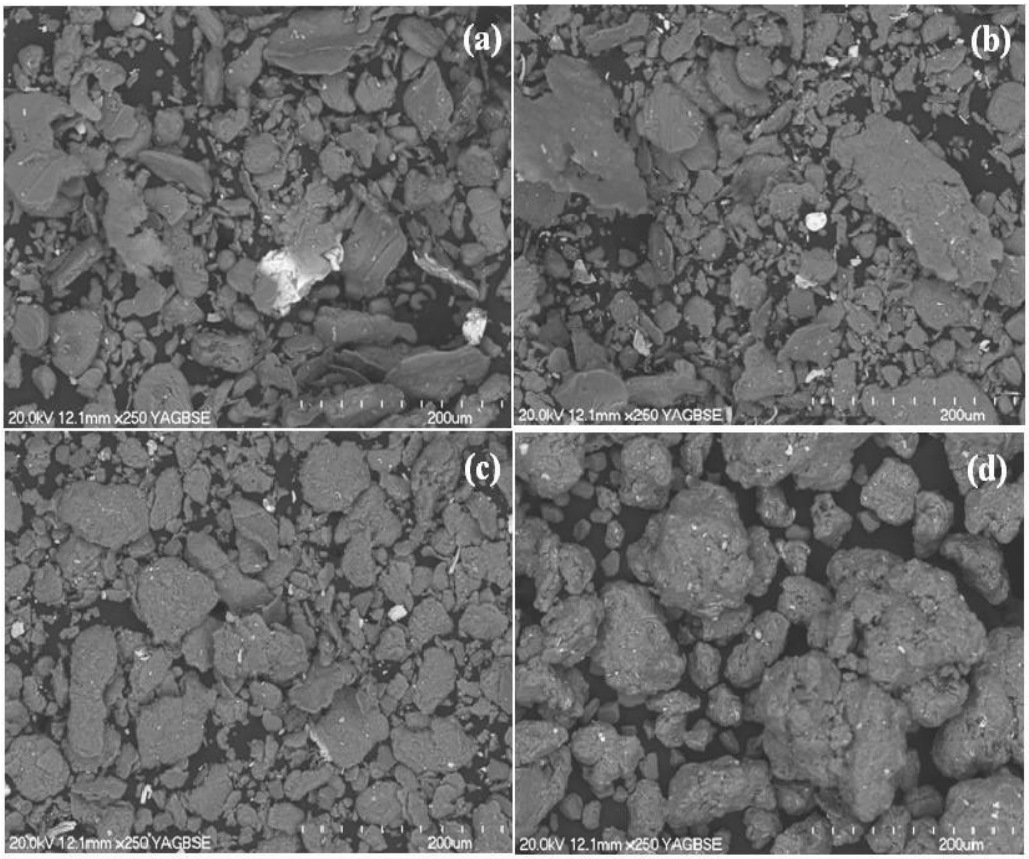

Figure 4.32: SEM backscattered electron images of the 12 hours milled powder of Al-4wt%Cu-SiC microcomposites powder particles: (a) 2.5vol.%SiC, (b) 5vol.%SiC, (c) 7.5vol.%SiC, (d) 10vol. %SiC.

XRD patterns from 12 hour milled Al-4wt%Cu-(2.5-10)vol.%SiC microcomposites powders (Figure 4.35) showed Al, Cu, and SiC peaks. Figure 4.36 shows the results of the average grain sizes and lattice strains of the 12 hours milled Al-4wt. %Cu-(2.5-10)vol.%SiC microcomposites powders. It can be seen that with increasing the volume fraction of SiC micro particles from 2.5% to 10%, the average grain size of the Al matrix increased from 167nm to 200 nm. In the meantime, the lattice strain changed little, being in the range of 0.10- 0.26%. Like alumina particles discussed previously, SiC particles will impede matrix grain growth. Smaller SiC particles are generally less effective in pinning moving grain boundaries, and since the SiC particle size was decreased by about 85% after

mechanical milling, this explains the varying estimated average grain size after 12 hours of milling [13].

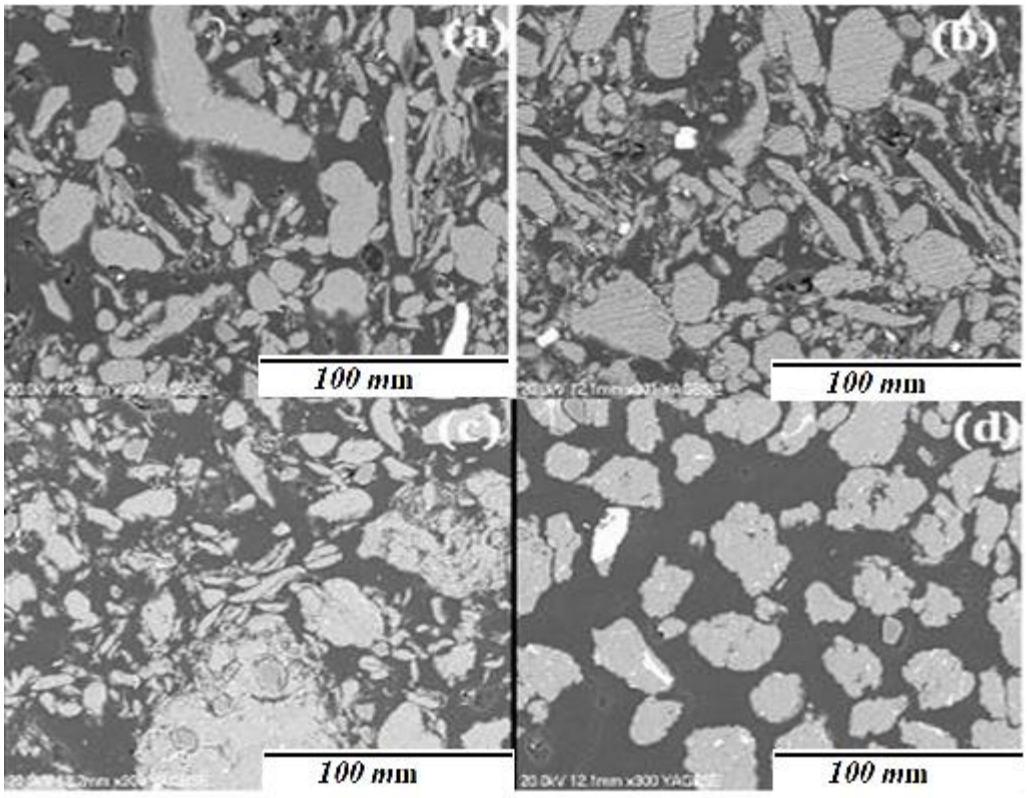

Figure 4.33: SEM backscattered electron images of the cross sections of the Al-4wt%-(2.5-10)vol.% SiC microcomposites powder particles produced by 12 hours of milling: :(a) 2.5vol.%SiC, (b) 5vol.%SiC, (c) 7.5vol.%SiC, (d) 10vol. %SiC. (20.0 kv 12.1mmX300 YAGBSE)

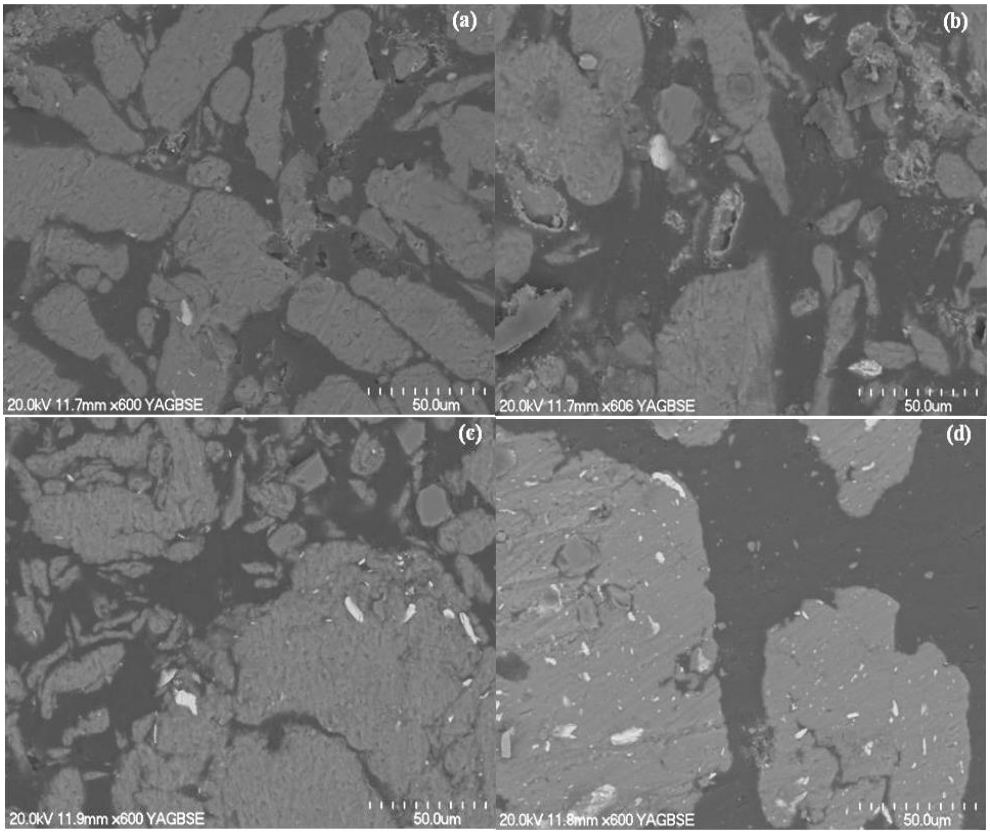

Figure 4.34: High magnification SEM backscattered electron images of the cross sections of the Al-4wt%-(2.5-10)vol.% SiC microcomposites powder particles produced by 12 hours of milling: :(a) 2.5vol.%SiC, (b) 5vol.%SiC, (c) 7.5vol.%SiC, (d) 10vol. %SiC.

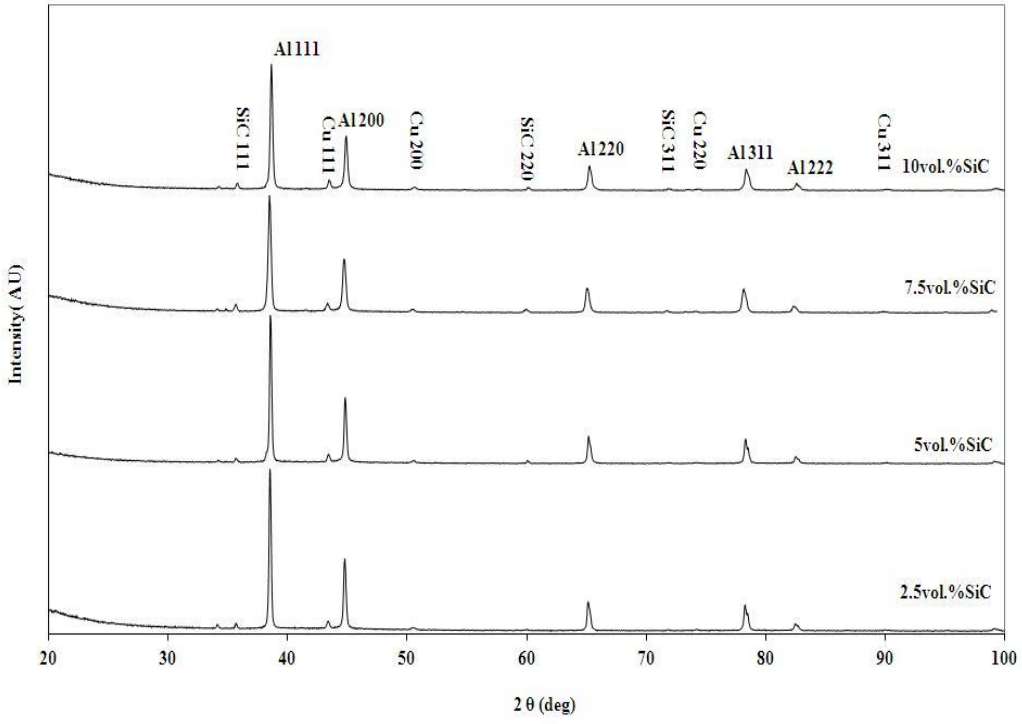

Figure 4.35: XRD diffraction patterns of Al-4wt%Cu- (2.5-10)vol%SiC microcomposites powders produced by 12 hours of milling.

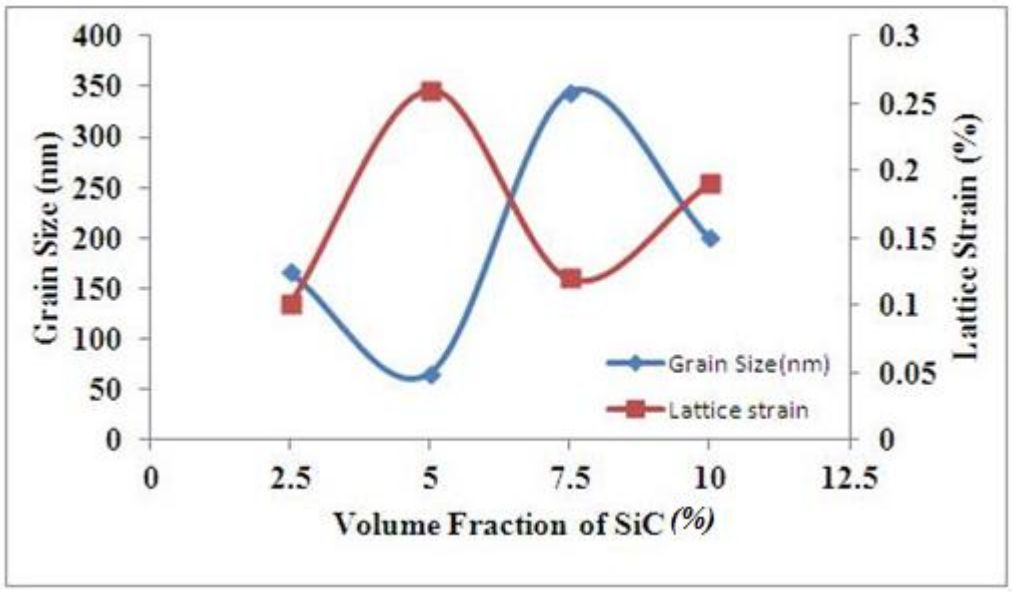

Figure 4.36: Average grain size and lattice strain of Al-4wt.%Cu-(2.5-10)vol.%SiC micro composite powders produced by 12 hours of milling as a functions of the volume fraction of SiC.

Figure 4.37 show the SEM micrographs of the cross-sections of Al-4wt%Cu-(2.5-10)vol%SiC micro-composite powder particles and corresponding EDX elemental mappings for Al, Si, and Cu. It can be seen that the SiC particles with sizes in the range of 0.5 to 25 μm are incorporated into the metal matrix particles. The average particle size of the starting SiC powder was 40 μm, so it is clear that the SiC particle sizes are significantly reduced due to fracturing of the SiC particles caused by milling.

The average microhardness of the Al-4wt%Cu- (2.5-10)vol.%SiC microcomposites powder particles produced after 12 hours milling (Figure 4.38) was much higher than that for Al powder particles, but changed little with increasing volume fraction of the micrometre sized SiC particles. This might be due to the non-uniform distribution of the SiC particles among the powder particles as shown by EDX elemental mappings in Figure 4.37.

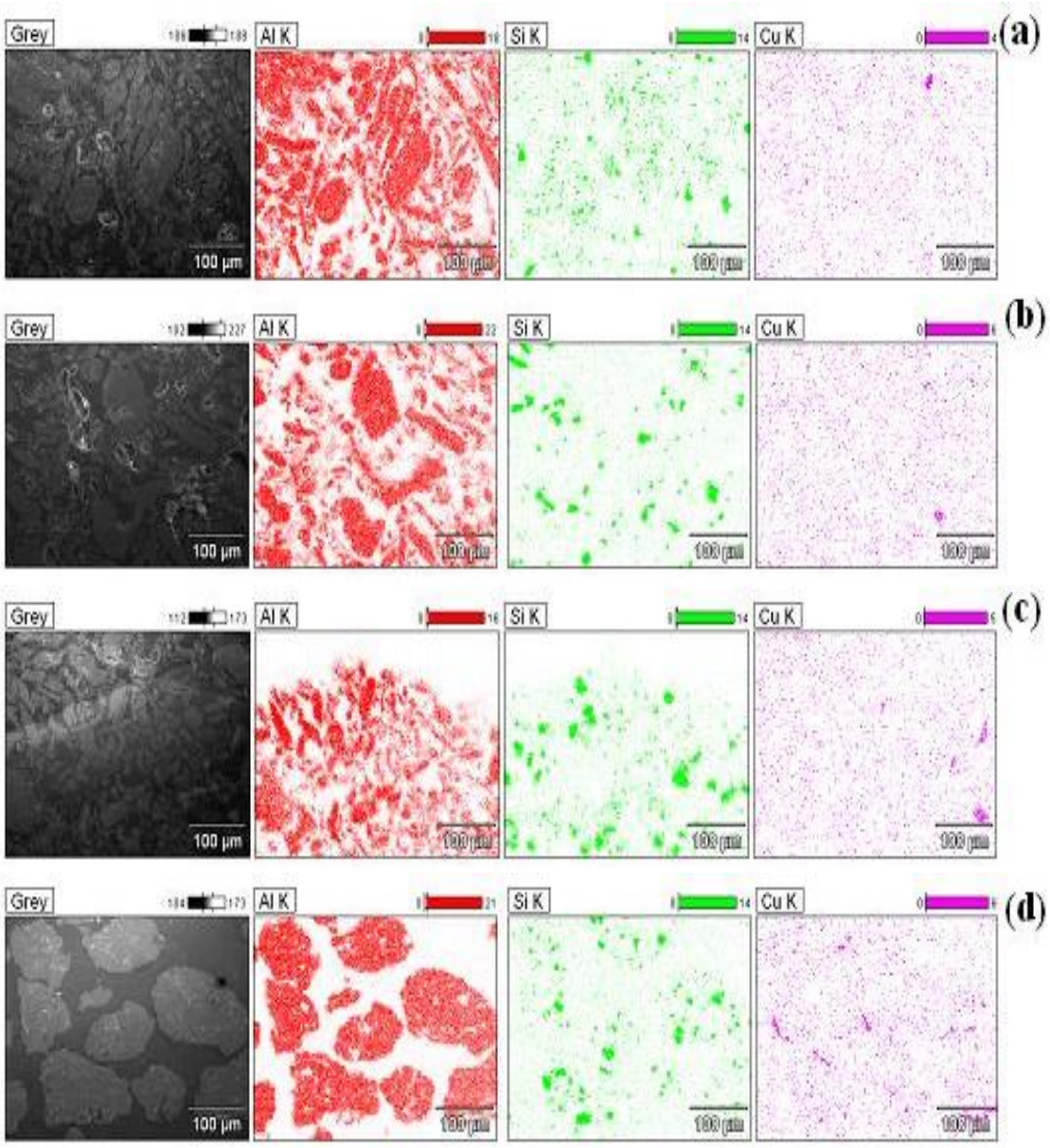

Figure 4.37: SEM micrographs and corresponding energy dispersive X-Ray Elemental (Al, Si, and Cu) maps of the cross section of Al-4wt%Cu-(2.5-10)vol.%SiC micro composite powder particles after 12 hours of milling: (a) 2.5vol%SiC , (b) 5vol%SiC , (c)7.5vol%SiC, and (d)10vol%SiC.

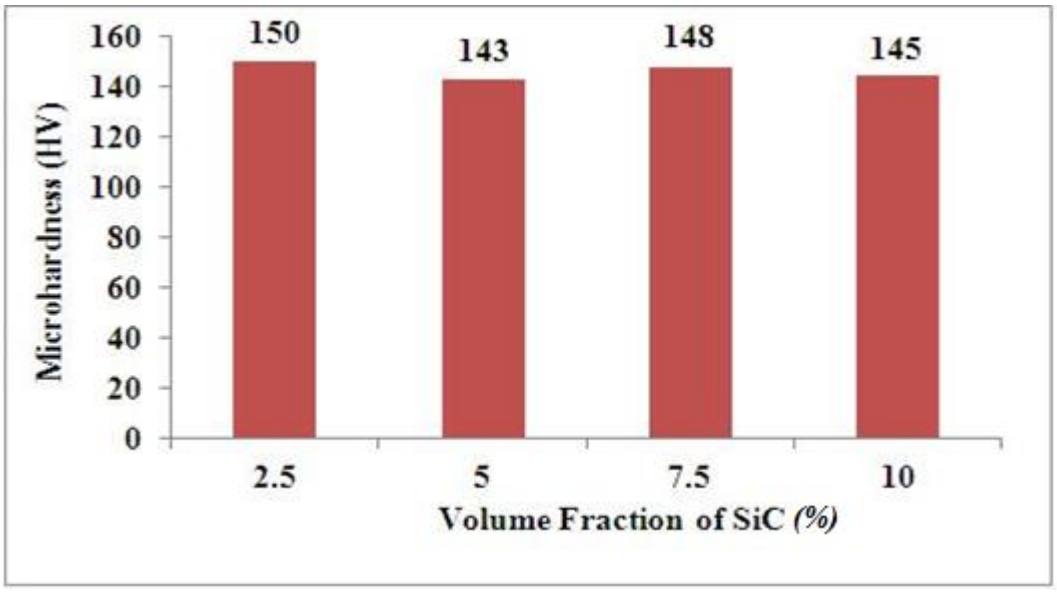

Figure 4.38: Average microhardness of Al-4wt%Cu- (2.5-10) vol.%SiC micro-composites powder particles produced after 12 hours of milling.

4.6 Discussion

4.6.1 Mechanical milling

High energy ball milling has been previously used to consolidate ductile powders such as Al- Al_2O_3 [14, 15], Al-Cu-Al_2O_3 [9], and Al-Cu-SiC [16]. The high energy ball milling of elemental powders resulted in producing powders/balls/granules after 12 and 24 hours of milling with or without using 1wt% PCA. This is used to prevent sticking of the milled powders to the discs or surface of the balls and the inner walls of the vial and to achieve a proper balance between cold welding and fracture when milling ductile materials. Milling was carried out for a maximum 12 hours of net time only, because by using 1 wt% of PCA a sufficient amount of powder with a negligible amount of loose powder was produced (Where the amount produced was >95% from starting powders). The oxygen content in the manufactured composite powder was not measured before and after milling, because the Al powder is already surrounded with a protective layer of aluminium oxide, which makes it difficult to measure the actual oxygen content of the powders. HEMM in which the process of creates a large number of

new surfaces due to the smaller size of the particles and the increased surface area attracts oxygen during the passivation of the milled powder.

Mechanical milling is feasible for dispersing reinforcement particles within the matrix, but with increased milling time there is no significant effect on microstructure because a steady-state condition is reached. This was noticed with alumina powders because they become very fine and higher energy is required to achieve ultra-fine particles. This study is in agreement with Zhang`s findings [17] and very effective way dispersing nanoscaled Al_2O_3 or SiC particles into small grain sized.

4.6.2 Effect of Nanoparticles on Milling

It appears that the addition of ceramic particles (Al_2O_3) to Al powder broadens the full-width at half-maximum (FWHM) aluminium XRD peaks, with a slight shift in the position of the XRD peaks being noticed. This can be explained by the effect on the lattice spacing of dissolution of impurities, particularly iron, in the lattice of aluminium. Based on the broadening of the XRD patterns and applying the Williamson-Hall method the average grain size of the Al-(2.5-10)vol.%Al_2O_3 nanocomposites and Al-4wt%Cu-(2.5-10)vol.%SiC ultra-fine grained and nanocomposites was reduced with 12 hours milling time and with an increasing volume of the reinforcement within the matrix. This was caused by severe plastic deformation affecting the elemental powders and the refining effect of adding the hard reinforcing particles to the Al powders. This is in agreement with Hesabi et.al [18] who found that the crystallite size of the Al powder decreased with the addition of ceramic particles especially in the case of nanoscaled alumina. XRD analysis revealed that the crystallite size of the aluminium matrix in the composite powders is smaller than that of the unreinforced aluminium. The addition of hard particles accelerates the milling process, leading to a faster work hardening rate

and fracture of the aluminium matrix. The acceleration of the grain refinement process by adding alumina particles can be attributed to the generation of a high dislocation activity, owning to interaction between the hard particles and dislocations. Because Al_2O_3 particles are hard and non-deformable, they can hinder dislocation movement, leading to an increase in the dislocation density. If the hard particles are small enough (<1 μm), the Orowan bowing mechanism leads to dislocation multiplication. The increased dislocation density accelerates the grain refining progress. Therefore, the grain refining process in the nanocomposite powder should be accelerated [18, 19].

XRD analysis and TEM images showed no evidence of new phase formation within the matrix. The nano sized Al_2O_3 and SiC particles were uniformly distributed within the soft ductile aluminium matrix as shown in Figures 4.23 and 4.30. A theory which explains a mechanism for this is as follows; **(1)** the very small size of reinforcements in nano measures in comparison to the size of the matrix (the Al grain size was fixed to be 40 μm in this study) **(2)** planetary mills can deliver a high energy density which creates a bigger mechanical impact on materials compared with other milling devices [20]. The difference in speeds between the balls and grinding jars produces an interaction between frictional and impact forces, which releases high dynamic energies [21] where the kinetic energy will be very high (at the interface surface of contact of the steel balls used for milling during MA). This result in high temperature generation at the point of contact, which softens the Al powder squeezed in between the balls and due to the force of impact, the nano reinforcement can penetrate the soft ductile surface of the Al so that the reinforcement becomes embedded.

The microhardness increased slightly with an increasing volume of reinforcement within the matrix and increased milling time due to strain hardening during

milling and high dislocation density in the heavily cold worked material. This indicates how the microhardness is affected by the composition of the material and the stage reached during milling. The overall microstructure was found to be homogeneous with grain sizes fluctuating between submicrometer and nanometres. It is noteworthy to point out that the reduction in the average crystallite size could also make a partial contribution to the resultant composite hardness due to grain refinement leading to grain size strengthening. It is also important to mention that plastic deformation caused by mechanical alloying generates lattice defects, such as dislocations, in the Al matrix. It is thought that these defects and their interaction with Al_2O_3nanoparticles contributes to the hardness increment [22].Slower rate in increasing of microhardness for Al-4wt%Cu-(2.5-10)vol.% SiC may be attributed to the completion of alloying and dynamic recovery due to high work hardening effects of deformed Al–Cu powders. It may be even ascribed to static recovery of high deformed Al matrix with local increase of temperature in particles during collisions [10].

4.7 Summary

In this study HEMM was used to fabricate UFG and nanostructured Al- (2.5-10) vol. %Al_2O_3 composite with a dispersion of nano alumina within the matrix and Al-4wt%Cu- (2.5-10) vol%SiC with two different sizes of SiC in micrometre and nanometre range. A sufficient amount of powder was produced after milling powders for 12 hours with a milling speed of 400 rpm and with the use of 1wt% of process control agent. The microstructure of the composite powder/balls/granules was studied in order to understand the morphology and microstructure evolution mechanism during HEMM and with changing volume percent of reinforcement added to the matrix. The SiC and Al_2O_3 nanoparticles were embedded into the aluminium matrix due to the high surface strain during

mechanical milling and the very small size of the embedded reinforcement particles relative to the size of the Al particles. The average microhardness increased with increasing volume fraction of reinforcement within the matrix.

4.8 References

[1] R. Sen, S. Das, and K. Das, "Effect of stirring rate on the microstructure and microhardness of Ni–CeO2 nanocomposite coating and investigation of the corrosion property," *Surface and Coatings Technology,* vol. 205, pp. 3847-3855, 3/25/ 2011.

[2] S. M. Zebarjad and S. A. Sajjadi, "Dependency of physical and mechanical properties of mechanical alloyed Al-Al_2O_3 composite on milling time," *Materials & Design,* vol. 28, pp. 2113-2120, 2007.

[3] B.Prabhu, C.Suryanarayana, L.An, and R.Vaidyanathan, "Synthesis and characterization of high volume fraction Al-Al_2O_3 nanocomposite powders by high-energy milling " *Materials Science and Engineering A,* vol. 425, pp. 192-200, 2006.

[4] G. K. Williamson and W. H. Hall, "X-ray line broadening from filed aluminium and wolfram," *Acta Metallurgica,* vol. 1, pp. 22-31, 1953.

[5] M. Zabihi, M. R. Toroghinejad, and A. Shafyei, "Application of powder metallurgy and hot rolling processes for manufacturing aluminum/alumina composite strips," *Materials Science and Engineering: A,* vol. 560, pp. 567-574, 2013.

[6] S.M.Zebarjad and S.A.Sajjadi, "Microstructure evaluation of Al-Al_2O_3 composites produced by mechanical alloying method," *Materials and Design,* pp. 684-688, 2006.

[7] Z. r. Hesabi, A.Simchi, and S. M. S. Reihani, "Structural evolution during mechanical milling of nanometric and micrometric Al_2O_3 reinforced Al matrix composites," *Materials Science and Engineering A,* vol. 428, pp. 159-168, 2006.

[8] M. S. Selamat, L. M. Watson, and T. N. Baker, "XRD and XPS studies on surface MMC layer of SiC reinforced Ti–6Al–4V alloy," *Journal of Materials Processing Technology,* vol. 142, pp. 725-737, 2003.

[9] H.Arami and A.Simchi, "Reactive milling synthesis of nanocrystalline Al-Cu/Al_2O_3 nancomposite," *Materials Science and Engineering A,* vol. 464, pp. 225-232, 2007.

[10] J. Safari, G. H. Akbari, and M. Delshad Chermahini, "The effect of reinforcement content and milling time on microstructure and mechanical properties of Al–10Mg/Al_2O_3 nanocomposites," *Materials Science and Engineering: A,* vol. 569, pp. 86-91, 2013.

[11] C. Suryanarayana, "Mechanical alloying and milling," *Progress in Materials Science,* vol. 46, pp. 1-184, 2001.

[12] A. Mukhtar, "Microstructure, Thermal Stability and Consolidation of Nanostructured and Ultrafine Structured Cu based Metal Matrix

Composite and Alloy powders Produced by High Energy Mechanical Milling," Doctor of Philosophy, Materials and Process Engineering, University of Waikato, Hamilton, 2010.

[13] S. Gustafsson, L. K. L. Falk, E. Lidén, and E. Carlström, "Pressureless sintered Al_2O_3–SiC nanocomposites," *Ceramics International,* vol. 34, pp. 1609-1615, 2008.

[14] K. D. Woo and H. B. Lee, "Fabrication of Al alloy matrix composite reinforced with subsive-sized Al_2O_3 particles by the in situ displacement reaction using high-enegy ball-milled powder," *Materials Science and Engineering A,* vol. 449-451, pp. 829-832, 2007

[15] A. H. Monazzah, A.Simchi, and S. M. S. Reihani, "Creep behavior of hot extruded Al-Al_2O_3 nanocomposite powder," *Materials Science and Engineering A,* vol. 527, pp. 2567-2571, 2010.

[16] Y.B.Liu, J.K.M.Kwok, S.C.Lim, L.Lu, and M.O.Lai, "Fabrication of Al-4.5Cu/15SiC_p composites: I.Processing using mechanical alloying," *Journal of Materials Processing Technology,* vol. 37, pp. 441-451, 1993.

[17] D.L.Zhang, "Processing of advanced materials using high-energy mechanical milling," *Progress in Materials Science,* vol. 49, pp. 537-560, 2004.

[18] Z. r. Hesabi, A.Simchi, and S. M. S. Reihani, "Structural evolution during mechanical milling of nanometric and micrometric Al_2O_3 reinforced Al matrix composites," *Materials Science and Engineering A,* vol. 428, pp. 159-168, 2006.

[19] I. Ozdemir, S. Ahrens, S. Mucklich, and B. Wielage, "Nanocrystalline Al-Al_2O_3 and SiC_p composites produced by high-energy ball milling," *Journal of Materials Processing Technology,* vol. 205, pp. 111-118, 2008.

[20] M.Huller,G.G.Chernik,E.L.Fokina, and N.I.Budim **"**Mechanical alloying in planetary mills of high accelerations," Rev.Adv.Mater.Sci, vol.18,pp.366-374,2008.

[21] R. S. I. M. a. Seiving. *Planetary Ball Mill PM 100*.

[22] J. L. H. Rivera, J. J. C. Rivera, V. P. d. Ángel, V. G. Febles, O. C. Alonso, and R. Martínez-Sánchez, "Structural and morphological study of a 2024 Al-Al2O3 composite produced by mechanical alloying in high energy mill," *Materials and Design,* vol. 37, pp. 96-101, 2012.

Chapter Five: Microstructure and Mechanical Properties of Bulk Ultrafine Structured Al-(2.5-10) vol.%Al_2O_3 Nanocomposites Produced by Powder Consolidation

5.1 Introduction

This chapter reports and discusses the results of a study on the microstructures and mechanical properties of bulk ultrafine structured Al-(2.5-10)vol.%Al_2O_3 nanocomposite produced by consolidation of nanostructured Al-(2.5-10) vol.%Al_2O_3 nanocomposite powders using powder compact forging and powder compact extrusion. The nanostructured Al-(2.5-10)vol.%Al_2O_3 nanocomposite powders were produced by high energy mechanical milling, as outlined in Chapter 3. The microstructure and mechanical properties of bulk ultrafine structured Al samples produced in the same way were compared. The purpose of this study is to achieve an understanding of the consolidation behaviour of nanostructured Al and Al-(2.5-10)vol.%Al_2O_3 nanocomposite powders and the relationships between the microstructures and mechanical properties of the consolidated samples.

5.2 Microstructures of Consolidated Samples Produced by Powder Compact Forging

Powder compacts were produced with a diameter of 25 mm and a height in the range of 29-35 mm, as shown in Figure 5.1. The densities of all powder compacts were determined by measuring their weights and dimensions. The theoretical densities of Al–(2.5-10)vol.%Al_2O_3 nanocomposites were calculated by using the rule of mixtures :

$$\rho_{composite} = \rho_{Al}V_{Al} + \rho_{Al2O3}V_{Al2O3} \quad \text{.....Equation 5.1}$$

Where ρ is the density of the material and V is the volume fraction. As shown in Table 5.1, the relative density of the Al–2.5vol.%Al_2O_3 nanocomposites powder compacts were higher than that of the Al powder compact. However for higher alumina contents the relative density decreased with increasing volume fraction of

Al_2O_3 nanoparticles. This is likely to be due to the increase of hardness of the mechanically milled Al–(2.5-10)vol.%Al_2O_3 nanocomposite powder particles with increasing volume fraction of Al_2O_3 nanoparticles, as shown in Chapter 4. As the hardness of the powder particles increases, their ability to deform under the same pressing pressure reduces and thus there is a lower degree of compact densification.

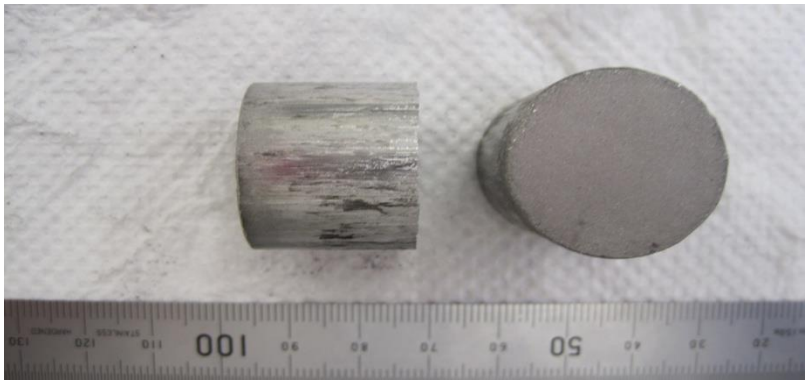

Figure 5.1: Side and top views of an Al–2.5vol.%Al_2O_3 nanocomposites powder compact .

Table 5.1: Theoretical and relative density of Al and Al –(2.5-10)vol.%Al_2O_3 nanocomposites and the corresponding powder compacts

Composition	Theoretical density (g/cm^3)	Density of compact (g/cm^3)	Relative density of compact (%)	Height of compact (mm)
Al-1wt%PCA	2.7	2.24	83.09	31.79
Al-2.5vol%Al_2O_3	2.73	2.40	87.98	29.75
Al-5vol%Al_2O_3	2.76	2.17	78.62	32.84
Al-7.5vol%Al_2O_3	2.79	2.18	78.402	32.52
Al-10vol%Al_2O_3	2.82	2.02	71.71	35.34

For powder compact forging experiments, the powder compacts were heated to 450 ºC using induction heating under argon atmosphere, and then forged using an open die set kept at room temperature. A 100-ton hydraulic press with a ram travelling speed of 7.7 mm/s was used to drive the open die halves for the forging experiments. The height reduction of the powder compact caused by the up-set forging was in the range of 82-88%. Circular discs were produced from the powder compact forging experiments, as shown in Figure 5.2. Tensile test

specimens were cut from the centre of the forged discs by using an electrical discharge machining (EDM) wire cutter. The density of the forged discs was determined using Archimedes method, and the values are shown in Table 5.2.

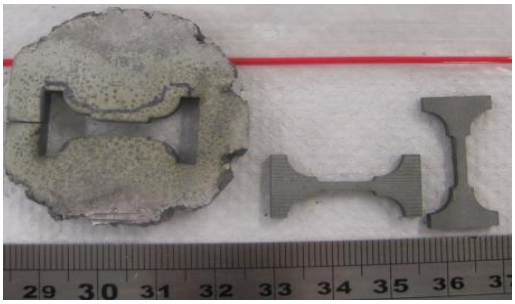

Figure 5.2: Images of an Al-5vol.%Al_2O_3 nanocomposites disc produced by PCF and two tensile test specimens cut from the disk.

Table 5.2: Theoretical and relative density of Al – (2.5-10)vol.%Al_2O_3 nanocomposite disks produced by PCF.

Composition	Theoretical density (g/cm^3)	Density of forged discs (g/cm^3)	Relative density of forged discs (%)	Height of forged (mm)
Al-1wt%PCA	2.7	2.477	91.7	4.98
Al-2.5vol%Al_2O_3	2.73	2.576	94.38	5.6
Al-5vol%Al_2O_3	2.76	2.549	92.36	5.4
Al-7.5vol%Al_2O_3	2.79	2.600	93.19	5.37
Al-10vol%Al_2O_3	2.82	2.599	92.17	4.55

Figures 5.3 show SEM micrographs of the cross sections of Al, and Al-(2.5-10) vol. %Al_2O_3 nanocomposite discs produced by PCF. It was observed that the volume fractions of pores in the discs produced by powder compact forging were very low. This is not in agreement with the relative densities of the discs measured using the Archimedes method and shown in Table 5.2. This significant discrepancy may be due to inappropriate use of Archimedes method for measuring density given the small mass and sizes of the specimens used.

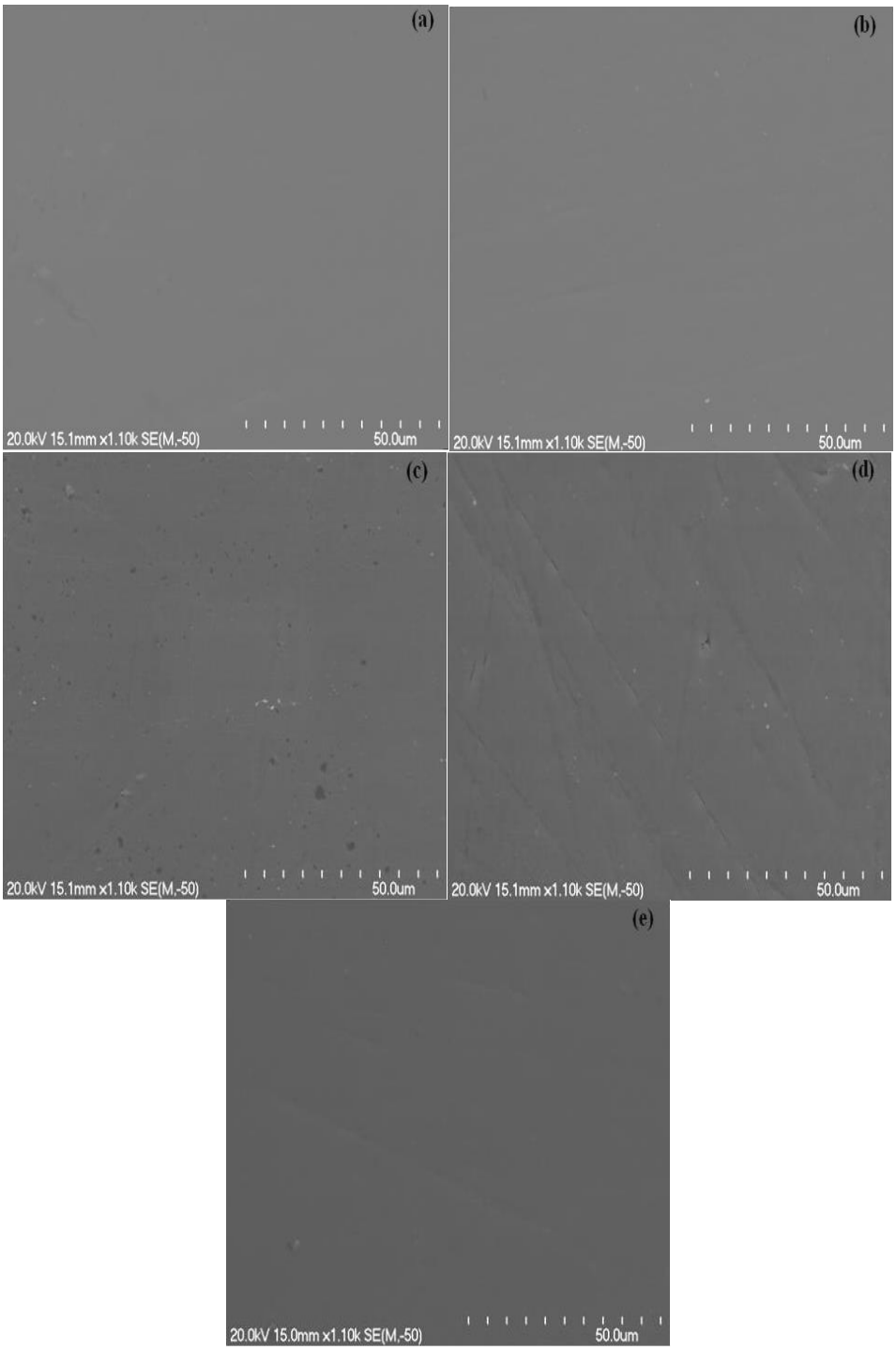

Figure 5.3: SEM micrographs of Al and Al-(2.5-10)vol.%Al_2O_3 nanocomposites discs produced by PCF: (a) Al , (b) 2.5vol.%Al_2O_3 , (c) 5vol.%Al_2O_3 , (d) 7.5vol.%Al_2O_3 ,(e) 10vol.%Al_2O_3 .

Figure 5.4 shows XRD patterns of Al and Al-(2.5-10)vol.%Al_2O_3 nanocomposite discs produced by PCF. They only show the Al peaks, but no Al_2O_3 peaks. This might be due to the small sizes and low volume fractions of Al_2O_3 nanoparticles and the low X-ray diffraction intensity of γ-Al_2O_3. The XRD patterns also showed that the Al peaks of Al-(7.5-10)vol.%Al_2O_3 nanocomposites slightly shifted to

higher angles compared to those of Al and Al-(2.505)vol.%Al_2O_3 nanocomposites. The average grain sizes and the lattice strain of the Al, Al- (2.5-10)vol.%Al_2O_3 nanocomposites discs were estimated based on the broadening of the XRD peaks and use of the Williamson-Hall method. The results are shown in Figure 5.5. The average grain size and lattice strain of Al-2.5vol.%Al_2O_3 nanocomposite discs were 200 nm and 0.20% , respectively, both much lower than those of the Al disk. When the volume fraction of Al_2O_3 nanoparticles was increased to 5%, the average grain size and lattice strain increased to 500 nm and 0.46% respectively. By further increasing the volume fraction of Al_2O_3 nanoparticles to 7.5%, the grain size and lattice strain decreased to 250 nm and 0.27% respectively. An increase of the volume fraction of Al_2O_3 nanoparticles to 10 vol%, had a little effect on the grain size and lattice strain. This is because of the thermal stability of the microstructure of the Al-(2.5-10)vol.% Al_2O_3 matrix of the nanocomposites, which increases with increasing volume fraction of the Al_2O_3 nanoparticles. This slower rate of microstructural coarsening with increasing Al_2O_3 nanoparticles content has been explained by other researchers as caused by the Zener-drag effect, where the nanoparticles resist the movement of grain boundaries [1], however no physical evidence for this was found in the TEM images presented in this work.

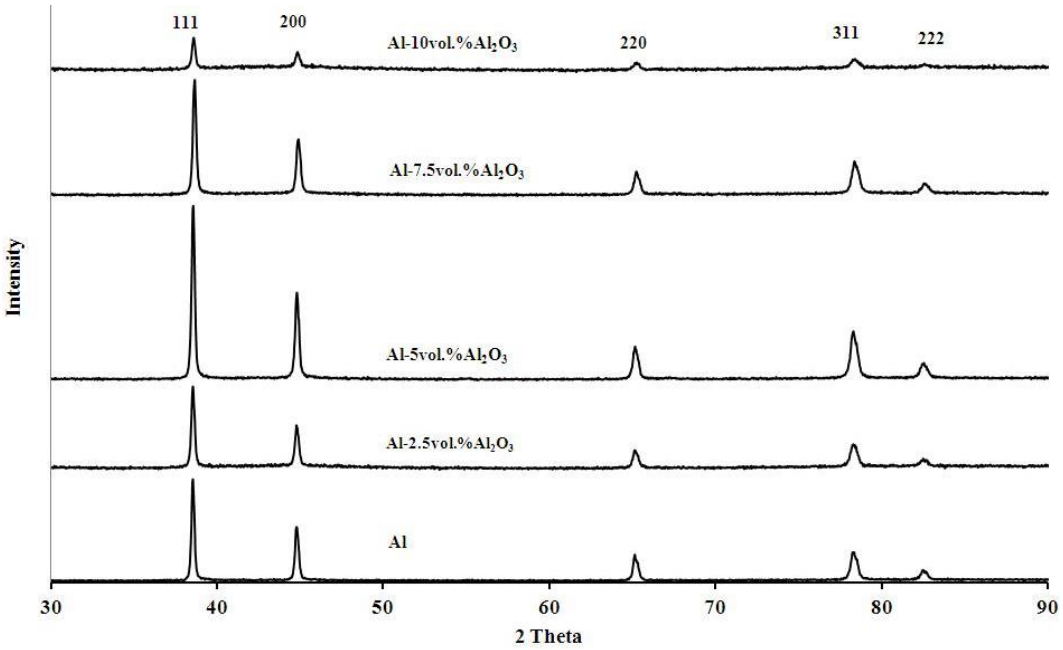

Figure 5.4: XRD patterns of Al and Al-(2.5-10)vol.%Al_2O_3 nanocomposite disks produced by PCF.

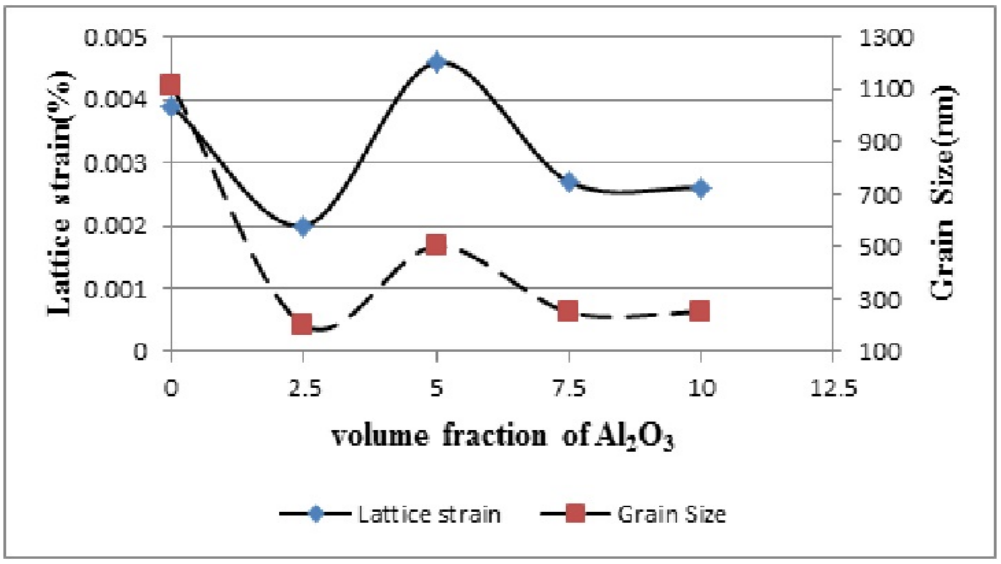

Figure 5.5: Average grain sizes and lattice strain of the Al and Al-(2.5-10)vol.%Al_2O_3 nanocomposites discs produced by PCF.

TEM was utilised to examine the microstructures of the Al and Al-(2.5-10)vol.% Al_2O_3 nanocomposites disks produced by PCF. As shown by the TEM bright field images (Figure 5.6), the Al matrix and Al-2.5vol.% Al_2O_3 nanocomposite discs had an ultrafine grained (UFG) microstructure consisting of Al grains with sizes ranging 100-700 nm and 100-500 nm, respectively. When the volume fraction of Al_2O_3 was increased to 5%, 7.5% and 10%, the Al matrix grain size range changed to 50-450 nm, 50-400 nm, and 50-300 nm, respectively. This

shows that the average grain size of the Al matrix decreases with increasing volume fraction of the Al_2O_3 nanoparticles. This is in general agreement with the trend in grain size changes with increasing volume fraction of Al_2O_3 nanoparticles from XRD analysis (Figure 5.5). The grain size values estimated from XRD peaks broadening (Figure 5.4) are in general agreement with the actual average grain sizes of the Al matrix observed by TEM. The TEM examination also shows that the Al grains contained a high density of dislocations.

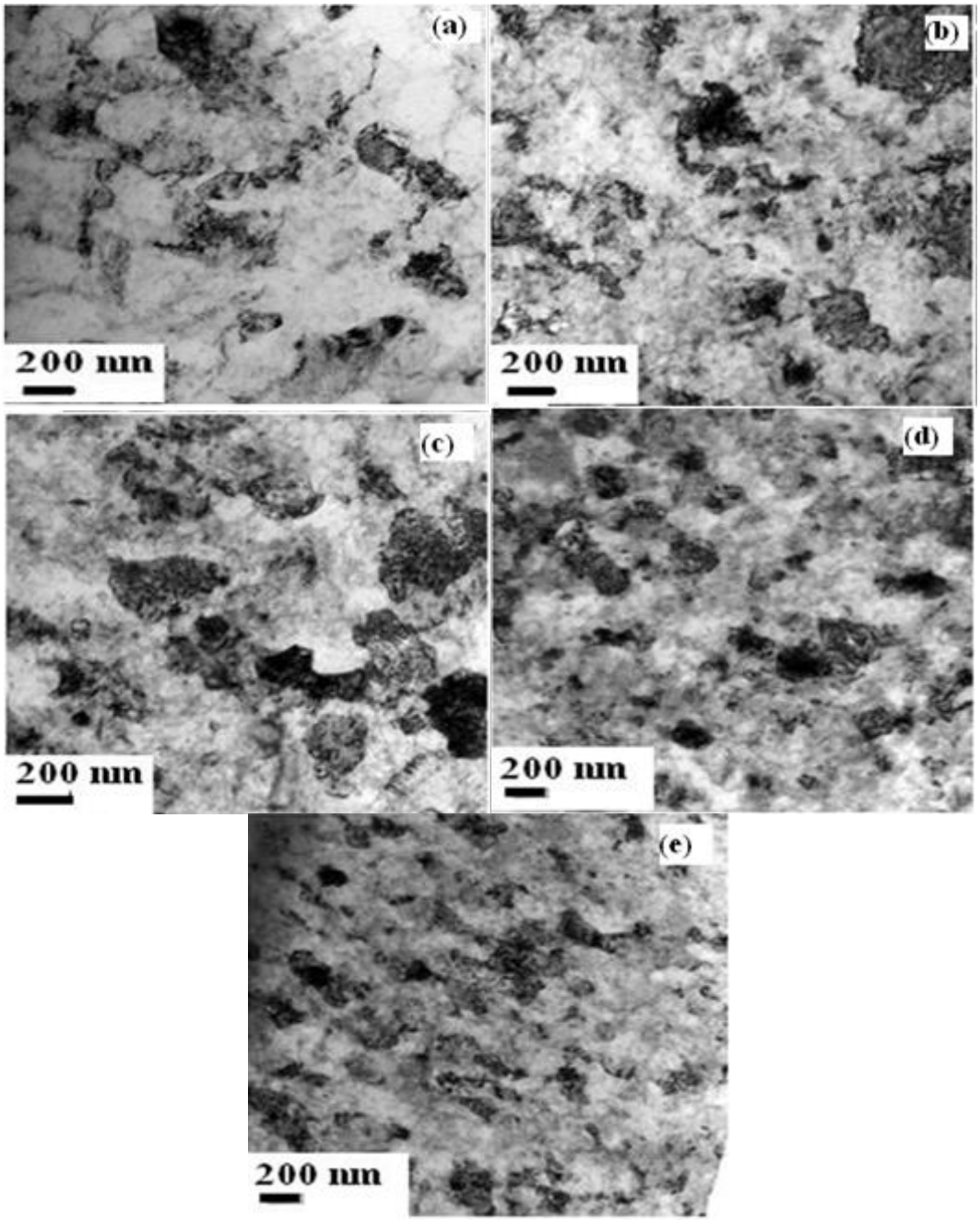

Figure 5.6: TEM bright field images of Al and Al-(2.5-10)vol.% Al_2O_3 nanocomposite discs produced by powder compact forging : (a) Al , (b) 2.5vol.% Al_2O_3,(c) 5vol.% Al_2O_3, (d) 7.5vol.% Al_2O_3, (e) 10vol.% Al_2O_3.

5.3 Mechanical Properties and Fracture Behaviour of Consolidated Samples Produced by Powder Compact Forging

The use of low strain rates and high temperatures during powder compact forging, make it an important thermomechanical processing technique for improving the quality of composites. From previous studies [2-4], as mentioned in chapter two, the tensile and yield strength of Al-(1-20)vol.%Al_2O_3 composites were reported to

be in the range of 80-400 MPa and 100-350 MPa, respectively. Figure 5.7 shows the tensile stress-strain curves for Al and Al/Al_2O_3 composites consolidated by PCF at varying alumina content. The pure Al showed yield strength of 280 MPa and elongation to fracture of just over 17%. The mechanical milling has significantly increased the yield strength and decreased the ductility of the aluminium compared with normal cold worked aluminium strip. The tensile properties, especially the ductility of the Al/Al_2O_3 nanocomposites were variable. Test pieces containing 2.5 and 10 vol.%Al_2O_3 exhibited little or no ductility, whereas specimens containing 5 vol.% Al_2O_3 showed good ductility with a yield strength of 343 MPa. The fracture appearance indicated that necking occurred prior to final fracture in the Al and Al-5vol.%Al_2O_3 samples, whereas the Al with 2.5 and 10 vol.% Al_2O_3 had very flat, brittle fracture surfaces. In the case of the 10vol.%Al_2O_3 sample the fracture was premature, outside of the gauge length. The reasons for good strength and ductility for Al-5vol.% Al_2O_3 and brittle behaviour for the other compositions can be explained as follows. The hardness and tensile behaviours of aluminium matrix composites reinforced with nanometric Al_2O_3 particulate have been found to increase with the volume fraction of the reinforcement. Kang et al [5] reported, above 4 vol. % of Al_2O_3, the strengthening effect levelled off because of the clustering of Al_2O_3 in the matrix. However the level of clustering was almost diminished in this study with 5 vol.%Al_2O_3 due to the use of MA and achieving a uniform distribution of reinforcement within the Al matrix, as seen in the TEM images for this specific composition. The improvement in yield strength diminished when the volume fraction of the nano-particulate in the composite exceeded 4% according to Kang et al [5]. This effect can be explained by three factors. Firstly, when nano-particulate content in the composites exceeded a critical value, the grain boundary

would be saturated with nano-particulates. Thus an increase in volume fraction exceeding 4% nano-particulates did not result in further grain-refinement. Secondly, grain boundary embrittlement, resulting from grain boundary aggregated nano-particulates, would weaken the strength and ductility of materials. Thirdly, the 'effective' nano-particulate content would reduce since particulates were easily agglomerated to form clusters. Therefore, in nano-particulate-reinforced aluminium matrix composite, the strengthening mechanisms include grain boundary strengthening and Orowan strengthening by effective dispersal of nano-Al_2O_3 particles. Orowan strengthening by effective dispersal of nano-Al_2O_3 particles proved the most significant mechanism. The local ultimate tensile stress in the composite may also be greater than that of the un-reinforced Al because of increased dislocation density and reduced grain-size [6]. It was reported by Koch that ductility is affected by grain size and that most nanostructured materials with grain sizes in the range of 20- 30 nm are "brittle" in tension (<5% elongation to fracture).

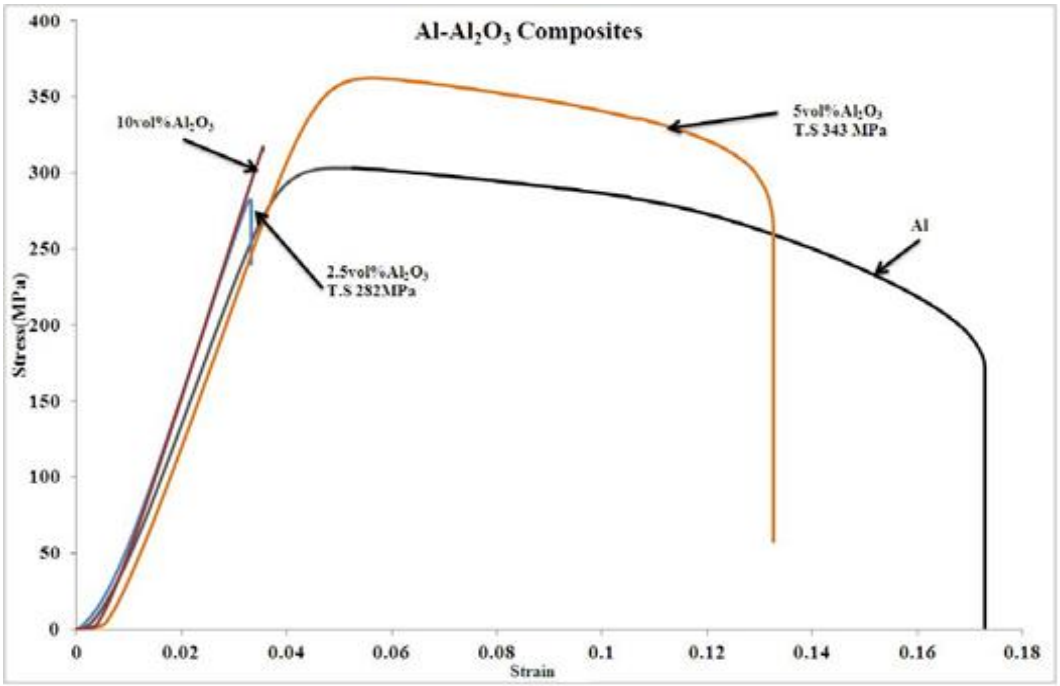

Figure 5.7: Tensile stress-strain curves of specimens cut from the Al and Al-(2.5-10)vol.%Al_2O_3 nanocomposites produced by PCF .

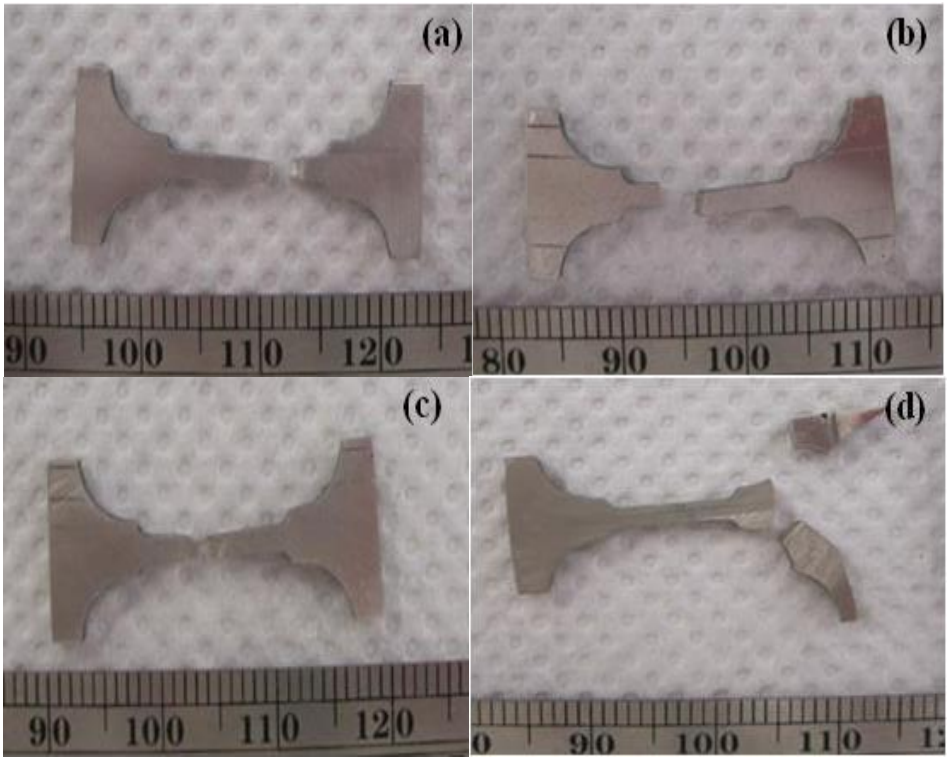

Figure 5.8: Fractured tensile test specimens cut from the Al and Al-(2.5-10)vol.%Al_2O_3 nanocomposites discs produced by PCF : (a) Al, (b) 2.5vol.%Al_2O_3, (c) 5vol.%Al_2O_3, (d) 10vol.%Al_2O_3.

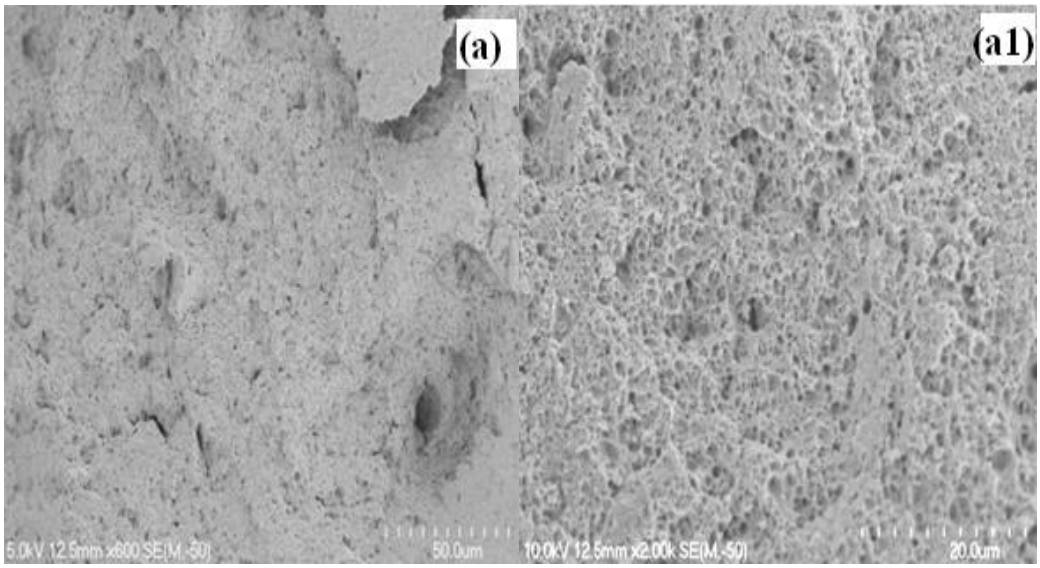

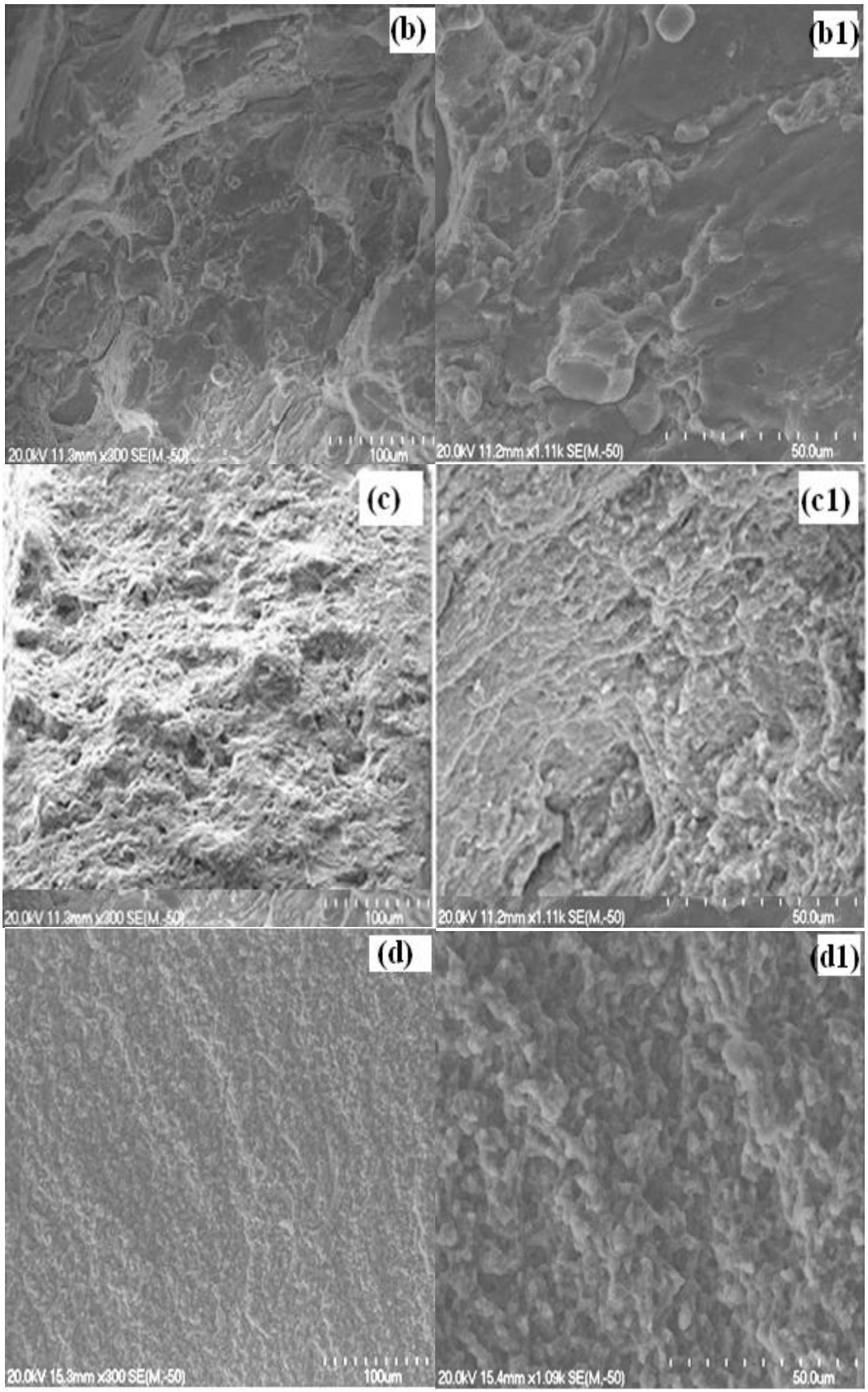

Figure 5.9: Fracture surfaces of tensile test specimens cut from Al and Al-(2.5-10)vol.%Al_2O_3 nanocomposites discs produced by PCF at two different magnifications: (a) and (a1) Al , (b) and (b1) 2.5vol.%Al_2O_3, (c) and (c1) 5vol.%Al_2O_3, (d) and (d1)10vol.%Al_2O_3.

Figure 5.9 (a)-(d) above shows the fracture surfaces of the tensile test specimens cut from the Al and Al-(2.5-10)vol%Al_2O_3 nanocomposite discs produced by PCF. The Al specimens showed ductile fracture surfaces with large dimples. Dimple formation is a typical feature in ductile fractures and it suggests that the powder particles are well bonded. Figures 5.9 (b) and (d) show that the Al – (2.5 and 10) vol.% Al_2O_3 specimens were brittle (no dimples). The fracture surfaces of Al – 5 vol.%Al_2O_3 specimens in Figures 5.9 (c) and (c1) indicate that the fracture of these specimens occurred through ductile fracture of the Al matrix (as reflected by the dimples).

Figure 5.10 , shows that a few cavities (indicated by the arrows) had formed near the fracture surfaces during tensile deformation and fracture of the specimens. From the shapes of the cavities, it appeares that they were not caused by separation of neighbouring powder particles due to weak interparticle bonding. Mechanical milling (MM) reduces the compressibility of the powders due to work hardening. Alumina act as barries that slow down the diffusion process required for proper sintering. However Poirier et al [7] observed that the bonding between the Al_2O_3 and the Al matrix was limited, as evidenced in their work by a large number of visible cavities at the Al_2O_3/Al interface. In this study, the regions away from the fracture surfaces were free from any cavities. This indicates that the cavities near the fracture surfaces were formed by nucleation in the solid material, rather than due to separation of weakly bonded powder particles.

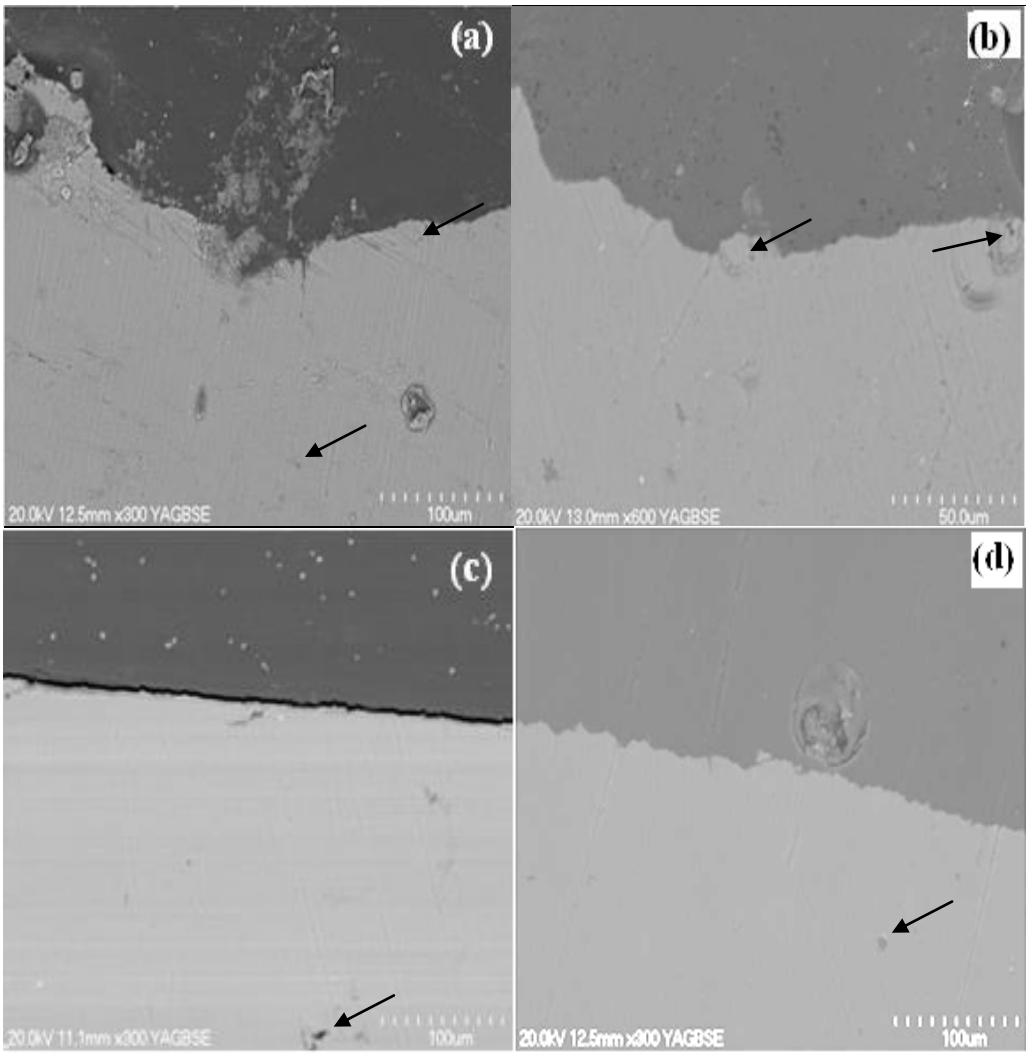

Figure 5.10: SEM micrographs of the longitudinal sections just below the fracture surfaces of the tensile tested specimens cut from the Al and Al-(2.5-10)vol.% Al_2O_3 nanocomposite disc produced by PCF: (a) Al, (b) 2.5vol.% Al_2O_3 ,(c) 5vol.% Al_2O_3, (d) 10.% Al_2O_3 .

Figure 5.11 shows the microhardness of the Al and Al-(2.5-10)vol.% Al_2O_3 nanocomposite disc produced by PCF together with that of the corresponding powder particles. It can be seen that the microhardness of the consolidated samples increased with increasing volume fraction of Al_2O_3 nanoparticles, and an improvement of ~5% in microhardness was achieved as a result of consolidation by powder compact forging.

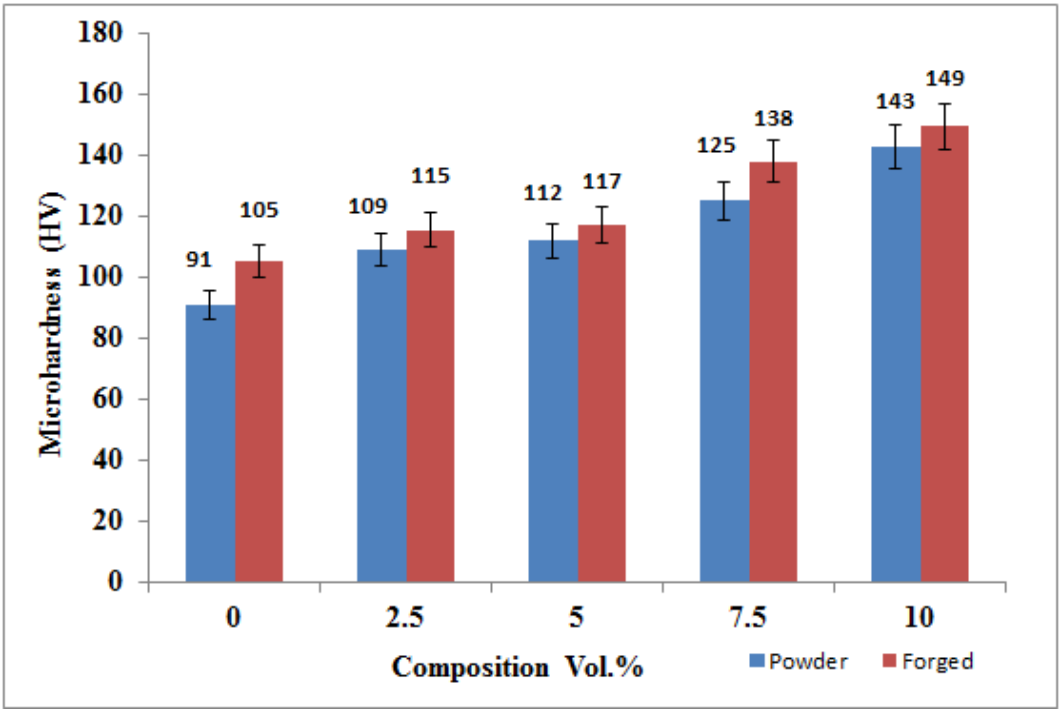

Figure 5.11: Microhardness of Al-(2.5-10)vol.%Al_2O_3 nanocomposites powder particles and corresponding discs produced by PCF. (Errors bars based on standard deviation, they all are within 5%)

5.4 Microstructures of Consolidated Samples Produced by Powder Compact Extrusion

The density of the cold compacts and their relative densities were determined using the rule of mixtures, and the values are shown in Table 5.3.

Table 5.3: Theoretical and relative density of Al – (2.5-10) vol. %Al_2O_3 nanocomposites and the corresponding powder compacts.

Composition	Theoretical density (gr/cm^3)	Density of cold compact (gr/cm^3)	Relative density of compacts (%)	Height of compact (mm)
Al- 1 wt% PCA	2.7	2.244	83.093	31.79
Al-2.5vol%Al_2O_3	2.73	2.344	85.867	21.72
Al-5vol%Al_2O_3	2.76	2.387	86.499	21.46
Al-7.5vol%Al_2O_3	2.79	2.366	84.814	21.52
Al-10vol%Al_2O_3	2.82	2.349	83.323	21.64

The SEM micrograph (Figure 5.12) of the cross section of the extruded bars showed that they were almost fully dense without any pores. This shows that the severe plastic deformation of the powder particles during extrusion of the powder compact enables full densification of the powder compact. However, this is not in agreement with the measured relative densities of the extruded bar using the

Archimedes method (Table 5.4). The reason for this significant discrepancy is possibly the small weight and sizes of the specimens used to measure the density.

Table 5.4: Theoretical, actual and relative densities of Al and Al – (2.5-10)vol.%Al_2O_3 nanocomposites bars produced by PCE.

Composition	Theoretical density(gr/cm^3)	Density of Extruded(gr/cm^3)	Relative density (%)
Al- 1 wt% PCA	2.7	2.66	98.61
Al-2.5vol%Al_2O_3	2.73	2.59	94.69
Al-5vol%Al_2O_3	2.76	2.58	93.38
Al-7.5vol%Al_2O_3	2.79	2.68	96.09
Al-10vol%Al_2O_3	2.82	2.61	92.54

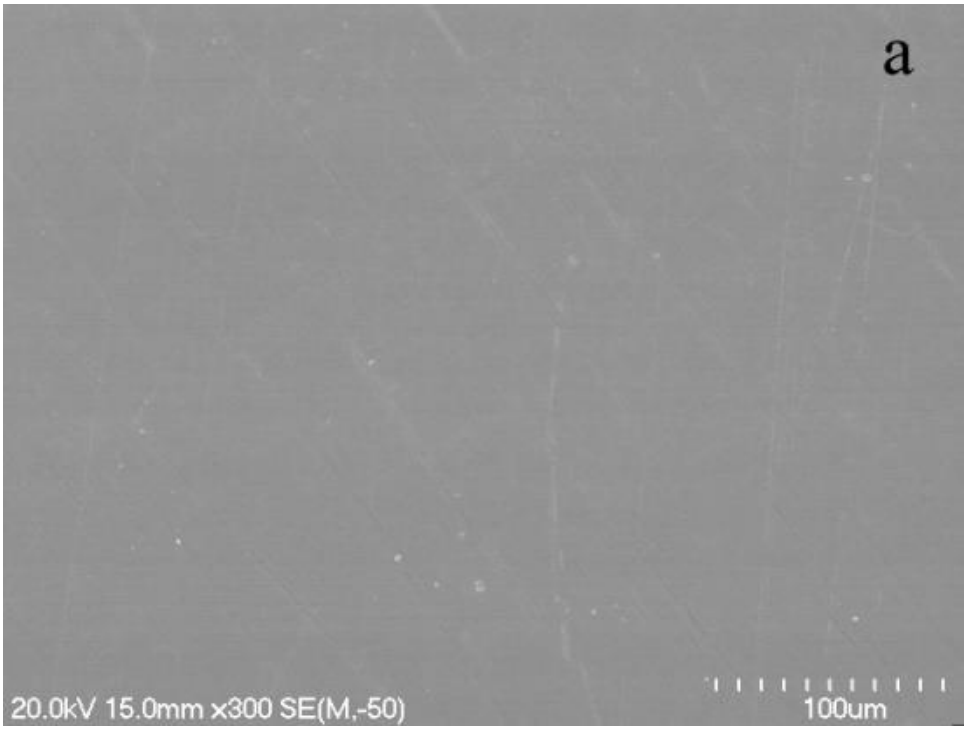

Figure 5.12: SEM micrograph of the cross section of the Al-2.5vol.%Al_2O_3 nanocomposites bar produced by PCE.

Figure 5.13 shows the XRD patterns of Al-(2.5-10)vol.%Al_2O_3 nanocomposites cylindrical bars produced by PCE. As before they only show Al peaks, due to the small sizes and volume fractions of Al_2O_3 nanoparticles and the low volume fraction intensity of γ-Al_2O_3.The average grain sizes and the lattice strain of the Al-(2.5-10)vol.%Al_2O_3 nanocomposites cylindrical bars were estimated based on the broadening of the XRD peaks and using the Williamson-Hall method (Figure5.14). The average grain size and lattice strain of Al-2.5vol. %Al_2O_3

nanocomposite extruded bar were 1666 nm and 0.31%, respectively, and those of Al-5vol. %Al_2O_3 nanocomposite extruded bar were 142 nm and 0.15%. When the volume fraction of Al_2O_3 nanoparticles was increased to 7.5% the grain size changed to 200 nm and lattice strain to 0.23%. For Al-10vol.%Al_2O_3 nanocomposite extruded bar, the grain size and lattice strain were 333 nm and 0.47%. These variances in the lattice strain are due to the thermal stability of the microstructure of the Al-(2.5-10)vol.% Al_2O_3 matrix of the nanocomposites increasing with the increase in the volume fraction of the Al_2O_3 nanoparticles.

TEM was utilised to examine the microstructures of the Al and Al-(2.5-10)vol.% Al_2O_3 nanocomposites cylindrical bars produced by PCE. As shown by the TEM bright field images shown in Figure 5.15, the Al and the Al matrix of the Al-(2.5-10) vol.% Al_2O_3 nanocomposite had an ultrafine grained (UFG) microstructure consisting of grains with sizes ranging 100-800 nm for Al ,100-600 nm for Al-2.5vol.% Al_2O_3. 50-500 nm for Al-5vol.%Al_2O_3, 50-400 nm for Al-7.5vol.% Al_2O_3, and 50- 300 nm for Al-10vol.% Al_2O_3. This shows that the average grain size of the Al matrix decreases with an increasing volume fraction of Al_2O_3 nanoparticles. Estimates of the average grain size were based on broadening of the XRD peaks using the Williamson-Hall method (Figure 5.14). These are in general agreement with the grain sizes of the Al matrix observed by TEM. The TEM examination also shows that the Al grains contained a high density of dislocations.

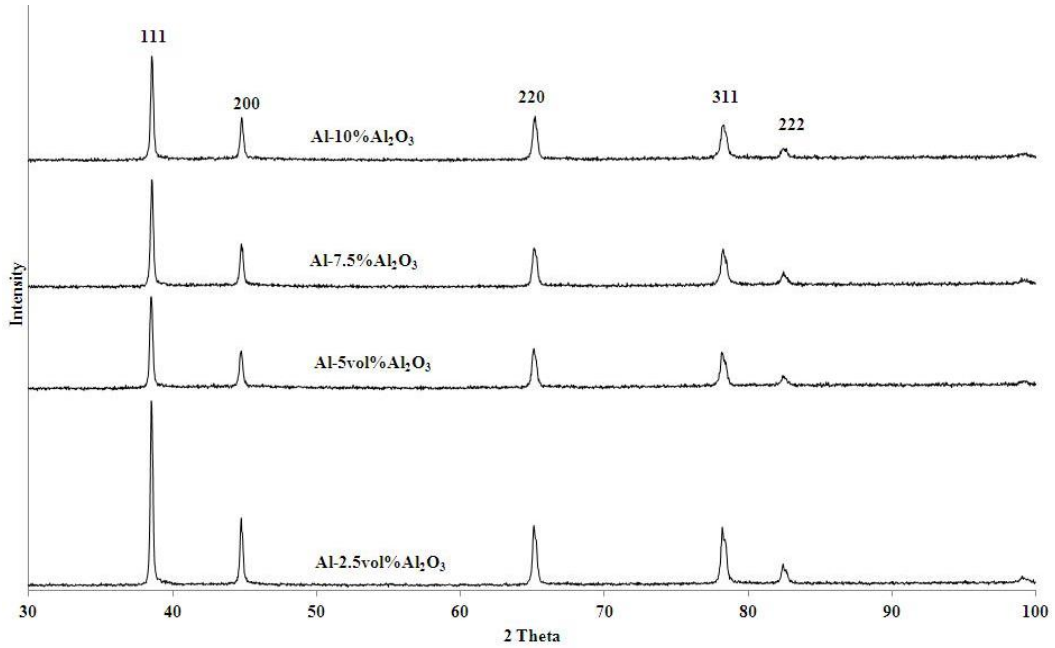

Figure 5.13: X-ray diffraction patterns of Al-(2.5-10)vol.%Al_2O_3 nanocomposite bars produced by PCE.

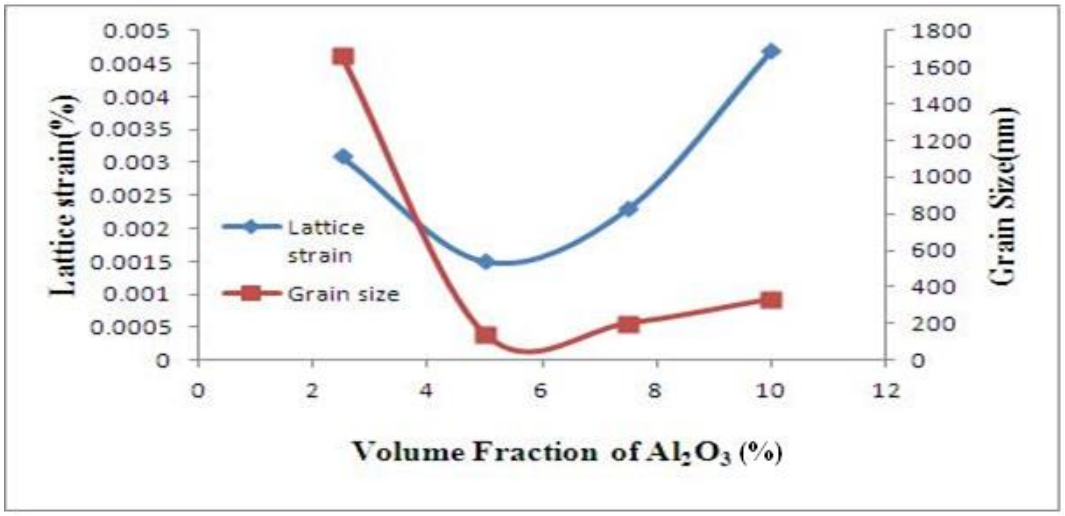

Figure 5.14: Grain size and lattice strain of the extruded Al-(2.5-10)vol.%Al_2O_3 nanocomposites bars produced by PCE as functions of the volume fraction of Al_2O_3 nanoparticles.

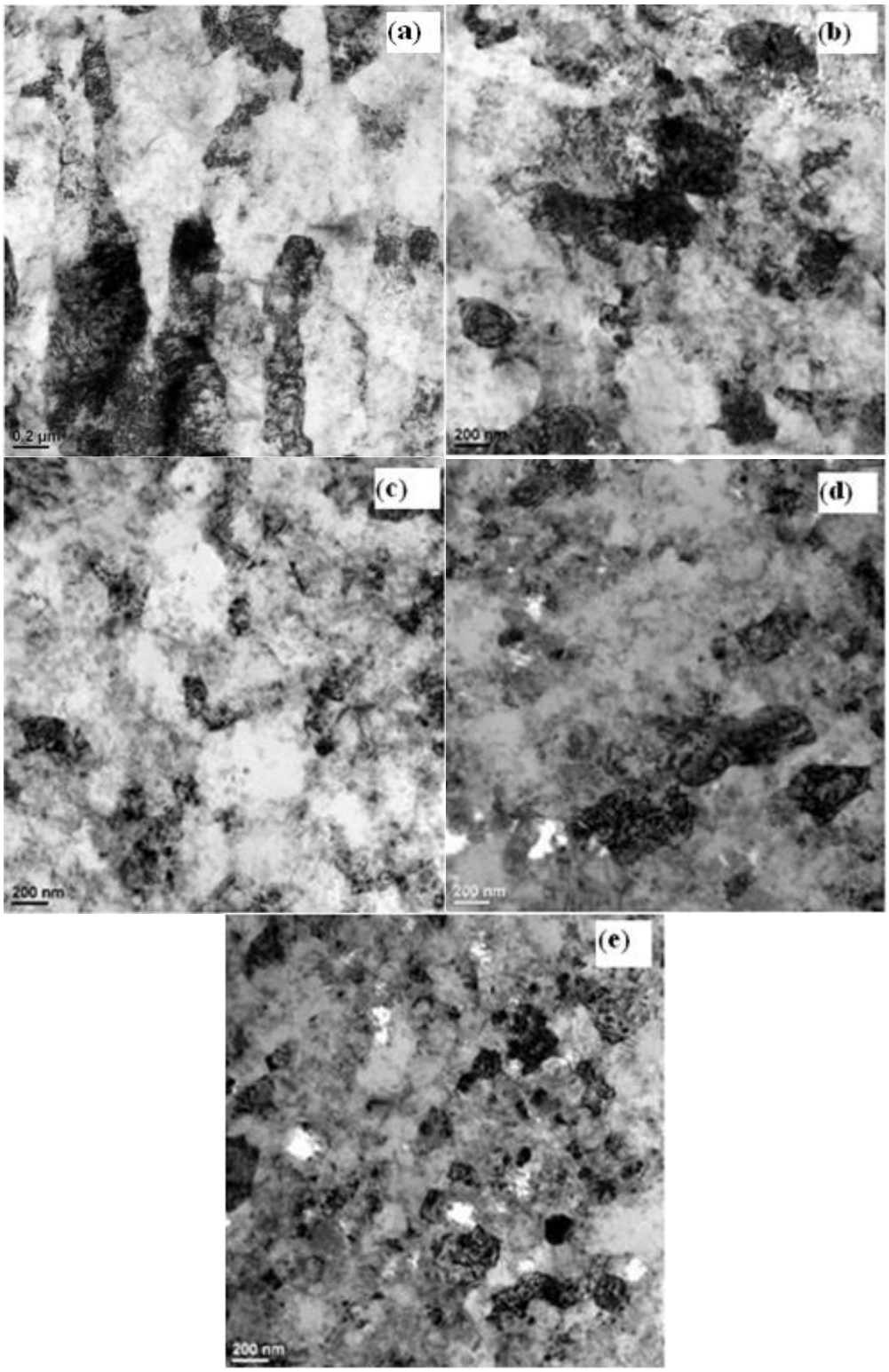

Figure 5.15: TEM bright field images of Al and Al-(2.5-10)vol.%Al_2O_3 nanocomposite produced by powder compact extrusion: (a) Al, (b) 2.5vol.% Al_2O_3,(c) 5vol.% Al_2O_3, (d) 7.5vol.% Al_2O_3, (e) 10vol.% Al_2O_3.

5.5 Mechanical Properties and Fracture Behaviour of Consolidated Samples Produced by Powder Compact Extrusion

Figure 5.16 shows the tensile engineering stress-strain curves of specimens cut from the Al and Al-(2.5-10)vol.%Al_2O_3 nanocomposites cylindrical bars produced by PCE. It can be seen that the Al and Al-5vol.%Al_2O_3 extruded bars showed a high tensile yielding strength (σ_y), of 321 MPa and 318 MPa respectively and good ductility as reflected by elongation to fracture of 1.5% and 8% ,respectively. The Al-2.5vol.%Al_2O_3 extruded bars showed the highest tensile yield strength of 364 MPa, but poor ductility as reflected by a small elongation to fracture of less than 1 %. No significant macroscopic plastic yielding was noticed for the 10 vol. %Al_2O_3 nanocomposites extruded bar, since it fractured prematurely at a stress of 347 MPa. The tensile mechanical properties of Al-7.5vol% Al_2O_3 was not determined as a due to tensile test specimen could not be produced.

The fractured tensile test specimens cut from Al and Al-5vol.%Al_2O_3 extruded bars showed clear necking before fracturing (Figure 5.17), while those cut from Al-(2.5 and 10) vol.%Al_2O_3 extruded bars showed no evidence of necking.

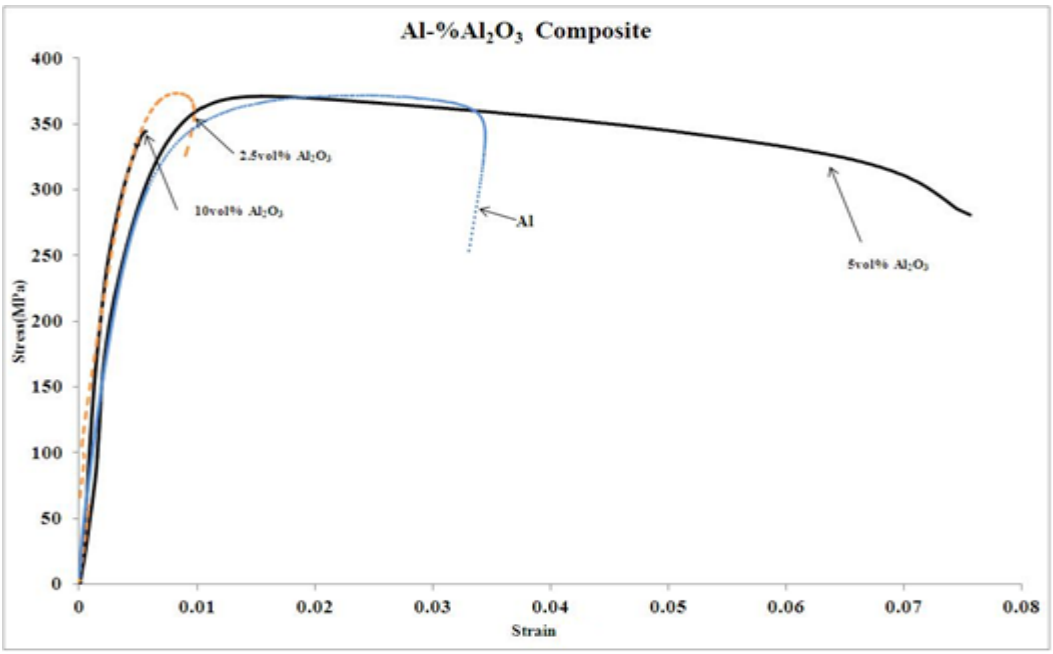

Figure 5.16: Tensile stress-strain curves of Al and Al-(2.5-10)vol.%Al_2O_3 nanocomposites bars produced by PCE.

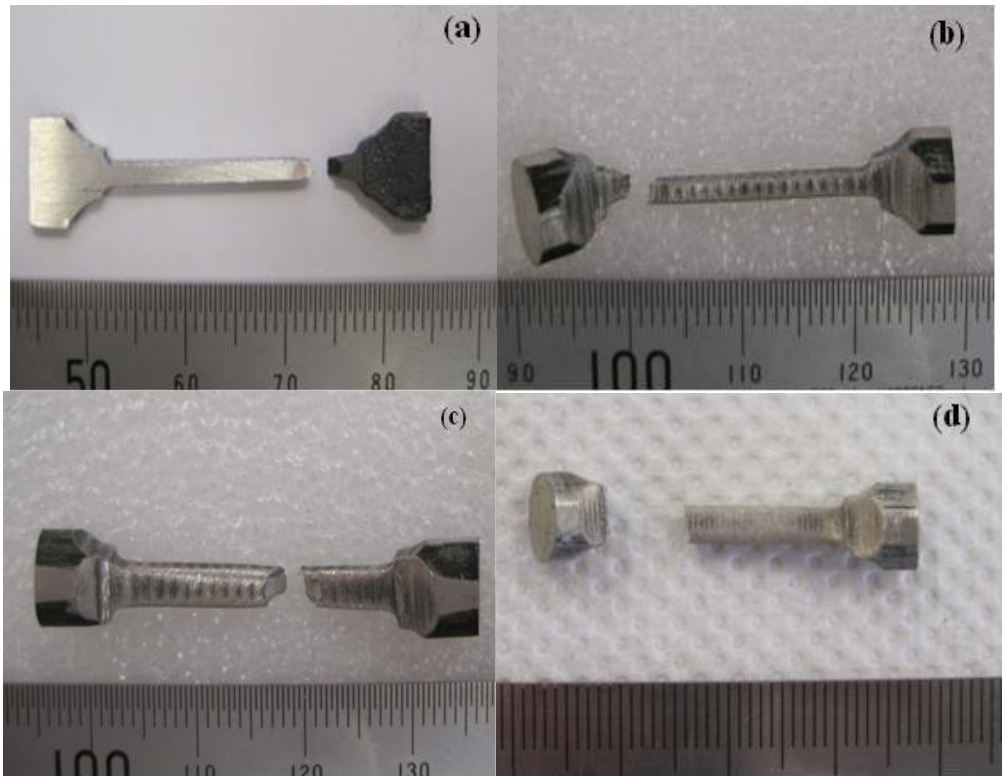

Figure 5.17: Fractured tensile test specimens cut from the Al and Al-(2.5-10)vol.% Al_2O_3 nanocomposites bars produced by PCE: (a) Al, (b) Al-2.5vol.% Al_2O_3 , (c) Al.5vol.% Al_2O_3, (d) Al -10vol.% Al_2O_3.

Further investigation was carried out on Al-5vol.% Al_2O_3 nanocomposites, under the same conditions as described in Chapter 3 . One noticeable difference after powder compact extrusion was the increase in relative density of the Al-5vol.% Al_2O_3 nanocomposites from 93 % to 99%. Figure 5.18 shows, the tensile engineering stress-strain curves of specimens cut from Al-5vol.%Al_2O_3 nanocomposites cylindrical bars produced by PCE. The mechanical properties have been summarized in Table 5.5 below. It can be seen from both Figure 5.18 and Table 5.5 that the Yield strength increased from 318 MPa (Figure 5.16) to more than 350 MPa in the new produced samples, which severely affected the ductility and reduced it to the range of 1.5-2 %. Increasing the volume fraction and/or decreasing the particle size of the reinforcement particles resulted in more frequent interactions between dislocations and the hard particles which accelerated the mechanical milling effectiveness. This leads to a refinement in the grain size of the powders produced. During extrusion, the reinforcing hard

particles fractured and thereby a uniform distribution of the particles in the matrix became evident (Figure 5.19). So with decreasing grain size and a more uniform distribution of the reinforcement particles within the matrix, the strength of the MMCs increased. By having these two effects working together for the 5vol.% material and knowing that during loading the specimen, yielding of the base alloy matrix occurs by the movement of dislocations along slip planes, the movement of dislocations is hindered by the presence of the hard Al_2O_3 homogenously distributed particles. This results in an accumulation of dislocations at the interface therefore a higher load is required for yielding. In other words the mechanical properties improved. According to Kang et al [5] when the volume fraction of the nano-particulate in the composite exceeded 4%, grain boundary aggregated nano-particulates cause the strength and ductility of the material to fall. Another reason for a drop off in ductility in metal matrix composites is that as the concentration of reinforcements in the matrix increases, damage accumulates leading to increased porosity, thus weakening the nanocomposite. This is explained by enhanced void formation between neighbouring particles which effectively increase the porosity of a fairly dense material. The presence of microspores between adhering particles and the reinforcement concentrations increases these damage accumulations [8]. This can be seen in the bright and dark field images shown in Figure 5.19 below.

In Figure 5.19 we can observe an almost homogeneous distribution of the nano Al_2O_3 particles within the matrix. From the nano particle distribution in the aluminium matrix, an estimation of the Orowan strengthening mechanism based on yield strength of the aluminium and particulate-dislocation interaction can be determined.

If we assume that the particles are evenly spaced we can find the estimated increase in tensile strength due to the addition of the alumina nanoparticles with average size of 50 nm. For aluminium the shear modulus **G** is 26 GPA and the Burgers vector **b**=0.286 nm. To calculate the estimated tensile strength we need first to find the average distance between the particles **λ**,

$$\lambda = 2r[\frac{0.8}{\sqrt[3]{f}} - 1]$$

Where, r the radius of the nanoparticles assumed to be spheres, f is the volume fraction of particles.

The shear yield strength increase deriving from dispersion strengthening is given by: $\tau = \frac{2T}{b\lambda}$

Where T is the dislocation line tension and b is the Burger`s vector. The line tension is given by: $T=Gb^2$

The expression for τ can now written as:

$$\tau = \frac{2Gb}{\lambda}$$

But **σ= 3** τ

By using the above equations and the given information we can simply now calculate the estimated increase in the strength for Al-5vol.%Al_2O_3 nanocomposites powders. The estimated yield strength of Al-5vol.%Al_2O_3 is 775.9 MPa. However, when comparing the calculated values of yield strength with the experimental values, a difference is noticed, possibly due to non-uniform dispersion of the nano-reinforcements in the actual sample. This in-homongeneity

in the distribution would have reduced the effective amount of particulates available for strengthening.

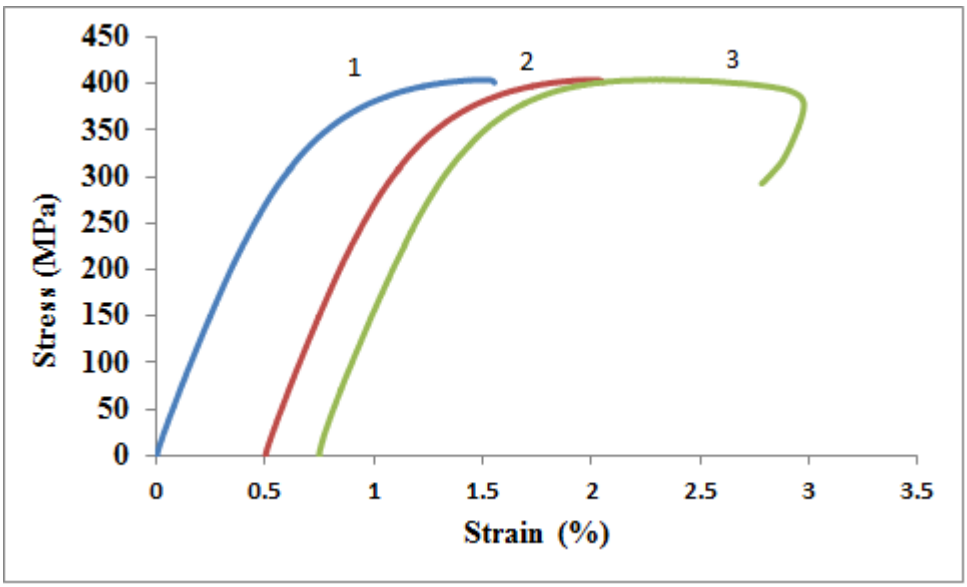

Figure 5.18: Tensile stress-strain curves of Al and Al-5vol.%Al_2O_3 nanocomposites bars produced by PCE. (All were shifted for clarification)

Table 5.5: Mechanical properties of Al – 5vol.%Al_2O_3 nanocomposites bars produced by PCE.

Sample	Yield strength (MPa)	Ultimate tensile strength (MPa)	Ductility (%)
1	367	404	1.5
2	359	378	1.5
3	372	404	2.1

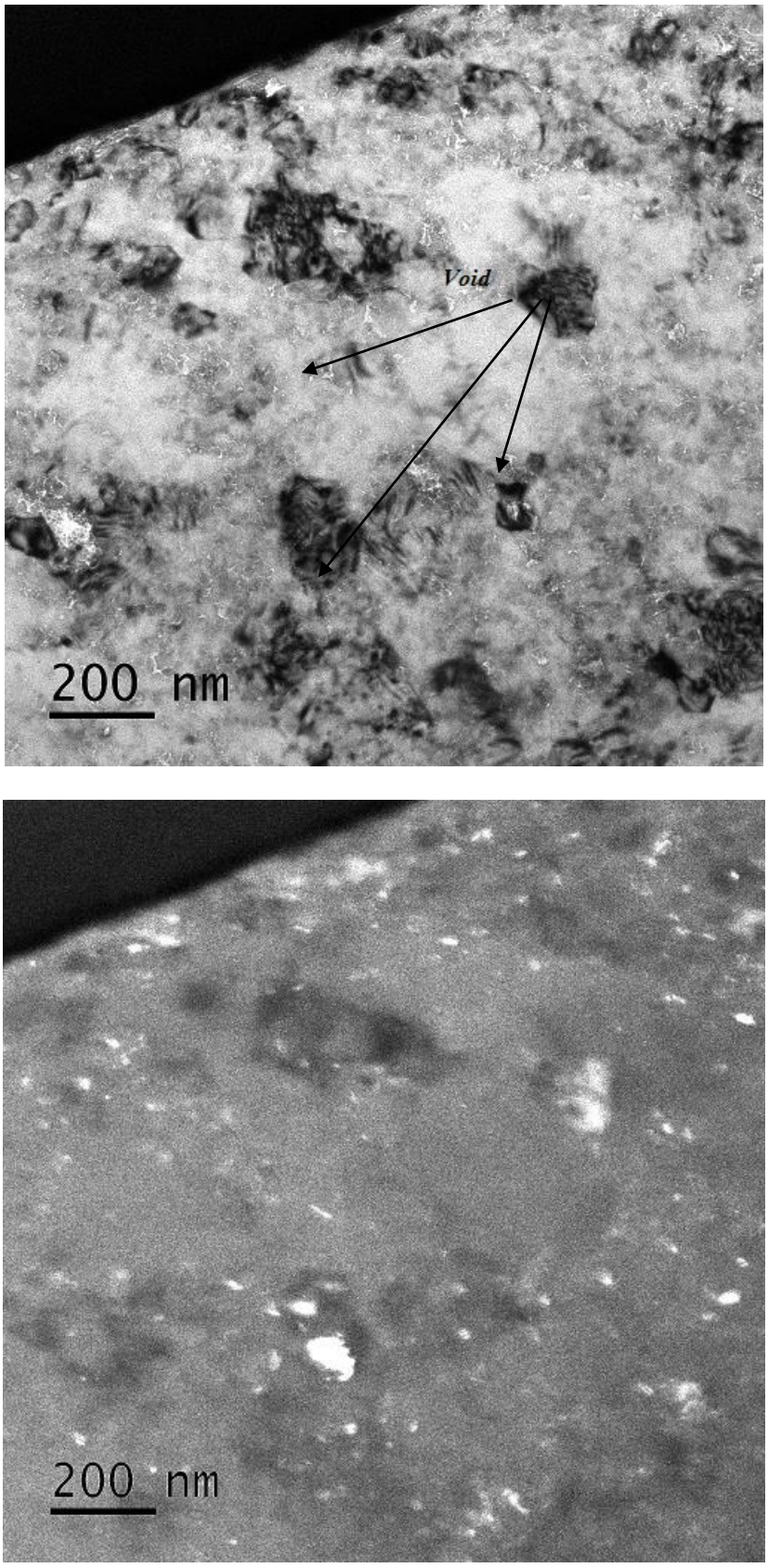

Figure 5.19: TEM bright field and dark field images of Al-5vol.%Al_2O_3 nanocomposite produced by powder compact extrusion showing void formation between neighbouring particles and the Alumina semi homogeneous distribution.

Figure 5.20 below shows the typical fracture surfaces of tensile test specimens cut from the Al and Al-(2.5-10)vol.% Al_2O_3 nanocomposite bars produced by PCE. The ductile fracture surfaces of Al and Al-5vol.%Al_2O_3 nanocomposite specimens clearly showed large dimples. In powder compact extrusion samples, dimples are typical of ductile fracture; this suggests that the powder particles were well bonded. Figures 5.20 (b) and (c) show that with an increasing volume fraction of Al_2O_3 nanoparticles from 2.5 to 5 vol%, the fracture surface exhibits more dimples indicating a higher degree of microscopic ductile fracture. The presence of veins and rivers patterns could be noticed in Figures 5.20 (b) and (c), this revealed that fractured particles were surrounded by ductile regions known as tear ridges and voids [9]. By increasing the Al_2O_3 volume fraction up to 10% the fracture surface of the composite showed a brittle failure which was dominated by intergranular fractures (Figures 5.20 (d) and (d1).

Figure 5.21 shows SEM micrographs of logitudinal cross-sections just below and well below the fracture surfaces of Al and Al-(2.5-10)vol.%Al_2O_3 tensile test specimens cut from the extruded bars. A few cavities (indicated by the arrows) formed near the fracture surface during tensile deformation and fracture of the specimen. From the shapes of the cavities, it appeares that they were not caused by separation of neighbouring powder particles due to weak interparticle bonding, but rather through void nucleation occuring as second phase particles or inclusions crack or debond from the matrix material during plastic deformation. In regions away from the fracture surfaces (Figures 5.21 (a1) and (c1)) there were some cavities, casued by a seperation of weakly bonded particles rather than the nucleation of cavities in the solid material. On the other hand, Figures 5.21 (d) and (d1) show that no cavities had formed near or away from the fracture surfaces of an Al-10vol.%Al_2O_3 specimen.

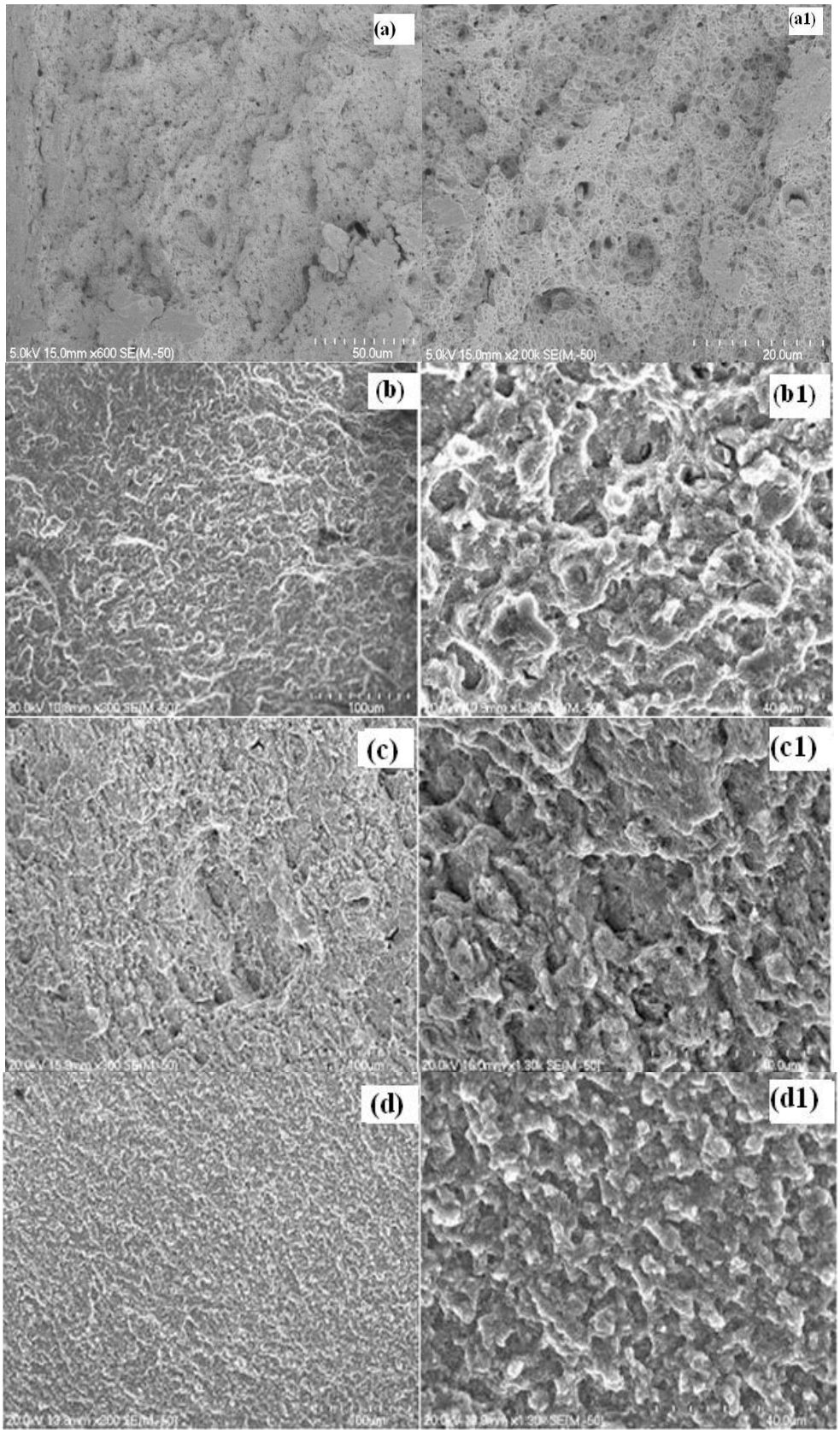

Figure 5.20: Fracture surface of tensile test specimens cut from Al and Al-(2.5-10)vol.% Al_2O_3 nanocomposite bars produced by PCE at two different magnifications: (a) and (a1) Al, (b) and (b1) 2.5vol.% Al_2O_3; (c) and (c1) 5vol.% Al_2O_3 ;(d) and (d1)10vol.% Al_2O_3 .

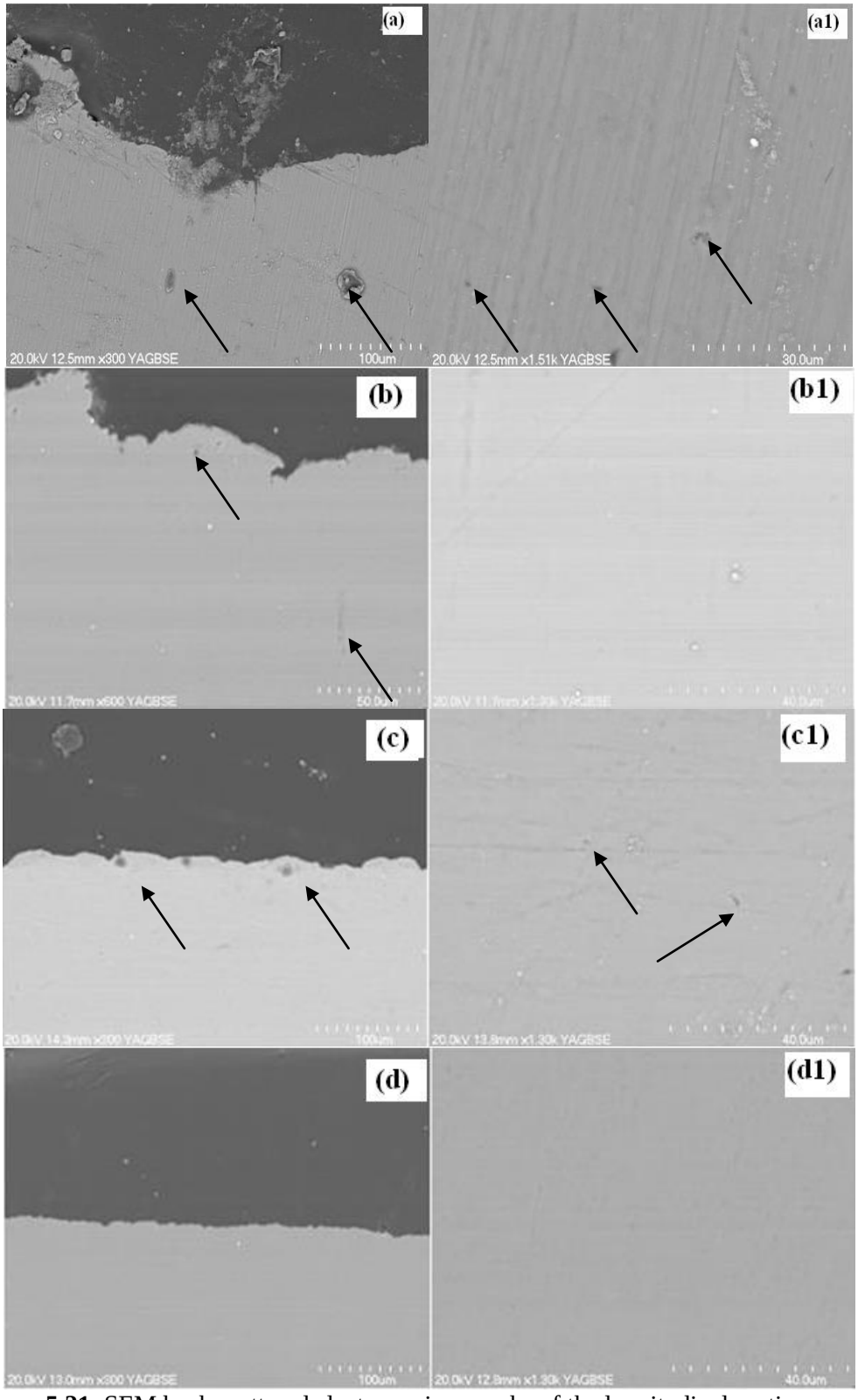

Figure 5.21: SEM back scattered electron micrographs of the longitudinal sections near ((a)-(d)) and away from the fracture surfaces (a1)-(d1) of the tensile test specimens cut from the Al and Al-(2.5-10)vol.% Al_2O_3 nanocomposite bars produced by PCE: (a) and (a1) Al, (b) and (b1) 2.5vol.% Al_2O_3 ,(c) and (c1) 5vol.% Al_2O_3, (d) and (d1) 10vol.% Al_2O_3.

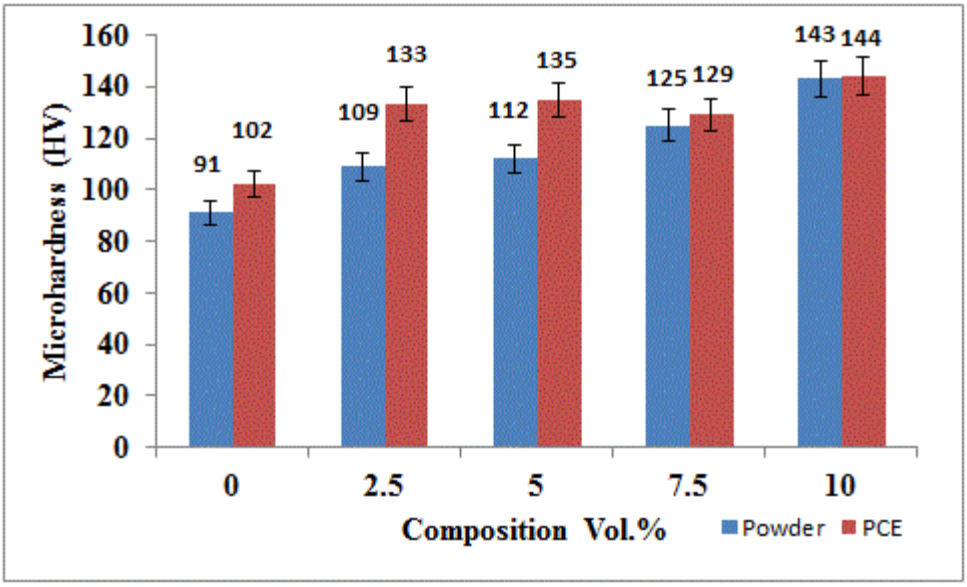

Figure 5.22: Microhardness of Al and Al-(2.5-10)vol.%Al_2O_3 nanocomposites powder particles and corresponding bars produced by PCE.

Figure 5.22 shows the microhardness of the Al and Al-(2.5-10)vol.% Al_2O_3 nanocomposite bars produced by PCE together with that of the corresponding powder particles. It can be seen that the microhardness of the consolidated samples has increased with increasing volume fraction of Al_2O_3, and an improvement up to ~20% in microhardness was achieved as a result of consolidation by powder compact extrusion.

5.6 Discussion

5.6.1 Powder preparation effects on consolidation

The consolidation of the nanocomposites powders through the application of heat and pressure results in fully dense compacts. Recrystallization and grain growth occurs during the high temperature consolidation, especially for the powders prepared from the HEMM process [10].

The high energy ball milling of the powders resulted in ultra-fine grain structures after 12 hours of net milling. The Al_2O_3 nanoparticles were embedded in the Al matrix, and there was no evidence of intermetallic or new phase formation within the matrix. The microhardness of the consolidated powder was slightly higher after consolidation, due to the initial strain hardening deriving from the milling process and the following thermomechanical treatment. Hardness was found to

increase with increasing the volume fraction of reinforcement within the matrix until a certain volume is reached after which it started to decrease due to clustering of the reinforcement. It has been reported that by reducing the Al_2O_3 particle size from 400 to 4 nm the nanocomposite powder hardness increases by 11% [7].

A homogeneous microstructure was found in the composites after consolidation. As expected, the density of composite compacts decreased with increasing volume fraction of Al_2O_3 nanoparticles in the Al matrix. This is because the degree of softening in the powder compacts during hot pressing is much higher for the 2.5 vol.%Al_2O_3 composite than that in the other composite compacts with higher alumina content. The theoretical densities of the Al-(2.5-10)vol.%Al_2O_3 nanocomposites were calculated using the rule of mixtures, while the actual densities of the powder compacts were calculated by dividing their weights by corresponding volumes. It was found that the relative densities for samples produced by both forging and extrusion were in the range of 92-99%. This is because of the increased hardness of the powder particles caused by work hardening during milling, and by the volume fraction of the hard Al_2O_3 nano particles in the composite structure.

5.6.2 Effects of consolidation on microstructure

Aluminium based particulate reinforced MMCs have limitations because of various structural defects causing poor forgability. Therefore utilising the severe plastic deformation (SPD) is one of the effective methods for making materials with nanometre or submicrometer sized grains. Powder compact extrusion has been used to consolidate metal nanopowders and nanostructured powders to obtain bulk materials with fine grain structure [4, 11].

Transmission electron microscopy has shown that the nano reinforcement was uniformly distributed within the Al matrix, which has a high dislocation density as a result of severe plastic deformation. Although, the density of green compacts is low and this affects the pressure distribution during forging, good consolidation characteristics were found despite the increase in the hardness of the starting powders due to strain hardening during milling.

No diffraction peaks from the Al_2O_3 phase can be detected in the XRD patterns for the specimens produced by PCF and PCE. This is probably because of the relatively small fraction and size of Al_2O_3 nano particles in the composite powder

It was observed that the samples produced from powder compact extrusion (PCE) have a finer microstructure than those produced by powder compact forging (PCF), based on average grain size estimations using the Williamson-Hall method [12] and the TEM examinations. This is important, because it shows that the composite microstructure after high temperature PCE processing was more refined. This grain refinement could be due to recrystallization of the heavily deformed ultra-fine grained Al matrix during heating to 500 ºC.

5.6.3 Mechanical Properties

Aluminium nanostructured powders give good properties for an extrusion temperature of about 400 °C. This work has shown that with increasing volume fraction of Al_2O_3 nanoparticles, the microstructure of the Al-(2.5-10) vol.% Al_2O_3 matrix of the bulk nanocomposite samples becomes finer. This is because an increase in the amount of Al_2O_3 in the starting powder microstructure increases the effectiveness of HEMM, and this creates a finer microstructure in the nanocomposite powder. This was confirmed by TEM examination of the milled powder particles.

For the Al-(2.5-10) vol. %Al_2O_3 nanocomposites produced by powder compact forging and powder compact extrusion. The Al-5vol. % Al_2O_3 composite produced from both processing methods showed the best ductility accompanied with the best tensile strength, and that is a result from what was mentioned and explained earlier in section 5.3.

It is well know that the yield stress is strongly dependent on the grain size and temperature. The Hall-Pitch relationship can be used to explain the effect of grain size on yield stress. The yield stress is proportional to $1/\sqrt{d}$ where d is the average grain diameter. The ultra-fine grained (UFG) Al metal matrix nanocomposites are characterized by high values of hardness and yield strength at low temperatures. It has been reported that nanostructured materials are "brittle" in tension (<5% elongation) [13]. A study has shown that the tensile strength of an Al matrix composites was enhanced to over 300 MPa with limited ductility of not more than 1% [14] while in other studies forged samples of an AA2618/20vol%Al_2O_3 composite achieve yield strengths of over 400 MPa with increased elongation at room temperature up to twice that found in an as-cast composite [15].

Brittle and ductile types of fracture surface were noticed after tensile testing. S.C.Tjong et al. [16] reported that the fracture surface for Al based composites reinforced with Al_2O_3 submicron particles were characterized by typical tear ridges and shallow dimple morphologies with submicron ceramic particles remaining intact with the matrix.

5.7 Summary

1. This study has clearly demonstrated, that a UFG structure of Al and Al-(2.5-10)vol.% Al_2O_3 nanocomposites can be synthesized by a combination of high energy mechanical milling and a severe plastic deformation process to

consolidate the powder compacts into nearly fully dense forged discs and extruded bars. The ultrafined grained structure of the milled composite powders and in the powder compact forgings and extrusions were confirmed by Transmission Electron Microscopy.

- Milled aluminium powder after forging and extruding showed high tensile yield strength (σ_y), of 299 MPa and 321 MPa, respectively. The broken tensile specimens for the forged and extruded composites showed that both specimens eventually necked before fracturing.
- No significant microscopic yielding was noticed in the Al-2.5 and 10 vol. %Al_2O_3 composites produced by powder compact forging. The Al-5vol. % Al_2O_3 composite showed a ductility of 8%. An Al-5vol. % Al_2O_3 composite shows the best fracture strength of 343MPa.
- No significant microscopic yielding was noticed in the Al- 10 vol. %Al_2O_3 composite material produced by powder compact extrusion. Al-2.5vol. % Al_2O_3 showed a ductility of ~1% with the highest tensile strength of 364 MPa while Al-5vol. % Al_2O_3 showed a ductility of 8%. Al-5vol. % Al_2O_3 specimen from the figure shows the a yielding strength of 318 MPa.

5.8 References

[1] H. Gleiter, "Nanostructured materials: basic concepts and microstructure," *ActaMaterialia,* vol. 48, pp. 1-29, 2000.

[2] S. M. Zebarjad and S. A. Sajjadi, "Dependency of physical and mechanical properties of mechanical alloyed Al-Al2O3 composite on milling time," *Materials & Design,* vol. 28, pp. 2113-2120, 2007.

[3] M.Kok, "Production and mechanical properties of Al2O3 particle-reinforced 2024 aluminium alloy composites," *Journal of Materials Processing Technology,* vol. 161, pp. 381-387, 2005.

[4] Z. R. Hesabi, A.Simchi, S. M. S. Reihani, and F.Simanick, "Fabrication and characterization of ultrafinee-grained Al-5vol%Al_2O_3nanocomposite," *international Journal of Nanomanufacturing,* vol. 5, p. 341, 2010.

[5] Y.C. Kang and S. L.I. Chan, "Tensile properties of nanometric Al2O3 particulate-reinforced aluminum matrix composites," *Materials Chemistry and Physics,* vol. 85, pp. 438-443, 2004.

[6] I. Mobasherpour, A. A. Tofigh, and M. Ebrahimi, "Effect of nano-size Al2O3 reinforcement on the mechanical behavior of synthesis 7075 aluminum alloy composites by mechanical alloying," *Materials Chemistry and Physics,* vol. 138, pp. 535-541, 2013.

[7] D. Poirier, R. A. L. Drew, M. L. Trudeau, and R. Gauvin, "Fabrication and properties of mechanically milled alumina/aluminum nanocomposites," *Materials Science and Engineering: A,* vol. 527, pp. 7605-7614, 2010.

[8] A. F. Zimmerman, G. Palumbo, K. T. Aust, and U. Erb, "Mechanical properties of nickel silicon carbide nanocomposites," *Materials Science and Engineering: A,* vol. 328, pp. 137-146, 2002.

[9] T. S. Srivatsan and A. Prakash, "The quasi-static fracture behavior of an aluminum alloy metal-matrix composite," *Composites Science and Technology,* vol. 54, pp. 307-315, 1995.

[10] A. Mukhtar, "MicroStructure, Thermal Stability and Consolidation of Nanostructured and Ultrafine Structured Cu based Metal Matrix Composite and Alloy powders Produced by High Energy Mechanical Milling," Doctor of Philosophy, Materials and Process Engineering, University of Waikato, Hamilton, 2010.

[11] O. N. Senkov, S. V. Senkova, J. M. Scott, and D. B. Miracle, "Compaction of amorphous aluminum alloy powder by direct extrusion and equal channel angular extrusion," *Materials Science and Engineering: A,* vol. 393, pp. 12-21, 2005.

[12] G. K. Williamson and W. H. Hall, "X-ray line broadening from filed aluminium and wolfram," *ActaMetallurgica,* vol. 1, pp. 22-31, 1953.

[13] C.C.Koch, "Ductility in nanostructured and ultra fine-grained materials: Recent evidence for optimism," *Journal of metastable and Nanocrystalline Materials*, vol. 18, pp. 9-20, 2003.

[14] F. Tang, H. Meeks, J. E. Spowart, T. Gnaeupel-Herold, H. Prask, and I. E. Anderson, "Consolidation effects on tensile properties of an elemental Al matrix composite," *Materials Science and Engineering: A*, vol. 386, pp. 194-204, 2004.

[15] L. Ceschini, G. Minak, and A. Morri, "Forging of the AA2618/20 vol.% Al_2O_3p composite: Effects on microstructure and tensile properties: Effects on microstructure and tensile properties," *Composites Science and Technology*, vol. 69, pp. 1783-1789, 2009.

[16] S. C. Tjong, G. S. Wang, and Y. W. Mai, "High cycle fatigue response of in-situ Al-based composites containing TiB2 and Al_2O_3 submicron particles," *Composites Science and Technology*, vol. 65, pp. 1537-1546, 2005.

Chapter Six: Microstructure and Mechanical Properties of Ultrafine Structured Al-4wt%Cu-(2.5-10) vol.%SiC Nanocomposites Produced by Powder Consolidation

6.1 Introduction.

Aluminium based metal matrix nanocomposites with nanostructured or ultrafine structured (UFS) matrices can be produced by a combination of high energy mechanical ball milling (HEMM) of the powders and their subsequent thermomechanical consolidation. The effects of nanoscaled reinforcement particles on the mechanical properties of metal matrix nanocomposites have been studied by many researchers. For instance, Narayansamy et al. [1] evaluated the effect of silicon carbide particle size on workability under a triaxial stress state of P/M performs of an Al-SiC composite. The authors, showed that the formability stress index, strain hardening index, and strength coefficient values vary significantly for different particle sizes and percentage content of SiC. Ogel et al.[2] produced an Al-Cu- SiC metal matrix composites by using a conventional hot pressing and found that the yield strength and tensile strength of the material were improved while the ductility reduced with increasing amounts of SiC particles. This chapter presents the results of an experiment on the microstructures and mechanical properties of UFS Al-4wt%Cu-(2.5-10) vol.%SiC nanocomposites. This nanocomposite was chosen because it's an age hardenable alloy, and to examine the effects of adding SiC reinforcement to the solid solution matrix. These were produced by a combination of HEMM of a mixture of Al, Cu, and SiC nanoparticles followed by powder consolidation using powder compact forging (PCF) and powder compact extrusion (PCE), respectively.

6.2 Microstructures and Mechanical properties of Ultrafine structured Al-4wt%Cu-(2.5-10)vol.%SiC composites Produced by Powder Compact Forging

The cylindrical Al-4wt%Cu-(2.5-10) vol. % SiC microcomposite powder compacts produced by hot pressing had a diameter of 25 mm and a height ranging from 28 to 32 mm, (Table 6.1). Theoretical densities of the Al-4wt%Cu-(2.5-10) vol. % SiC microcomposites were calculated by using the rule of mixture, while the actual densities of the powder compacts were calculated by dividing their weights by corresponding volumes. Table 6.1, shows that the relative densities decreased with increasing SiC content by up to 7.5 vol. % in the milled Al-4wt%Cu-SiC powder. This is likely related to the increased hardness of the powder particles caused by work hardening during milling and to the increased volume fraction of the hard micrometre sized SiC particles in the composite structure.

Table 6.1: Theoretical and relative density of Al –4wt% Cu-(2.5-10)vol.%SiC microcomposites and the corresponding compacts.

Composition	Theoretical density (gr/cm^3)	Density of compacts (gr/cm^3)	Relative density (%)	Height of compacts (mm)
Al-4wt%Cu-2.5vol%SiC	2.71	2.55	94	28
Al-4wt%Cu-5vol%SiC	2.72	2.38	87	30
Al-4wt%Cu-7.5vol%SiC	2.74	2.26	83	31.5
Al-4wt%Cu-10vol%SiC	2.75	2.3	84	31

Figure 6.1 shows the SEM micrographs of the samples obtained from the central region of forged discs taken in two different magnifications. SEM examination revealed that the forged discs were almost fully dense with the volume fraction of pores being <1%. The Al_2Cu and SiC fine particles were homogenously distributed within the Al(Cu) solid solution matrix. The sizes of the SiC particles (grey particles in Fig. 6.1) were in the range of 5-15 μm which indicates the reduction of SiC particle sizes by up to 85% during milling. The Al_2Cu particles (bright particles in Fig. 6.1) were formed by a reaction between Al and Cu, with

shapes ranging from equiaxially stretched to elongated to a diameter/thickness in the range of 1-10 μm. Fig. 6.2 shows the XRD patterns of the forged Al-4wt%Cu-SiC microcomposites discs which showed Al (Cu) and SiC peaks. The XRD peaks of the Al (Cu) phase are fairly broad, suggesting the grains of Al (Cu) phase were very fine. Based on the Williamson-Hall method (Fig. 6.3), the estimated grain size and lattice strain of the Al-4wt%Cu-(2.5-10) vol.%SiC nanocomposites are summarized in Table 6.2. The grain size and lattice strain remained almost unchanged. This is due to the thermal stability of the composite microstructure as the volume fraction of SiC in the matrix increases. This may be explained by the increased Zener-drag effect with increasing volume fraction of nanoparticles, which resist the movement of grain boundaries. This effect leads to a slower rate of microstructural coarsening with increased content of nanoparticles [3], but no physical evidence for this was found from the TEM images.

Table 6.2: Average grain size and lattice strain for milled Al-4wt%Cu-(2.5-10)vol.%SiC microcomposites produced by powder compact forging.

Composition	**Milling Time (Hr)**	**Average grain size (μm)**	**Lattice Strain (%)**
Al-4wt%Cu-2.5vol.%SiC	12	2	0.34
Al-4wt%Cu-7.5vol.%SiC	12	2.5	0.30
Al-4wt%Cu-10vol.%SiC	12	1.667	0.36

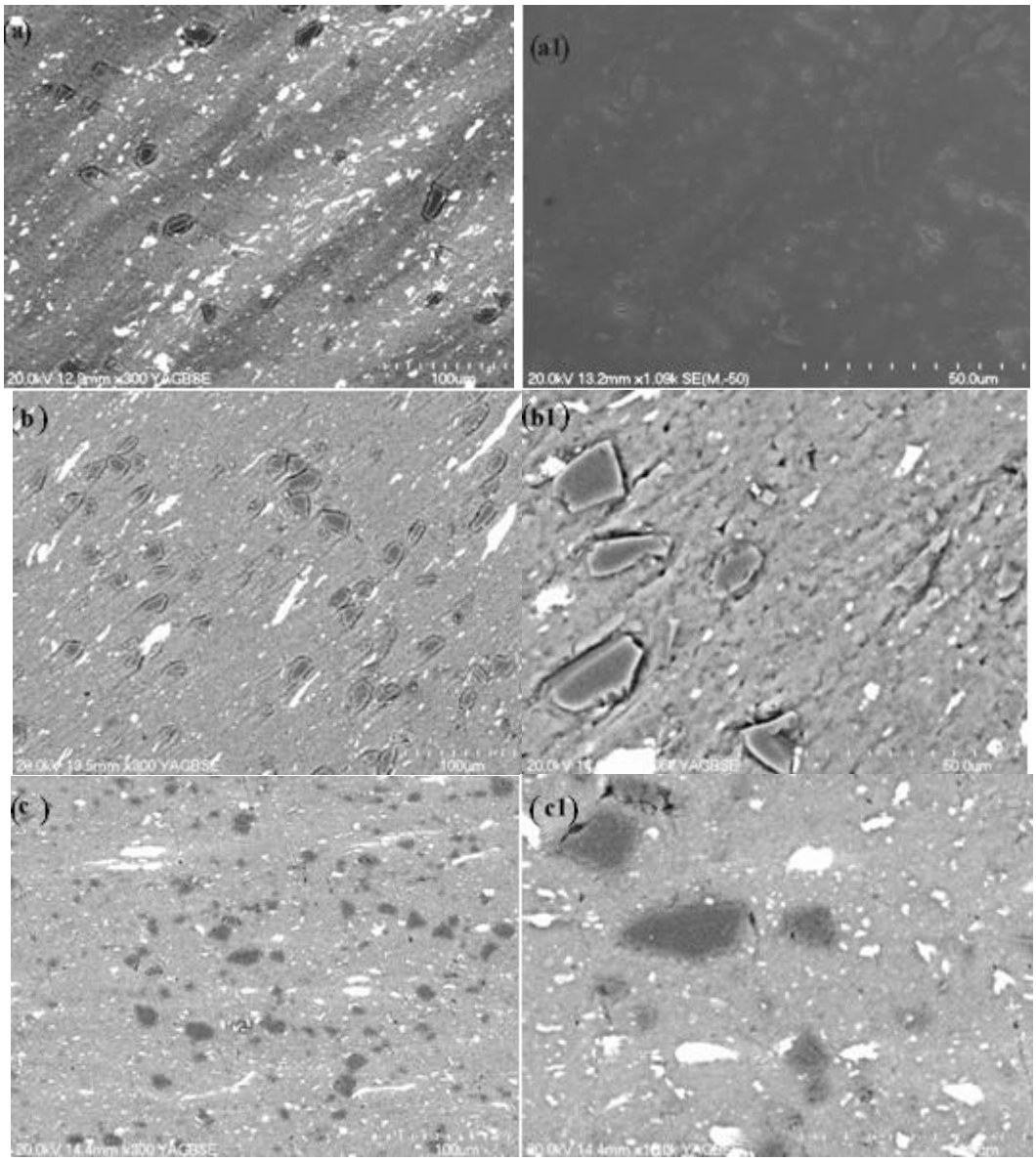

Figure 6.1: SEM micrographs of samples from the centre regions of the Al-4wt%Cu-(2.5-10)vol.%SiC microcomposite discs produced by PCF: (a) and (a1) 2.5vol.%SiC; (b) and (b1) 7.5vol.%SiC; (c) and (c1) 10vol.%SiC.

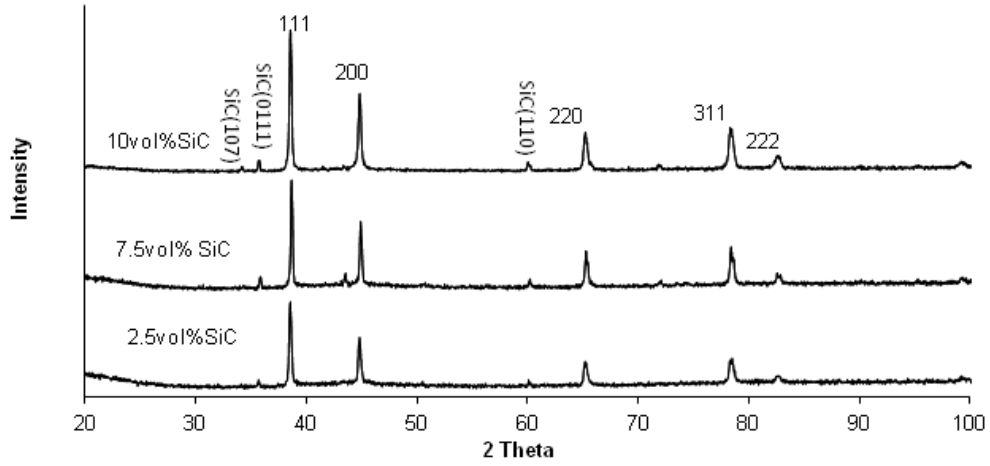

Figure 6.2: XRD patterns of forged Al-4wt%Cu-(2.5-10)vol.%SiC microcomposites discs.

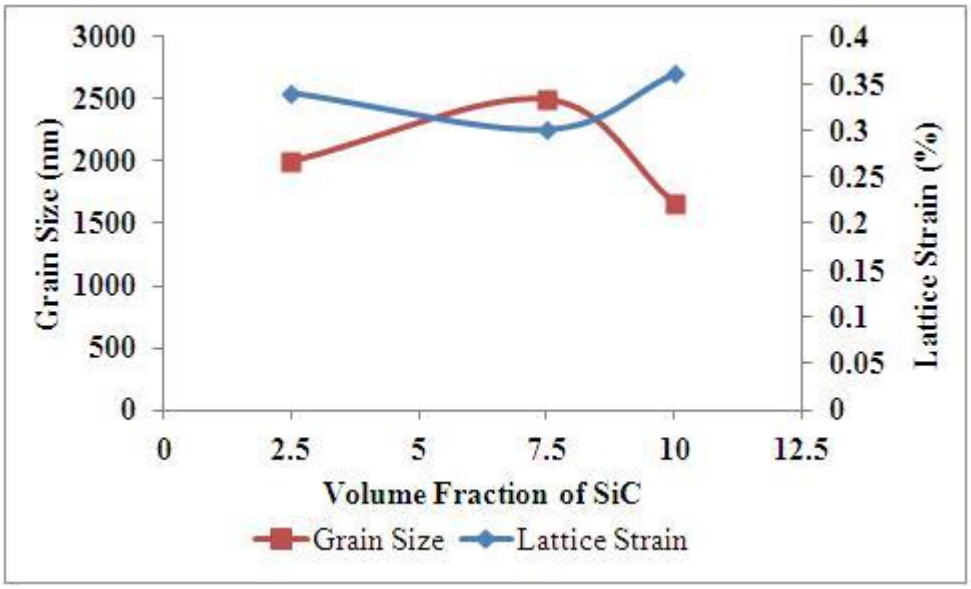

Figure 6.3: Average grain size and lattice strain of the Al-4wt%Cu-(2.5-10)vol.% SiC microcomposites disc produced by PCF as a function of the volume fraction of SiC particles.

The average microhardness of the forged discs was 73HV, 105HV and 162HV for Al-4wt%Cu-(2.5, 7.5 and 10) vol. % SiC, respectively. Figure 6.4 shows the tensile engineering stress-strain curves of specimens cut from the Al-4wt%Cu-(2.5-10) vol.%SiC microcomposite discs produced by PCF. The Al-4wt%Cu-2.5vol.%SiC microcomposite specimens fractured at an average stress of 225MPa without yielding, while the Al-4wt%Cu-(7.5 and 10) vol. %SiC microcomposites specimens did yield prior to fracturing and with a small plastic strain to fracture (~1%) at an average stress of 191 to 384 MPa, respectively. The fracture strength

of the forged discs increased from 225 to 412 MPa with increasing volume fraction of SiC particles from 2.5% to 10%. The broken tensile test specimens did not show evidence of necking. The fractured surfaces were very flat and the fracture mostly occurred at the locations closet to the point of section thickness change. Figure 6.5 shows the fracture surfaces of the specimens. The fracture of the specimen occurred through fracturing of SiC particles (shown by the arrows), debonding of the powder particles and ductile fracture of the Al (Cu) matrix (as reflected by the dimples).

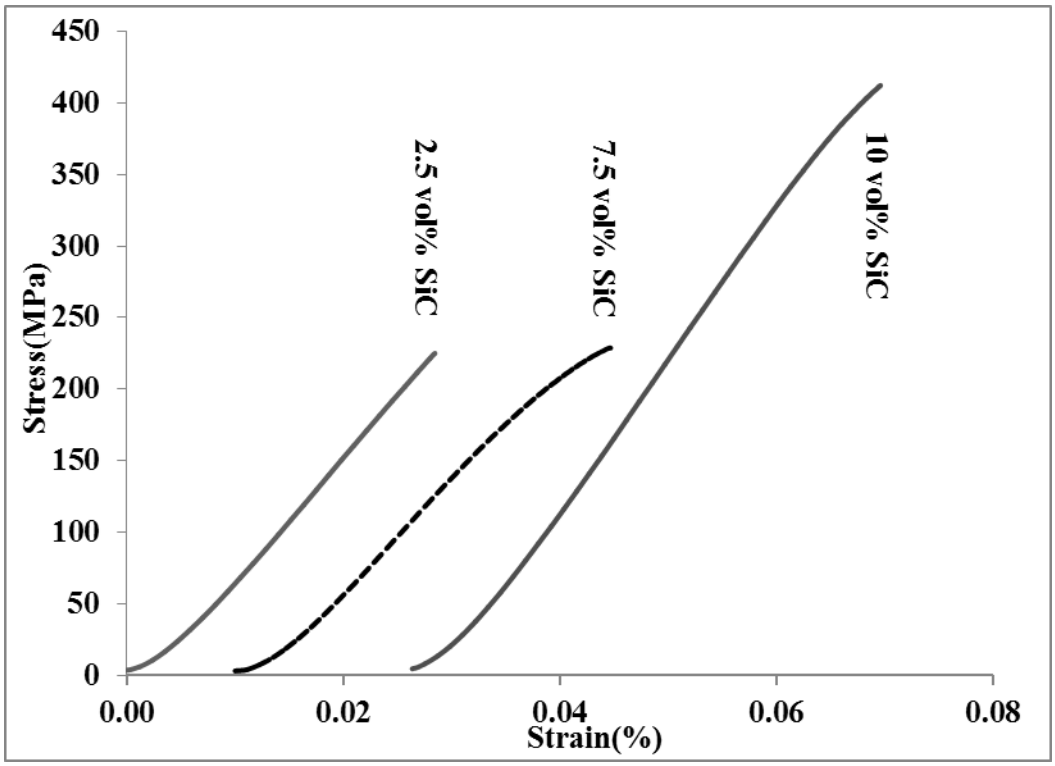

Figure 6.4: Tensile stress- strain curves of the specimens cut from the Al-4wt%Cu-SiC composite forged discs. (Two curves were moved to the right for clarity).

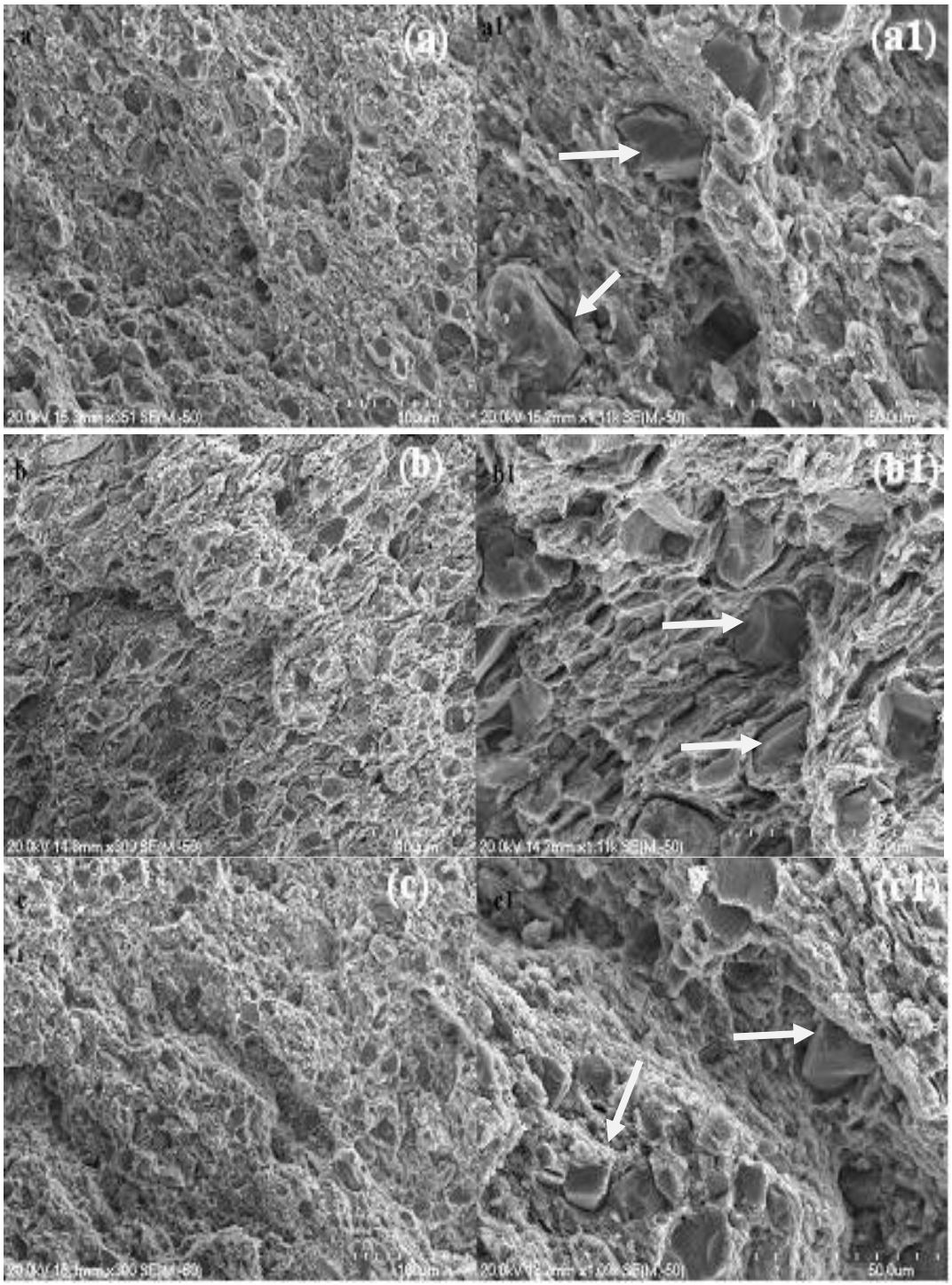

Figure 6.5: SEM images of the fracture surfaces of the tensile testing specimens at two magnifications: (a) and (a1) Al-4wt%Cu-2.5vol%SiC; (b) and (b1) Al-4wt%Cu-7.5vol%SiC; and (c) and (c1) Al-4wt%Cu-10vol%SiC.

6.3 Microstructures and Mechanical properties of Ultrafine Structured Al-4wt%Cu-(2.5-10) vol.%SiC Nanocomposites Produced by Powder Compact Forging

The Al-4wt%Cu-(2.5-10)vol.%SiC nanocomposite powders produced by HEMM of mixtures of Al powder, Cu powder and SiC nano powder with 1 wt% of PCA were first compacted using uniaxial hot pressing. The Al–4wt%Cu-(2.5-

10)vol.%SiC nanocomposite powder compacts had a diameter of 25 mm and height in the range of 29-41 mm (Table 6.3). The densities of all composite compacts were derived by measuring their weights and dimensions. Theoretical densities of Al–4wt%Cu-(2.5-10)vol.%SiC nanocomposites were calculated using the rule of mixture (Equation 5.1).

Table 6.3: Theoretical and relative density of Al –4wt% Cu-(2.5-10)vol.%SiC nanocomposites and the corresponding compacts.

Composition	Theoretical density (gr/cm^3)	Density of compact (gr/cm^3)	Relative density of compacts	Height of compact (mm)
Al-4wt%Cu-2.5vol%SiC	2.71	2.55	94.23	30.48
Al-4wt%Cu-5vol%SiC	2.72	1.767	64.85	40.21
Al-4wt%Cu-7.5vol%SiC	2.74	1.74	63.67	39.3
Al-4wt%Cu-10vol%SiC	2.75	2.074	75.3	29.5

With the exception of Al-4wt%Cu-10vol.%SiC, the relative densities of the nanocomposite powder compacts decreased with increasing volume fraction of SiC in the milled nanocomposite powder (Table 6.3). This is possibly caused by the increased hardness of the mechanically milled Al–4wt%Cu-(2.5-10)vol.%SiC nanocomposite powder particles with increasing volume fraction of SiC for the reasons described in Chapter 4. It follows that the higher the powder particle hardness, the lower is their deformation under the same powder pressing pressure and thus there is a lower degree of densification caused by powder particle deformation.

The density of the forged discs was determined using the Archimedes method, and the values are shown in Table 6.4. It should be noticed that the specimens produced after powder compact forging are almost fully dense.

Table 6.4: Theoretical and relative density of Al –4wt%Cu- (2.5-10)vol.%SiC nanocomposite discs produced by PCF.

Composition	Theoretical density (gr/cm^3)	Density of forged (gr/cm^3)	Relative density of forged (%)
Al-4wt%Cu-2.5vol%SiC	2.71	2.71	99.94
Al-4wt%Cu-5vol%SiC	2.72	2.64	96.95
Al-4wt%Cu-7.5vol%SiC	2.74	2.70	98.72
Al-4wt%Cu-10vol%SiC	2.75	2.73	99.24

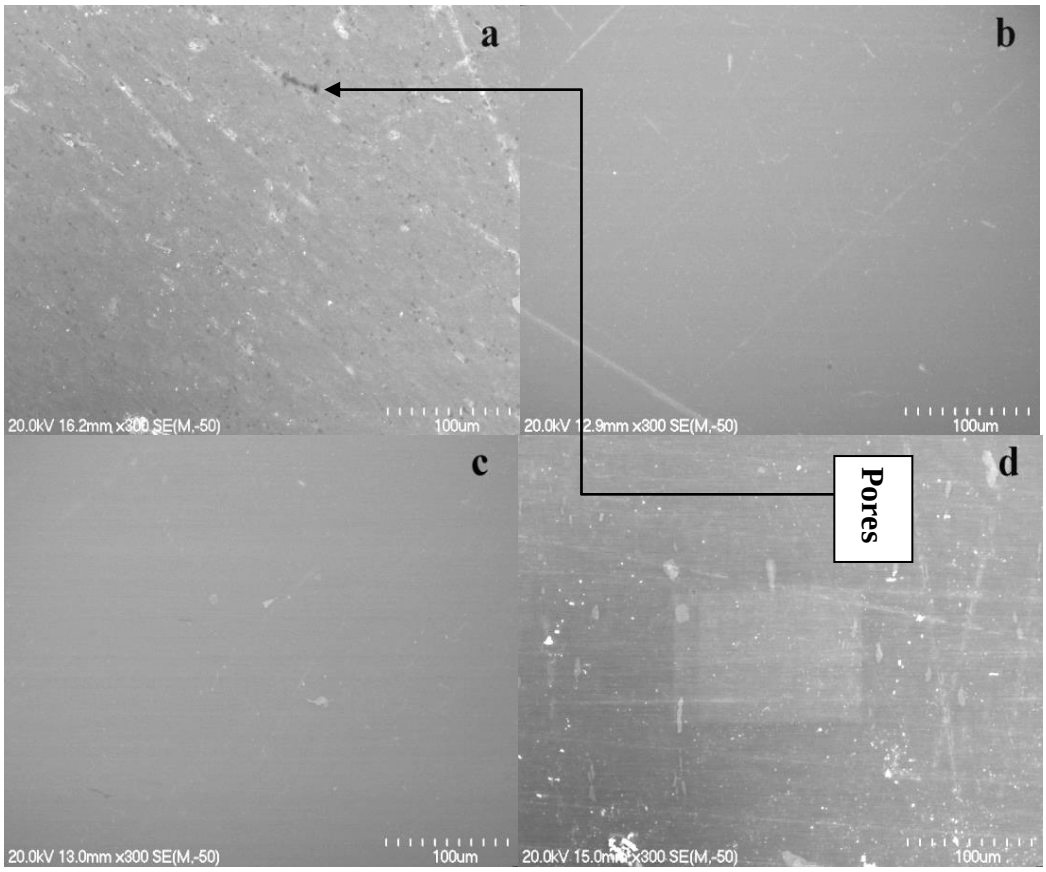

Figure 6.6: SEM micrographs of Al-4wt.%Cu-(2.5-10)vol.%SiC nanocomposite discs produced by PCF: (a)2.5vol.%SiC, (b) 5vol.%SiC,(c) 7.5vol.%SiC, (d) 10vol.%SiC

Figure 6.6 shows the SEM micrographs of Al-4wt.%Cu-(2.5-10) vol.%SiC nanocomposite discs produced by PCF. It is clear that the pores were less than 1% in the samples. Figure 6.7 shows the XRD pattern of the Al-4wt%Cu-(2.5-10)vol.%SiC nanocomposites forged discs. The XRD patterns shows strong Al peaks and weak SiC and Cu peaks, due to their small sizes and volume fractions. The average grain sizes and the lattice strain of the Al-4wt%Cu-(2.5-10) vol. %SiC nanocomposites were estimated from the broadening of the XRD peaks

(Figure 6.8). Based on the Williamson-Hall method (Figure 6.8), the estimated grain size and lattice strain of the Al-4wt%Cu-(2.5-10)vol.%SiC nanocomposites were determined and are summarized in Table 6.5. The presence of SiC particles impedes matrix grain growth. Smaller SiC particles are generally less effective in pinning moving grain boundaries, which can explain the inconsistency of the estimated average grain size [4].

Table 6.5: Average grain size and lattice strain for milled Al-4wt%Cu-(2.5-10)vol.%SiC nanocomposite produced by powder compact forging.

Composition	Milling Time (Hr)	Average grain size (μm)	Lattice Strain (%)
Al-4wt%Cu-2.5vol.%SiC	12	10	0.29
Al-4wt%Cu-5vol.%SiC	12	3.3	0.42
Al-4wt%Cu-7.5vol.%SiC	12	3.3	0.44
Al-4wt%Cu-10vol.%SiC	12	0.5	0.46

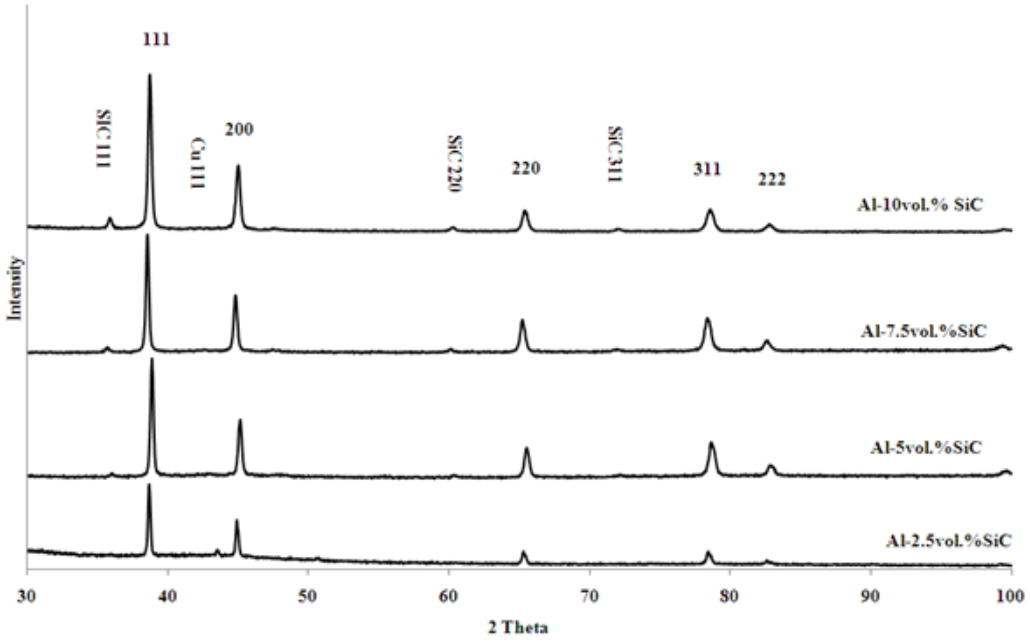

Figure 6.7: X-ray diffraction patterns for Forged Al-4wt%Cu-(2.5-10)vol.%SiC nanocomposites**.**

.

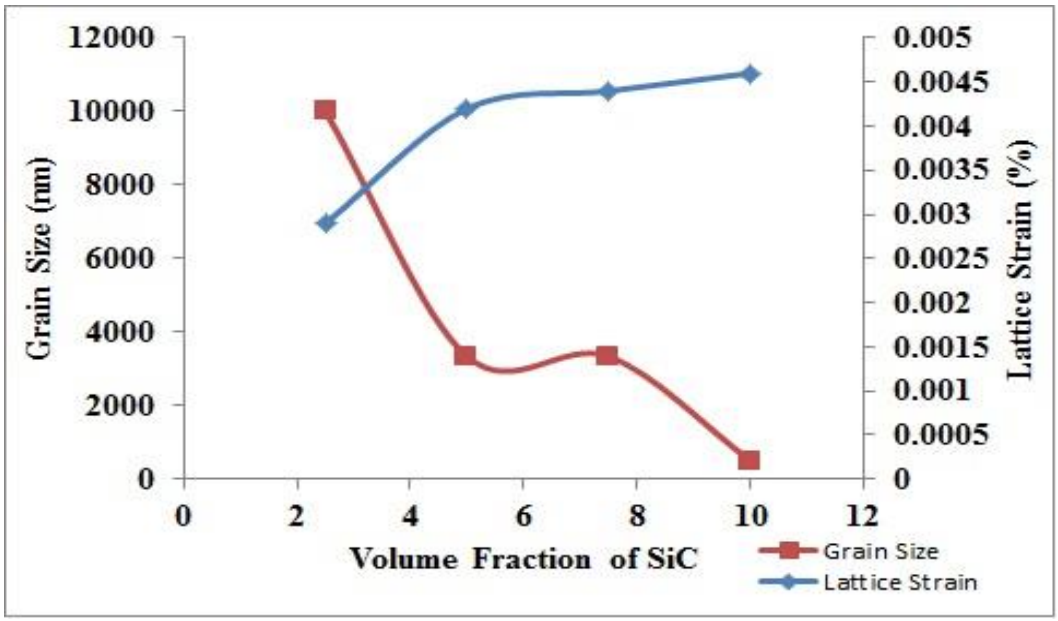

Figure 6.8: Grain size and lattice strain data of the Al-4wt%Cu-(2.5-10)vol.%SiC nanocomposites after powder compact forging.

TEM was utilised to examine the microstructures of the Al-4wt%Cu-(2.5-10) vol.%SiC nanocomposite discs produced by PCF. The bright field images (Figure 6.9), shows that the Al matrix had an ultrafine grained (UFG) microstructure consisting of grain sizes in the range of 400-2000 nm , 200 -1500 nm, 100-1000 nm, and 50-500 nm for Al-4wt%Cu-(2.5, 5, 7.5, and 10) vol.%SiC nanocomposites respectively. This shows that the average grain size (Figure 6.8) is clearly larger than the actual average Al grain size estimated by TEM, and this difference is likely due to an under estimation of the XRD peak widths.

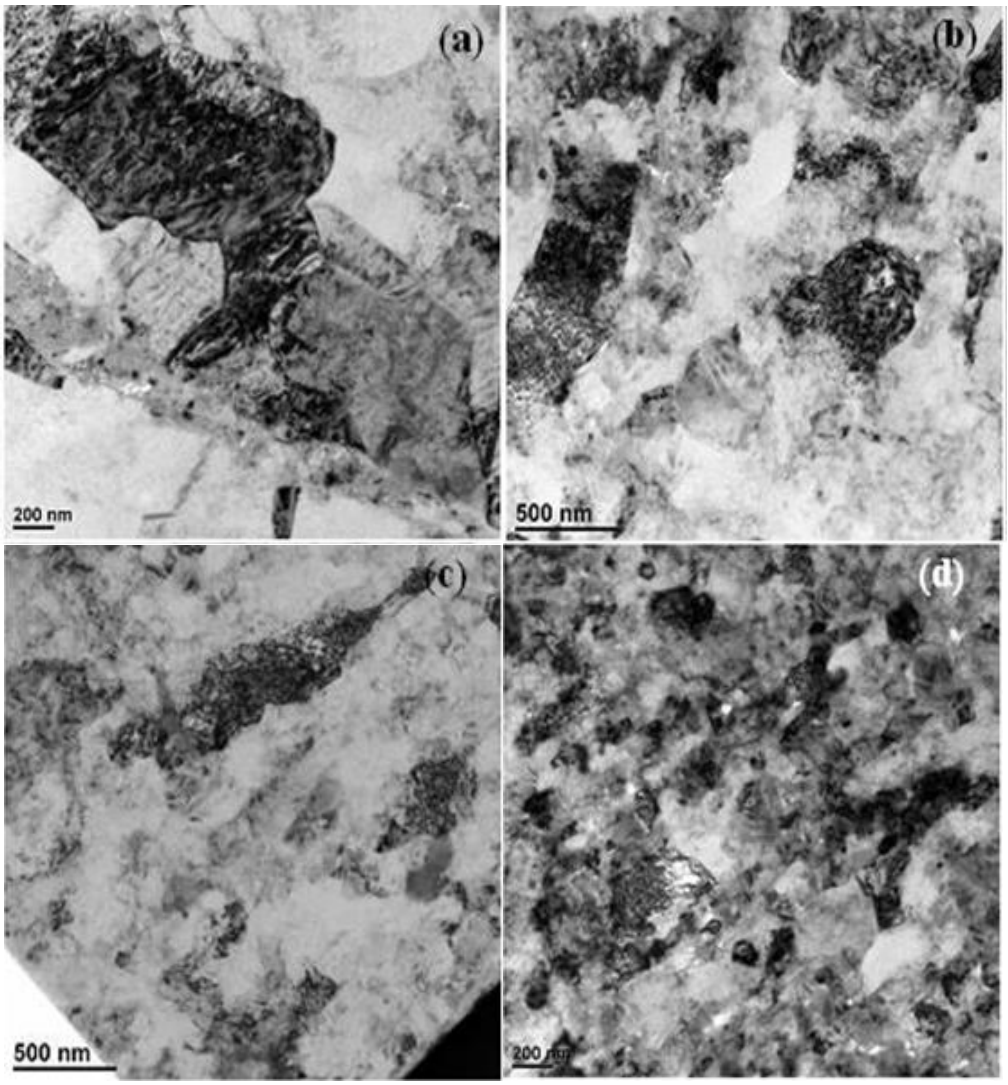

Figure 6.9: TEM bright field images ofAl-4wt%Cu-(2.5-10)vol.%SiC nanocomposites discs produced by PCF: (a) 2.5vol.% SiC ,(b) 5vol.% SiC,(c) 7.5vol.% SiC,(d)10vol.% SiC.

Stress-strain curves for the specimens cut from the Al-4wt%Cu-(2.5-10) vol. %SiC nanocomposites discs produced by PCF are shown in Figure 6.10. The Al-4wt%Cu-2.5vol. %SiC specimens fractured at an average stress of 205MPa without yielding. The fracture strength of the forged disks increased from 200 to 450 MPa by increasing the volume fraction of SiC nano particles from 5 to 7.5 vol. % but the Al-4wt%Cu- 10 vol. %SiC specimens exhibited pre-mature fracturing. To gain more information about the nature of the fractures, and the bonding between the powder particles, the fracture surfaces, and longitudinal sections, near to and away from the fracture surfaces of the specimens, were examined using the SEM. Figure 6.11 shows that the broken tensile test

specimens did not show significant void formation during deformation and fractures. Figure 6.12 shows the fracture surfaces of the specimens and these indicate a ductile fracture of the Al matrix as reflected by the tear ridges. The average microhardness of the Al-4wt5Cu-(2.5-10)vol.%SiC nanocomposite forged discs increased from 105 HV to 231 HV, with increasing volume fraction of SiC nanoparticles from 2.5% to 10%, as shown in Figure 6.13.

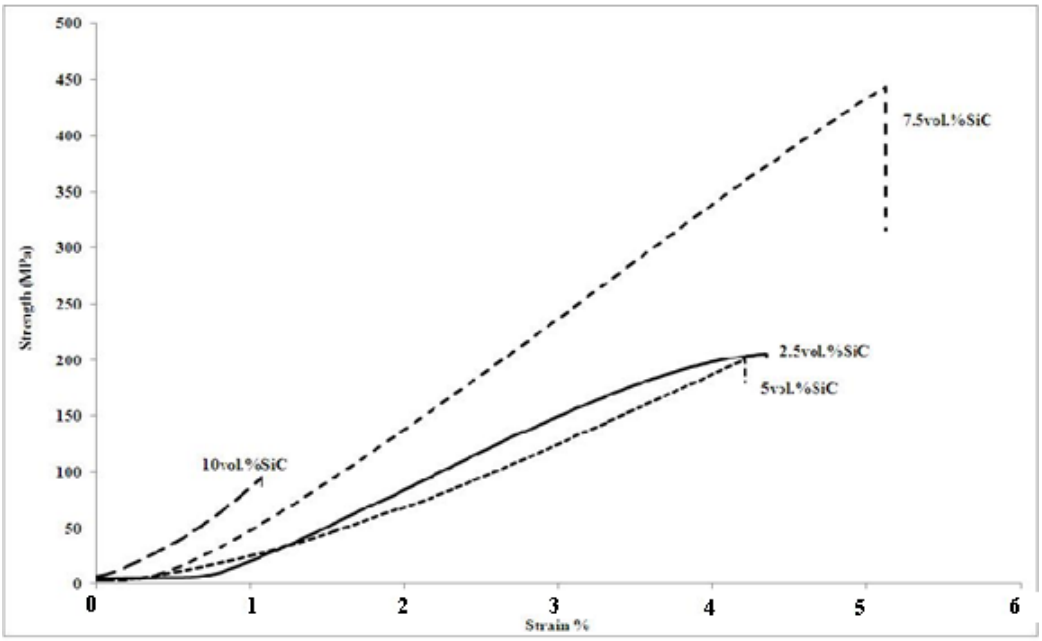

Figure 6.10: Tensile engineering stress-engineering strain curves of the specimens from the Al-4wt%Cu-(2.5-10)vol.%SiC nanocomposites produced by PCF reinforced with nano SiC.

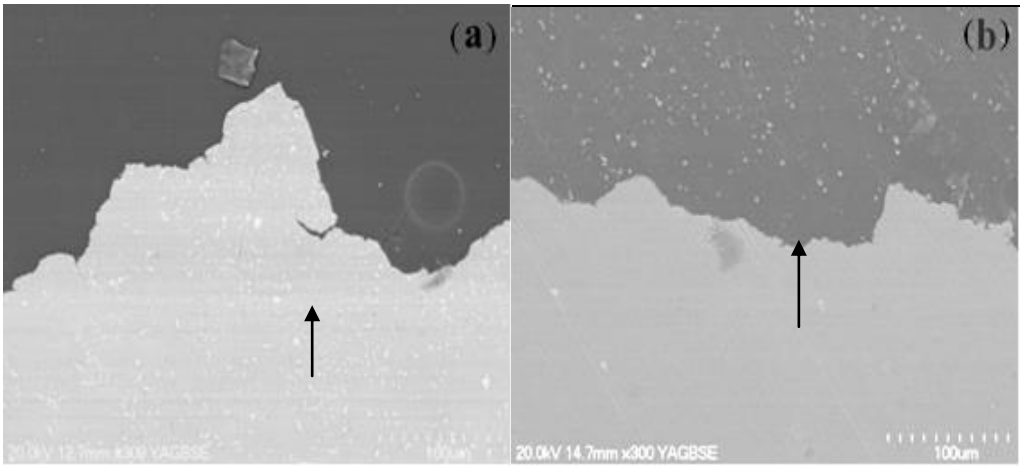

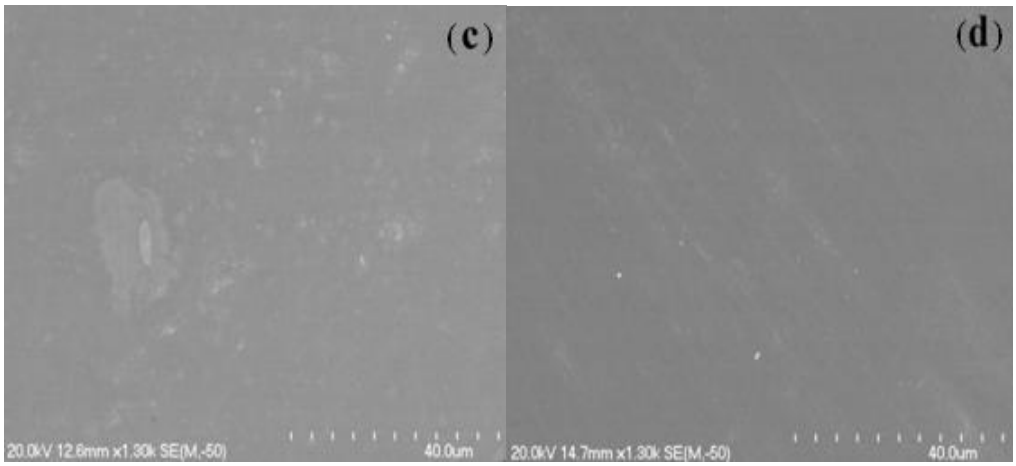

Figure 6.11: SEM micrographs of longitudinal sections of the tensile test specimens cut from the Al-4wt%Cu-(5 and 7.5)vol.% SiC nanocomposite disc produced by PCF: (a) just below the fracture surface, 5vol.% SiC ; (b) just below the fracture surface, 7.5vol.% SiC; (c) away from the fracture surface, 5vol.% SiC; (d) away from the fracture surface, 7.5vol.% SiC.

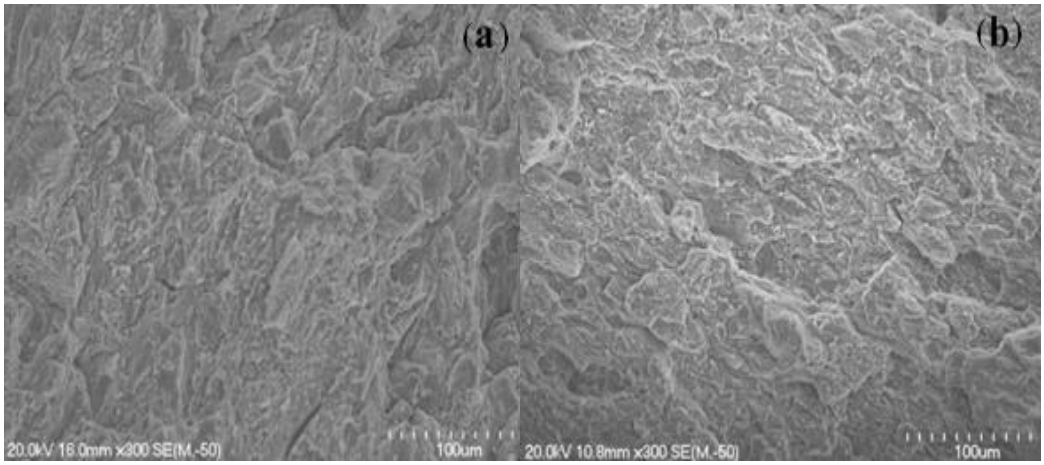

Figure 6.12: SEM micrographs of the fracture surfaces of the tensile tested specimens cut from Al-4wt%Cu-(7.5 and 10) vol.% SiC nanocomposite discs produced by PCF (a) 5vol.%SiC and (b) 7.5vol.%SiC.

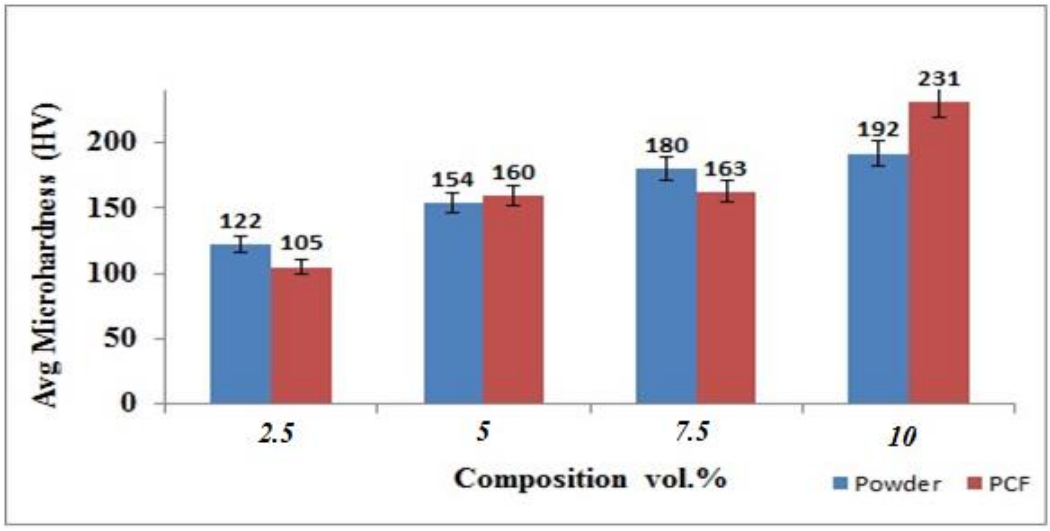

Figure 6.13: Microhardness for Al-4wt%Cu-(2.5-10)vol.%SiC nanocomposites discs produced by PCF.

6.4 Microstructures and Mechanical Properties of UFSAl-4wt%Cu-(2.5-10)vol.%SiC Nanocomposites Produced by Powder Compact Extrusion

6.4.1 Microstructure of Consolidated Samples Produced by Powder Compact Extrusion

The Al–4wt%Cu-(2.5-10)vol.%SiC nanocomposite compacts had a diameter of 25 mm and height in the range of 16-22mm (Table 6.6). The densities of all the powder compacts were measured by measuring their weights and dimensions. The theoretical densities of Al–4wt%Cu-(2.5-10)vol.%SiC nanocomposites were calculated using the rule of mixtures as described in Chapter 5. The relative density of the nanocomposite powder compacts decreased with increasing volume fraction of SiC nanoparticles in the milled nanocomposite powder.

Table 6.6: Theoretical and relative density of Al–4wt% Cu-(2.5-10)vol.%SiC nanocomposites and the corresponding powder compacts.

Composition	Theoretical density (g/cm^3)	Density of cold compact (g/cm^3)	Relative density of compacts (%)	Height of compact (mm)
Al-4wt%Cu-2.5vol%SiC	2.71	2.657	97.949	19.74
Al-4wt%Cu-5vol%SiC	2.72	2.376	87.166	21.84
Al-4wt%Cu-7.5vol%SiC	2.74	2.469	90.165	20.75
Al-4wt%Cu-10vol%SiC	2.75	2.433	88.428	16.86

Circular bars (8 mm in diameter) were produced from the powder compact extrusion experiments. The tensile test samples were cut from the centre of the extruded bars using an electrical discharge machining (EDM) wire cutter. The relative densities of the extruded bars were determined using Archimedes` method and are shown in Table 6.7.

SEM micrographs (Figure 6.14) of the extruded bars showed that they were almost fully dense with no apparent porosity. This is in agreement with the relevant densities of the cylindrical bars measured using the Archimedes` method.

Table 6.7: Theoretical and relative density of Al – 4wt.% Cu-(2.5-10)vol.%SiC extruded nanocomposites cylindrical bars produced by PCE.

Composition	Theoretical density (g/cm^3)	Density of Extrusion (g/cm^3)	Relative density (%)
Al-4wt%Cu-2.5vol%SiC	2.71	2.670	98.446
Al-4wt%Cu-5vol%SiC	2.72	2.715	99.604
Al-4wt%Cu-7.5vol%SiC	2.73	2.699	98.547
Al-4wt%Cu-10vol%SiC	2.75	2.722	98.950

Figure 6.15 shows XRD patterns of Al-4wt%Cu-(2.5-10)vol.%SiC nanocomposite cylindrical bars produced by PCE. The XRD patterns show strong Al peaks with weak SiC and Cu peaks, due to the small sizes and volume fractions of SiC and Cu particles. The average grain sizes and the lattice strain in the Al-4wt%Cu-(2.5-10)vol.%SiC nanocomposite cylindrical bars were estimated using the XRD data (Figure 6.16). The estimated average grain size and lattice strain of the Al-4wt%Cu-2.5vol.%SiC nanocomposites are 250 nm and 0.39%, respectively. With increasing volume fraction up to 5% of SiC nanoparticles, the grain size and lattice strain changed to 500 nm and 0.37%, respectively. For Al-4wt%Cu-7.5vol.%SiC nanocomposites, the grain size and lattice strain are 1250 nm and 0.36%, respectively. For Al-4wt%Cu-10vol.%SiC nanocomposites, the grain size and lattice strain are 1666 nm and 0.42%, respectively. The average grain size increased with increasing volume fraction of the SiC nanoparticles in the nanocomposite, while the lattice strain was little affected by the volume fraction of SiC.

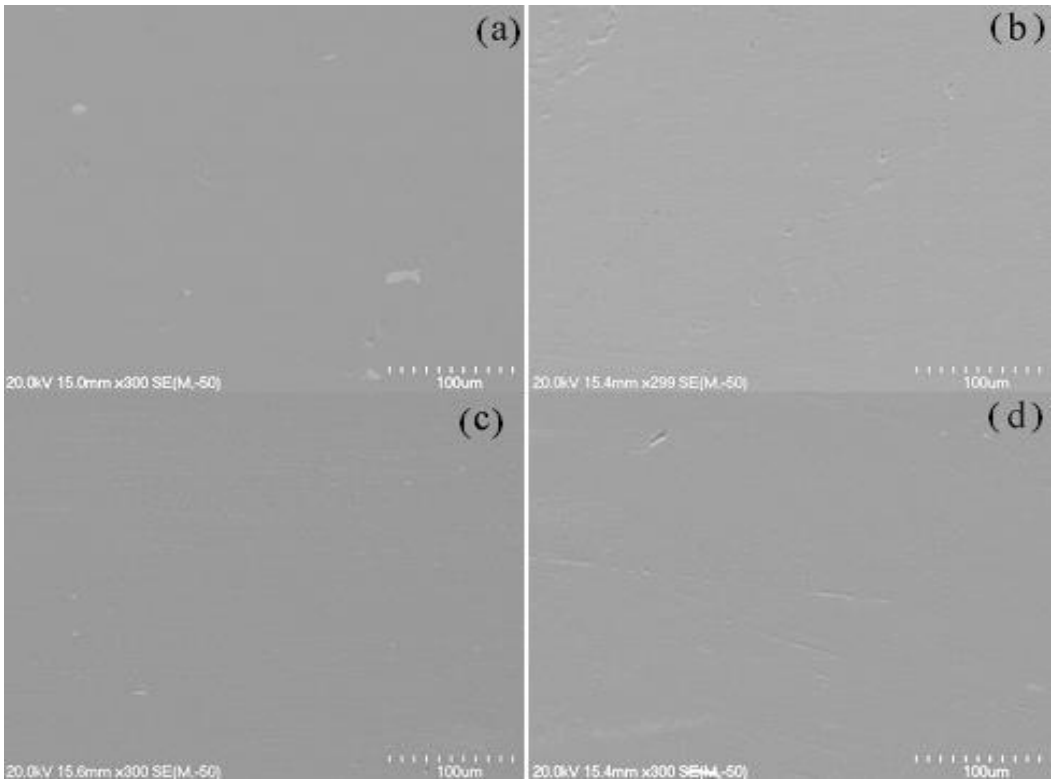

Figure 6.14: SEM micrographs of the Al-4wt.%Cu-(2.5-10)vol.% SiC nanocomposite bars produced by PCE: (a)2.5vol.%SiC, (b) 5vol.%SiC, (c) 7.5vol.%SiC, (d) 10vol.%SiC.

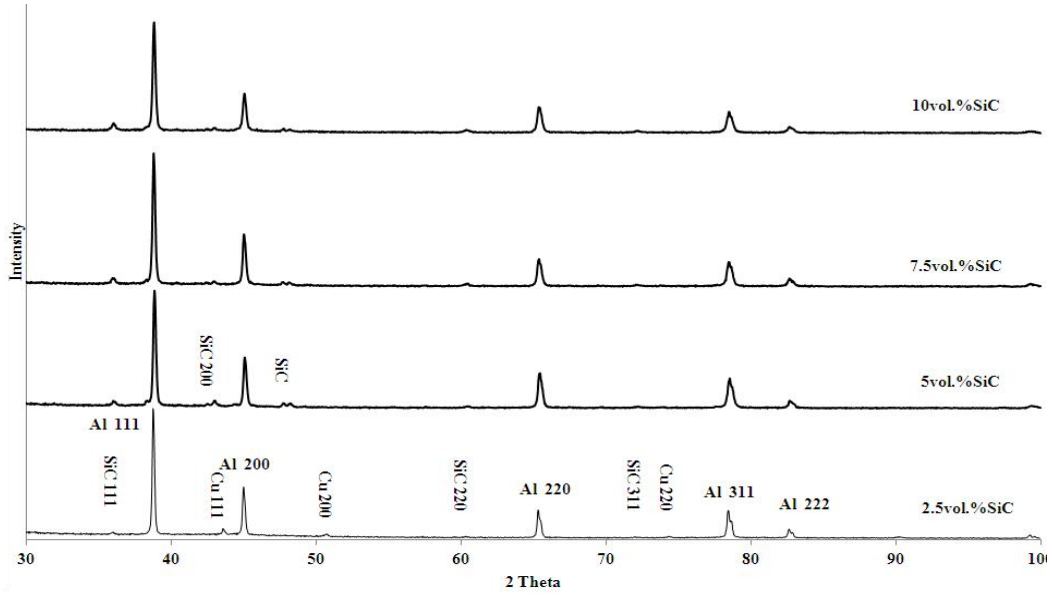

Figure 6.15: X-ray diffraction patterns of the Al-4wt%Cu-(2.5-10)vol.%SiC nanocomposite bars produced by powder compact extrusion**.**

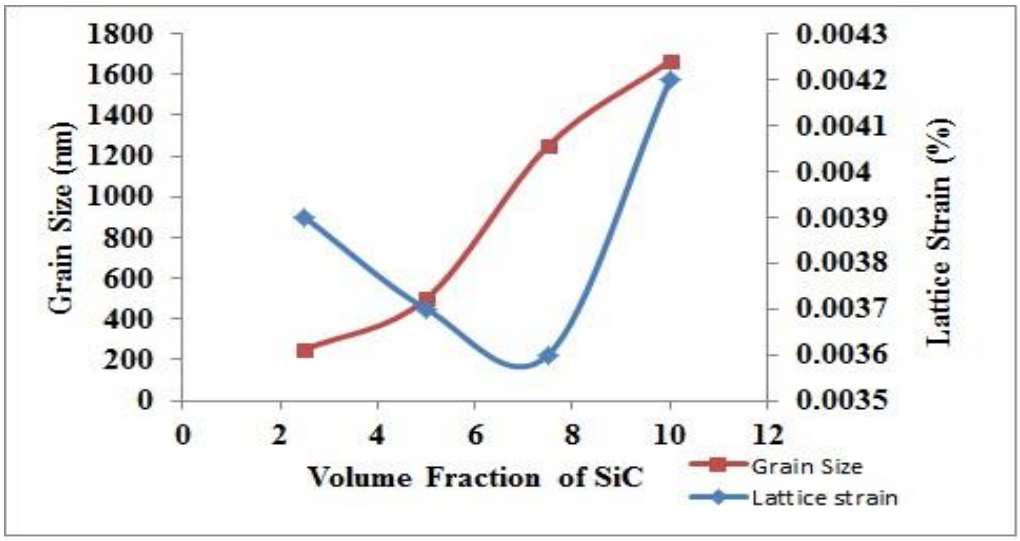

Figure 6.16: Grain size and lattice strain of the Al-4wt%Cu-(2.5-10)vol.%SiC nanocomposites bars produced by PCE as a function of the volume fraction of SiC nanoparticles.

Figure 6.17 shows bright field TEM images of the Al-4wt%Cu-(2.5-10)vol%SiC nanocomposite extruded bars. The microstructure had an ultrafine grain size (UFG), consisting of Al grains with sizes ranging from 100-800 nm for Al-4wt%Cu-2.5vol.%SiC, 200-600 nm for Al-4wt%Cu-5vol%SiC, 100-500 nm for Al-4wt%Cu-7.5vol%SiC, and 50-300 nm for Al-4wt%Cu-10vol%SiC. This shows that the average grain size estimated using the broadening of the XRD peaks (Figure 6.16) is clearly larger than the actual average Al grain size found in TEM. The TEM micrographs show a high dislocation density in the Al grains.

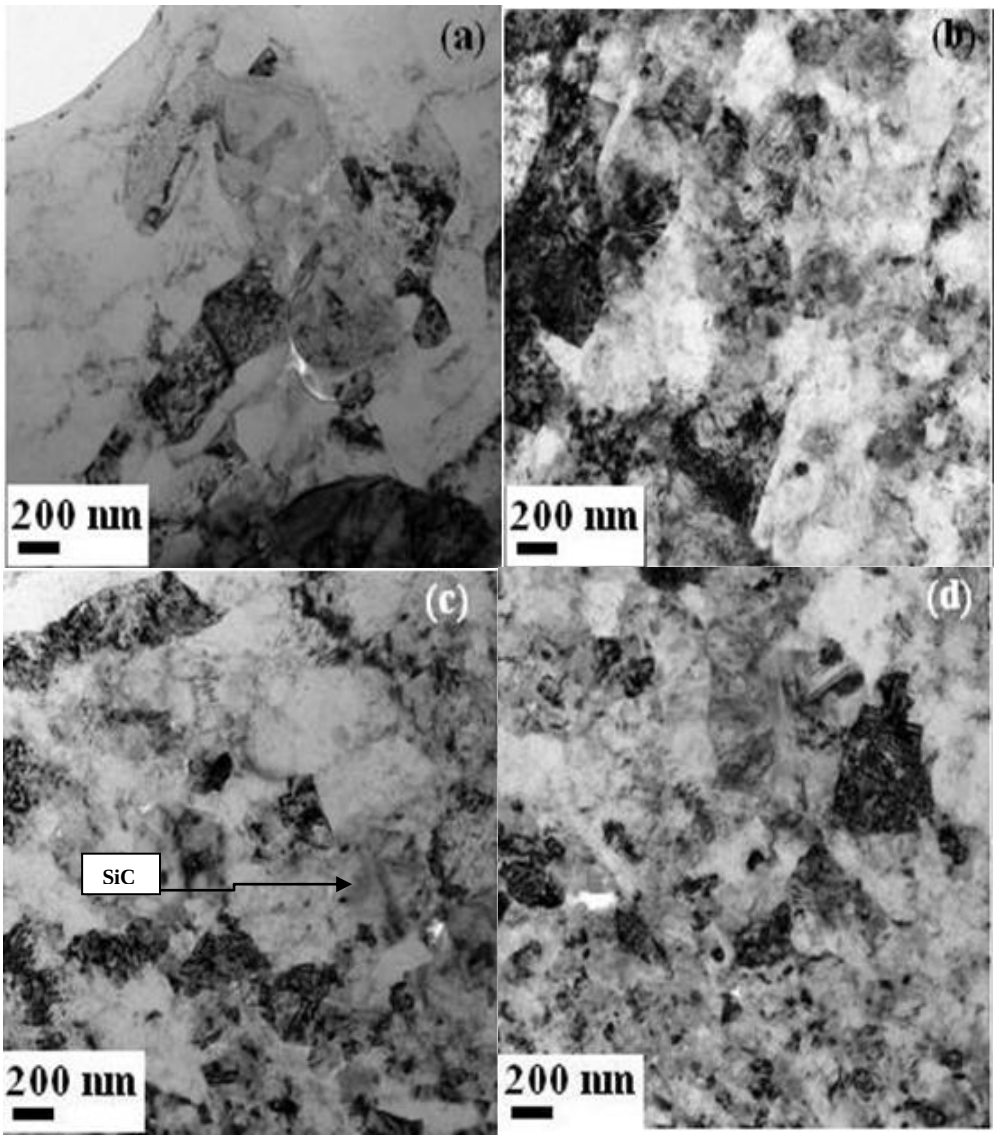

Figure 6.17: TEM bright field images ofAl-4wt%Cu-(2.5-10)vol.% SiC nanocomposites bars produced by PCE (a) 2.5vol.% SiC, (b) 5vol.% SiC, (c) 7.5vol.% SiC, (d) 10vol.% SiC.

6.4.2 Mechanical Properties and Fracture Behaviour of Consolidated Samples Produced by Powder Compact Extrusion

Figure 6.18 shows the tensile engineering stress-strain curves for specimens cut from the Al-4wt%Cu-(2.5-10)vol.%SiC nanocomposite bars produced by PCE. The tensile data after PCE are summarized in Table 6.8. The tensile testing specimens cut from the extruded bars of Al-4wt%Cu-(7.5 and 10) vol. %SiC nanocomposite fractured prematurely at stresses of 270 MPa and 325 MPa respectively. Thus, it is not clear what their yield strength and TS are. The overall

premature fracture may have been caused by easy fracturing of the SiC nanoparticles agglomerates within the Al matrix in the extruded bars.

Table 6.8: Yield strength, tensile strength, and plastic strain for Al – 4wt.% Cu-(2.5-10)vol.%SiC extruded nanocomposites cylindrical bars produced by PCE.

Composition	Yield Strength (MPa)	Tensile Strength (MPa)	Plastic Strain (%)
Al-4wt.%Cu-2.5 vol. %SiC	98	168	6.8
Al-4wt.%Cu-5 vol. %SiC	391	400	1.2
Al-4wt.%Cu-7.5 vol. %SiC	N/A	N/A	N/A
Al-4wt.%Cu-10 vol. %SiC	N/A	N/A	N/A

Figure 6.19 shows typical fracture surfaces of the tensile test specimens cut from the composite bars. It can be seen that the fracture of the Al-4wt%Cu-(2.5 and 5) vol. % SiC nanocomposite specimens occurred through ductile fracture of the Al matrix, with the fracture surfaces showing dimples and ligaments. It appears that with increasing SiC nanoparticles content from 2.5 vol. % to 5%, the depth of the dimples and height of the ligaments becomes significantly smaller, as shown in Figure 6.19 (a) and (b). The fracture surfaces of the Al-4wt%Cu-(7.5 and 10) vol. %SiC nanocomposite specimens were very flat, suggesting that their fracture was brittle in nature. To reveal more information about the nature of the bonding between the powder particles, the longitudinal sections of the fractured specimens just below the fracture surfaces were also examined using SEM (Figure 6.20). It can be seen that only a few cavities(indicated by the arrows) formed near the fracture surfaces during tensile deformation and fracture of the specimens. The shapes of the cavities suggest that they were not caused by separation of neighbouring powder particles due to weak interparticle bonding in the broken tensile test specimens. The average microhardness of the Al-4wt.%Cu-(2.5-10)

vol. %SiC nanocomposite bars produced by PCE increased from 104 HV to 205 HV with increasing the volume fraction of SiC nanoparticles from 2.5 to 10% (Figure 6.21).

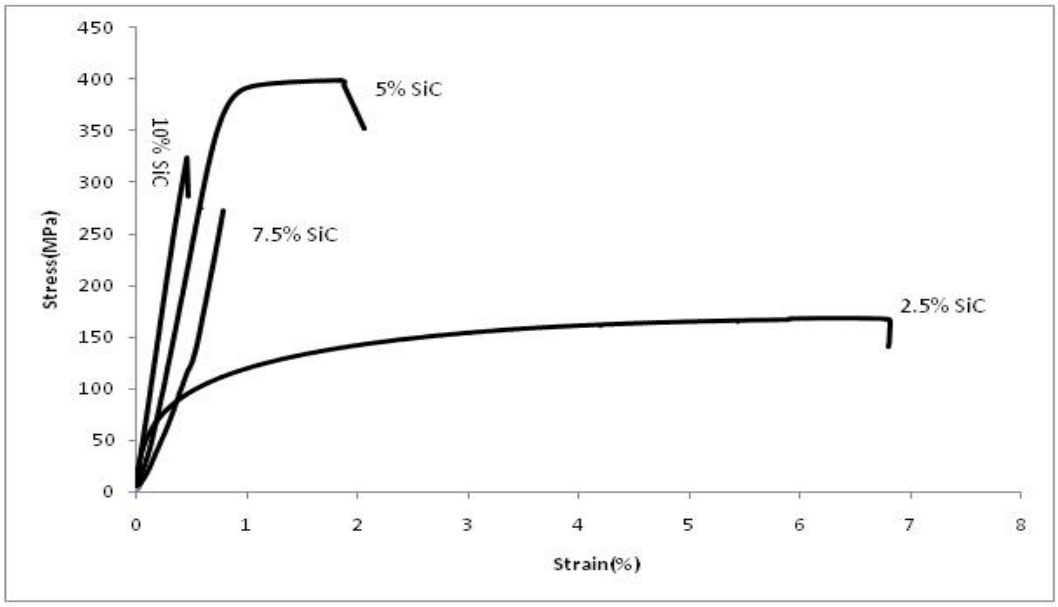

Figure 6.18: Tensile stress-strain curves of specimens cut from Al-4wt%Cu-(2.5-10) vol. % SiC bars produced by PCE.

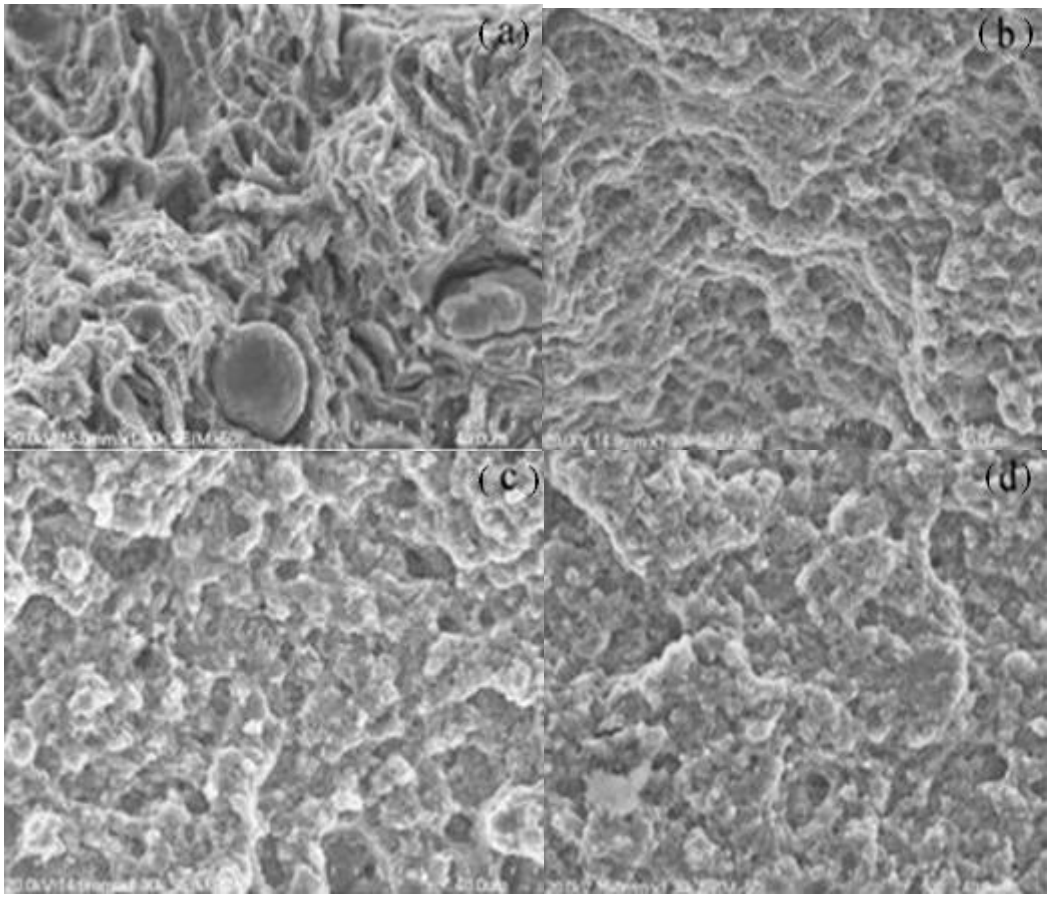

Figure 6.19: SEM micrographs of the fracture surfaces of the tensile test specimens cut from Al-4wt%Cu-(2.5-10) vol.% SiC nanocomposite bars produced PCE: (a) 2.5vol. %SiC (b) 5 vol. %SiC (c) 7.5vol. %SiC (d) 10vol. %SiC.

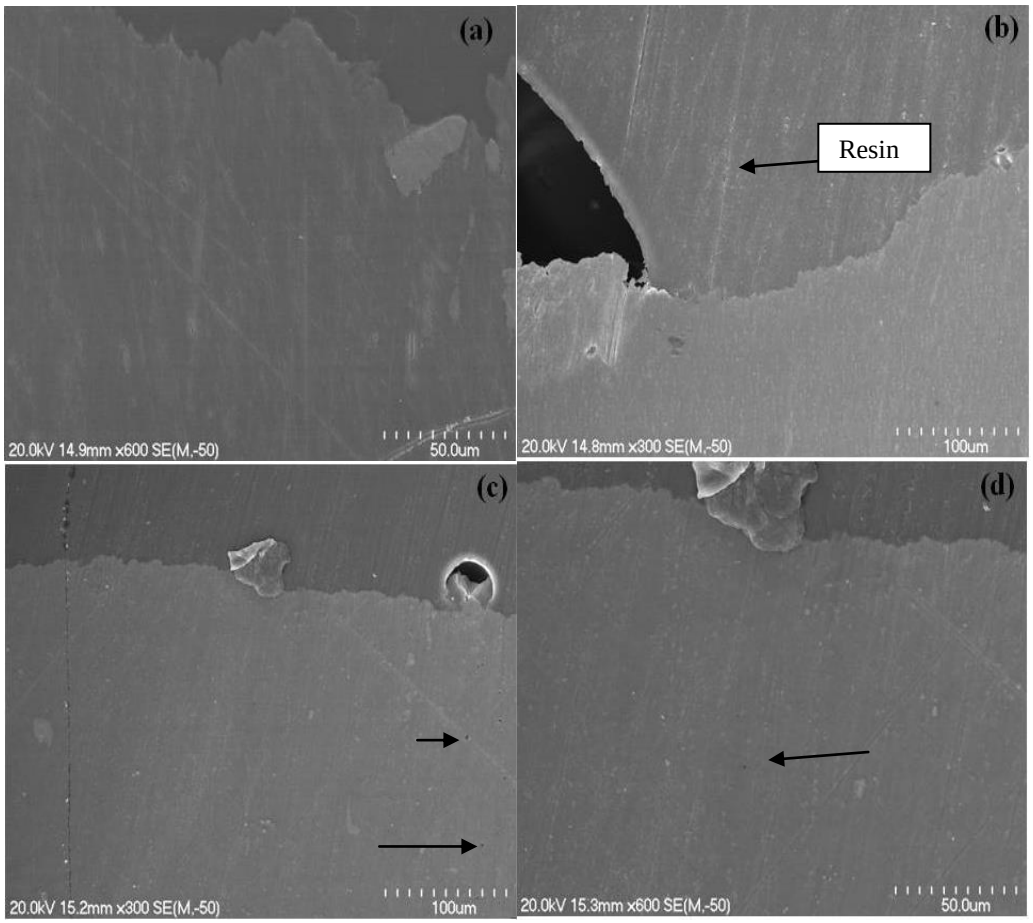

Figure 6.20: SEM micrographs of the longitudinal sections just below the fracture surfaces of the tensile test specimens cut from the Al-4wt%Cu-(2.5-10)vol.% SiC nanocomposite bars produced by PCE: (a) 2.5vol.% SiC ; (b) 5vol.% SiC; (c) 7.5vol.% SiC; (d) 10vol.% SiC.

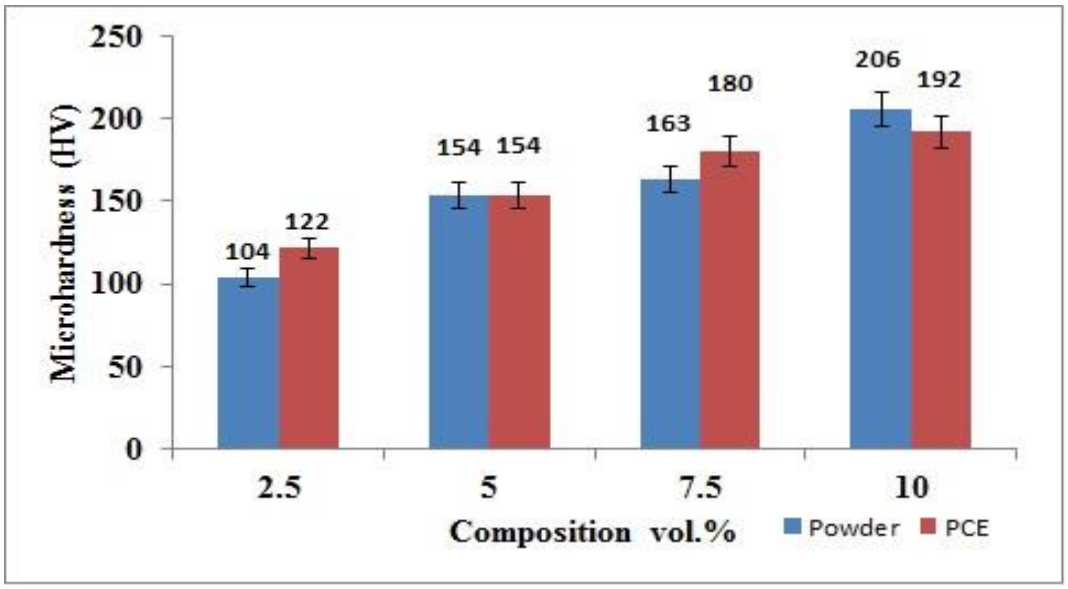

Figure 6.21: Microhardness for Al-4wt%Cu-(2.5-10)vol.%SiC nanocomposites bars produced by PCE.

6.5 Electrical Properties

Electrical resistivity is a measure of how strongly a material opposes the flow of electrical current. Conductivity (σ) is the inverse of the electrical resistivity and measured by Siemens per meter. The electrical resistivity is calculated by the following equation (see also Figure 6.22);

$$\rho = R\frac{A}{L} \qquad (6.1)$$

where; R is the electrical resistance of a uniform specimen of the material (measured in ohms, Ω), ℓ is the length of the piece of material (measured in meters, m), A is the cross-sectional area of the specimen (measured in square meters, m^2).

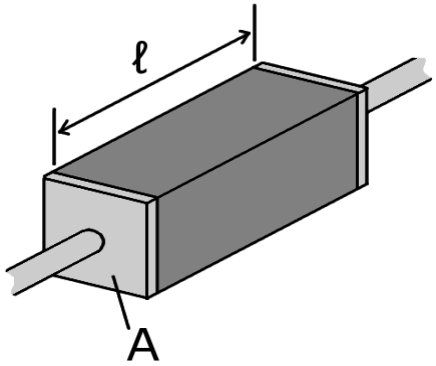

Figure 6.22: Piece of resistive material with electrical contacts on both ends.

Table 6.9: The resistivity, conductivity and temperature coefficient of various materials at 20 °C [5, 6].

Material	**P(Ω.m) at 20 C**	**σ(S/m) at 20 C**
Aluminium	2.82×10^{-8}	3.5×10^{7}
Copper	1.68×10^{-8}	5.96×10^{7}

Table 6.10: The electrical resistivity for Al-4wt%Cu-(2.5-10)vol.%SiC nanocomposite produced by powder compact extrusion.

Specimen	Voltage (v)	Current (I)	Length (m)	Resistivity (P) (Ω)	Conductivity (1/p) ($S \cdot m^{-1}$)
Al-4wt%Cu-2.5vol.%SiC	0.000766	10	0.00629	4.4E-08	2.27 E7
Al-4wt%Cu-5vol.%SiC	0.00113	10	0.0063	6.2E-08	1.6E7
Al-4wt%Cu-7.5vol.%SiC	0.000855	10	0.00658	5.5E-08	1.8E7
Al-4wt%Cu-10vol.%SiC	0.00106	10	0.00666	7.04E-08	1.42E7

The R was fixed to be 0.007 Ω.

The Al-4wt%Cu-(2.5-10)vol.%SiC nanocomposite bars produced by PCE were used to measure the electrical conductivity as there were enough specimens available for this test. It was noticed that with increasing volume percentage of SiC nanoparticles within the matrix, the conductivity of the nanocomposite extruded bars decreased due to their hindering the movement of the electrons within the Al matrix. This is in agreement with observations made by Chang et al. and Akthars et al. [7, 8].

6.6 Discussion

6.6.1 Effect of SiC Volume Fraction on Microstructure

With increasing volume fraction of SiC nanoparticles, the microstructure of the Al-4wt%Cu matrix of the bulk nanocomposite samples becomes finer. There are two reasons for this: (i) an increase in the number of SiC nanoparticles in the starting powder microstructure increases the effectiveness of HEMM, causing the microstructure of the powder to be finer. This process is confirmed by TEM examination of the milled powder particles. (ii) The thermal stability of the Al-4wt%Cu matrix increases with increasing volume fraction of SiC nanoparticles. This effect leads to a slower rate of microstructural coarsening with increased content of SiC nanoparticles.

With increasing volume fraction of SiC, a high dislocation density around the SiC promotes dynamic recrystallization (DRX), giving rise to small sub-grains during hot deformation. This suggests that the dynamically recrystallized grains are influenced significantly by the SiC volume fraction. When the deformation temperature is increased, the dislocation density decreases and the grain size increases for all of the composites [9], no clear evidence from TEM was observed, but that what is expected as mentioned from other researchers. During deformation, the mismatch between a non-deforming particle and ductile metal matrix during deformation leads to an enforced strain gradient in the matrix near to a particle. The strain gradient creates a region which contains a high dislocation density and large orientation gradient. These regions are called particle deformation zones (PDZ). In other words, the addition of particles refines the matrix grain structure of matrix during hot deformation [10].

6.6.2 Mechanical Properties and Fracture Behaviour

Figure 6.10 shows stress-engineering strain curves for specimens from the Al-4wt%Cu-(2.5-10)vol.%SiC nanocomposite forged discs reinforced with nano SiC. It is known that aluminium based particulate reinforced MMCs have their limitations because of their low forgability resulting from defects. These defects may arise from the presence of nondeformable particles, a non-uniform distribution of these particles and porosity [10-12]. A study showed that forged samples had yield strengths of over 400 MPa with increased elongation at room temperature up to twice that in an AA2618/20vol%Al_2O_3 composite [13].

The yield strength of the bulk nanocomposite samples produced by powder compact extrusion increases significantly from 98 to 391 MPa with increasing volume fraction of the SiC from 2.5 to 5 vol. %, showing that SiC nanoparticles are effective in strengthening this material. Also, a further refinement of the Al-

4wt%Cu microstructure also contributes to an increase in yield strength. The high effectiveness of these two factors in strengthening the composite is also reflected by the observation that the yield strength of an ultrafine structured Al-4wt%Cu-5vol.%SiC nanocomposite (391 MPa) is more than 2.5 times higher than that of a coarser structured Al-4wt%Cu-10vol.%SiC composite with an average particle size of 23μm [11]. The significant decrease in the ductility of bulk nanocomposite samples with increasing volume fraction of SiC nanoparticles from 2.5 to 5% may be for two reasons: (i) The existence of SiC nanoparticles agglomerates in the microstructure, which makes the formation of cavities under tensile stress easier, and (ii)a refinement of the microstructure of the Al-4wt%Cu matrix, which makes it easier to lose stability of deformation under tension [13]. Similarly, the premature fracture of the Al-4wt%Cu-(7.5 and 10)vol.%SiC nanocomposite samples during tensile testing may also be due to the existence of SiC nanoparticles agglomerates in their respective microstructures, making it very easy to form cavities under tensile stress. With a high total volume fraction of SiC nanoparticles at volume fractions of 7.5 or 10%, the number of such SiC nanoparticles agglomerates per unit volume of the sample can be quite high, so it is easy for cracks to form and propagate, causing fracture to occur before macroscopic yielding.

According to Narayanasamy et.al [1], with increasing amounts of SiC in the composites, the SiC particles impede the dislocation motion and hence the stress required for further plastic deformation increases, which cause all the stresses to increase. This is not true for all of the composites examined in this study due to the low interparticle bonding, which resulted in a brittle material. The material may fracture pre-maturely.

Brittle and ductile types of fracture surface were noted after tensile testing. In Figure 6.19, it can be seen that the fracture of the Al-4wt%Cu-(2.5 and 5)vol. % SiC nanocomposite specimens occurred through ductile fracture of the Al matrix, with the fracture surfaces showing dimples and ligaments. It appears that with increasing SiC nanoparticle content from 2.5 vol. % to 5%, the depth of the dimples and height of the ligaments becomes significantly smaller. On the other hand, the fracture surfaces of the Al-4wt%Cu-(7.5 and 10) vol. %SiC nanocomposite specimens were macroscopically flat, suggesting that the cracks propagated with ease under tensile stress, causing the tensile test specimens to fracture prematurely. At microscopic level, the fracture surfaces were fairly rough, and the sizes of the fracture surface features scaled with the grain sizes, indicating that at a microscopic level, the fracture occurs through intergranular fracture. With SiC reinforcement in the Al matrix a partial ductile fracture was observed and there are dimples with embedded SiC particles and no clear separation between the SiC and matrix interface. Such findings have also been reported by Badini [14].The same observation was reported by Ogel et.al. [2] Who also found that SiC reinforced specimens had a partially ductile fracture containing dimples with SiC embedded in them. These observations indicate that because there is no clean separation at the SiC/matrix interface there is good interfacial bonding.

6.7 Summary

- The fracture strength of the Al-4wt%Cu-micro-SiC was increased from 225MPa for Al-4wt%Cu-2.5vol. %SiC to 412 MPa for Al-4wt%Cu-10vol. % SiC. The Al-4wt%Cu-2.5vol. %SiC forged disc did not show any macroscopic plastic yielding, while the Al-4wt%Cu-(7.5 and 10)vol. %SiC forged disc showed macroscopic plastic yielding with a small plastic strain to fracture (~1%).

- The average microhardness of the extruded bars increased from 104 HV to 205 HV with increasing volume fraction of SiC in the metal matrix nanocomposites.
- The average microhardness of the extruded bars for Al-4wt%Cu-(2.5-10)vol.% SiC increased from 104 HV to 205 HV with increasing volume fraction of SiC nanoparticles from 2.5 to 10%. The tensile strength increased from 168 MPa to 400 MPa with increasing the volume fraction of SiC nanoparticles from 2.5 to 5% while the ductility dropped from 6.8% to 1.2 %.

6.8 References

[1] R.Narayanasamy, T.Ramesh, and M.Prabhakar, "Effects of particle size of SiC in aluminium matrix on workability and strain hardening behaviour of P/M composite," *Materials Science and Engineering A*, vol. 504, pp. 13-23, 2009.

[2] B. Ogel and R. Gurbuz, "Microstructural characterization and tensile properties of hot pressed Al-SiC composites prepared from pure Al and Cu powders," *Materials Science and Engineering: A*, vol. 301, pp. 213-220, 2001.

[3] H. Gleiter, "Nanostructured materials: basic concepts and microstructure," *Acta Materialia*, vol. 48, pp. 1-29, 2000.

[4] S. Gustafsson, L. K. L. Falk, E. Lidén, and E. Carlström, "Pressureless sintered Al_2O_3–SiC nanocomposites," *Ceramics International*, vol. 34, pp. 1609-1615, 2008.

[5] R. A. Serway, *Principles of Physics* 2ed. Fort Worth, Texas; London: Saunders College Pub, 1998.

[6] D. Griffiths, *Introduction to Electrodynamics* 3ed. Upper Saddle River, New Jersey: Prentice Hall, 1999.

[7] S.-Y. Chang, C.-F. Chen, S.-J. Lin, and T. Z. Kattamis, "Electrical resistivity of metal matrix composites," *Acta Materialia*, vol. 51, pp. 6191–6302, 2003.

[8] F. Akhtara, S. J. Askaria, K. A. Shaha, X. Dua, and S. Guoa, "Microstructure, mechanical properties, electrical conductivity and wear behavior of high volume TiC reinforced,'Materials Characterization, vol 60, pp. 327-336,2009.

[9] V. Massardier, L. Pelletier, and P. Merle, "Influence of the introduction of ceramic particles in Al-Cu alloys on GP zone formation," *Materials Science and Engineering: A*, vol. 249, pp. 121-133, 1998.

[10] Y. Xirong, Z. Xicheng, and F. Wenjie, "Deformed Microstructures and Mechanical Properties of CP-Ti Processed by Multi-Pass ECAP at Room Temperature," *Rare Metal Materials and Engineering*, vol. 38, pp. 955-957, 2009.

[11] Gupta M.,Lai M.O. and Soo C.Y. Effect of type of processing on the microstructural features and mechanical properties of Al-Cu/SiC metal matrix composites. Materials Science and Engineering A .1996;210:114-122.

[12] C.-H. Lee, H.-H. Lu, C.-A. Wang, P. K. Nayak, and J.-L. Huang, "Microstructure and mechanical properties of TiN/Si_3N_4 nanocomposites by spark plasma sintering (SPS)," *Journal of Alloys and Compounds*, vol. 508, pp. 540-545, 2010.

[13] Ma,E. (2003) “Nanocrystalline materials: controlling plastic instability.” Nature Materials 2(1): 7-8.

[14] C. Badini, G. M. La Vecchia, P. Fino, and T. Valente, "Forging of 2124/SiCp composite: preliminary studies of the effects on microstructure and strength," *Journal of Materials Processing Technology*, vol. 116, pp. 289-297, 2001.

Chapter Seven: Conclusions and Recommendations

7.1 Conclusions

- High energy mechanical milling was used to produce Al , Al-(2.5-10)vol.% Al_2O_3 ,and Al-4wt%Cu-(2.5-10)vol.%SiC composite balls/granules/powder particles. It was found that Al_2O_3 and SiC nanoparticles can be uniformly dispersed in an Al matrix.
- An addition of 1 weight percent, of PCA was added for all the milling conditions to improve the milling and reduce the effect of Al welding and powder sticking to the inner wall of the vial.
- The nano SiC and Al_2O_3 were embedded into the aluminium matrix due to the high strains affecting the surface during the milling and the very small size of the reinforcement relative to the size of the Al particles.
- For Al-(2.5-10)vol.% Al_2O_3 the XRD patterns showed only Al peaks, due to the small fraction and the very small size of the Al_2O_3 nanoparticles. XRD analysis of the as milled nano-structured Al-(2.5-10)vol. % Al_2O_3 composite showed that extensive milling in Route 2 caused clear broadening of the Al peaks with a reduction in the intensity which are indications of grain size reduction with increased milling time.
- Two different grain sizes of SiC reinforcement was used to produce the Al-4wt%Cu-(2.5-10)vol.%SiC UFG structured composites. XRD patterns of milled Al-4wt%Cu- (2.5-10)vol%SiC composites showed a mix of Al peaks, Cu peaks , and SiC peaks. The Cu and SiC peaks both had very weak intensities which could be explained by the small weight and volume percentage of Cu and SiC, respectively, in the aluminium matrix. It is clearly that with increasing volume fraction of SiC particles within theAl-4wt%Cu matrix the XRD peaks were becoming sharper and broader,

suggesting that the Al matrix grains were decreasing in size. The average grain sizes and lattice strains of the milled powder were determined using the Williamson-Hall method. TEM examination confirmed a reduction in the Al matrix grain size for the Al-4wt%Cu-(2.5-10)vol%SiC composite with increasing volume fraction of reinforcement within the matrix.

- There was a gradual increase in the average microhardness of the Al and the Al- (2.5-10) vol.% Al_2O_3 composite powders with increasing alumina content after 12 hours of milling with increasing alumina content. The microhardness also increased with increasing volume fraction of micro SiC within the matrix but not increase at a steady rate. This was probably because of a lack of uniformity of the SiC within the matrix and the clustering of the SiC within the matrix.
- The UFG structure Al-(2.5-10)vol.% Al_2O_3 and Al-4wt%Cu-(2.5-10)vol.%SiC composites can be synthesized by a combination of high energy mechanical milling and severe plastic deformation which was utilized to consolidate the powder compacts into nearly fully dense forged discs and extruded bars.
- The relative densities of forged samples for both the Al –(2.5-10)vol.% Al_2O_3 and the Al-4wt%Cu –(2.5-10)vol.%SiC composites reached 95% and 99% respectively.
- For powder compact extrusion experiments, the powder compacts were heated to a sintering temperature of 500 ºC using induction heating under an argon atmosphere, and then extruded through an open die pre-heated to 450 ºC using a 100-ton hydraulic press . The relative densities were calculated for the extruded samples for both the Al–(2.5-10)vol.% Al_2O_3 and the Al-4wt%Cu –(2.5-10)vol.%SiC composites produced. SEM

micrographs taken from a random sample cut from the extruded bars showed no porosity.

- No significant microscopic yielding was noticed for the Al-2.5 and 10 vol. % Al_2O_3 composites produced by powder compact forging. Al-5vol. % Al_2O_3 showed plastic yielding of 8%.No significant microscopic yielding was noticed for the Al- 10 vol. % Al_2O_3 composite produced by powder compact extrusion. Al-2.5vol. % Al_2O_3 showed plastic yielding of ~1% with the highest tensile strength of 364 MPa while Al-5vol. % Al_2O_3 showed plastic yielding of 8%. An Al-5vol. % Al_2O_3 specimen achieved a yield strength of 318 MPa with good ductility.
- The ultimate tensile strength increased from 168 MPa to 400 MPa with increasing volume fraction of SiC nanoparticles from 2.5 to 5% while the ductility dropped from 6.8% to 1.2 %. The average microhardness of the extruded bars for Al-4wt%Cu-(2.5-10)vol.% SiC increased from 104 HV to 205 HV with increasing the volume fraction of SiC nanoparticles from 2.5 to 10%.

7.2 Recommendations for Future Work

- Improve the powder production technique by reducing the usage of PCA; transfer the powder directly to the powder compacting steps.
- Perform heat treatment and annealing on Al-(2.5-10)vol. % Al_2O_3 and Al-4wt%Cu-(2.5-10)vol.% SiC composites.
- Study the effect of nano reinforcement on the physical and electrical properties.

- Carry out high temperature tensile testing for the forged and extruded composites to study their mechanical behaviour and to develop an in-depth understanding of the effect of temperature.
- Study the effect of a rolling process on improvements in material quality.
- Further TEM studies of the UFG and nanostructured materials to get an in-depth understanding of microstructure/processing/ property relationships.

Appendix

Example Williamson-Hall method to illustrate how I calculated lattice strain and grain size for Figure 4.21 and Figure 4.22

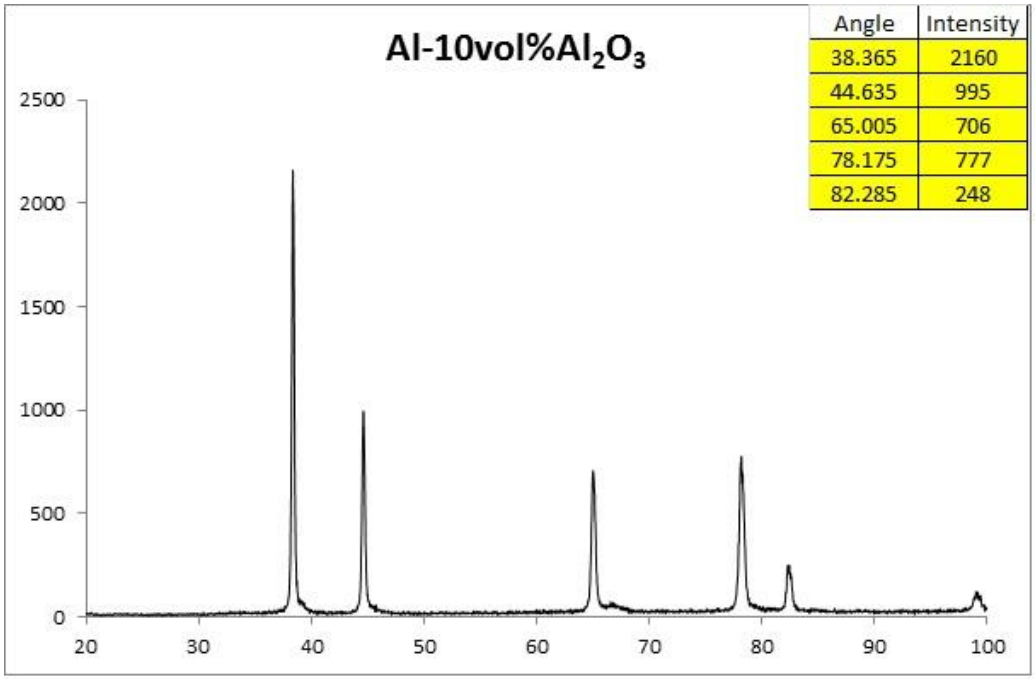

Peak 1:

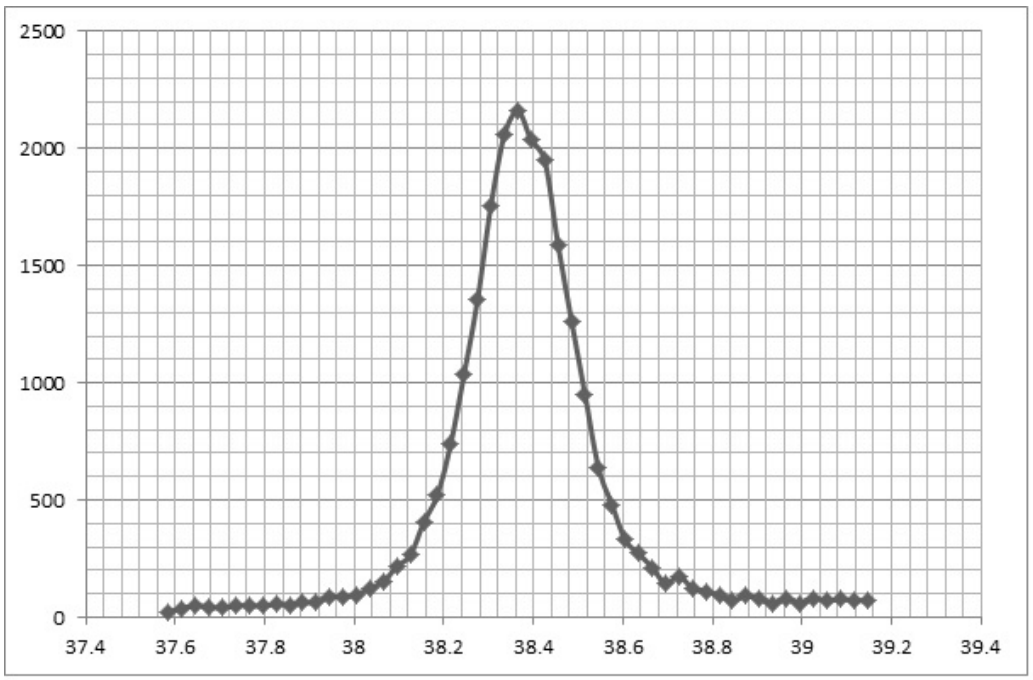

Peak 2:

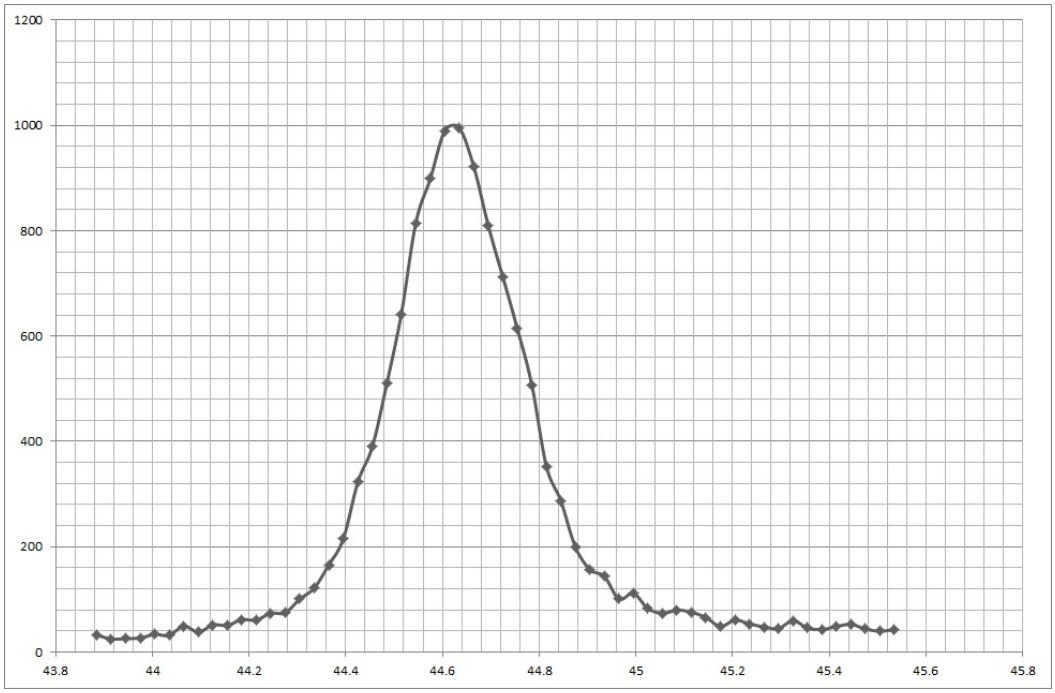
1200
1000
800
600
400
200
0
43.8
44
44.2
44.4
44.6
44.8
45
45.2
45.4
45.6
45.8

Peak 3:

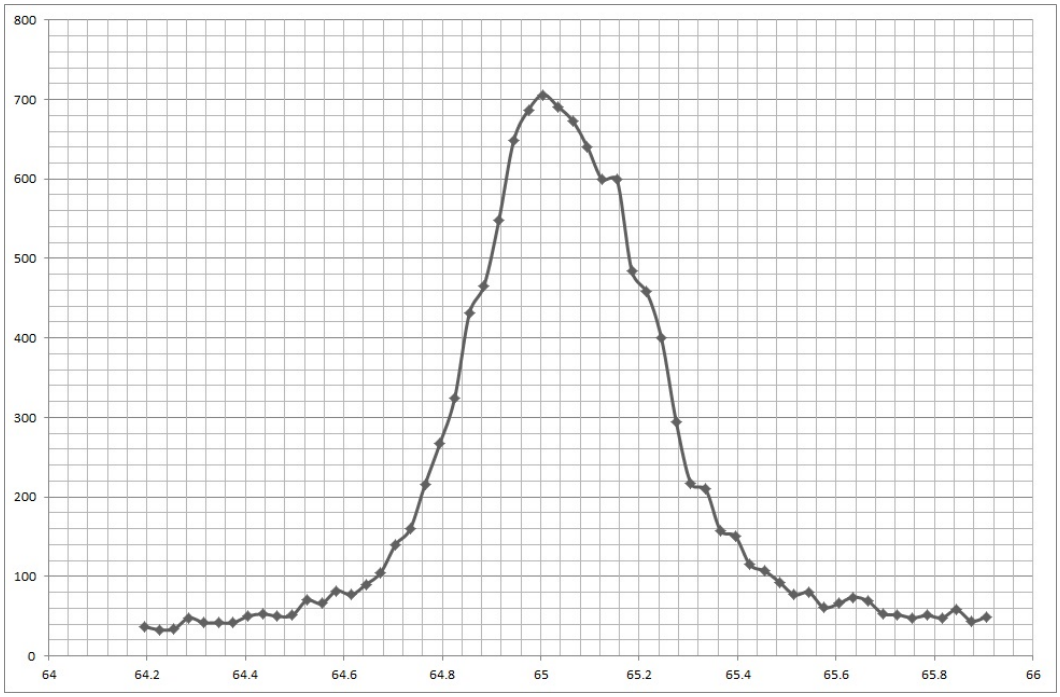
800
700
600
500
400
300
200
100
0
64
64.2
64.4
64.6
64.8
65
65.2
65.4
65.6
65.8
66

Peak 4:

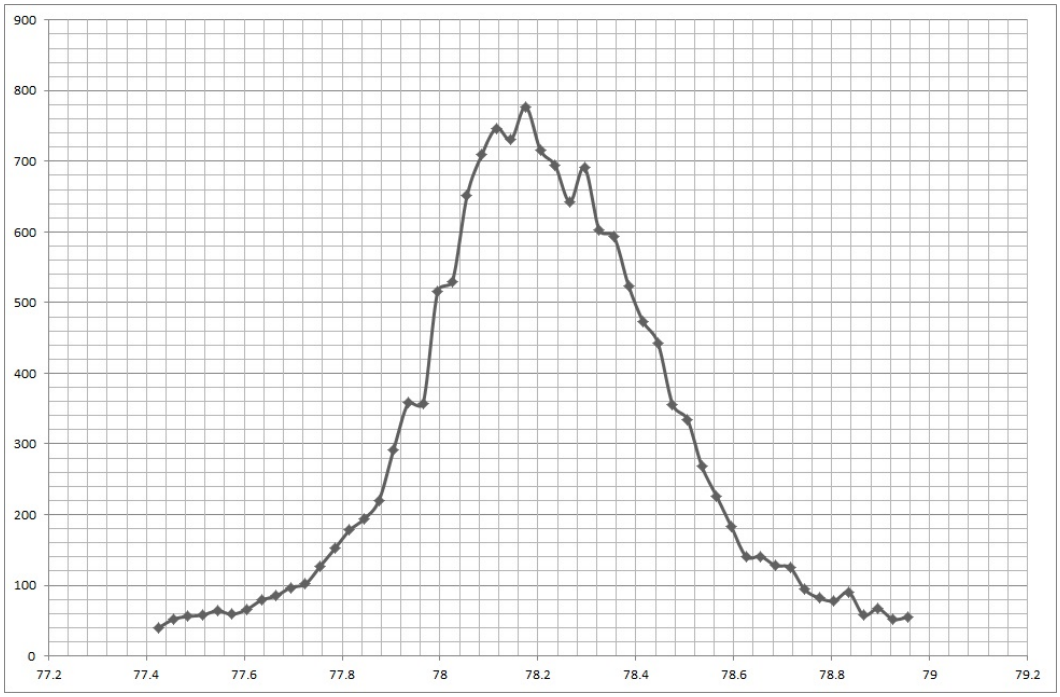

Peak 5:

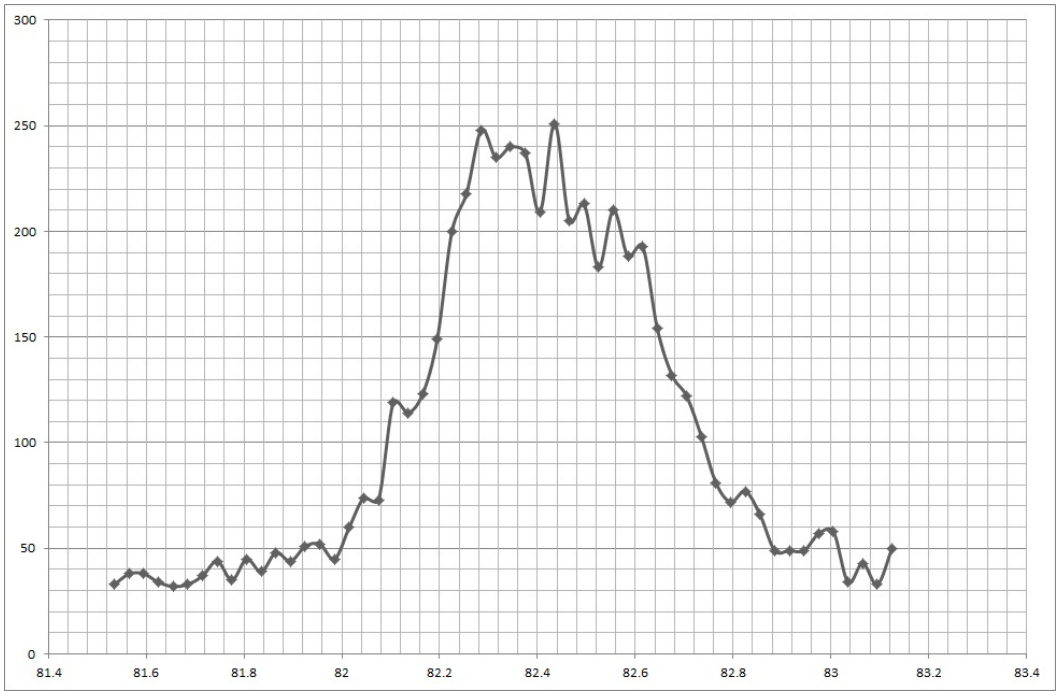

Calculations:

0.9	λ 1.54E-10	K 1.39E-10

Al-10vol%Al2O3 12 h

2 Theta	Theta	Cos θ	Max Int	Lev Int	Half Int	Actual Int	2 Theta		Λ θ β	θ β inst	(1) θ β ^2	(2) θ β ^2	β	β = (Λ θ β * π) / 180
2θ	2θ/2		M	L	(M - L)/2		$2\theta_1$	$2\theta_2$	$(\theta_2 - \theta_1)/2$		Λ θ β^2	θ β inst ^2	((1)-(2))^0.5	
38.365	19.183	0.944477	2160	100	1030	1130	38.255	38.5	0.1225	0.0853	0.0150	0.00728	0.0879	1.53E-03
44.635	22.318	0.925094	995	40	477.5	517.5	44.49	44.78	0.1450	0.0883	0.0210	0.00780	0.1150	2.01E-03
65.005	32.503	0.843368	705	40	333	373	64.84	65.255	0.2075	0.1008	0.0431	0.01016	0.1814	3.17E-03
78.175	39.088	0.776184	777	60	358.5	418.5	77.98	78.445	0.2325	0.1116	0.0541	0.01245	0.2040	3.56E-03
82.285	41.143	0.753076	243	40	104	144	82.185	82.66	0.2375	0.1134	0.0564	0.01286	0.2087	3.64E-03

	λ	K	
0.9	1.54E-10	1.39E-10	1.540598

sample

2 Theta	Theta	Cos θ	Sin θ	β*Cos θ	β*Cos θ/λ	Sin θ/λ	2 Theta		Λ θ β					β = (Λ θ β * π) / 180
2θ	2θ/2						$2\theta_1$	$2\theta_2$	$(\theta_2 - \theta_1)/2$					
38.365	19.183	0.944477	0.328578	0.00145	0.00094	0.21328	38.475	38.72	0.122					1.53E-03
44.635	22.318	0.925094	0.379739	0.00185	0.00121	0.246488	44.72	44.97	0.125					2.01E-03
65.005	32.503	0.843368	0.537836	0.00267	0.00173	0.348784	65.085	65.41	0.178					3.17E-03
78.175	39.088	0.776184	0.630506	0.00275	0.00179	0.409261	78.22	78.655	0.218					3.56E-03
82.285	41.143	0.753076	0.657934	0.00274	0.00178	0.427064	82.445	82.915	0.235					3.64E-03

lattice parameter

Smaple	2Theta	Theta	Sin θ	ain Size	a
	38.365	19.1825	0.326827	2.36E-10	4.08E-10

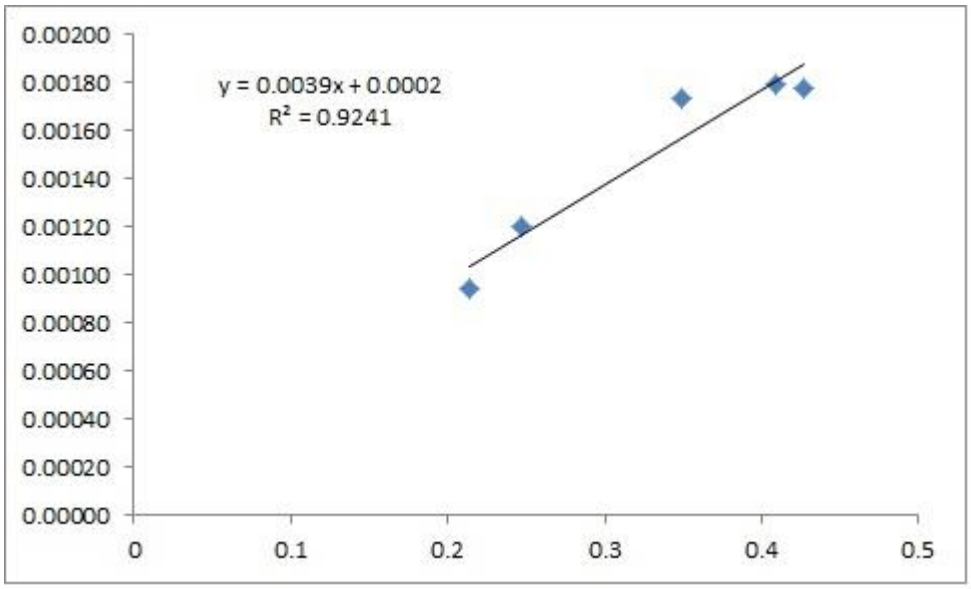

From the trend line equation we can find the lattice strain and estimated grain size in this case:

The lattice strain is 0.39%

The grain size: (1/0.0002) / 10= 500 nm